Na-ijlende gevolgen steenkolenwinning Zuid-Limburg

Final report
on the results of the working group
5.2.1 - ground movements

by

Projectgroup
"Na-ijlende gevolgen van de steenkolenwinning in Zuid-Limburg"
(projectgroup GS-ZL)

on behalf of

Ministerie van Economische Zaken - The Netherlands

Delft, Maastricht and Aachen (D), 31. August 2016
(Rev. a: 02. December 2016)

This report consists of 222 pages, 5 appendices and 4 plans

Na-ijlende gevolgen steenkolenwinning Zuid-Limburg

WG 5.2.1 - ground movements -
Final report

Parts A and part D of this report are edited by

Delft University of Technology
Department of Geoscience and Remote Sensing
Stevinweg 1
2628 CN Delft
Netherlands
Telephone: +31 (15) 2783546
E-mail: r.f.hanssen@tudelft.nl

Authors: Dr. ir. Hans van der Marel
Dr. ir. Freek van Leijen
Prof. dr. ir. Ramon Hanssen

Part B of this report is edited by

GeoControl
Meidoorn 93
6226 WG Maastricht
Netherlands
Telephone: +31 (43) 3628523
E-mail: info@geocontrol.nl

Author: Dr. Roland F. Bekendam

Parts C and D of this report are edited by

Ingenieurbüro Heitfeld Schetelig GmbH
Jean-Bremen-Straße 1-3
52080 Aachen
Germany
Telephone: +49 (241) 70516 -0
E-mail: info@ihs-online.de

Authors: Dr.-Ing. Michael Heitfeld
Dr. Peter Rosner
M.Sc. Stefan Pietralla
M.Sc. Dennis Rosin

Contents

Figures

Part A

Part B

Part C

Part D

Tables

Part A

Part B

Part D

Appendix

Appendix 1: Vertical displacement from 5 year levelling intervals

Appendix 2: Integrated PSI-GNSS-levelling time series at key levelling points

Appendix 3: Cross-profiles

Appendix 4: InSAR deformation maps

Appendix 5: Bow-Tie-Analysis

Plans

Plan 1: Potential impact areas, overview; scale 1:125.000
(Drawing No: 107-11-001a)

Plan 2: Potential impact area 1 - Heerlerheide fault, Geleen,
with monitoring measures; scale 1:25.000
(Drawing No: 107-11-002a)

Plan 3: Potential impact area 2 - Feldbiß fault, Brunssum,
with monitoring measures; scale 1:25.000
(Drawing No: 170-11-003a)

Plan 4: Potential impact area 3 - Feldbiß fault, Eygelshoven,
with monitoring measures; scale 1:25.000
(Drawing No: 170-11-004a)

Preface

After abandonment of the coal mines in the South Limburg mining district, significant ground heave induced by the rising mine water was observed since the 1960s. Derived from the previous progression of mine water rise, it has to be assumed that mine water is going to rise over a long period (at least 15 to 20 years) until a stable hydraulic equilibrium is reached (see report WG 5.2.4/5.2.5). Owing to the ongoing rise of mine water, further ground heave has to be expected for the future. In the context of the project, WG 5.2.1 had to give answer to the question: What impacts, related to ground heave and affecting the ground surface, have to be expected for the future?

In part A an evaluation of the available information of ground movements was carried out by using levelling data, GNSS (Global Navigation Satellite System) data, and satellite data (InSAR). The results provide a detailed overview of both the spatial extent of ground movement and the kinematic of the ground movements.

Based on the results of part A, the modelling of ground movements for prediction of future ground movements is discussed in part B. A „prognosis-tool“ is presented and tested for representative key points.

In part C potential impact areas with a potential remaining risk of damage to buildings in the future are defined. The risk factors that might induce discontinuities in zones of differential ground heave are described and the impact potential is estimated.

Based on a Bow-Tie-Analysis of the threats and consequences that might lead to or arise from differential ground heave preventive measures and a monitoring concept are presented in part D.

Part A - Measurements

1 Objectives

This part of the report describes the collection and analysis of ground movement measurements for the mining region in South Limburg. In the first phase of the project, all available geodetic data about historic ground movement in the region has been collected. The collected data sets are described in chap. 2.

A large part of these data are analysed and converted to various ground movement products, such as maps and profiles, see chap. 3. Hereby, the focus has been on the period after termination of the mining activities in 1974.

2 Available data

Various geodetic techniques are available to measure ground movements. In particular, levelling, continuous Global Navigation Satellite Systems (GNSS, such as GPS), and satellite radar interferometry (InSAR) are able to provide relevant measurements, each with their own characteristics regarding temporal and spatial resolution, and precision. In addition, campaign GNSS, tachymetry, and gravimetry can be used to provide information about ground movement.

Here, an effort is made to try to collect all available measurements in the South Limburg mining region made in the past. The characteristics of the available data sets are described here. All data is stored in a database by TNO for future use.

2.1 Levelling data

Fig. A 1 shows the levelling benchmarks in the South Limburg area. The levelling benchmarks in the mining area (+ 1 km) are colour coded with the number of available epochs. The dots represent levelling benchmarks with only a single measurement or outside the area of interest.

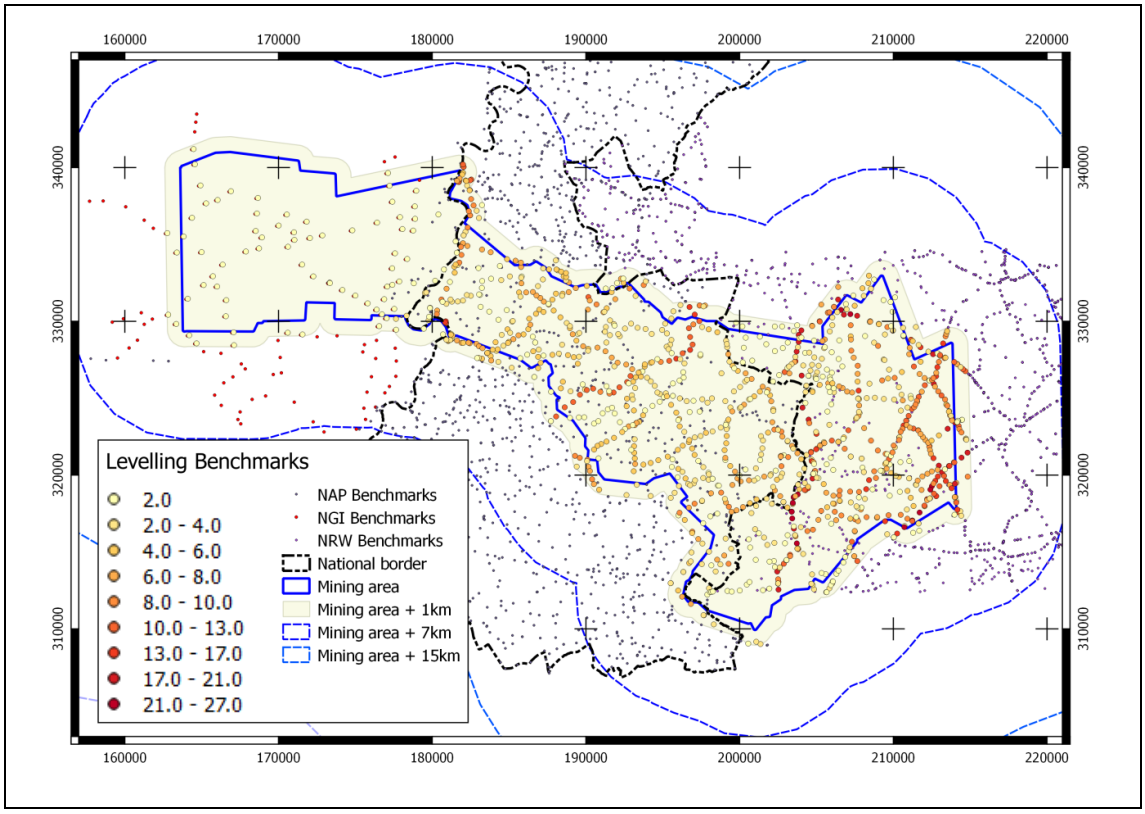

Fig. A 1: Levelling benchmarks with colour coded number of epochs in area of interest

The levelling data for the benchmarks in Fig. A 1 were provided by

- Rijkswaterstaat Centrale Informatievoorziening (RWS/CIV), Afdeling NAP, Delft, Netherlands.
- Nationaal Geografisch Instituut (NGI), Brussels, Belgium.
- Ingenieurbüro Heitfeld-Schetelig GmbH (IHS), Aachen, Germany, using data from Vermessungs- und Katasterverwaltung Nordrhein-Westfalen.

Historic heights of NAP benchmarks in South Limburg were provided by RWS for a bounding box [156.000, 221.000, 303.000, 348.000]. The heights refer to NAP, before, and after, the NAP revision in 2005. Some of the NAP heights are given both in the revised and unrevised NAP system, which makes it possible to apply corrections for the revision (see chap. 3.1). The horizontal coordinates of the benchmarks are in RD.

Fig. A 2 zooms in to the Dutch mining area, showing the levelling benchmarks with number of measurements. Several points are levelled only once (the dots in the Figure) and do not contribute to the computation of surface movement.

Fig. A 3 gives the distribution of the NAP measurements over time for the bounding box in Fig. A 1. The main concentration of measurements is between January 1974 and May 2012. For the period before 1974 the data is very scarce. Most of the levelling data from the mining companies that have been done in the period before 1994 has not been digitised. Only data from the mining companies that was shared with RWS has been digitised and made available to the project. The other levelling data still exists in written form at various archives.

The Belgium levelling data contains two main epochs: the 2nd half of 2013, and data from before 2000. The data that was provided contains the ID of the levelling benchmarks, the Lambert72 coordinates, height in TAW and date of computation.

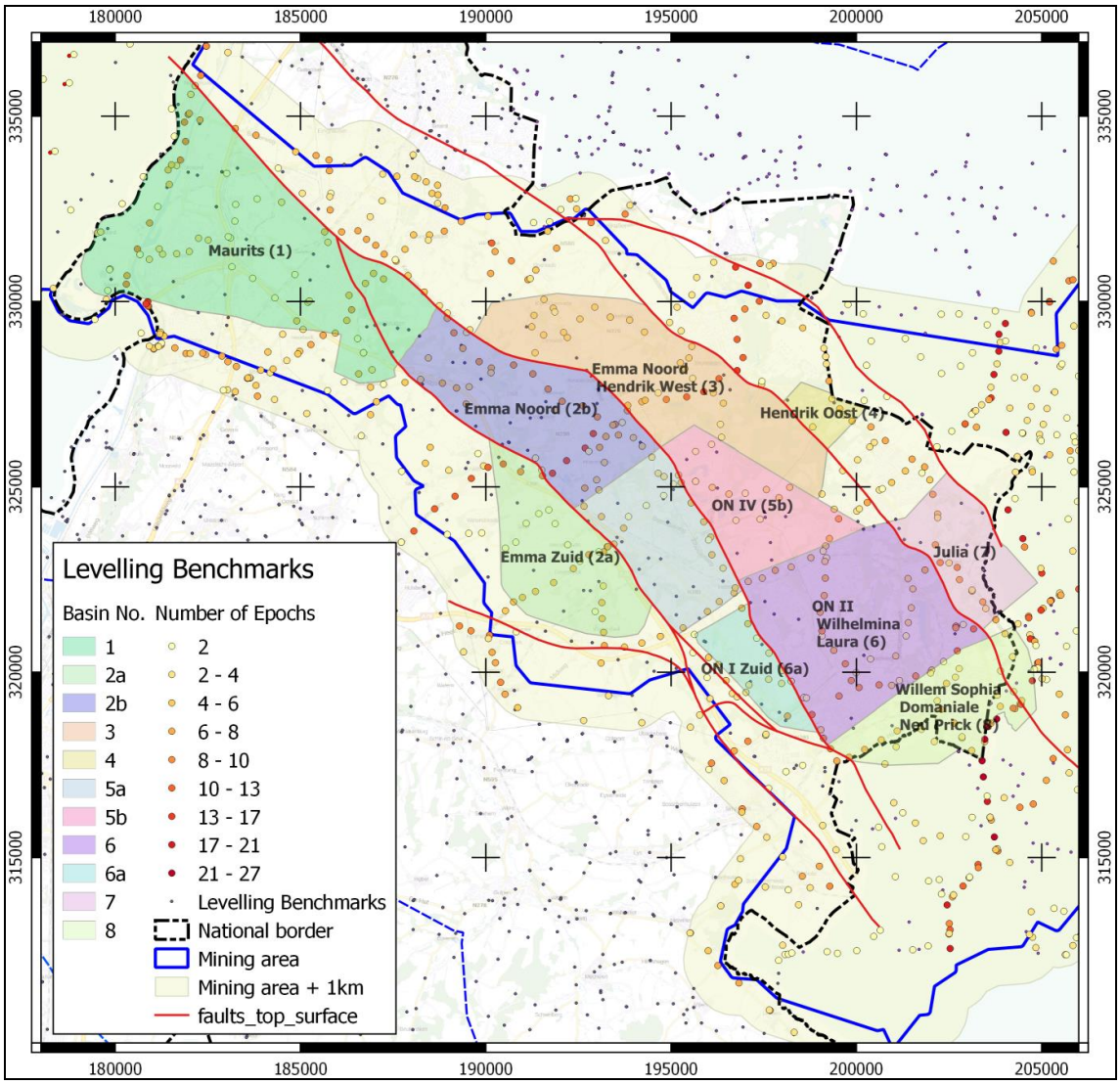

Fig. A 2: Levelling benchmarks (detail for the Netherlands), including the various basins. The colour coding of the levelling benchmarks indicates the number of available epochs

Historically, the "Tweede Algemene Waterpassing" was conducted for a first time over Belgium between 1946 and 1967, and a second time between 1980 and 2000. Since 2000 no systematic levellings over the whole of the Belgium territory were carried out. There have been only occasional levellings in areas with known problems. One of these areas was Limburg in 2013, but not all points

in that area have been re-measured. The heights before 1968 are only available on paper at NGI.

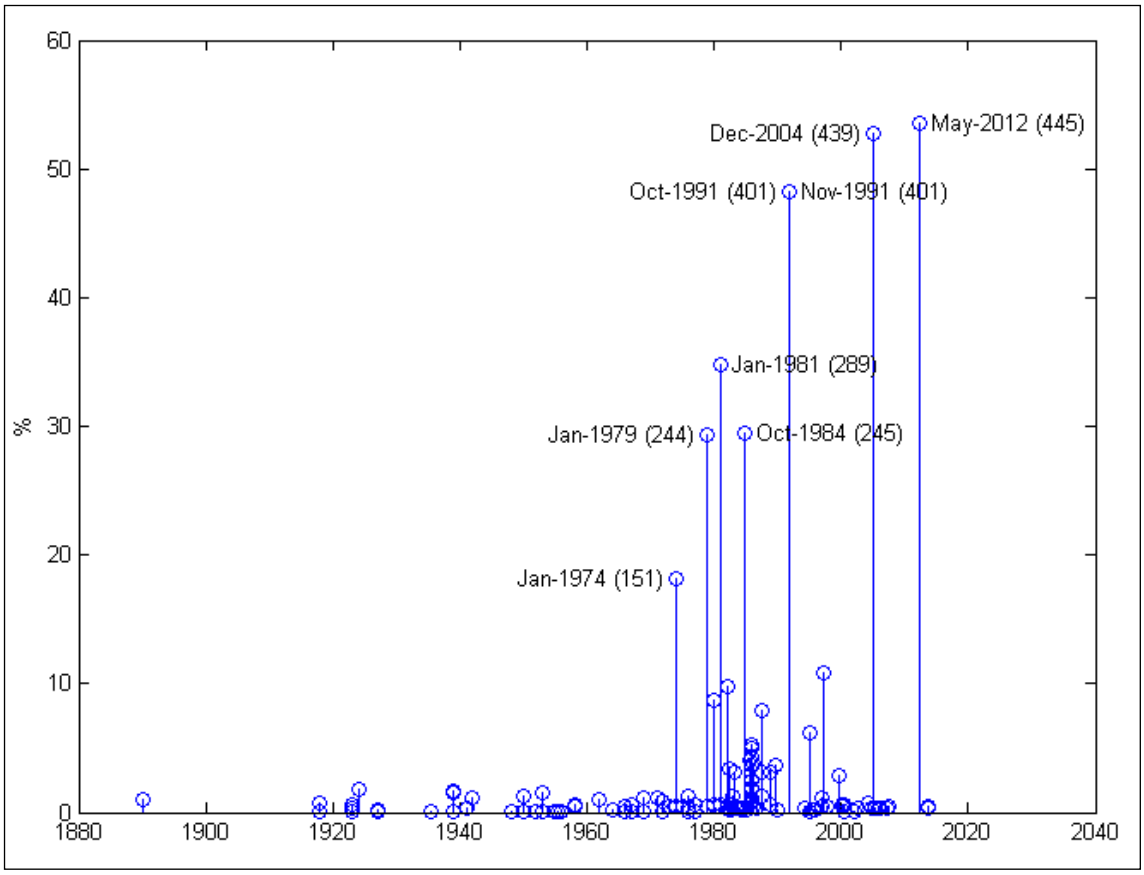

Fig. A 3: Levelling epochs

The levelling data North Rhine-Westphalia covers more or less the same period as the NAP data, but levelling has been carried out on a more regular basis. The heights refer to the same datum as NAP, although a small offset (1-2 cm) is possible. The horizontal coordinates are in the German Gauss-Krüger (zone 2) projection.

The Belgium Lambert72 and the German Gauss-Krüger (zone 2) coordinates have been converted to Dutch RD system (EPSG 28992) using the proj.4 software. The datum of the heights is not converted, except for the NAP data, as

we are only interested in height differences. For the NAP data set corrections were made in relation to the NAP revision in 2005, such that the historic data can be compared over time (see chap. 3.1 for details).

2.2 Continuous GNSS data

Fig. A 4 shows the locations of GPS Continuously Operating Reference Station (CORS) in the general region of the South Limburg mining area.

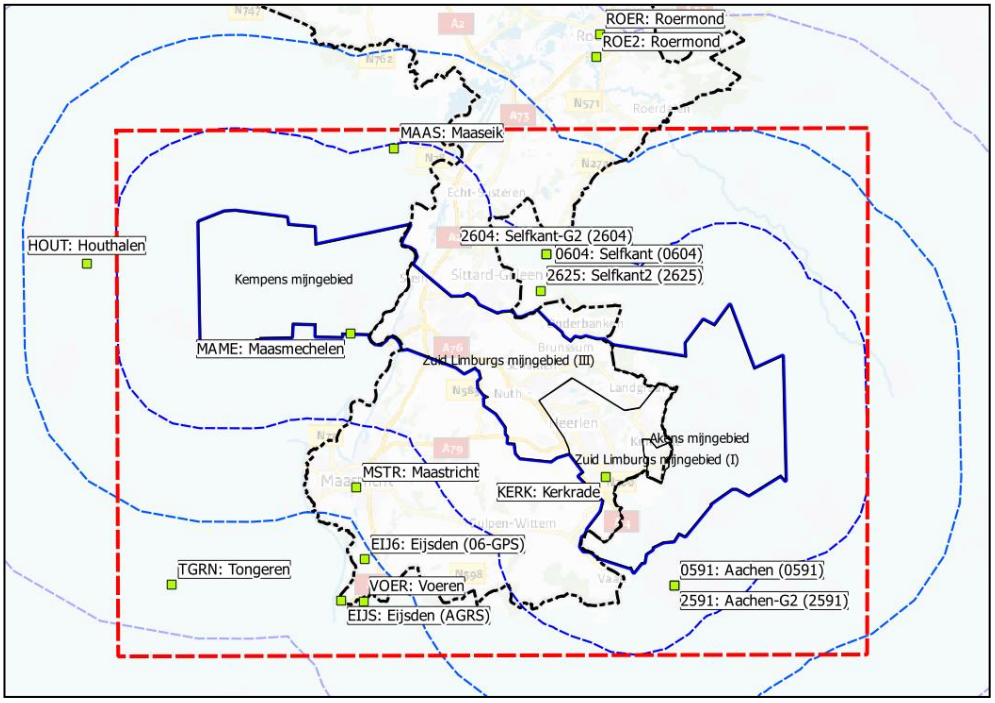

Fig. A 4: Continuous GNSS stations

Basically all possible CORS within the bounding box [156.000, 221.000, 303.000, 348.000] defined during the initial phase of the project were selected, with a few exceptions: Roermond (ROER/ROE2) and Houthalen (HOUT) were added simply because these stations were close to the bounding-box.

Tab. A 1 gives the four letter ID, station name, coordinates, start and stop time for each of the stations.

Tab. A 1: GPS CORS stations

id	start	end	x	y	H	station name
EIJS	2007-12-16		175916.4121	307629.9527	57.7844	Eijsden (AGRS)
KERK	2006-10-13		198627.3407	318186.0944	189.5578	Kerkrade
MSTR	2005-08-08		177216.6843	317268.6690	69.3919	Maastricht
ROER	2005-08-02	2011-08-28	198079.5707	356057.4907	51.0009	Roermond
ROE2	2011-08-29		197793.4135	354110.0369	35.8889	Roermond
EIJ6	2002-12-23		177925.3322	311112.3387	57.1277	Eijsden (06-GPS)
0591	2002-11-19	2009-10-30	204472.4721	308897.6767	216.8765	Aachen (0591)
2591	2009-11-01		204471.1814	308901.5444	216.8710	Aachen-G2 (2591)
0604	2007-09-23	2009-10-30	193520.3578	337257.0930	61.1666	Selfkant (0604)
2604	2009-11-01	2013-02-01	193522.8583	337263.1032	61.1545	Selfkant-G2 (2604)
2625	2013-02-02		193030.5879	334119.4031	55.4520	Selfkant2 (2625)
HOUT	2003-05-04		154088.0804	336450.8805	57.8367	Houthalen
MAAS	2003-05-04		180455.2281	346317.3017	42.7734	Maaseik
MAME	2004-06-13	2014-06-20	176725.2127	330442.1390	60.3329	Maasmechelen
TGRN	2003-05-04		161395.5451	308960.7867	101.4012	Tongeren
VOER	2003-05-04		177802.2890	307551.6041	72.7308	Voeren

The oldest available data is from 1997 for the AGRS station EIJS, but most stations only started to deliver data in the period 2003-2005. Several stations, such as Roermond (ROER/ROE2), Aachen (0591/2591), and Selfkant (0604/2604/2625), were re-located once or twice. Maasmechelen was discontinued in 2014 and not replaced. This is a pity, as there are only two stations in the mining area: Maasmechelen (MAME) and Kerkrade (KERK). Furthermore, the future of the station in Kerkrade (KERK) is uncertain. The building hosting the station is currently on the market for a new renter, and it is not certain if the contract with the previous renter for hosting the GPS station can be continued with a new renter.

Raw GPS data in RINEX (Receiver Independent EXchange) format was collected from various providers. RINEX data from the AGRS.NL network (EIJS), NETPOS network (KERK, MSTR, ROER, ROE2), and 06-GPS network

(EIJ6, 0591, 2591, 0604, 2604, 2625) was already routinely collected at the TU Delft GNSS local data centre. The station EIJ6 is operated by 06-GPS; 0591, 2591, 0604, 2604, 2625 are operated by Vermessungs- und Katasterverwaltung Nordrhein-Westfalen, and their data is shared with 06-GPS; KERK, MSTR, ROER, and ROE2 are operated by the Dutch Kadaster; and EIJS is an EUREF station build by the TU Delft, Kadaster and RWS, and operated by the Kadaster and TU Delft.

RINEX data for Belgium GNSS stations, HOUT, MAAS, MAME, TGRN, and VOER were provided specially for this project by NGI, Brussels. The GPS RINEX data, which covers a period of up to 17 years, is of the order of 50 Gb. The Raw GPS data has been processed by the TU Delft using the Gipsy/Oasis software of the Jet Propulsion Laboratory (JPL), Pasadena, USA. The processing and resulting time series in latitude, longitude and height are discussed in chap. 3.2.

2.3 Satellite radar interferometry data

The area of South Limburg is captured by four data stacks of satellite radar imagery. This enables the estimation of ground movement based on radar interferometry. In particular, Persistent Scatterer Interferometry (PSI) analyses are applied to all four data sets:

1. ERS-1/2 satellite, 1992-2000.
2. ENVISAT satellite, 2003-2010.
3. RadarSAT-2 satellite, 2010-2014.
4. TerraSAR-X satellite, 2013-2015.

A PSI analysis results in a set of detected Persistent Scatterers (PS), for which the deformation time series [mm] could be estimated (FERRETTI et al., 2001, VAN

LEIJEN, 2014, CROSETTO et al., 2016). All time series are relative with respect to a certain reference PS. Based on the time series, derived parameters can be obtained, such as a linear deformation velocity [mm/y].

The PSI analysis of the ERS-1/2 and ENVISAT data sets is performed by the TU Delft, whereas the RadarSAT-2 and TerraSAR-X data sets are provided by SkyGeo, the Netherlands. For the RadarSAT-2 data set, an additional analysis is applied by SkyGeo to detect distributed scatterers. Hereby, the number of detected scatterers is further increased for this data set (from 602.288 to 942.893 scatterers). The characteristics of the data sets are summarised in Tab. A 2.

Tab. A 2: Mission and PSI characteristics of the available data sets

	ERS-1/2	**ENVISAT**	**RadarSAT-2**	**TerraSAR-X**
Orbit	Descending	Descending	Descending	Descending
Wavelength	0,056 m	0,056 m	0,055 m	0,031 m
Incidence angle	26°	26°	34°	24°
Heading	196°	196°	191°	192°
Nominal repeat orbit	35 days	35 days	24 days	11 days
Number of images	66	70	64	47
Date first acquisition	23.04.1992	21.12.2003	03.06.2010	22.11.2013
Date last acquisition	31.12.2000	05.09.2010	28.10.2014	28.06.2015
Number of PS	267.191	245.203	942.893	3.572.891
Deformation direction	Line-of-Sight	Line-of-Sight	Line-of-Sight	Vertical

An overview of the results is given in Figures Fig. A 5- Fig. A 8. The velocities are provided in the radar Line-of-Sight (LOS) direction or in vertical direction (TerraSAR-X), and are relative to an arbitrary chosen reference PS.

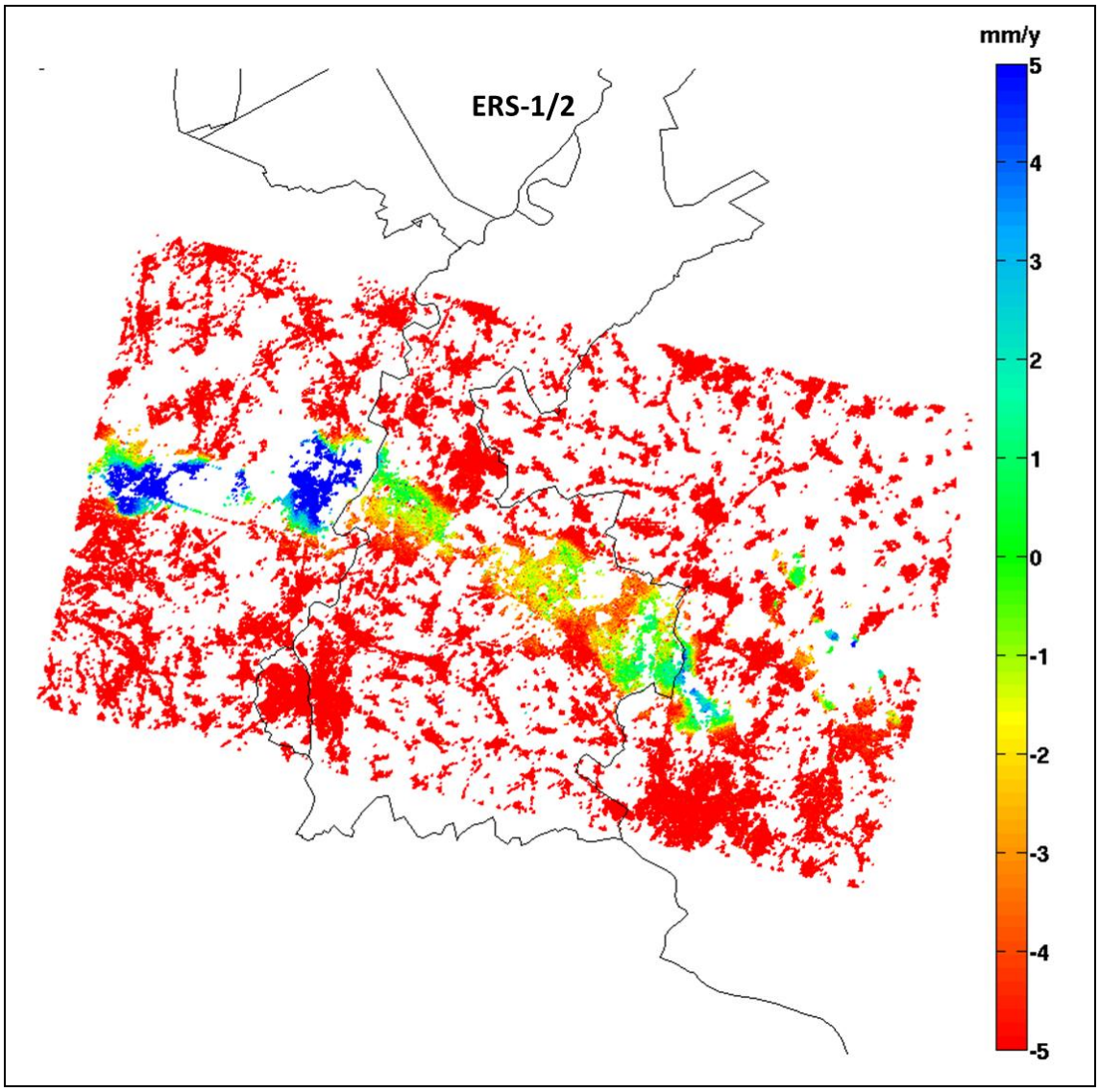

Fig. A 5: Linear deformation velocity [mm/y] of detected Persistent Scatterers in the 1992-2000 period (ERS-1/2 data set). The deformation velocities are given in the radar Line-of-Sight. All PS deformation velocities are relative to an arbitrary chosen reference PS. In this case, the reference PS appears to be chosen in the ground heaving mining area, resulting in negative deformation velocities in the surrounding areas. In chap. 3.3.1 GNSS measurements are used to refer the PS deformations to an Earth-fixed reference frame

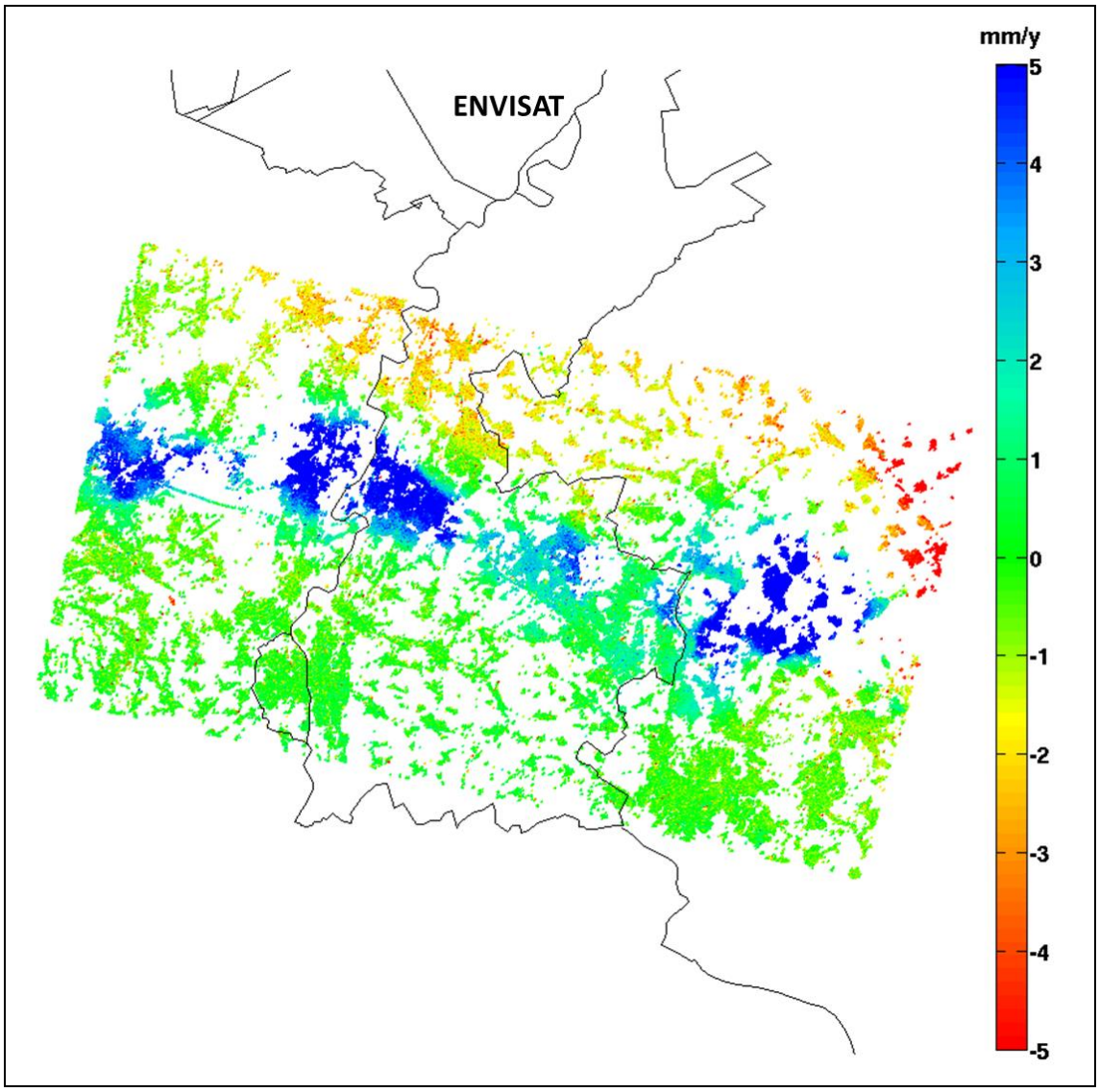

Fig. A 6: Linear deformation velocity [mm/y] of detected Persistent Scatterers in the 2003-2010 period (ENVISAT data set). The deformation velocities are given in the radar Line-of-Sight. In this case, a North-South trend in the PS deformation velocities is visible, possibly caused by errors in the orbit parameters of the satellite. In chap. 3.3.1 GNSS measurements are used to refer the PS deformations to an Earth-fixed reference frame, thereby removing any artificial trends in the PS data

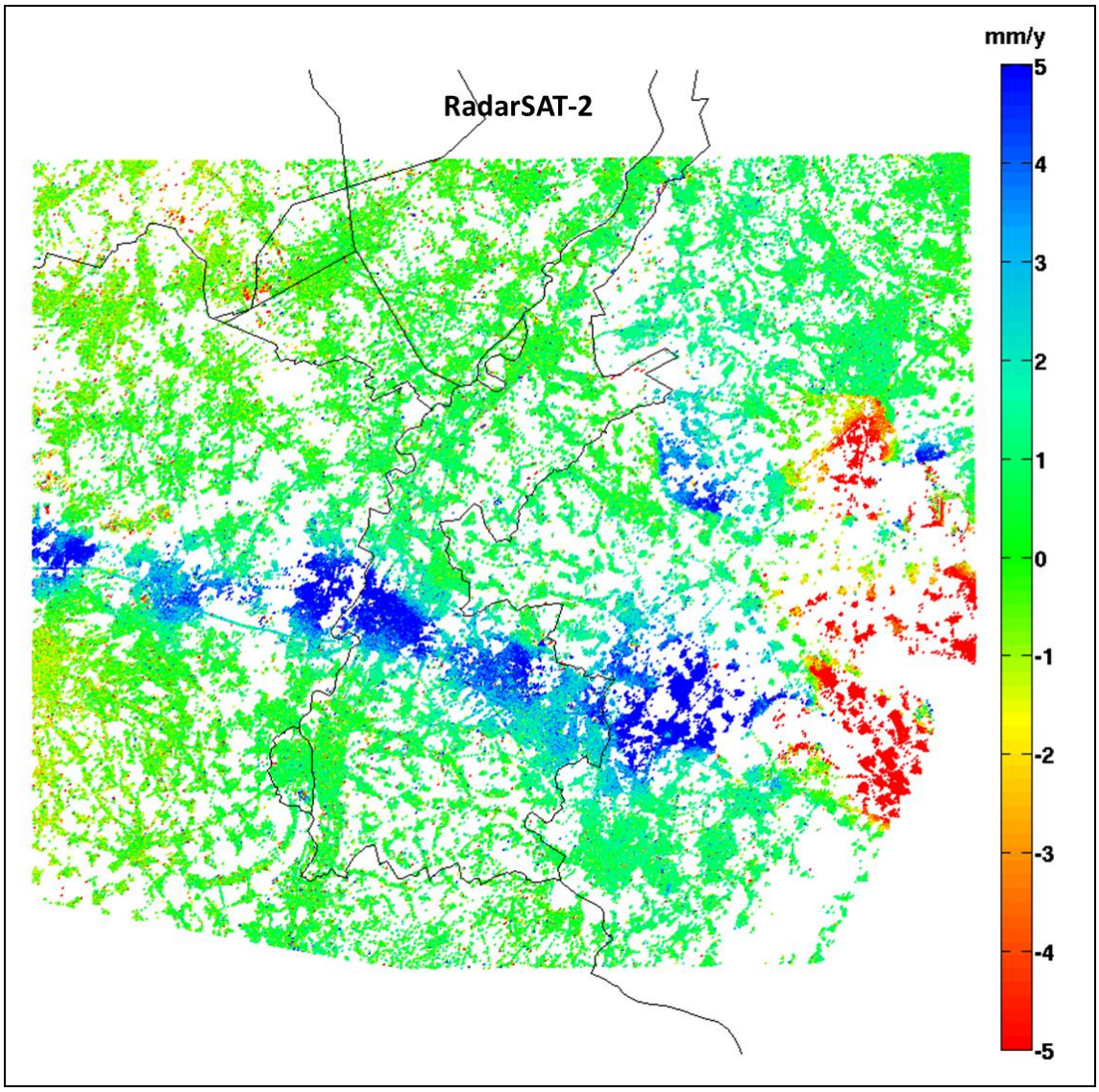

Fig. A 7: Linear deformation velocity [mm/y] of detected Persistent Scatterers in the 2010-2014 period (RadarSAT-2 data set). The deformation velocities are given in the radar Line-of-Sight

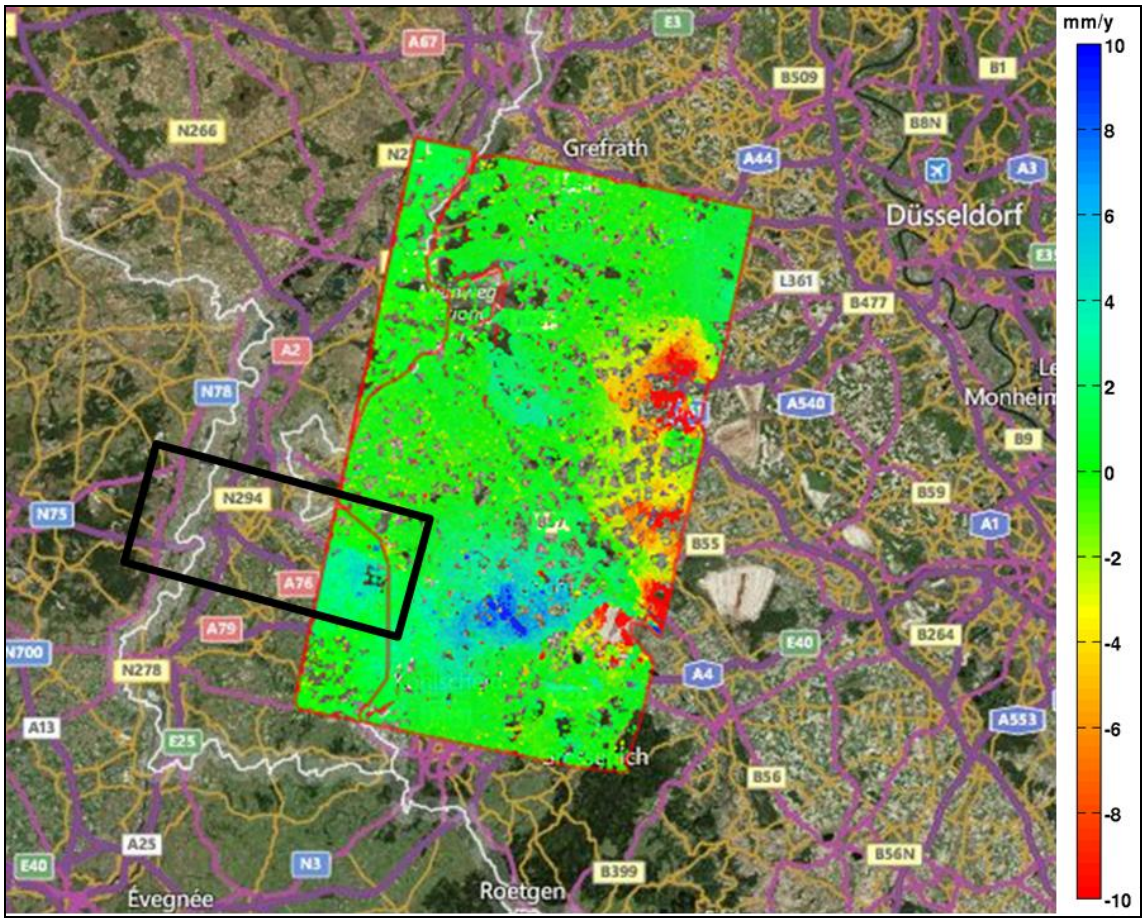

Fig. A 8: Linear deformation velocity [mm/y] of detected Persistent Scatterers in the 2013-2015 period (TerraSAR-X data set). The deformation velocities are given in vertical direction. The black box indicates the area of interest. As can be seen, only a part of this area is covered by the available TerraSAR-X data

Regarding the precision of these results, a comparative study (CROSETTO et al., 2009) has shown that the standard deviation of estimated displacements in C-Band PSI time series is between 1,1 and 4,0 mm. In a controlled experiment using corner reflectors, a standard deviation of 2,6 mm for ERS and 1,6 mm for ENVISAT time series is estimated (MARINKOVIC et al, 2007). The inaccuracies in the estimates are mainly caused by scattering noise and inaccuracies in the estimation of the atmospheric signal delays.

2.4 Additional data

Apart from the levelling, continuous GNSS and satellite radar interferometry data, additional data sets are available that contain information regarding ground movements. We collected campaign GNSS measurements, historic topographic maps, and gravimetry measurement. In addition, we added seismic data to the collection.

2.4.1 Campaign GNSS data

Fig. A 9 shows the location of campaign GNSS data points, also known as "GPS Kernnet" points. The GPS Kernnet, consisting of about 400 points in the Netherlands, is maintained by the Dutch Kadaster (DE BRUIJNE et al., 2005). The GPS Kernnet was started in the 1990s to facilitate the GPS users in the Netherlands. GPS Kernnet points were both connected to nearby RD triangulation markers and NAP levelling markers, as well, a network of GPS measurements was formed between the GPS Kernnet points. Thus, for the GPS Kernnet points two different types of heights are available:

- Ellipsoidal heights in ETRS89/ETRF2000 from GPS measurements
- NAP heights from levelling to nearby NAP benchmarks

The data spans a period from 1989 to 2013. The GPS Kernnet played a pivotal role in the early adaption of GPS in the Netherlands and the construction of a correction grid for the transformation between RD and ETRS89 coordinates. Since 2005 the GPS Kernnet is maintained as backup facility for the CORS networks in the Netherlands.

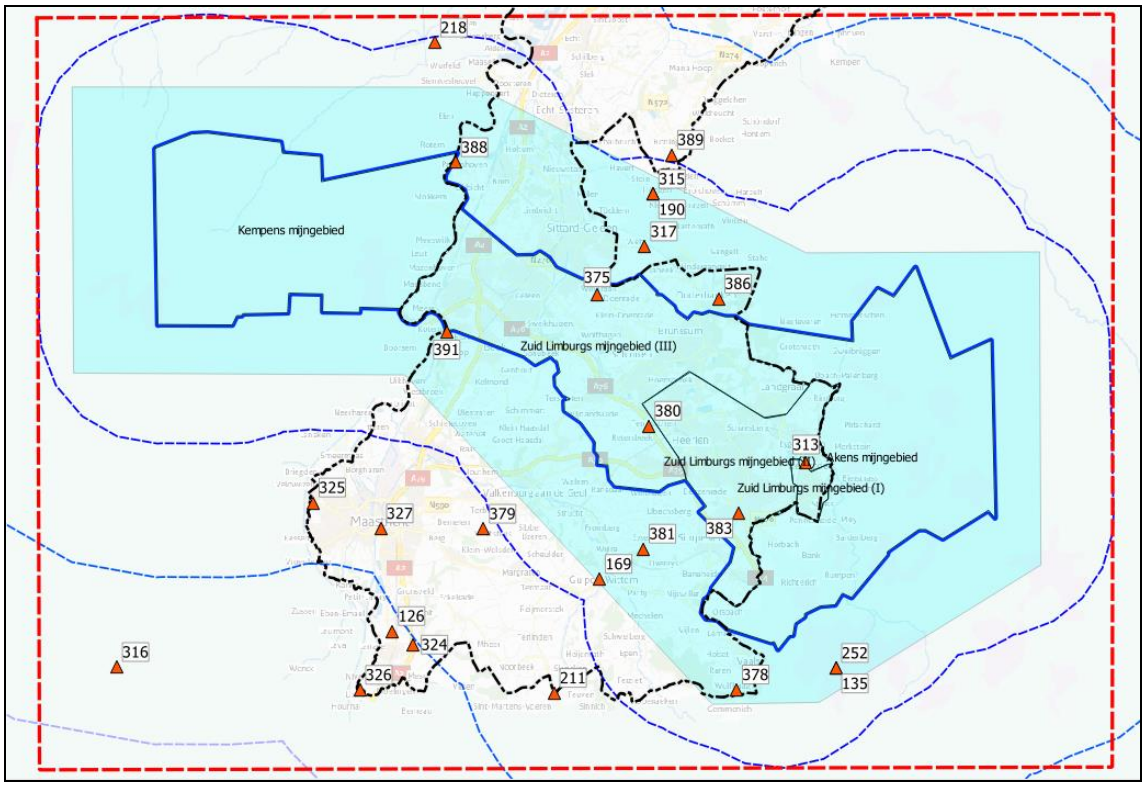

Fig. A 9: Campaign GNSS

In the South Limburg mining area four GPS Kernnet points are located. See Fig A 9.

For the computation of ellipsoidal heights different measurement procedures and analysis software have been used for different periods:

1. Until 2004 GPS baselines between GPS Kernnet points, using Trimble Geomatics Office for computing the baselines, and using Move3 adjustment of the baselines and to connect to AGRS stations.
2. From 2004-2010 the Bernese GPS Software 5.0, using baselines between GPS Kernnet points and AGRS stations.
3. After 2010, Geo++ GNSMART, partitioned model using real-time NETPOS-network parameters.

The changes in measurement procedure and analysis software result in rather non-homogeneous GPS time series, and also considering that only four points are

located inside the mining area, significantly reduces its value for the analysis of surface movement in the South Limburg area. Reprocessing of the raw GPS data would have been useful, but unfortunately, the original raw GPS data has not been archived, and reprocessing is not possible.

2.4.2 Historic topographic maps

Other sources of historic height information are topographic maps. Here, height information in the form of contours is provided, supplemented with annotated heights at certain road crossings. The height information is in general obtained by stereo photogrammetry. Although the accuracy of the height contours will be limited, the total subsidence in the area exceeds 10 m at certain locations (PÖTTGENS, 1985). Hence, it may be feasible to retrieve an indication of the total subsidence in the area based on these maps.

For the mining region in South Limburg seven historic topographic maps are available, published in 1925, 1936, 1955, 1960, 1968, 1979, and 1989. However, visual inspections shows that only the maps of 1925, 1960, and 1989 contain new, updated, height information, see Fig. A 10. Unfortunately, the height information in the maps is not available as separate (digital) data sets. Hence, the heights should be (manually) extracted from the maps.

Apart from the topographic maps, two other data sets with height information can be added here. In 1975, the TOPhoogteMD data set was finalised based on barometric measurements. The accuracy of these heights is unknown. In 2012, the height in the Limburg region was measured by terrestrial laser altimetry (LIDAR) in the framework of the AHN-2 project (VAN DER ZON, 2013). This data set provides height measurements with a maximum standard deviation of 5 cm, a maximum systematic bias of 5 cm, and a point density of 10-20 points/m^2.

Fig. A 10: Topographic maps with updated height contours. Left) 1925, middle) 1960, right) 1989

2.4.3 Tachymetry data

The Kadaster, who maintains the Dutch RD triangulation network, has had in the past several problems connecting GPS and tachymetry measurements for RD points in the mining area. The underlying cause of the problem is that RD is assumed to be static, and no horizontal movements are taking into account. When coordinates do not agree, the assumption is that there is a distortion of the monument. These assumptions obviously do not hold in the mining area. Therefore, the observed discrepancies could potentially be interpreted as horizontal movements.

The Kadaster has provided information on horizontal displacements computed from triangulation and GPS data. However, interpretation of this data is complicated, because the reported differences are either the result of

- two independent measurements of the same point,
- two independent measurements of the same point, but based on the nearby triangulation points,
- re-computations using the same data, but reporting different periods.

Only the first category will result in a true displacement. This category usually involves triangulation measurements in one epoch, and GPS measurements in the other. The second category may yield useful displacements depending on the

triangulation points that have been used for the connection of the local measurements (inside or outside the deformation area). The third category will probably not be very useful for deformation studies.

The interpretation is further complicated by the fact that the Kadaster has not stored the measurement epoch in their data bases, but the epoch of computation. So re-computations, using the same measurements, result in slightly different coordinates reporting an epoch that is later than the measurement epoch. It will be necessary to consult the full computation dossiers for a correct interpretation of the displacements, which have been scanned for this reason.

The main priority for this project was to collect and archive this data for future analysis. Fig. A 11 gives an example of the available information. Interpretation of this data is not a priority in this project.

Fig. A 11: Tachymetry

2.4.4 Gravimetry data

Time series of gravimetry measurements at the surface can provide insights into changes of mass distribution in the sub-surface, for instance due to groundwater flow. Unfortunately, the number of available historic gravimetry measurements in the Limburg mining region is limited. Three data sets have been retrieved:

1 Measurements in the South Limburg region acquired in 1979 (BLESS et al., 1980).
2 Measurements in the South Limburg region acquired in 1989 (NOHLMANS, 1990).
3 A set of measurements collected by Prof. Wim Bredewout, Utrecht University (dates unknown).

The locations of the various measurement points are visualised in Fig. A 12.

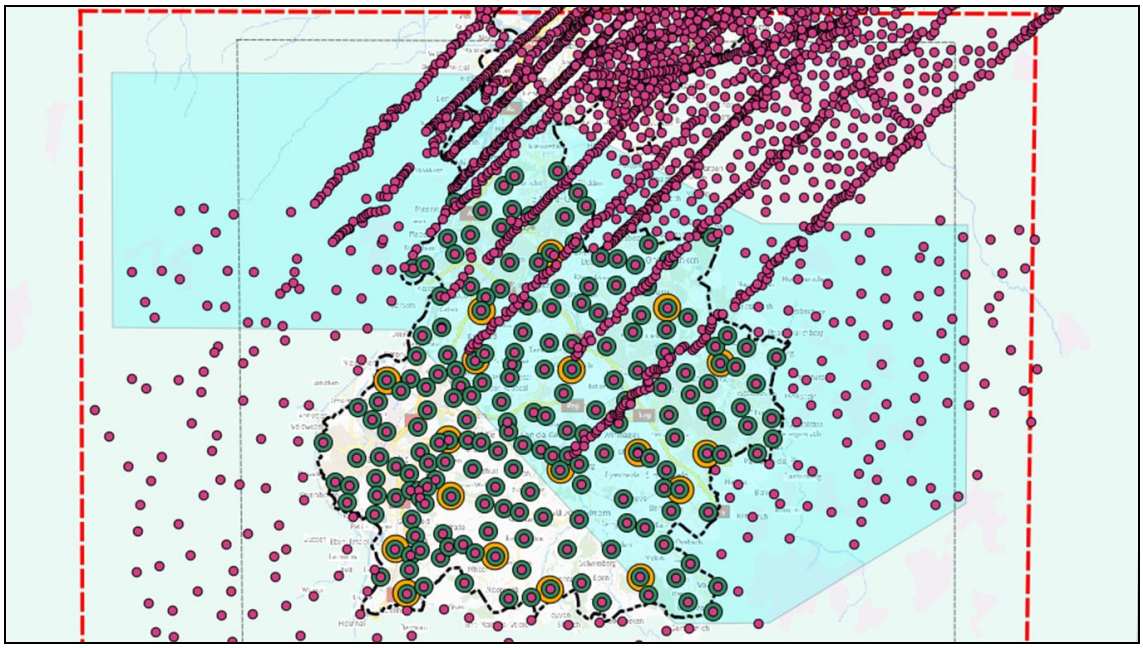

Fig. A 12: Available gravimetric measurements. Green dots: measured in 1979 (BLESS et al., 1980). Orange dots: measured in 1989 (NOHLMANS, 1990). Purple dots: measurements collected by Prof. Wim Bredewout, Utrecht University (dates unknown)

2.4.5 Seismic data

In the Netherlands seismic data is collected by the Royal Dutch Meteorological Institute (KNMI). Both tectonic and induced seismics are recorded and made public, see Fig A 13 and http://www.knmi.nl/seismologie/aardbevingen-nederland.html. The seismic data is collected for the project, but users are referred to the website stated above for the most recent version of the data. The analysis of this data is described in the report of WG 5.2.7.

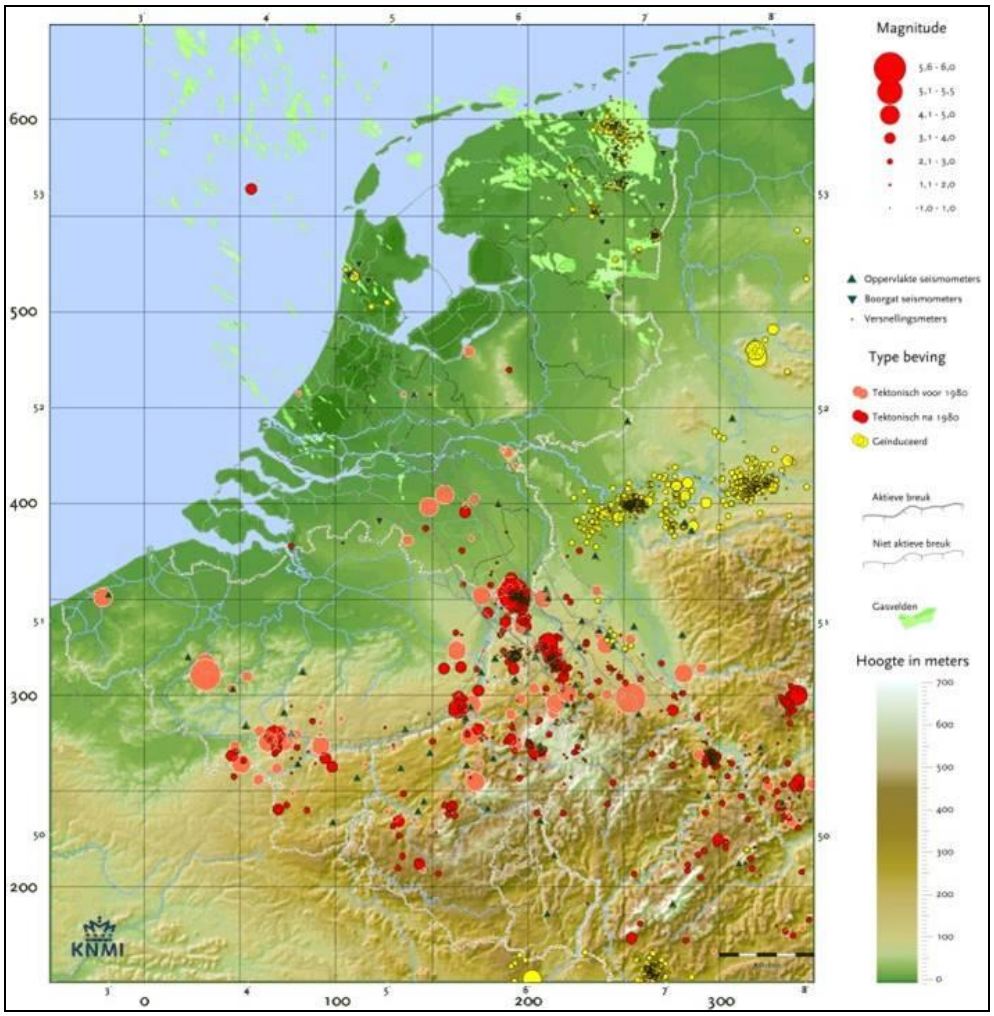

Fig. A 13: Overview of historic tectonic and induced earthquakes in the Netherlands (source: KNMI)

2.5 Conclusions available data

A large range of data sets of ground movements is available. The largest information content is provided by the levelling, continuous GNSS, and satellite radar interferometry measurement. Therefore, these data sets are further analysed in chap. 3. The seismic data is analysed by WG 5.2.7. For the other data sets holds that they are not used within this project, but that they are stored in the database of TNO for potential use in the future.

3 Data analysis

3.1 Levelling data analysis

3.1.1 NAP redefinition and levelling data conversion

Levelling data for the Netherlands, Germany, and Belgium was first converted into a uniform data format. The Gauss-Krüger and Lambert coordinates were converted to RD. The height datum for the German and Belgium data was not adjusted as we are only interested in height differences.

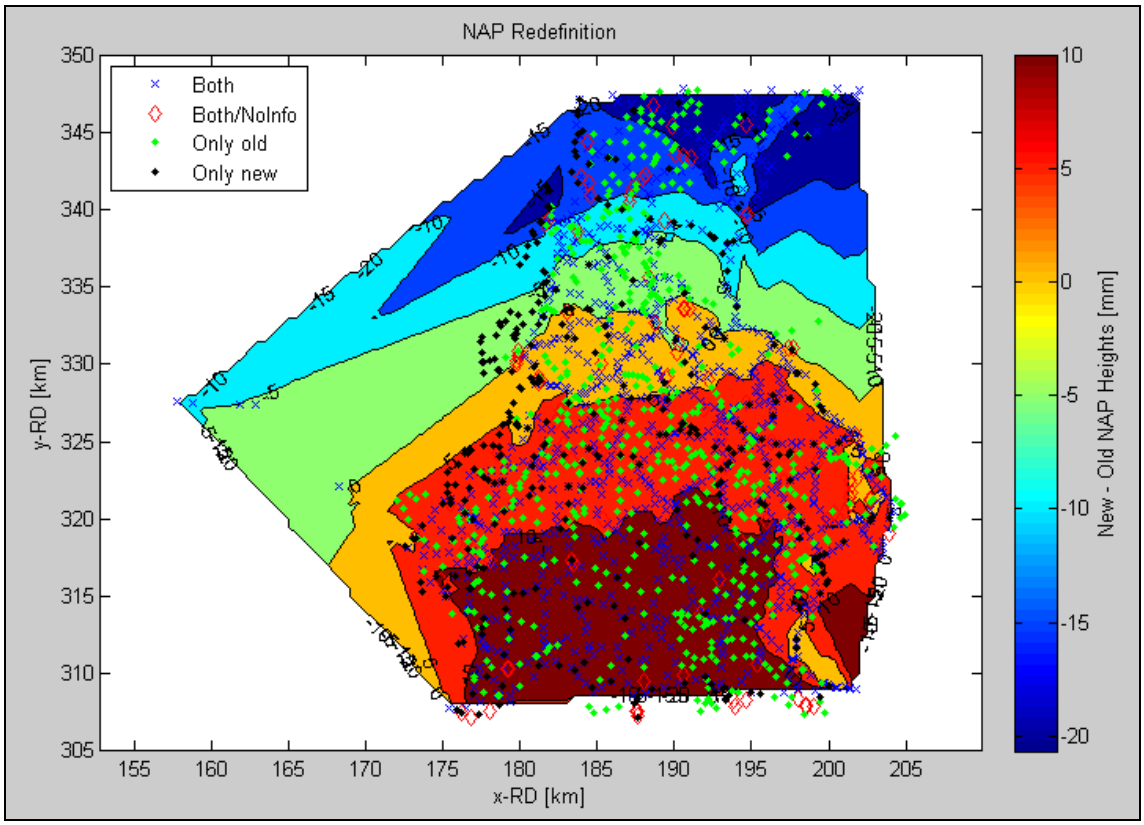

Fig. A 14: Corrections for the NAP redefinition

The Dutch data contained two datums: old NAP, and revised (new) NAP. The Dutch data is organised around so-called projects: each project has a date (hence

all levelling data from a project has the same date) and levelling order. Several projects were stored in both the old NAP and revised NAP system. For the levelling points in these projects is was straightforward to compute corrections to transform the old into the new system. However, for many points only heights in the old system, or both in the old and new system, but without projects in both systems, were available. For these points corrections were computed by interpolating data from projects in both systems. The results of this interpolation are shown in Fig. A 14.

We decided to convert all old heights into the new system, but going the other way would give the same results.

3.1.2 Matlab levelling data interrogation tools

In order to interrogate the database several Matlab scripts were developed. Functions were developed to retrieve historic height data: the function does corrections for the NAP redefinition, suppress redundant projects, select data based on levelling order, and remove identified outliers. Another group of functions finds all benchmarks within a specified radius from a given benchmark or given coordinates, or within a polygon. These functions are used to select data within concessions and basins. Other functions do plotting of selected benchmarks. The plot in Fig A 15 shows an example: plotted are the height differences with the last epoch for all benchmarks within a 1,5 km radius of levelling point 060C0236 (the levelling point was selected arbitrarily and did not contain usable height data). Using the data cursor information on the data points can be obtained. The inset shows the location of the levelling benchmarks, fault lines concession and basin borders. Fig. A 16 shows another example: plotted are the location of benchmarks within a basin, together with fault lines and border, with selected points highlighted.

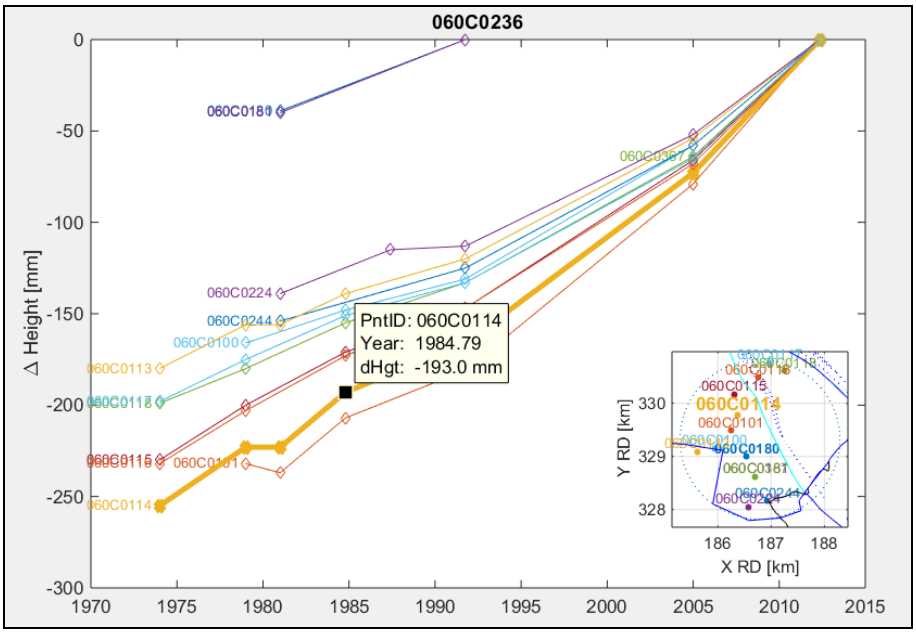

Fig. A 15: Screenshot of an example height evolution plot using the data cursor to highlight marker 060C0114 and interrogate a particular data point. (The plot has been optimised for on-screen viewing and is included here as an example)

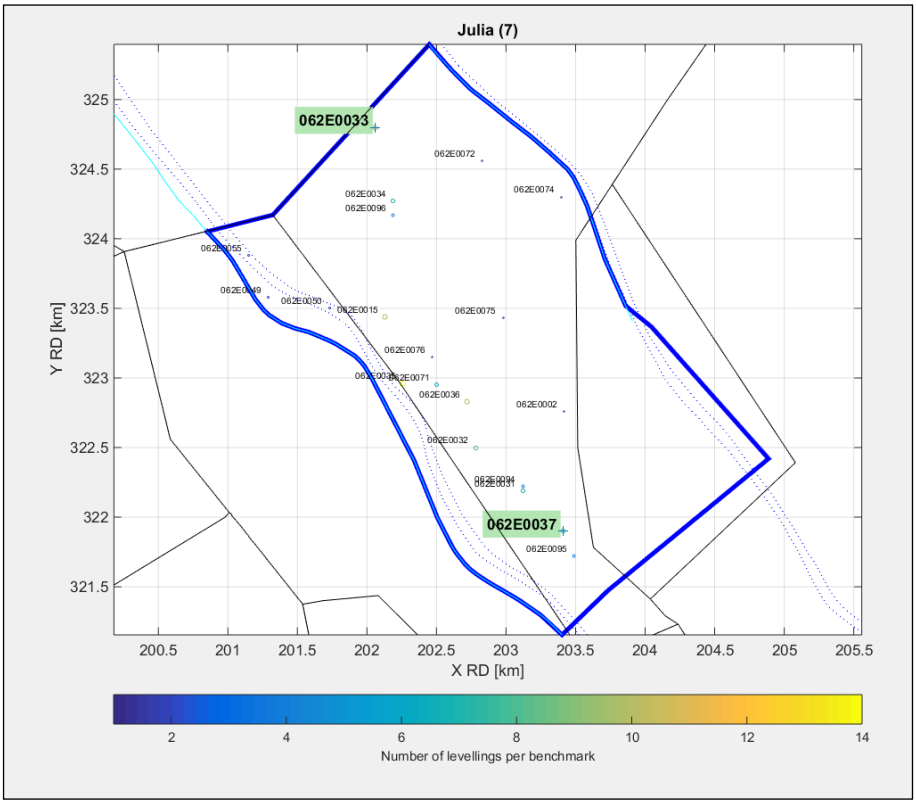

Fig A 16: Example plot showing a hydrological basin with levelling points, fault lines and concession borders. The heighted points were selected as key levelling points

These tools were used extensively during the early stages in the project to check the available data and to find representative levelling points for specific areas.

3.1.3 Representative levelling points for mining areas

During the initial phase of the project a search was made for representative levelling points for each hydrological basin.

Initially, a list of key benchmarks was selected at locations of suspected maximum deformation. This initial list was updated in several iterations, looking for nearby benchmarks with better data, better being more data and/or larger deformation. It turned out to be impossible to find a single point per basin: often two or more points per basin had to be selected in order to get a good impression of the representative time-deformation for each basin. The search was further complicated by the requirement that the key levelling points should also be located near a sufficient number of permanent InSAR scatterers.

The final list of representative levelling benchmarks and their historic heights have been used together with InSAR data in chap. 3.3.2 to show representative time-deformation diagrams.

3.1.4 Time-Deformation diagrams by hydrological basin

Because of the difficulties in finding representative levelling points for each basin a different approach was developed using a simple model to derive the time-deformation deformation diagrams for all levelling points in a basin, see Fig. A 17.

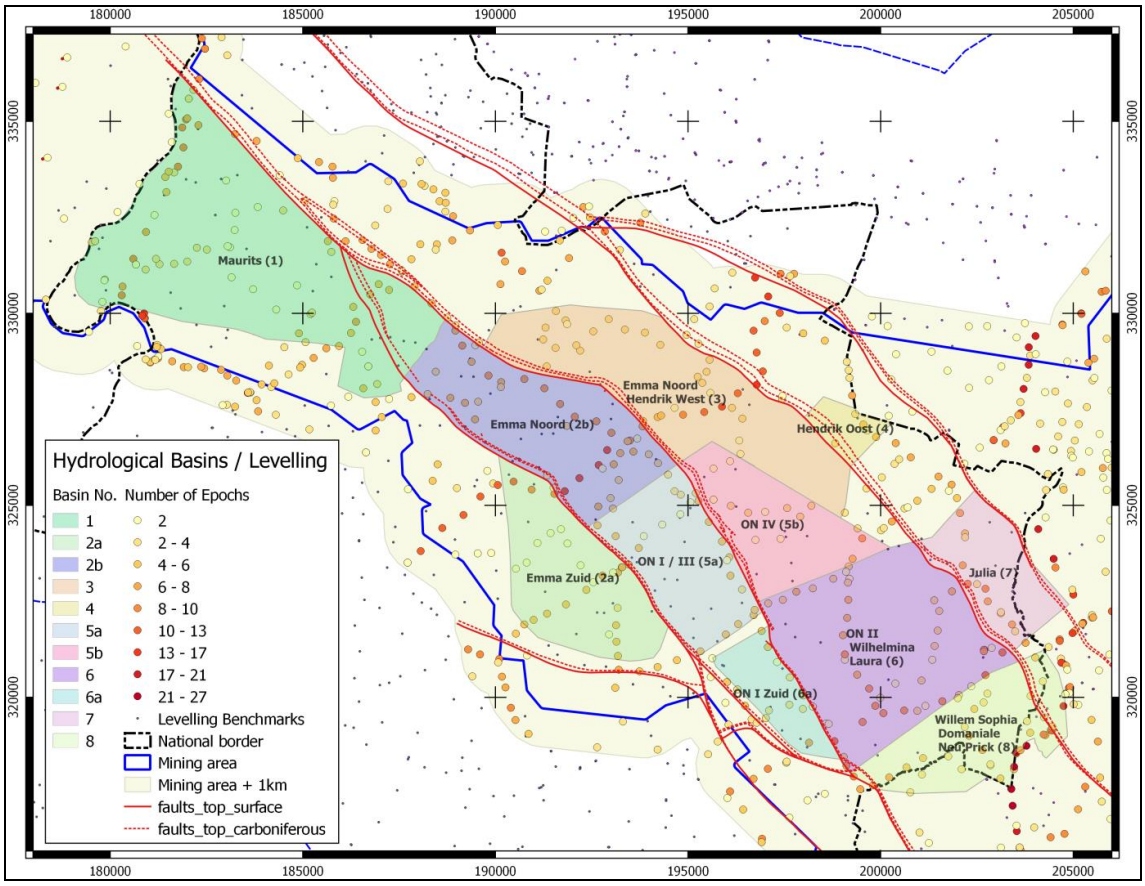

Fig. A 17: Overview of hydrological basins with levelling points. The colour coding of the levelling benchmarks indicates the number of available epochs

From all available levelling data in a basin, except for a few levelling points that show different behaviour e.g. near the border of a basins, or levelling points of bad quality, the characteristic time-deformation profile is estimated for a given period. After all data is used, the time-deformation profile is scaled to the levelling point with maximum deformation in the basin. The functional model is

$$y_{lk} = c_l \cdot \Delta h_k + h0_l \quad (1)$$

with y_{lk} the levelled height for point l at epoch t_k, $\Delta h_k = h_k - h_{2012}$ the height difference at epoch t_k with respect to the most recent measurement in 2012, $h0_l$ an offset which is different for each point and c_l an impact factor (scaling) that depends on the amount of deformation and is different for each point. Δh_k, c_l and

$h0_l$ are estimated using an iterative least-squares adjustment with the average of, c_l initially constrained to one (minimum norm solution); later, c_l and Δh_k are rescaled so that the maximum value of c_l is one (except for points with very short series) such that Δh_k represents the maximum deformation in the basin. The epochs are clustered within a half year window.

Some levelling points have been excluded from the analysis for various reasons. For instance, the data did not fit the other points or the estimated c_l was close to zero (no deformation), close to the border of the basin, or poor quality. The levelling benchmarks that have been excluded are listed in Tab. A 3.

Tab. A 3: Basin name, RMS fit and excluded levelling benchmarks

Basin name (number)	**RMS fit [mm]**	**Excluded levelling benchmarks**
1 - Maurits (1)	3,6	'060C0150' '060C0224' '060C0137'
2 - Emma Zuid (2a)	1,9	'062B0242' '062B0281' '062B0197' '062B0241'
3 - Emma Noord (2b)	3,1	'060C0123'
4 - Emma Noord/Hendrik West (3)	4,0	
5 - Hendrik Oost (4)	2,4	
6 - ON I, III (5a)	4,5	'062B0194' '062B0217' '062B0185'
7 - ON IV (5b)	5,2	'062B0083'
8 - ON I Zuid (6a)	2,8	'062B0141' '062B0150'
9 - ON II, Wilhelmina, Laura (6)	3,2	'062E0022' '062B0099' '062B0100' '062B0247' '062B0091' '062B0139’
10 - Julia (7)	4,9	'062E0034'
11 - Willem Sophia, Domaniale, Neu Prick (8)	3,5	'062E0017'

During the iterative least-squares adjustment the following output is produced:

- For each iteration of the iterative least-squares with overall RMS error of the fit.
- For each levelling point the number of measurements, period, impact factor c_l, RMS of the residuals of the observations and RMS of the height differences.

- For each epoch, the number of available measurements, the period (result from clustering), estimated Δh_k, estimated standard deviation Δh_k, RMS of the height residuals and RMS of the observation residuals, ratio of largest residual with RMS of the residuals (wmax) and the levelling projects that are involved with levelling order in brackets.

- Plot with the estimated heights.

The overall RMS error of the fit is given in Tab. A 3.

Fig. A 18 up to and including Fig. A 28 show the characteristic time-deformation for each basin. Each plot shows a line connecting the estimated heights with an estimate for the error bar (two sigma). The original data after rescaling and levelling with c_l and $h0_l$ are shown as diamonds in the plot. The numbers above each point represent the number of available levelling points; the italic numbers below each point are the (average) order of the levelling data. The inset shows the location of the levelling points. The size and colours of the circles is a function of c_l.

Users should be aware that 2nd and 3rd order levelling may sometimes be connected directly to an earlier 1st order levelling. If this is the case, there will be little or no apparent deformation over this period. These cases are to some extent identifiable from the plots, and should be ignored in the interpretation.

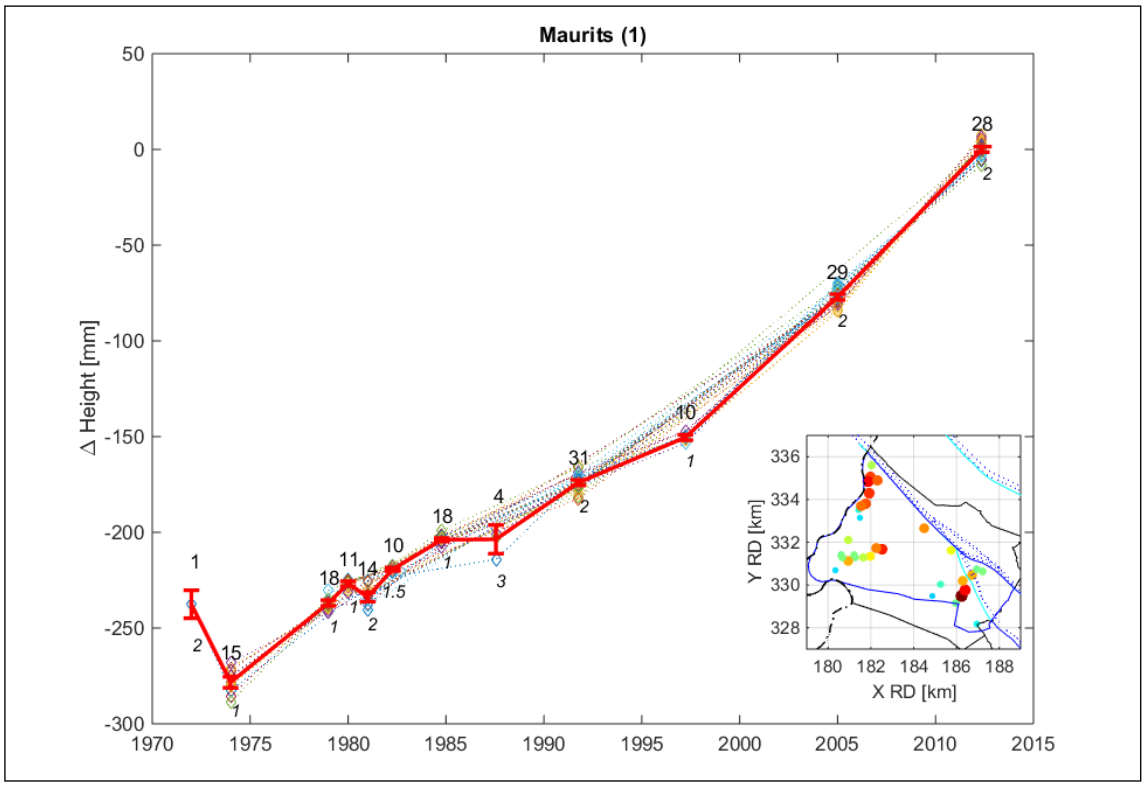

Fig. A 18: Time-deformation diagram Maurits (1) basin

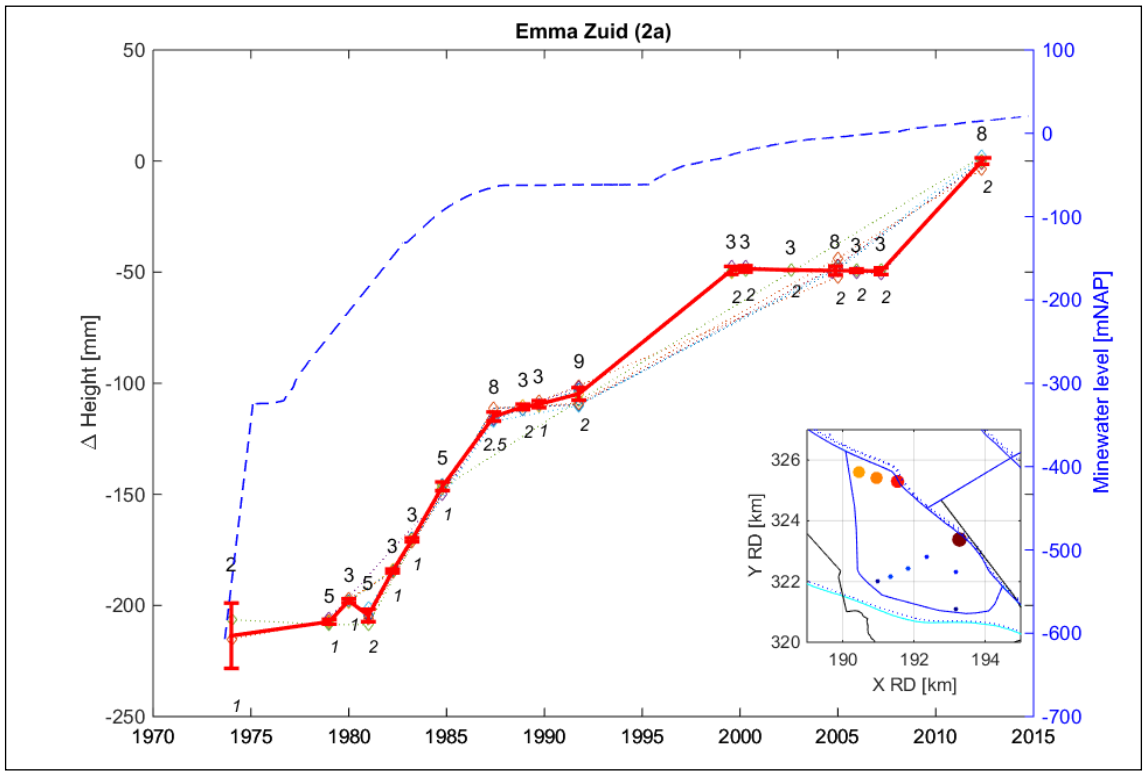

Fig. A 19: Time-deformation diagram Emma Zuid (2a) basin

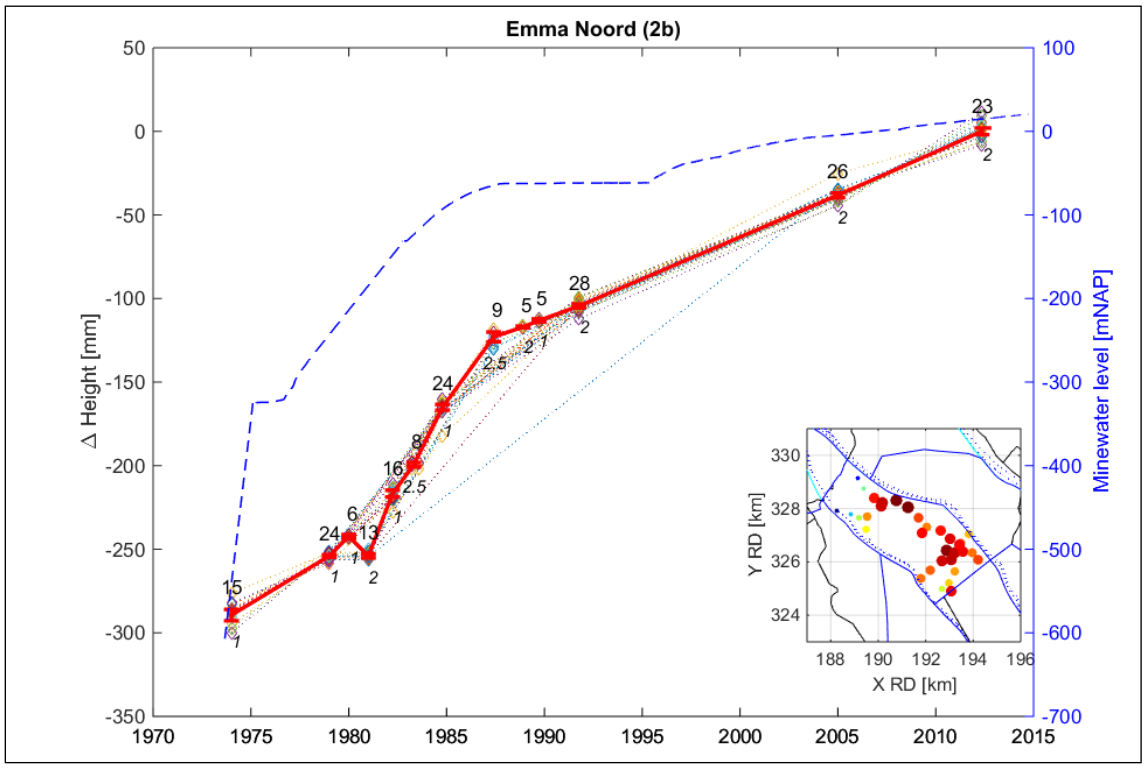

Fig. A 20: Time-deformation diagram Emma Noord (2b) basin

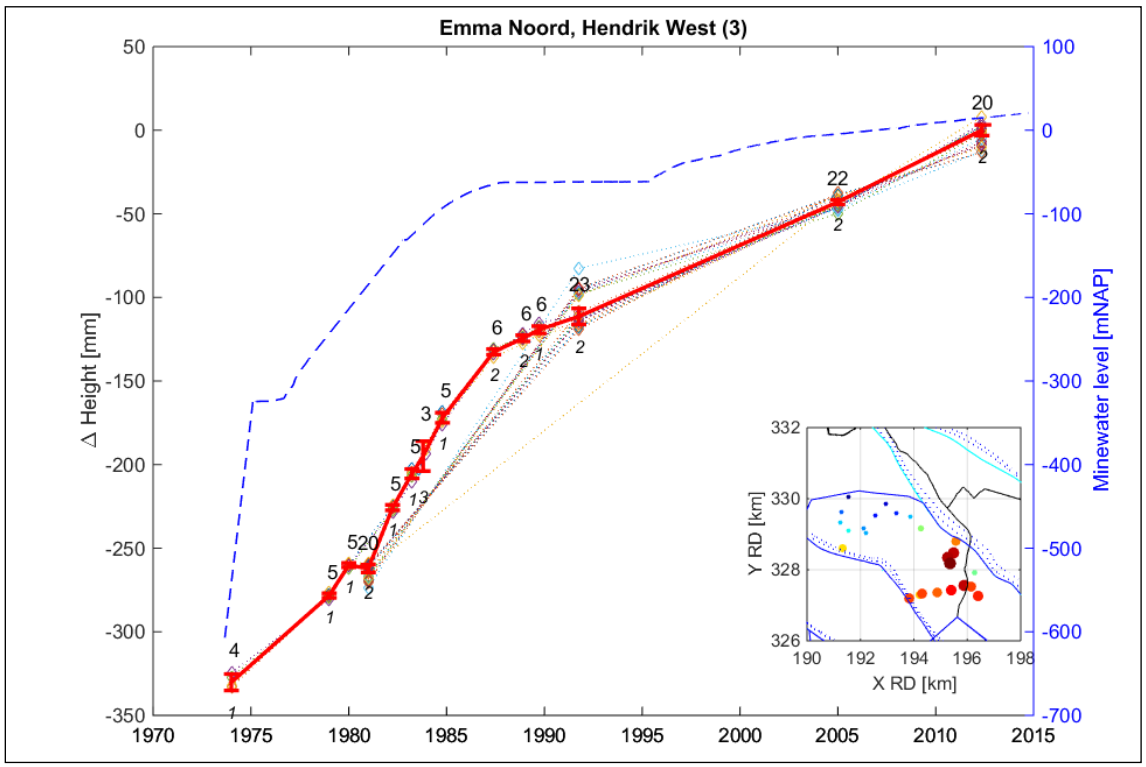

Fig. A 21: Time-deformation diagram Emma Noord and Hendrik West (3) basin

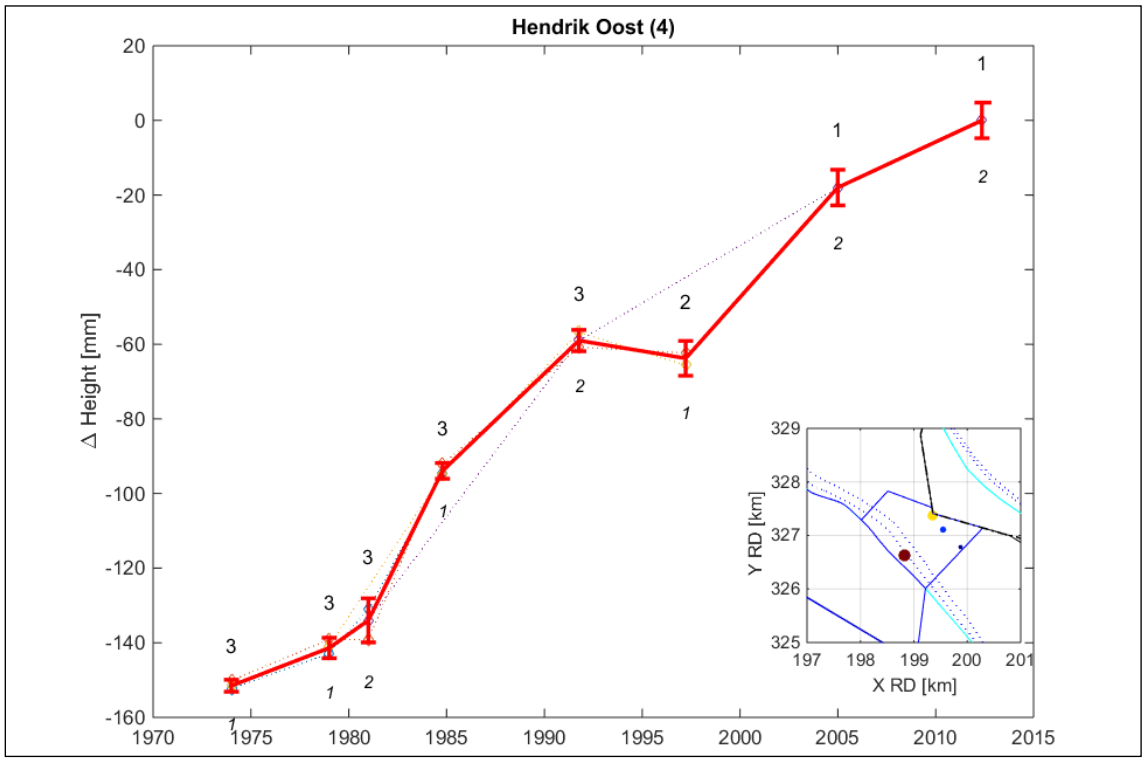

Fig. A 22: Time-deformation diagram Hendrik Oost (4) basin

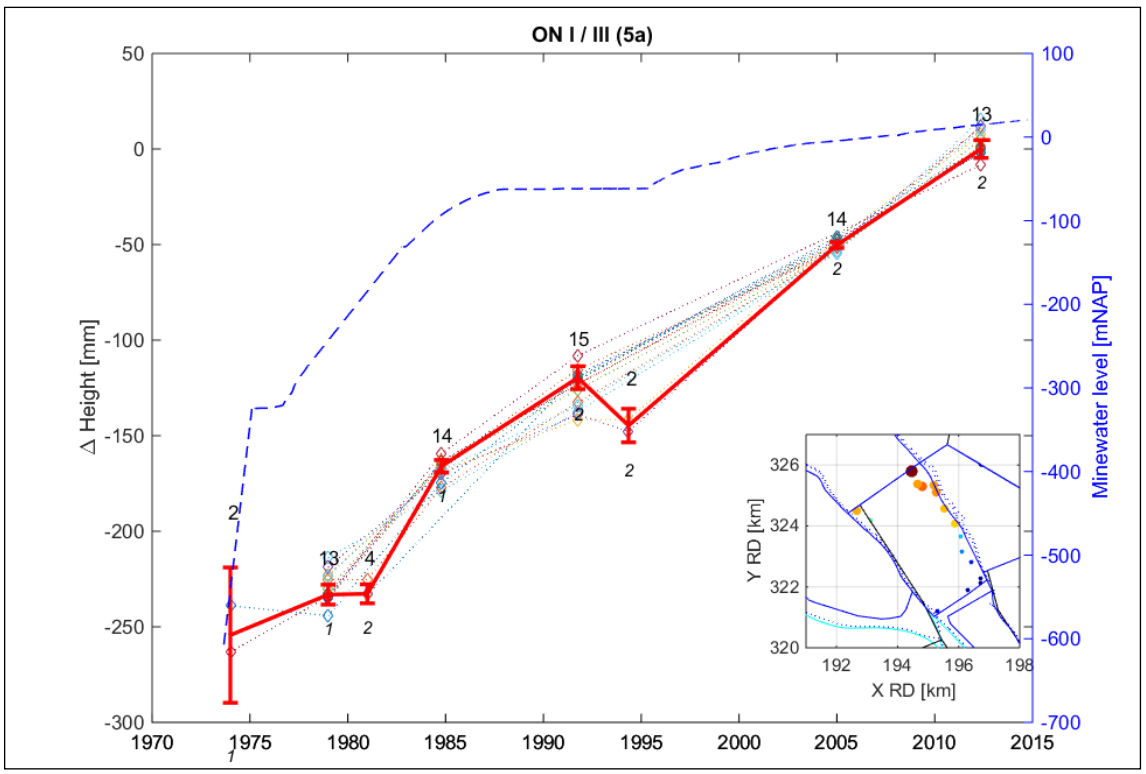

Fig. A 23: Time-deformation diagram Oranje Nassau ON I, III (5a) basin

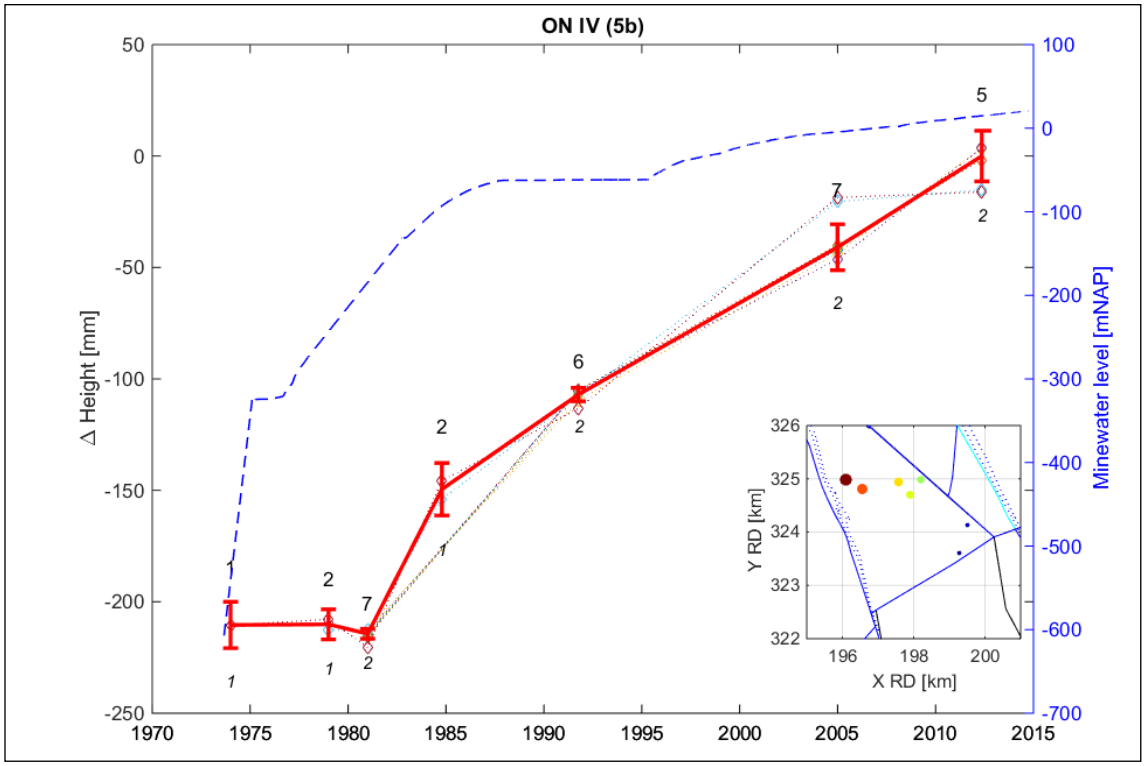

Fig. A 24: Time-deformation diagram Oranje Nassau ON IV (5b) basin

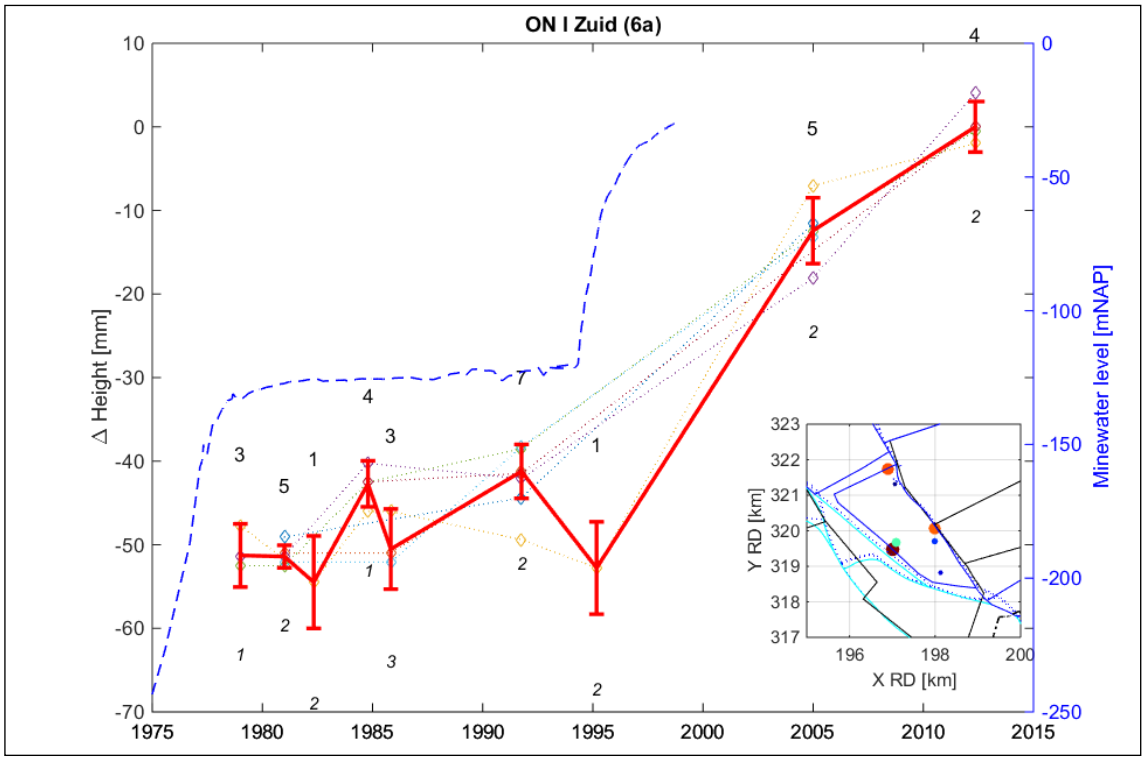

Fig. A 25: Time-deformation diagram Oranje Nassau ON I Zuid (6a) basin

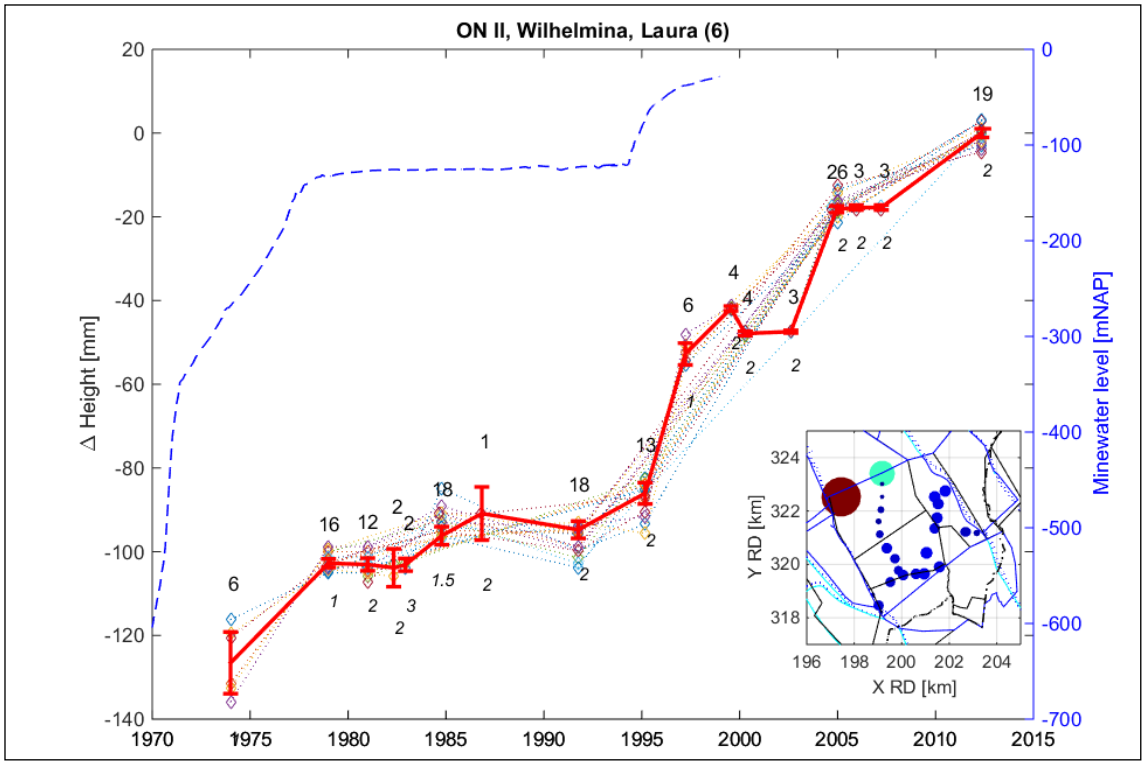

Fig. A 26: Time-deformation diagram Oranje Nassau ON II, Wilhelmina and Laura (6) basin

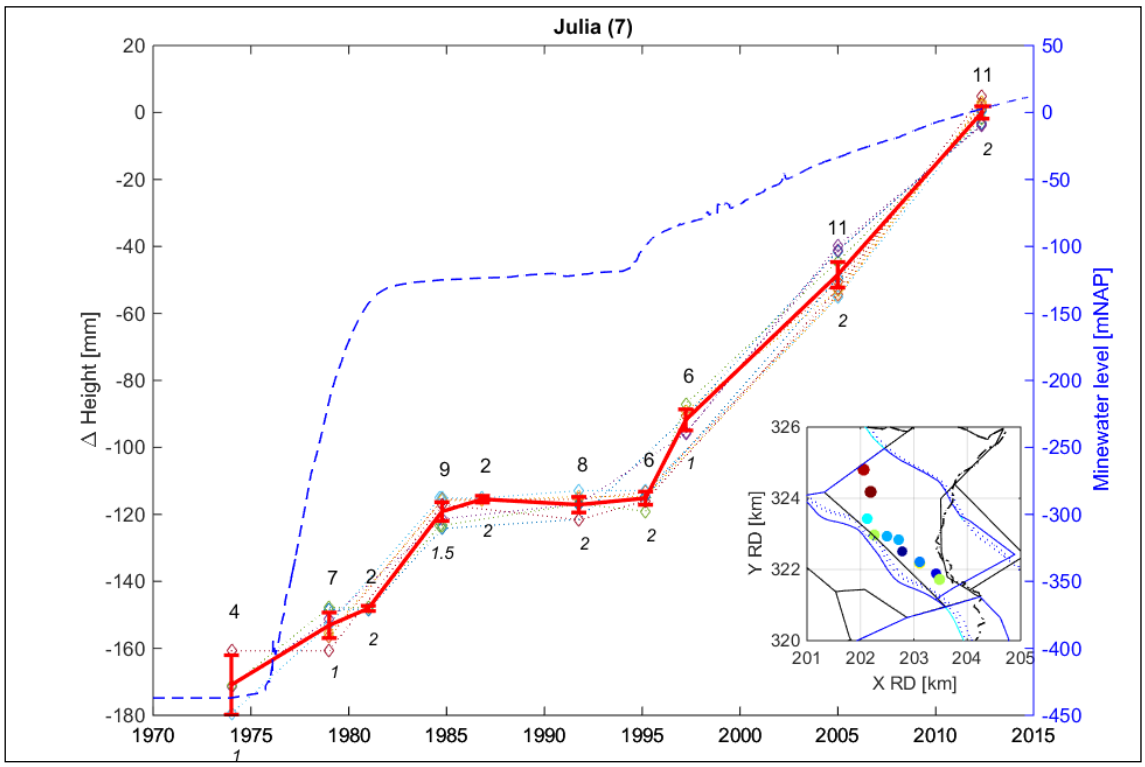

Fig. A 27: Time-deformation diagram Julia (7) basin

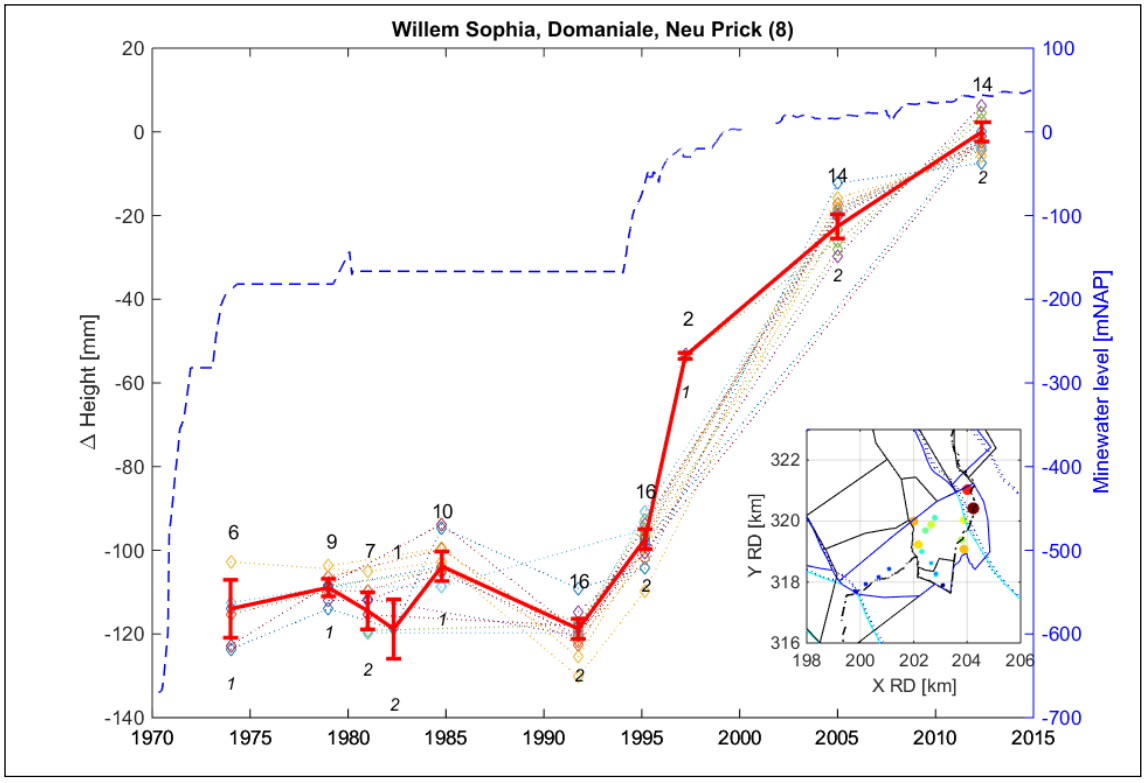

Fig. A 28: Time-deformation diagram Willem Sophia, Domaniale, Neu Prick (8) basin

3.1.5 Data fitting

In order to be able to produce contour plots the heights differences need to be interpolated to specific times. Several interpolation functions have been tried: the best results were obtained by modified piecewise Hermite cubic splines. At both ends of the data interval the interpolation is based on a linear interpolation/extrapolation, allowing to extend the data a little into the future and past. Within both end points piecewise Hermite cubic splines are used. An example is show in Fig A 29.

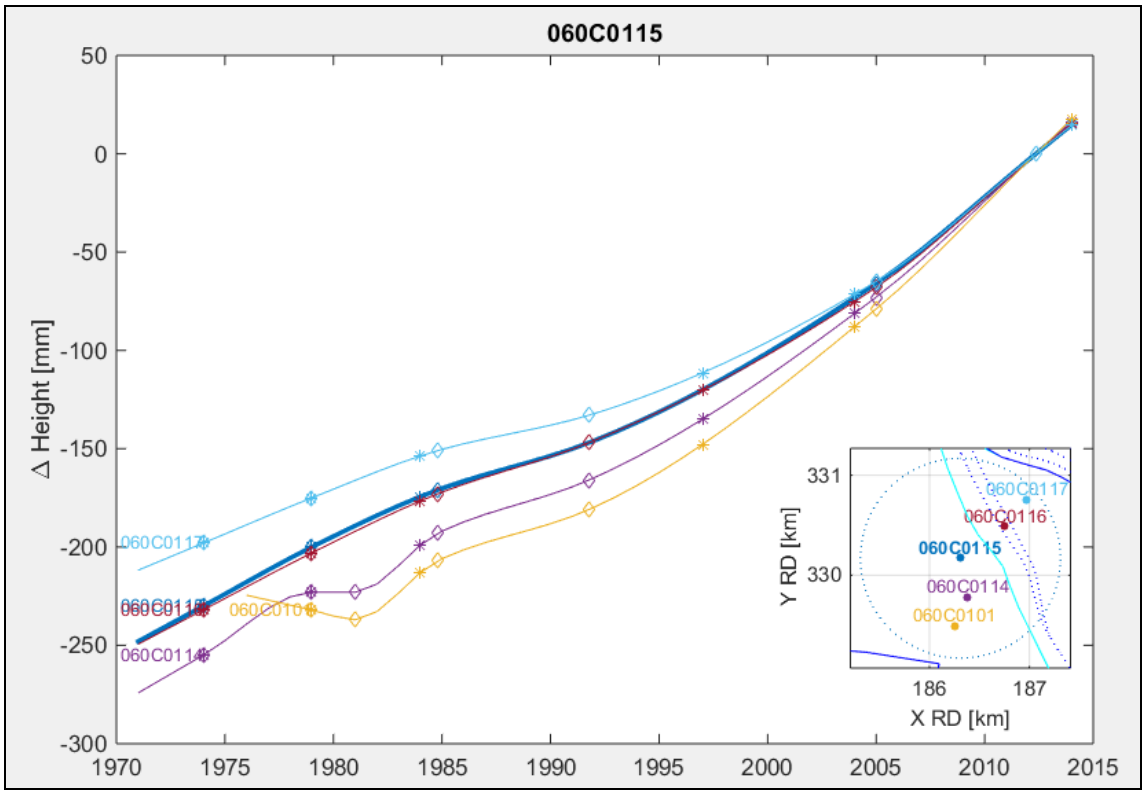

Fig. A 29: Screenshot with example of interpolation/extrapolation by modified piecewise Hermite cubic splines (The plot has been optimised for on-screen viewing and is included here as an example)

3.1.6 Contour plots

Fig. A 30 and Fig. A 31 show the result of contouring for the period 01.01.1974 until 23.04.1992, and for the period 23.04.1992 until 28.10.2014. This last period has been chosen to coincide with the period for which InSAR data is available. For the first period only levelling data is available. In chap. 3.3.3, Fig. A 61 the combined levelling and InSAR result is shown. In Fig. A 32 the total vertical displacement for the period 1974-2014 is given. Fig. A 32 is computed by summing individual grids, each covering 5 years of deformation, from 1974 until 2014. The contour plots for each of these 5 year periods are shown in Appendix 1.

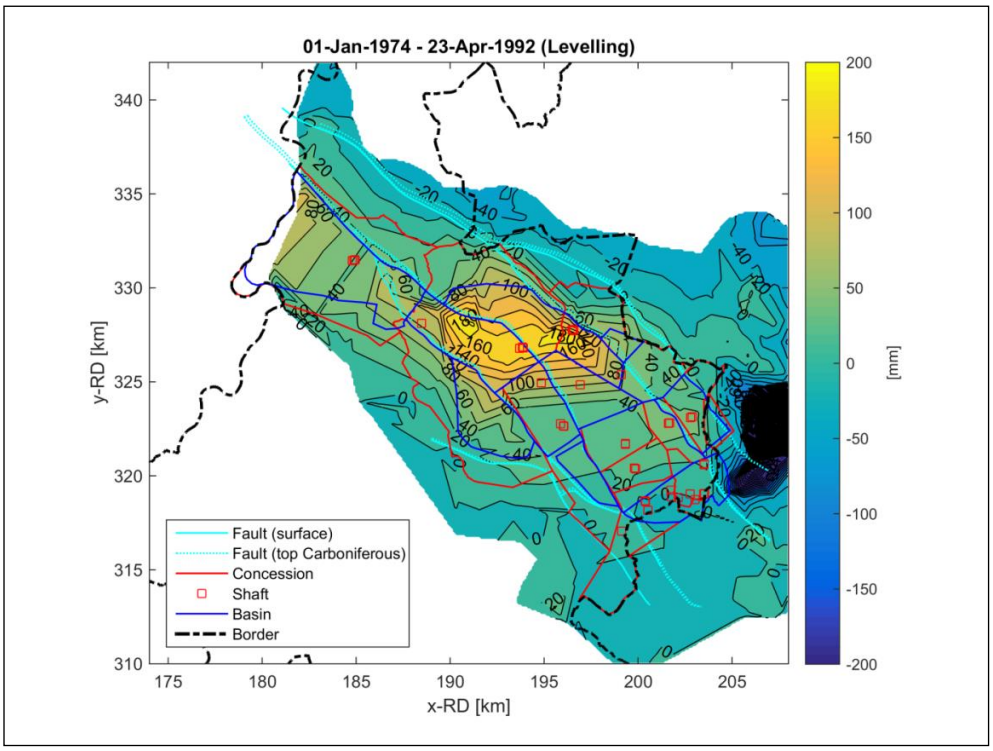

Fig. A 30: Contour plot showing the vertical displacement [in mm] for the South Limburg mining area between 01.01.1974 and 23.04.1992

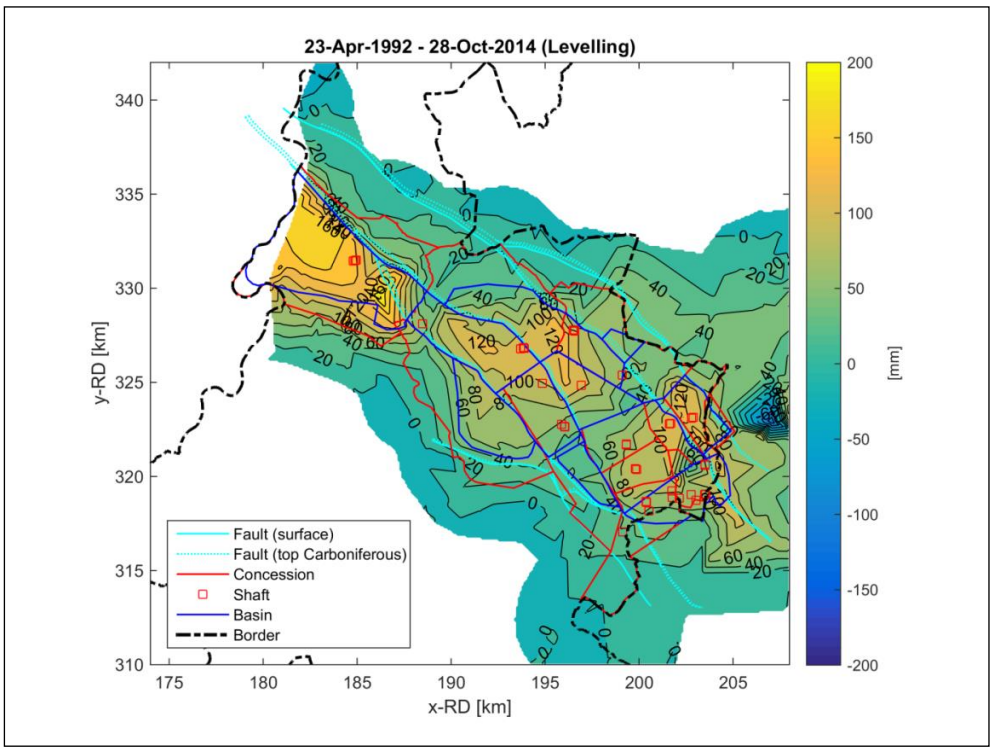

Fig. A 31: Contour plot showing the vertical displacement [in mm] for the South Limburg mining area between 23.04.1992 and 28.10.2014

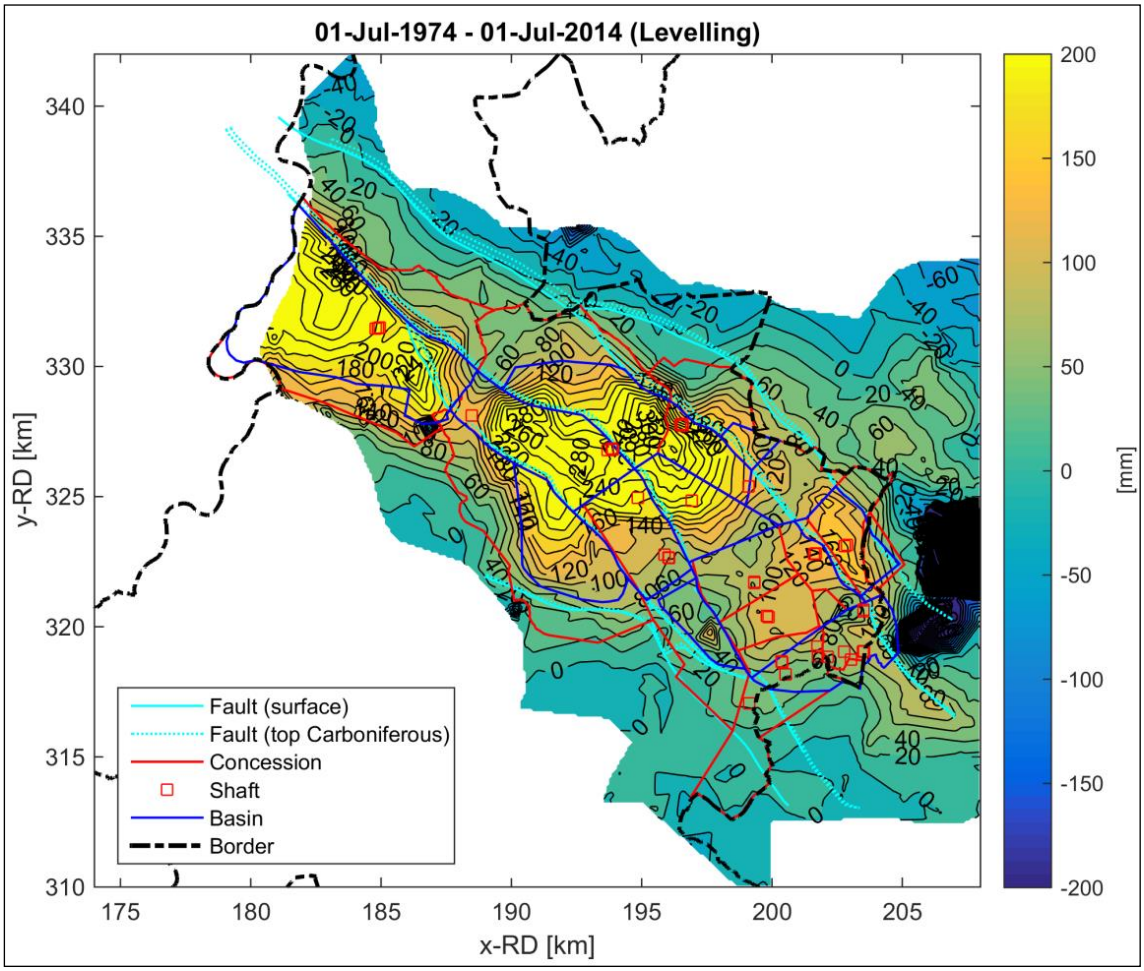

Fig. A 32: Contour plot showing the vertical displacement [in mm] for the South Limburg mining area between 01.07.1974 and 01.07.2014

3.1.7 Aalbeek-Hoensbroek-Schinveld profile

In PÖTTGENS (1985) a profile generated from levelling points along a line Aalbeek-Hoensbroek-Schinveld is shown. The profile is plotted again in Fig. A 33 using the most recent levelling data.

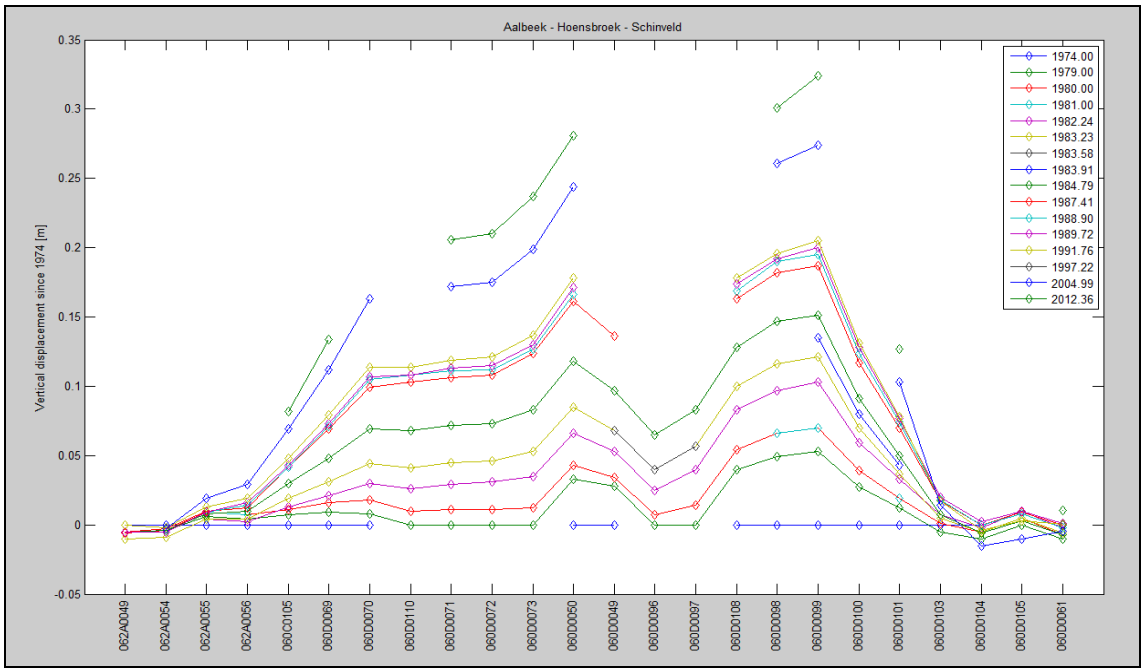

Fig. A 33: Aalbeek-Hoensbroek-Schinveld profile. Heights for benchmarks along the line Aalbeek-Hoensbroek-Schinveld are shown with respect to the height of the benchmark at 1974.0. Data of the same epoch are connected by lines; the epoch is shown in the legend

3.2 Continuous GNSS data analysis

The objective for processing data from Continuous Operating GNSS Stations (CORS) is to obtain:

1. Time series of ground movement from existing CORS stations in the area of interest,
2. Time series of existing CORS in the wider area (inside and outside area of interest) that can be used to tie ground movement from InSAR to the reference frame provided by GNSS,
3. Insight into the use of GNSS CORS stations for the monitoring ground movement in the mining area, e.g. the expected accuracy and processing methods (technical); feasibility and cost (economics); number trade-off and location of stations (advise).

Fig. A 4 shows the location of existing GNSS CORS stations in the wider area. Only two stations are in the area of interest: Kerkrade (KERK) in the East and Maasmechelen (MAME) in Belgium just over the border. Tab. A 1 gives an overview of the stations with the date that observations were started. The oldest data is from 1997, for station EIJS, but most stations only started observations in the period 2003-2005. Several stations, such as Roermond (ROER/ROE2), Aachen (0591/2591), and Selfkant (0604/2604/2625) were re-located once or twice. Maasmechelen was discontinued in 2014 and not replaced. Other stations had equipment changes during their lifetime.

The GNSS processing consists of the following steps:

1. Data collection, screening and preparation
   - Collect RINEX observables on the TU Delft GNSS Local Data Center (gnss1.tudelft.nl/dpga/)
   - Screen the RINEX headers and produce tables with meta data; check with station log files; and if necessary, correct the headers.
   - Compute tables with ocean tide loading parameters for the GNSS stations (holt.oso.chalmers.se/loading/).
   - Preparation of robot antenna calibrations (Geo++).
2. Processing on the TU Delft GRS high performance cluster (hpc03.tudelft.nl)
   - Precise Point Positioning (PPP) using GIPSY/OASIS 6.3 GNSS software from JPL (Jet Propulsion Laboratory, Pasadena, USA)
   - Latest models and orbits/clocks from 2nd IGS reprocessing
   - In–house developed parallel processing scripts
   - Processing 10-18 years of data
3. Time Series analysis
   - In-house developed Matlab software (runs on workstations & PC)
   - Transformation from IGS08 to ETRF2000 reference frame
   - Decomposition into individual components: tectonic, secular trend, temperature influence, atmospheric loading, harmonics, jumps, noise
   - Analysis of the horizontal and vertical components
   - Computation of time series in the line of sight for radar satellites

The settings used for the GIPSY/OASIS (version 6.3) processing are given in Tab. A 4.

Tab. A 4: Main settings for the GIPSY/OASIS (v6.3) Precise Point Positioning (PPP)

Pre-processing	Carrier Phase decimated to 5 minutes; Pseudorange carrier aided smoothing to 5 minutes; Cycle slip detection
Basic Observable	Undifferenced ionosphere-free carrier phase (LC) and pseudorange (PC); Elevation cut-off 7 degrees; Weighting Sigma^2=1/sin(e); Data weight LC 1 cm, PC 1 m.
Main processing mode	Precise Point Positioning with ambiguity resolution (PPP)
Satellite orbits and clocks	Reprocessed GPS orbits/clocks (JPL final orbits) in the IGS08 reference frame
Adjustment	Stochastic Kalman filter/smoother implemented as square root information filter with smoother.
Estimated parameters	Station position, receiver clock, troposphere delay and gradients, phase ambiguities.
Station position	Estimate of daily station marker coordinates; dN, dE, dU eccentricities from RINEX file applied.
Receiver clock	Estimate every 5 minutes
Troposphere	A priori Wet and Dry delay from GPT2 model (Boehm et al, 2007); Mapping Function GPT2 model; Zenith delay and horizontal gradients estimated; Zenith delay random walk 5.0d-8 km/sqrt(sec); Horizontal delay gradients random walk 5.0e-9 km/sqrt(sec)
Ionosphere	1st order effect removed by LC and PC combinations; 2nd order effect modelled
Ambiguities	Resolved to integers (where possible)
Antenna calibration	PCV model from igs08_wwww.atx applied
Tidal loading	Solid earth and pole tide IERS 2010 Conventions; Permanent tide NOT removed from model, so NOT in estimated site coordinates; Ocean Tide Loading GOT4.8ac model with respect to instantaneous centre of mass; Ocean Pole Tide Loading Applied
Non tidal loading	Not applied (thus in coordinates)

The main outputs of the GIPSY/OASIS processing (step) are time series with daily station positions in latitude, longitude, and ellipsoidal height in the IGS08 reference frame. The IGS08 reference frame is based on ITRF2008 reference frame. The latitude, longitude, and height have been converted into North, East, and Up components with respect to an average position, whereby a correction has been applied for the known velocity of the Eurasian plate in the ITRF2008 reference frame. The correction is done in such a way that the resulting North, East and Up components are with respected to the ETRF2000 reference frame.

The resulting time series contain a couple of effects

1. Long-term surface movement.
2. Monument movement as result of the environmental conditions, residual Earth tides and ocean loading, atmospheric loading, groundwater effects, etc., Tidal loading effects have been modelled in GISPY/OASIS, but small residual effect may remain. Atmospheric loading has not been modelled in GIPSY/OASIS and remain in the time series, as well as groundwater effects, and other motions of the monument, for instance, under the influence of temperature changes.
3. Apparent motions, but no real motions, as the result of for instance unmodelled elevation and azimuth dependent antenna phase delays (can only be partly covered by antenna calibration), site multipath, and unmodelled atmosphere effects. The GPS processing, which include the estimation of rather correlated receiver clock, troposphere zenith delay, and height parameters, is very sensitive to elevation dependent effects in the observations and models used by the processing. As result of the repeating GPS satellite constellation these effects can result into several harmonic effects in the time series.

4. Common mode signals. These are effects that are (more or less) the same for all stations, which can be due to the used reference frame, common atmosphere effects, or errors in the used satellite orbits and clocks.
5. Jumps due to equipment changes.
6. Measurement noise.

To separate these effects a decomposition of the GPS time series is made. Each component of the time series, $\Delta N, \Delta E, \Delta U$ (North, East, Up), can be described by the following model

$$\Delta = s(t) + \Delta_{AtmLd}(P-P_0) + \Delta_{TempI}(T-T_0) + \Sigma(a_{si}\cdot\sin 2\pi\cdot f_i\cdot t + a_{ci}\cdot\cos 2\pi\cdot f_i\cdot t) + \Delta''_{CM} + \Sigma\Gamma_T + \varepsilon \quad (2)$$

with s(t) the *trend*, Δ_{AtmLd} an *atmospheric loading* coefficient and Δ_{TempI} a *temperature influence* coefficient, a_{si} and a_{ci} *harmonic* coefficients, Δ''_{CM} a common mode signal that is the same for all stations, $\Sigma\Gamma_T$ the cumulative effect of jumps (with $\Gamma_T(t < T) = 0$), $\Gamma_T(t < T) = 0$ and ε the residual *noise*, t time in decimal years and f_i frequency in cycles/year.

The trend model s(t) can be a linear trend, higher order polynomial or spline function. In this project a spline function is used. The spline consists of *piecewise polynomials* of order three with continuity in the first derivative (velocity) at the *breakpoints*. The length of each piecewise polynomial is about one year.

For each coordinate component an atmospheric loading coefficient and a coefficient for station deformation under influence of temperature are estimated, using observed atmospheric pressure P and temperature T from the KNMI meteo station in Maastricht. The harmonic terms that are estimated have periods of 1 cycle/year (annual), 0,95 cycle/year (GPS draconitic period), and 2 cycles/year (semi-annual) and 14,2 days/year (lunar). The 0,95 cycles/year period is very close to the GPS draconitic year of 351 days and period of 350 days that the

satellite constellation repeats. These periods are very common periods in GPS time series, but often not related to real motion. For each station several plots are made

- Plot with raw time series, corrected for jumps, with the total fit, estimated trend, and trend plus atmospheric loading
- Plot with the estimated components (Temperature effect, harmonics, atmospheric loading)
- Plot with the residuals

All plots include information on the reliability intervals (95 %) from the estimated standard deviations and identify the equipment changes. An example for the GPS station in EIJSden is shown in Fig. A 34, Fig. A 35, and Fig. A 36.

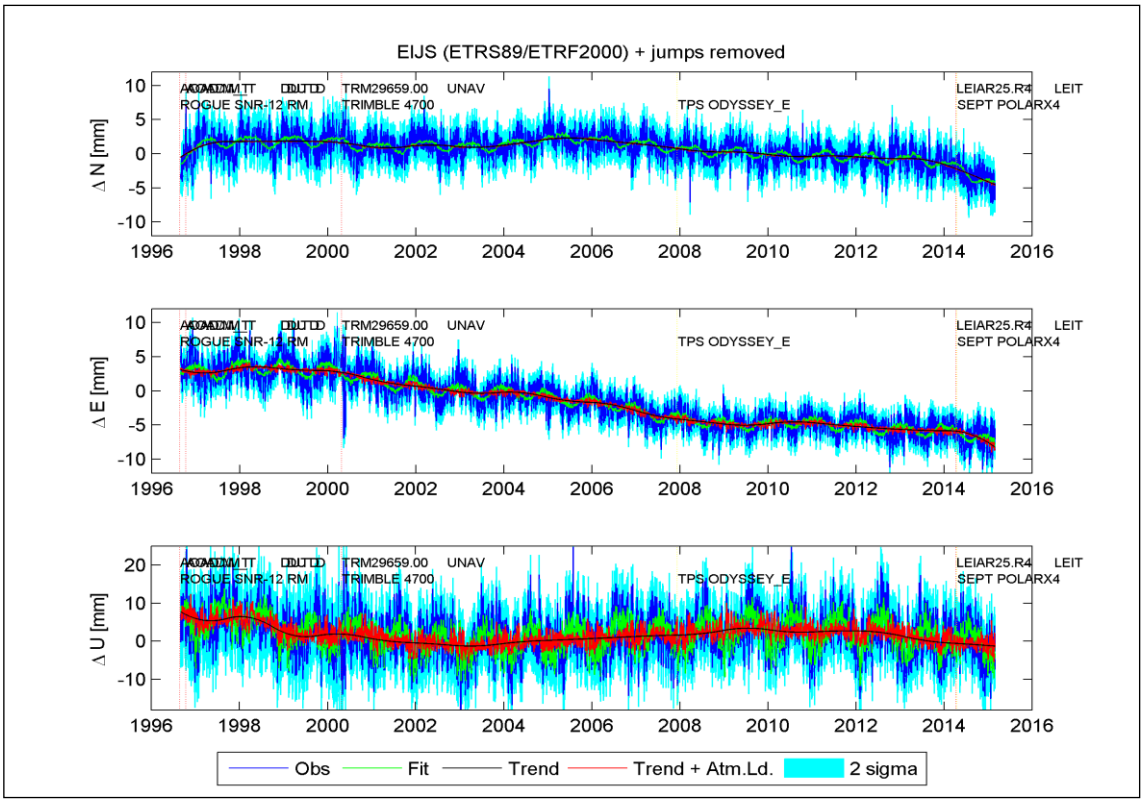

Fig. A 34: GPS Time Series for EIJSden in the ETRS89/ETRF200 reference frame, with jumps due to equipment changes removed, and showing the fitted trends

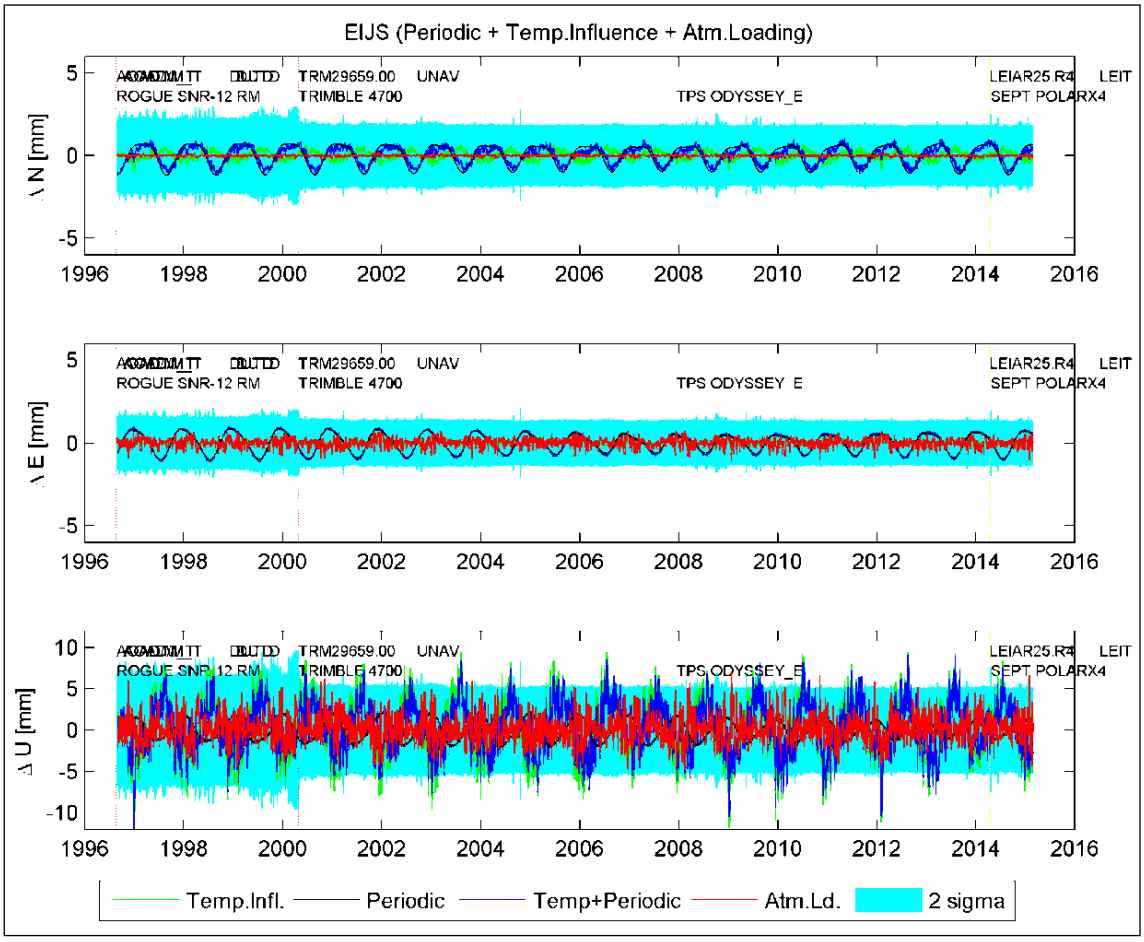

Fig. A 35: Periodic effects, temperature influence and atmospheric loading in the EIJSden time series

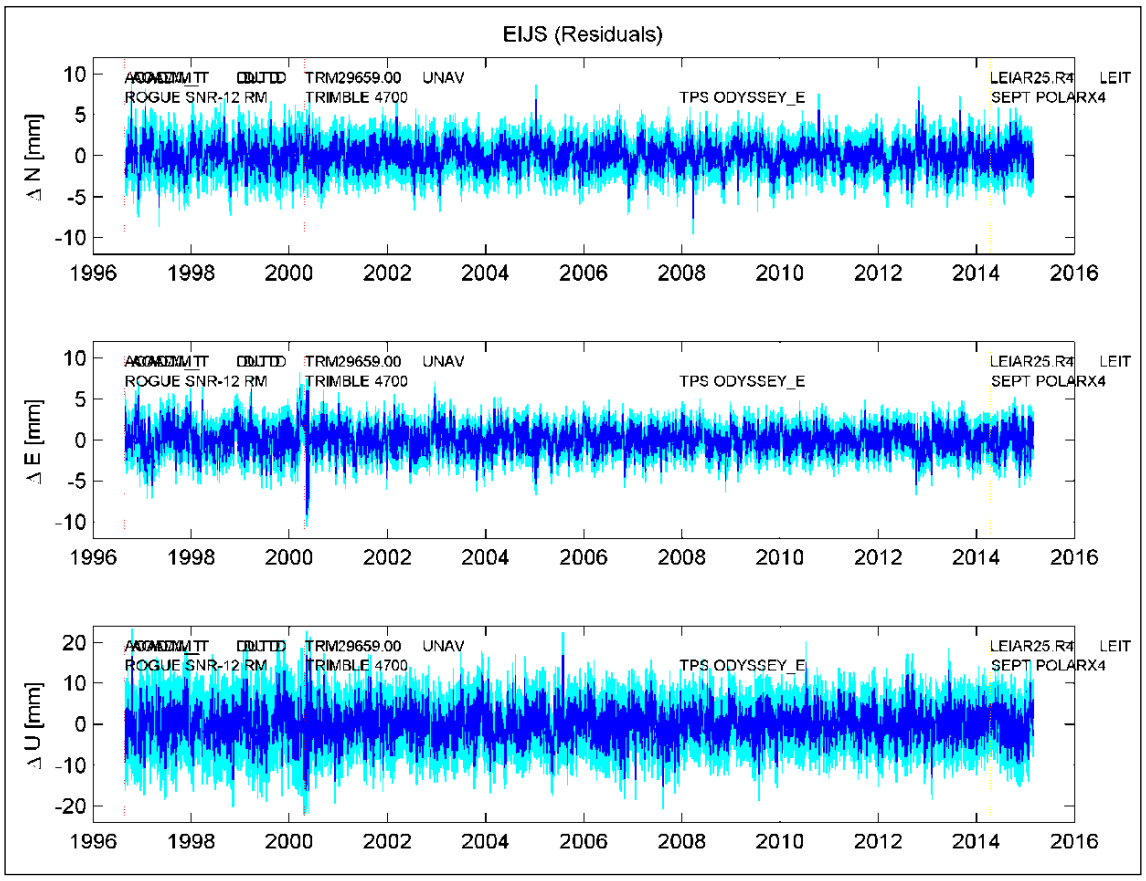

Fig. A 36: Residuals in the EIJSden time series after fitting the model

Another useful way to present the results is to plot all station together in a single plot, off-setting each time series by a certain amount on the y-axis. Examples for the vertical component are shown in Fig. A 37, Fig. A 38, and Fig. A 39.

The final fitted trends for all three components, North, East, and Vertical, are shown in Fig. A 40 to Fig. A 42, including the effect of atmospheric loading. The estimated atmospheric loading is only significant in the vertical component, Fig. A 42. Fig. A 43 shows the vertical component without the loading effect. Since the atmospheric loading is more or less the same for all station in the area, Fig. A 43, the vertical without atmospheric loading, is the final result in the vertical.

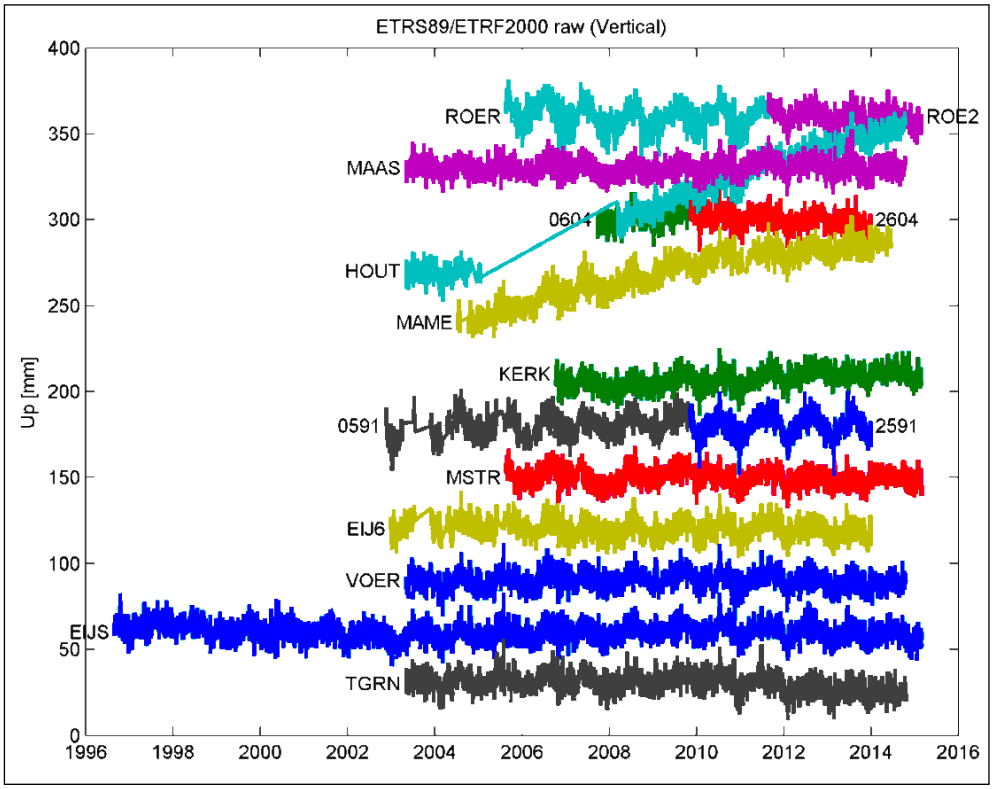

Fig. A 37: Raw height time series, with jumps removed, for all stations

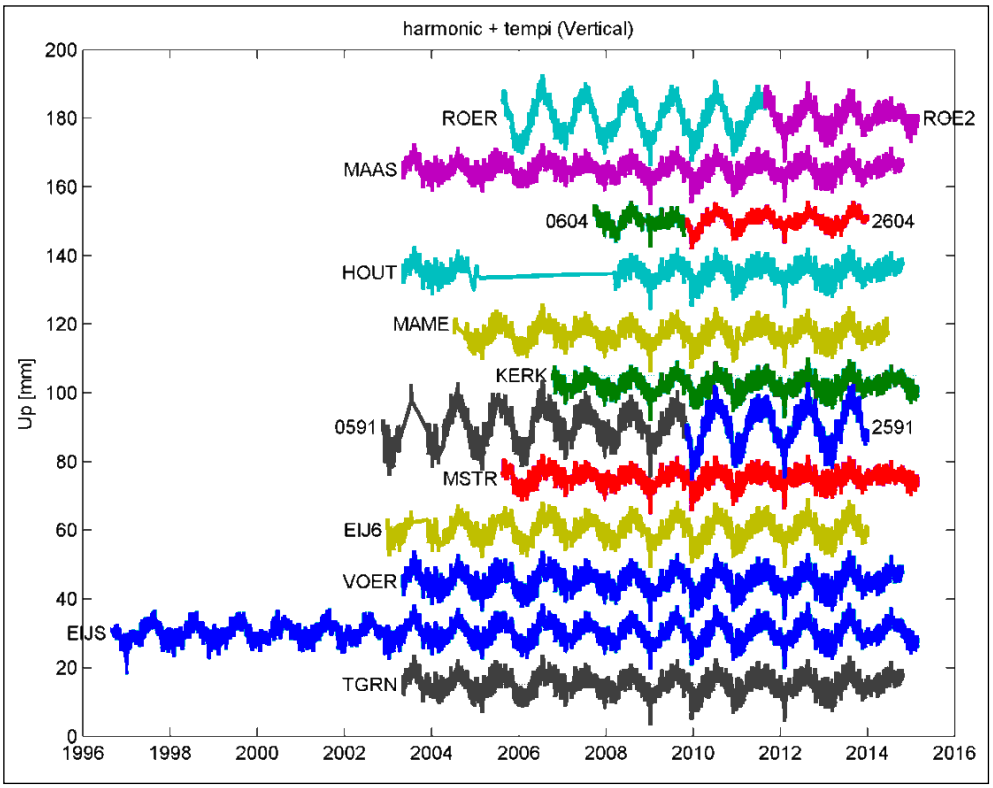

Fig. A 38: Harmonic components and temperature influence in the height component

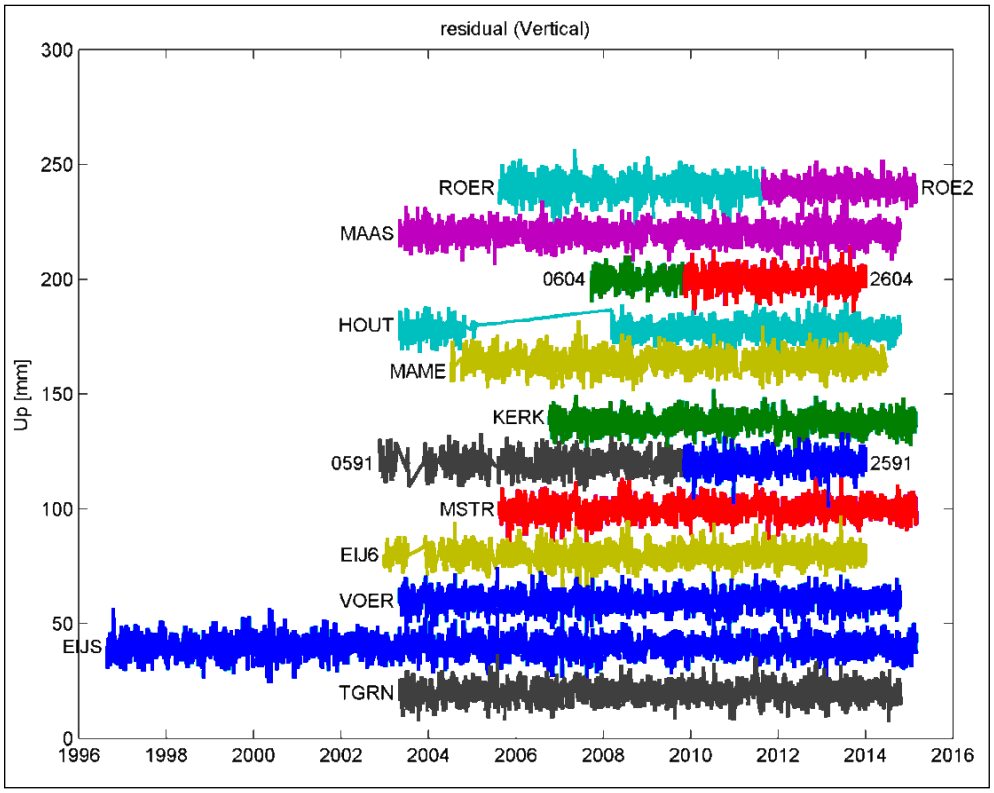

Fig. A 39: Residuals in the height component

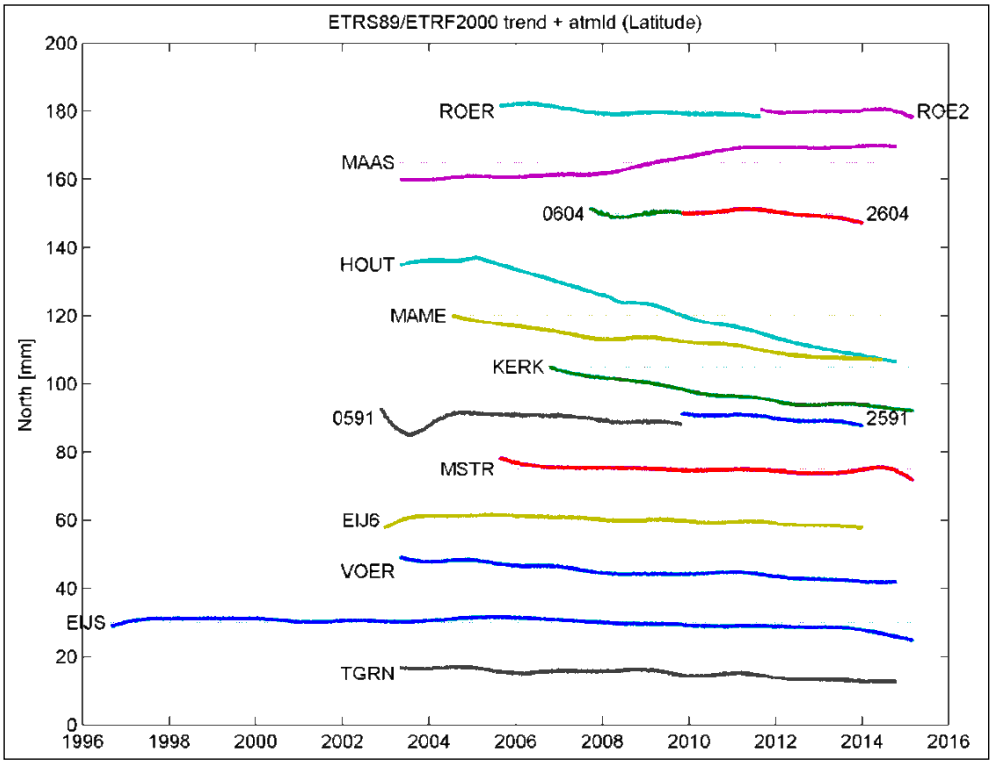

Fig. A 40: Estimated trend (with atmospheric loading) for the North (latitude) component

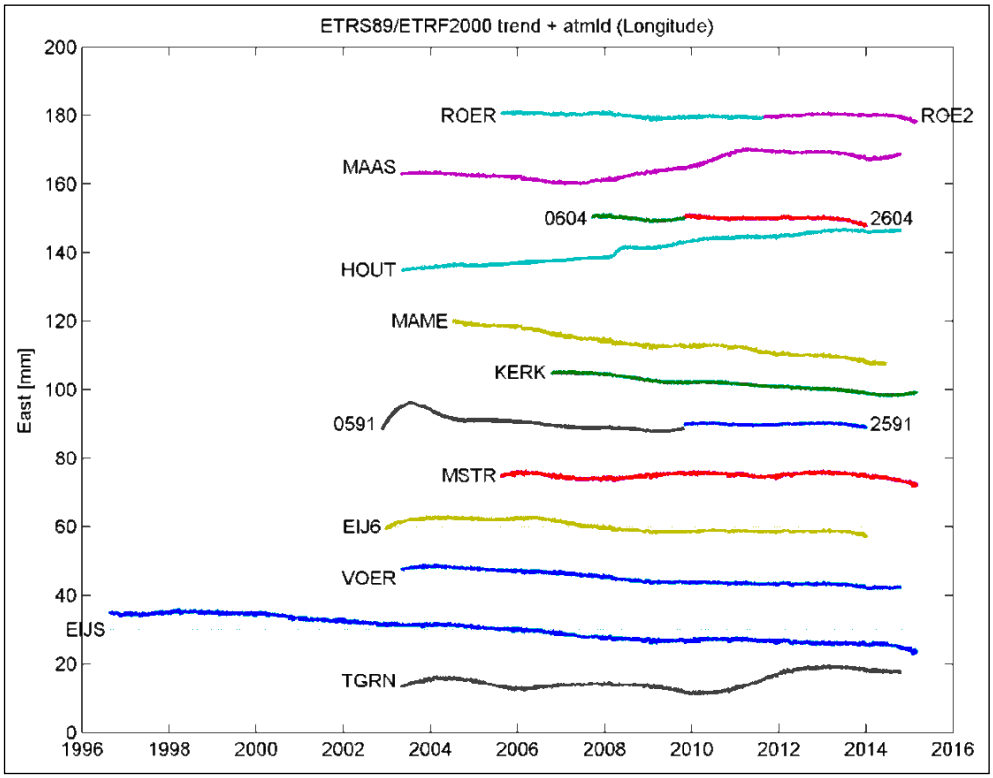

Fig. A 41: Estimated trend (with atmospheric loading) for the East (longitude) component

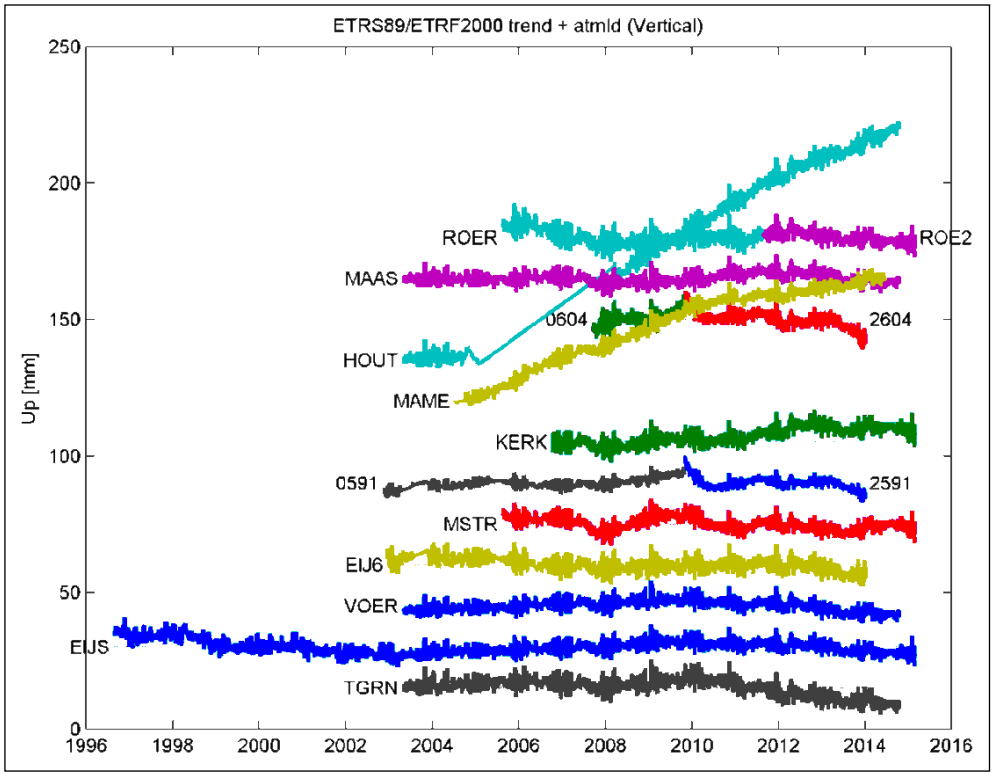

Fig. A 42: Estimated trend, with atmospheric loading, for the Vertical (Up) component

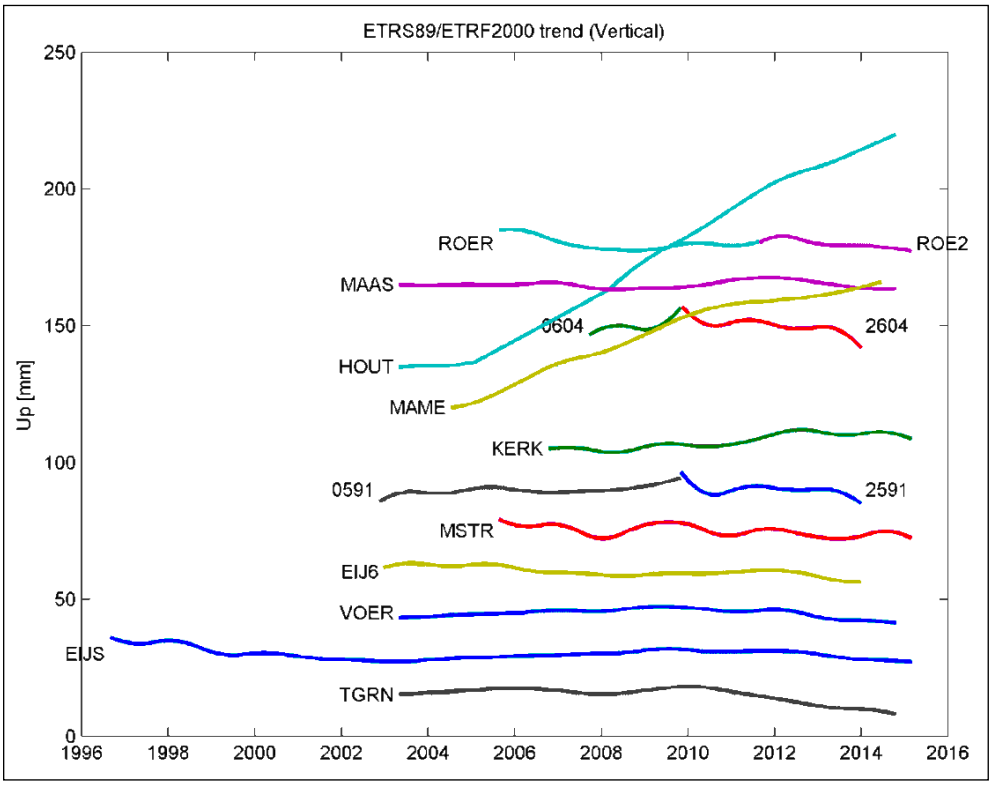

Fig. A 43: Estimated trend, without atmospheric loading, for the vertical (Up) component

Tab. A 5 gives the estimated parameters and estimated standard deviations. Three different types of standard deviations for the daily positions have been computed:

1. The mean standard deviation as given by Gipsy (StdF)
2. Empirically determined standard deviation (StdE), computed from the differences between successive days std(diff(neu))./sqrt(2)
3. The standard deviation of the residuals after the least-squares fit (StdR).

The estimated horizontal precision is better than 2 mm/day; the vertical precision is about 3-4 mm/day.

Tab. A 5: Estimated parameters from the GPS processing

		Vel1 mm/y	Vel2 mm/y	AtmLd mm/kPa	TempI mm/daK	365d mm	347d mm	183d mm	14d mm	StdF mm	StdE mm	StdR mm
EIJS	Lat	16.02	-0.67	0.06	0.39	0.84	0.10	0.24	0.02	0.95	1.04	1.40
EIJS	Lon	18.51	-0.33	0.27	-0.08	0.70	0.19	0.16	0.05	0.69	1.03	1.42
EIJS	Rad	0.86	0.53	-1.76	5.21	1.47	0.47	0.31	0.15	2.73	3.10	3.81
KERK	Lat	16.00	-0.08	-0.08	0.04	0.10	0.55	0.18	0.04	0.91	1.01	1.46
KERK	Lon	18.55	-1.30	0.10	-0.88	1.17	0.13	0.21	0.04	0.66	0.89	1.23
KERK	Rad	0.87	2.57	-1.99	5.31	2.34	0.32	0.28	0.15	2.56	2.67	3.47
MSTR	Lat	16.02	-0.11	0.07	0.55	0.52	0.34	0.14	0.00	0.91	1.04	1.39
MSTR	Lon	18.49	0.18	0.26	0.19	1.67	0.22	0.32	0.05	0.66	0.98	1.45
MSTR	Rad	0.87	-3.83	-1.80	5.31	2.71	0.60	0.28	0.06	2.57	2.81	3.68
ROER	Lat	15.99	0.46	0.07	-0.19	0.12	0.71	0.10	0.02	0.91	1.01	1.34
ROER	Lon	18.45	-0.92	0.22	0.03	0.76	0.10	0.25	0.07	0.66	0.89	1.32
ROER	Rad	0.87	1.01	-2.43	5.21	2.18	1.01	0.54	0.26	2.56	3.41	4.30
ROE2	Lat	15.99	0.30	-0.10	-1.46	0.53	0.38	0.74	0.01	0.91	1.00	1.20
ROE2	Lon	18.46	0.11	0.15	0.11	1.26	0.89	0.41	0.03	0.66	0.90	1.18
ROE2	Rad	0.87	-2.50	-1.93	5.85	5.57	4.18	0.89	0.17	2.55	2.64	3.31
EIJ6	Lat	16.02	0.89	-0.08	1.60	0.62	0.49	0.36	0.02	0.91	0.98	1.33
EIJ6	Lon	18.51	-0.95	0.21	-0.15	0.62	0.23	0.14	0.06	0.66	0.87	1.24
EIJ6	Rad	0.86	1.44	-2.15	5.50	2.26	0.73	0.15	0.15	2.60	2.78	3.57
0591	Lat	16.00	-0.44	0.20	-1.28	0.98	0.18	0.43	0.03	0.92	1.04	1.48
0591	Lon	18.59	-1.38	0.05	0.35	2.13	0.36	0.23	0.06	0.67	0.98	1.62
0591	Rad	0.86	0.25	-1.20	7.27	2.71	1.75	0.35	0.19	2.60	2.89	3.80
2591	Lat	16.00	-2.06	0.12	-1.86	0.27	1.16	0.49	0.06	0.89	1.07	1.42
2591	Lon	18.59	0.61	0.11	0.69	2.65	0.39	0.63	0.06	0.65	0.94	1.51
2591	Rad	0.86	-2.51	-1.32	6.11	5.23	3.73	0.83	0.25	2.49	2.89	3.83
0604	Lat	16.00	2.02	0.22	-1.04	0.48	1.60	0.46	0.07	0.90	0.83	1.16
0604	Lon	18.49	-1.02	0.18	1.24	1.91	0.76	0.51	0.12	0.66	0.83	1.17
0604	Rad	0.87	-0.02	-2.19	4.89	9.64	7.18	0.81	0.38	2.56	2.58	3.25
2604	Lat	16.00	-1.93	0.06	-1.00	0.95	0.68	0.43	0.09	0.90	0.95	1.30
2604	Lon	18.49	0.21	0.20	0.50	1.47	0.79	0.45	0.00	0.65	0.86	1.22
2604	Rad	0.87	-4.90	-1.83	3.43	2.46	2.60	0.51	0.25	2.52	3.02	3.75
HOUT	Lat	16.04	-3.94	-0.01	0.30	0.66	0.28	0.40	0.03	0.91	0.93	1.24
HOUT	Lon	18.38	2.05	0.16	-0.48	0.86	0.26	0.28	0.05	0.66	0.85	1.21
HOUT	Rad	0.87	8.93	-2.07	5.77	2.73	0.39	0.16	0.17	2.56	2.80	3.47
MAAS	Lat	16.01	2.85	0.04	-1.27	0.40	0.38	0.22	0.02	0.91	0.89	1.34
MAAS	Lon	18.43	2.07	0.21	-1.21	0.96	0.24	0.10	0.05	0.67	0.88	1.48
MAAS	Rad	0.87	0.65	-1.88	5.41	2.28	0.41	0.31	0.18	2.58	2.79	3.60
MAME	Lat	16.02	-1.12	0.05	-0.55	0.96	0.29	0.22	0.03	0.92	0.91	1.40
MAME	Lon	18.46	0.19	0.28	0.22	0.12	0.30	0.05	0.07	0.66	0.86	1.31
MAME	Rad	0.87	5.87	-1.60	5.47	1.64	0.19	0.27	0.18	2.58	2.93	3.80
TGRN	Lat	16.04	-0.63	0.07	-1.31	0.98	0.26	0.41	0.01	0.95	0.93	1.32
TGRN	Lon	18.47	-1.32	0.21	0.41	0.84	0.27	0.16	0.03	0.70	0.87	1.33
TGRN	Rad	0.86	1.80	-2.14	5.90	2.26	0.14	0.03	0.22	2.77	2.80	3.60
VOER	Lat	16.02	0.02	0.07	-0.47	0.44	0.25	0.28	0.04	0.91	0.92	1.26
VOER	Lon	18.52	-0.81	0.21	0.33	1.10	0.19	0.11	0.05	0.67	0.87	1.24
VOER	Rad	0.86	1.01	-1.78	6.13	2.65	0.39	0.28	0.17	2.58	2.79	3.59

Adding a term for the temperature effect gives a significant improvement in the fit, but the underlying causes need to be further investigated. It could be local effects, in particular for the height; also a regional common mode effect in the vertical can be observed.

The annual harmonics term and temperature coefficient are both well estimable. Sometimes both terms amplify each other, in other cases it is the opposite.

Atmospheric loading has been estimated for the horizontal terms, but it is very small as expected, as can be seen from Tab. A 5. For the vertical component the estimates of atmospheric loading agree well between stations, which is as expected because of the small region in this study.

MAME (Maasmechelen) and HOUT (Houthalen) show a clear vertical ground heave, also KERK (Kerkrade) has a small vertical ground heave.

The stations also have very noticeable horizontal movements that could be related to the rising mine water, but this has not been further investigated.

Clusters of nearby stations, like EIJS and VOER, have similar movements. This gives confidence that the time series are indeed reliable.

Only one of the GNSS stations (KERK) was located in the South Limburg mining area, and two in the Belgium area. The two Belgium stations show considerable ground heave, but unfortunately these are outside the study area and we also have no other data to provide an interpretation. KERK shows a ground heave of 2,5 mm/year, but is comparable in magnitude to the ground heave and subsidence on several GNSS stations outside the mining area. This makes it difficult to draw any conclusions on the observations GNSS alone, especially because only one of the GNSS is in the mining area, and because the stations outside the mining area do exhibit similar behaviour: the observed behaviours could also be explained by autonomous site motion (of the antenna), site related effects and/or effects due to equipment changes.

The GNSS data has been converted to radar Line-of-sight (LOS) using all three components (vertical and horizontal) and is then used to combine and adjust the ERS-1/2, ENVISAT, and RadarSAT-2 radar stacks, see chap. 3.3.

3.3 Satellite radar interferometry data analysis

The three available Persistent Scatterer Interferometry (PSI) data sets covering the full mining region, as described in chap. 2.3, are used for further analysis regarding ground heave. The ERS-1/2, ENVISAT, and RadarSAT-2 data sets cover a time span from 1992 to 2014. To improve the interpretation of the PSI results, the data is integrated with continuous GNSS and levelling measurements. Hereby, a two-step approach is applied:

1. Referencing of each PSI data set with respect to GNSS
2. Integration of PSI data sets with levelling

The procedure and results of these steps are discussed in chap. 3.3.1 and chap. 3.3.2. Based on the results, cross-profiles and contour maps are created, see chap. 3.3.3. A comparison between the PSI-based and levelling-based ground movement maps is given in chap. 3.3.4. For all PSI analysis holds that the measurements are converted to the vertical direction. Hence, any possible horizontal components in the Line-of-sight deformation vector are neglected.

3.3.1 Referencing PSI data sets with GNSS

The first step in the applied integration of the techniques is the referencing of each PSI data set with respect to the continuous GNSS measurements. This step is required since 1) each PSI data set is referenced to a unique reference Persistent Scatterer (PS), of which its own movement is unknown, and 2) a

spatial trend in the PSI estimates may occur due to inaccuracies in the orbit parameters of the satellites used. Since the GNSS measurements are processed in the same Earth-fixed reference frame, they provide a good framework to remove the unknown offset of the reference PS and potential remaining trends.

A six-step procedure is applied to integrate each PSI data set with the GNSS measurements. The integration is based on the linear velocity rates of both the PSI and GNSS data. Hence, the PSI time series are adapted with an offset and spatial trend in the linear deformation velocity. The six steps applied are:

1. Conversion of the GNSS time series of the various stations (see chap. 2.2) in East, North, Up components to the local line-of-sight (LOS) direction of the SAR satellites.
2. Estimation of a linear deformation velocity [mm/y] for each GNSS station.
3. Selection of PS within a radius of 400 m around each GNSS station.
4. Prediction of a PSI linear velocity based on the selected PS by Kriging.
5. Estimation of a trend and offset based on the difference between the measured GNSS velocities and the predicted PSI velocities.
6. Adaption of the PSI time series and linear deformation rates.

The procedures and results of each of these steps are described below.

1. Conversion of GNSS time series

Since PSI analyses (from a single ascending or descending orbit track) only provide measurements in the radar line-of-sight (LOS), whereas for GNSS time series in local East, North, Up components are available, as discussed in chap. 3.2, the integration of PSI and GNSS is performed in the radar LOS. Hence, the three GNSS time series components are transformed into a single radar LOS time series for each GNSS station. For each station, the local radar incidence angle and SAR satellite heading are used. Unfortunately, not sufficient

GNSS stations were operational during the ERS-1/2 acquisition period (1992 - 2000). Therefore, only time series for the ENVISAT and RadarSAT-2 periods are available, see Fig. A 44 and Fig. A 45. To estimate the trend and offset of the ERS-1/2 data set, the assumption is made that the GNSS measurements obtained during the ENVISAT period are also representative for the ERS-1/2 period.

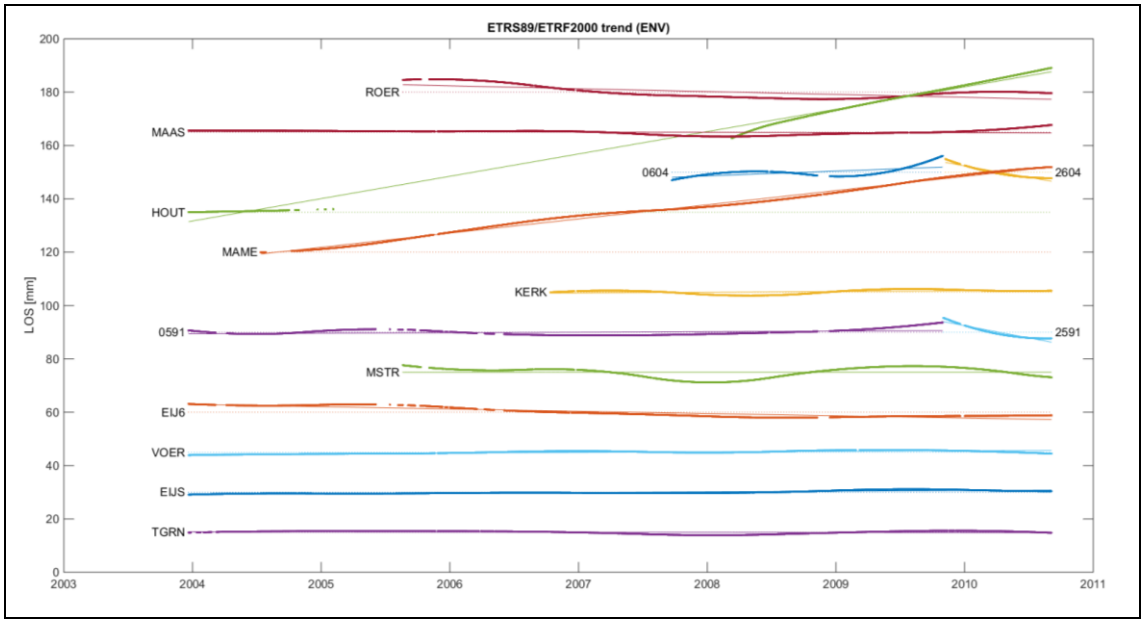

Fig. A 44: GNSS time series of various stations in the radar line-of-sight direction during the ENVISAT acquisition period (2003 - 2010). To increase the visibility, each time series was given an offset. Hence, the Y-axis should not be interpreted in absolute sense

2. Estimate of linear GNSS velocity

For each GNSS station, a linear deformation rate is estimated from the LOS GNSS time series using a least-squares inversion. Hereby, deformation rates in mm/y are obtained, which are directly comparable with the PSI velocity estimates. However, there are no PS at the exact GNSS station locations. This would be different if a collocated GNSS and Coherent Active Transponder (CAT) setup would have been available (MAHAPATRA, 2013). Since this is not

the case, a spatial prediction of the PSI deformation rate at the GNSS station locations is required.

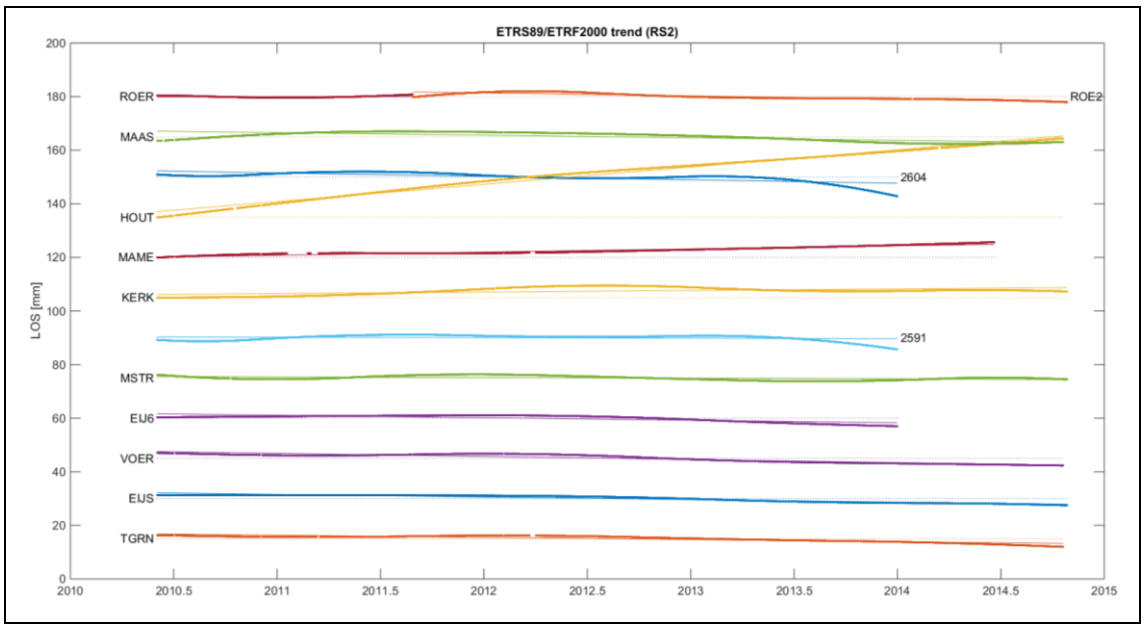

Fig. A 45: GNSS time series of various stations in the radar line-of-sight direction during the RadarSAT-2 acquisition period (2010 - 2014). To increase the visibility, each time series was given an offset. Hence, the Y-axis should not be interpreted in absolute sense

3. Selection of PS

To predict the PSI deformation rate at the GNSS station location, surrounding PS are selected. Ideally, PS located at the same building as the GNSS antenna should be used, since they are sensitive to the same movement, such as settlement of the building and seasonal thermal expansion. To enable a prediction, a minimal number of 3 PS on the building is set. In many cases, these PS are not available. As the alternative, a spatial prediction based on a larger area is applied. Here, PS within a 400 m range around the station are selected. As a result, the number of selected PS is strongly dependent on the level of urbanisation in the area around the stations.

Examples of this approach are given in Fig. A 46 and Fig. A 47. For the station Kerkrade, minimal 4 PS are available for the ENVISAT and RadarSAT-2 data sets. However, the building did not exist yet at the time of the ERS-1/2 acquisitions. Therefore, for this data set the PS within the 400 m radius are taken. The same has been done for the station in Maastricht, see Fig. A 47. Also here, the buildings around the station appear to be rather new, since no PS are detected in the area in the 1992-2000 period.

Application of the approach to all stations resulted in only 4 cases where sufficient PS on the same building are available. Hence, in all other cases a 400 m radial selection was applied, resulting in a minimum number of 20 selected PS (up to a maximum of 480 PS).

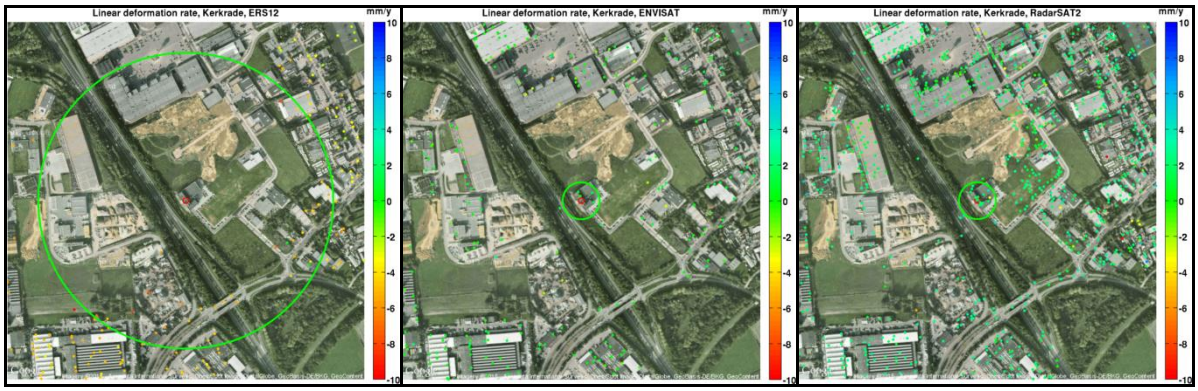

Fig. A 46: Selection of PS around the GNSS station Kerkrade (KERK). Left) ERS-1/2 data set, middle) ENVISAT data set, right) RadarSAT-2 data set. For the ENVISAT and RadarSAT-2 data sets, PS on the same building as the GNSS antenna are selected, for the ERS-1/2 data set surrounding PS within a 400 m radius are used, since the building did not exist during this time frame

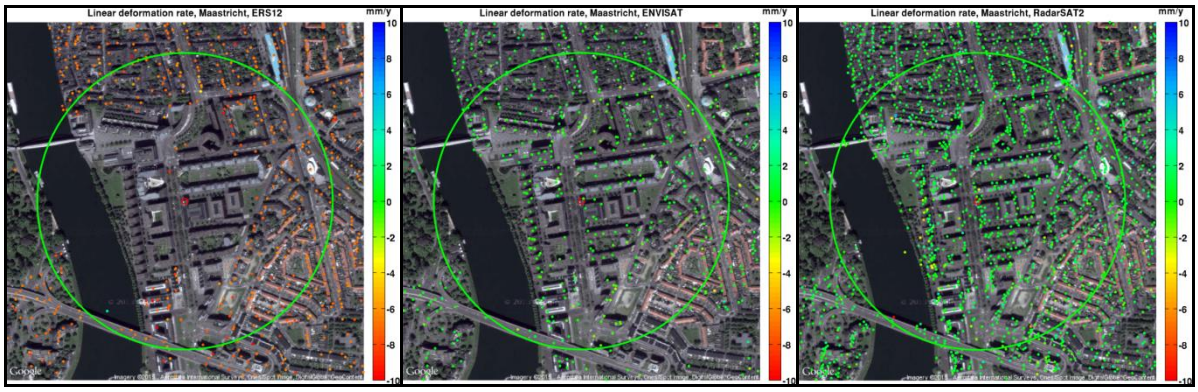

Fig. A 47: Selection of PS within a 400 m radius of the GNSS station Maastricht (MSTR). Left) ERS-1/2 data set, middle) ENVISAT data set, right) RadarSAT-2 data set. Note that the buildings around the GNSS station appear to be relatively new, since no PS are detected within this area in the ERS-1/2 (1992-2000) data set

4. Prediction of PSI velocity

The PSI deformation rates at the GNSS station locations are predicted based on the selected PS using Kriging. For each PSI data set a Gaussian variogram with a nugget is estimated to model the spatial correlation. Because the number of PS in the surrounding of the GNSS stations varies strongly (between 20 and 480 PS), the reliability of the estimated variogram per location varies as well. Since spatial variation of the deformation signal is assumed to be rather smooth, the choice is made to use the variogram obtained based on the data around the Maastricht station for all stations.

The result of the predictions is shown in Fig. A 48. Here, the original PS deformation rates (small dots), the predicted PSI deformation rates for the stations (circles), and the GNSS deformation rates (big dots) are given. The differences between the PSI predictions and GNSS estimates are clearer in Fig. A 49, where the offsets are shown. It is clear that there is a relatively strong offset between the ERS-1/2 data set and the GNSS results. Hence, the ERS-1/2 reference PS experiences a strong motion.

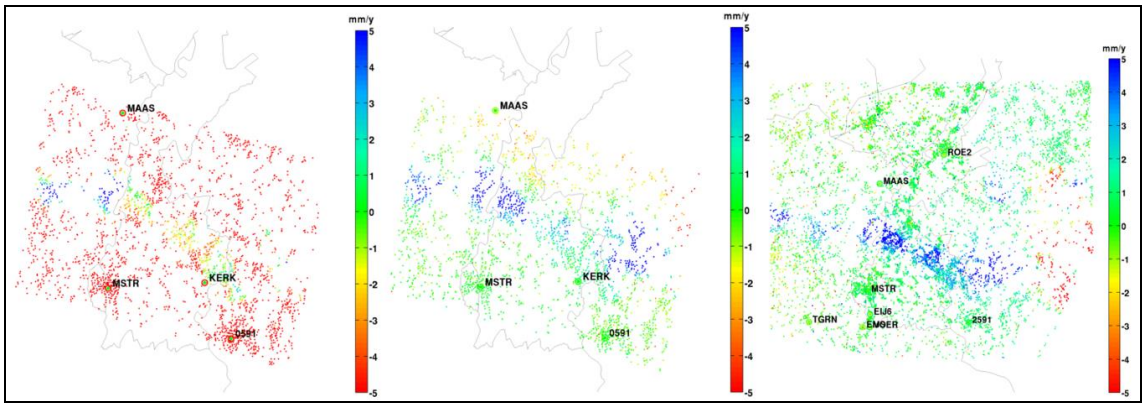

Fig. A 48: Predicted PSI velocities at the GNSS station locations (circles), together with the GNSS estimates (big dots) and the original PS (small dots). Left) ERS-1/2 data set, middle) ENVISAT data set, right) RadarSAT-2 data set

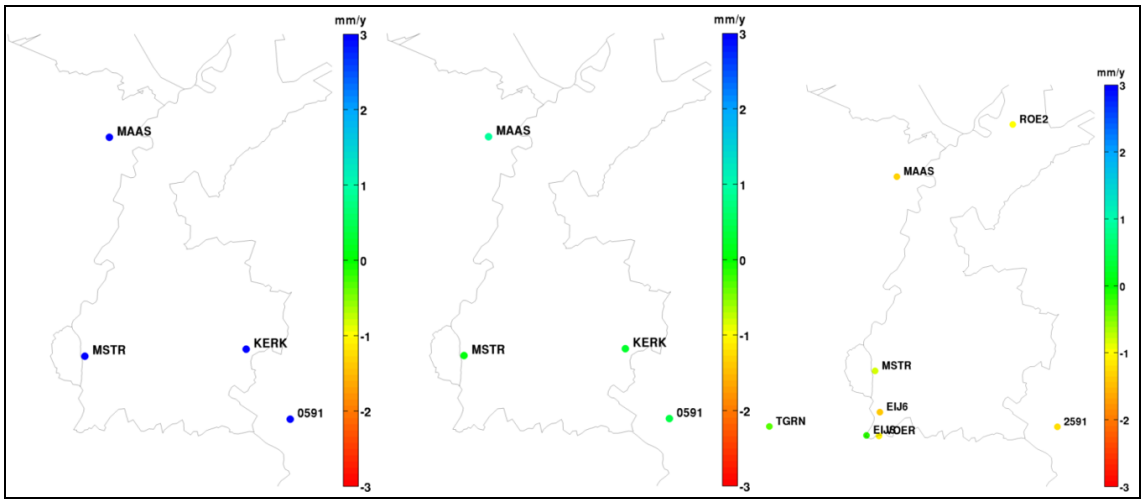

Fig. A 49: Differences between predicted PSI velocities and the GNSS estimates at the GNSS station locations. Left) ERS-1/2 data set, middle) ENVISAT data set, right) RadarSAT-2 data set

5. Estimation of trend and offset

The differences between the GNSS velocity estimates and the PSI predictions at the GNSS station locations are used to estimate a spatial trend and offset for each PSI data set. An iterative outlier detection and removal scheme is applied based on the Delft school of geodetic parameter estimation and testing. Hereby, an a-priori standard deviation of the velocity differences of 0,5 mm/y and a level of significance α of 0,05 is assumed. Minimally, 4 stations should remain; otherwise the testing scheme is aborted. For the ERS-1/2 and ENVISAT data sets, all tests are accepted within the first iteration. The residuals in the differences between PSI predictions and GNSS estimates are shown in Fig. A 50. As can be seen, the residuals are well below 0,5 mm/y.

In case of the RadarSAT-2 data set, more GNSS stations are available, see Fig. A 51. By applying the testing scheme, two stations are removed (EIJ6 and EIJS). After the third iteration, all residuals are well below 0,5 mm/y.

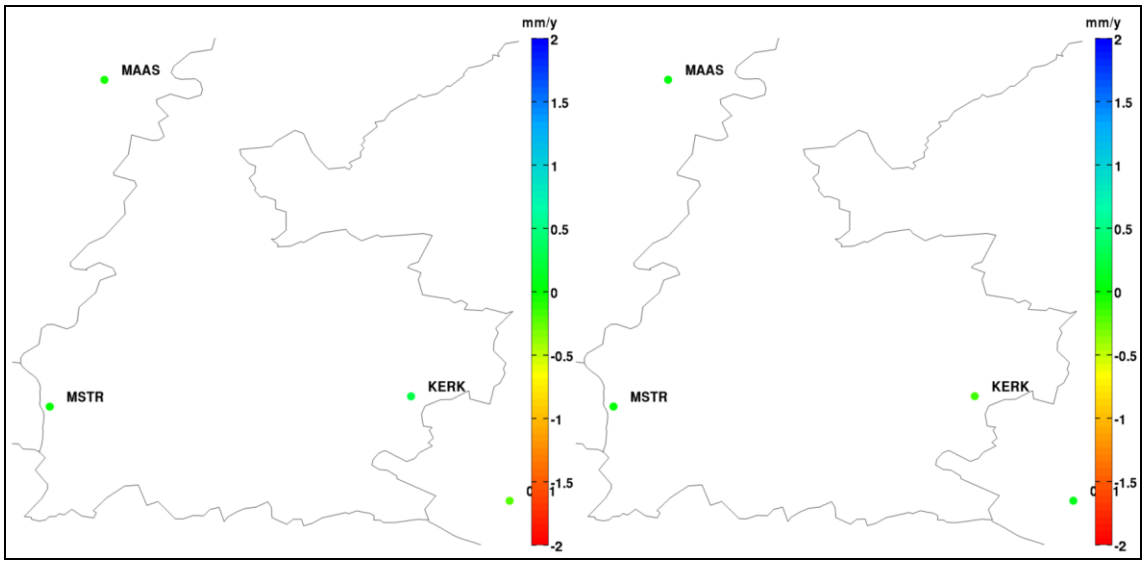

Fig. A 50: Residuals between the PSI-GNSS differences and the estimated trend + offset. Left) ERS-1/2 data set, right) ENVISAT data set

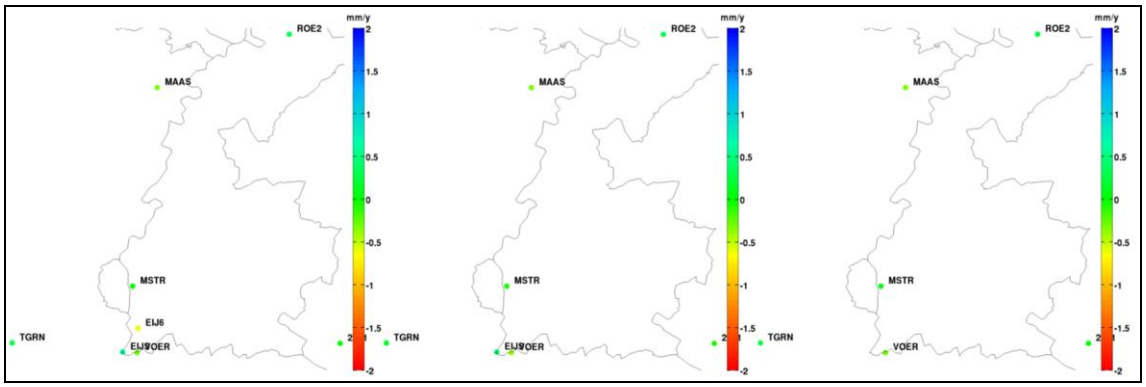

Fig. A 51: Residuals of trend + offset estimate for the RadarSAT-2 data set after 3 iterations of outlier detection (from left to right). The differences between the GNSS estimates and predicted PSI linear velocity rates for the stations EIJ6 and EIJS are too big and are removed by the outlier detection

6. Adaption of PSI time series

The estimated offsets and trends are applied to the original PSI data sets. Hereby, the PSI data sets are integrated with the GNSS measurements in the area. The results are shown in Fig. A 52.

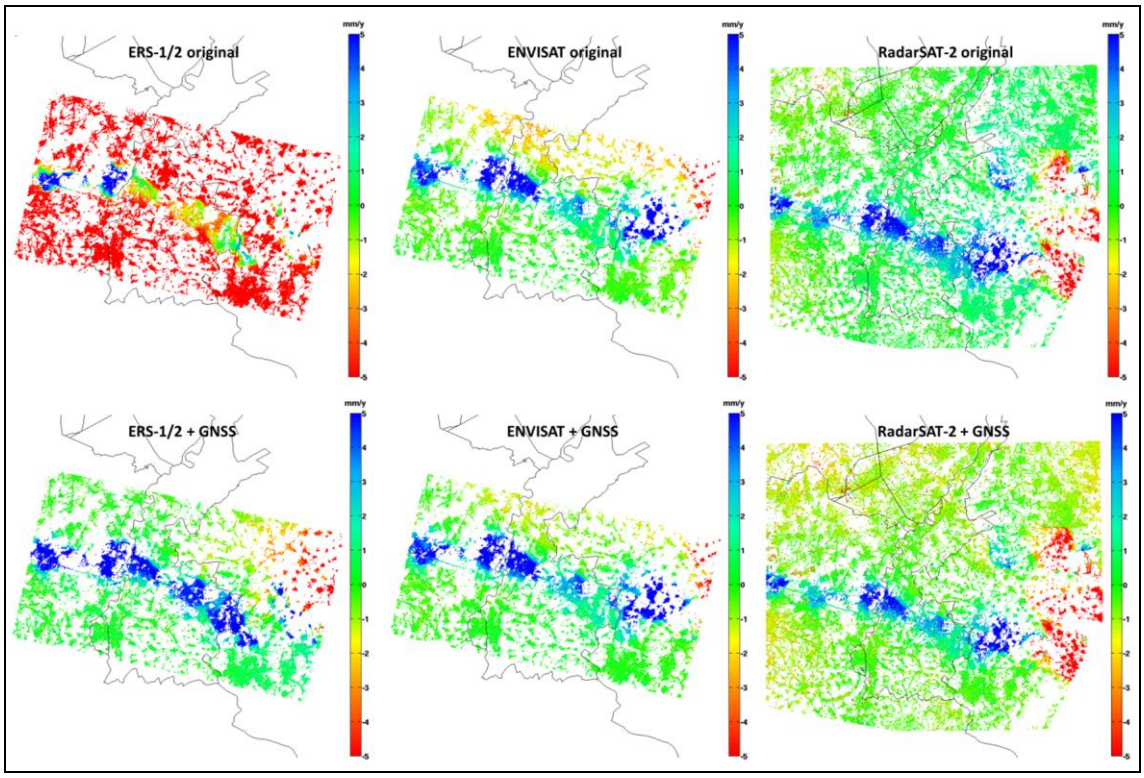

Fig. A 52: Linear deformation velocities before (top row) and after integration with GNSS measurements (bottom row)

3.3.2 Integration PSI with levelling

After the integration of the PSI data sets with GNSS measurements, the second step is the integration with the levelling measurements. Here, a three-step approach is applied:

1. Selection of levelling benchmarks.
2. Prediction of PSI time series at levelling benchmark locations.
3. Merging of the PSI and levelling time series.

The procedures applied and results obtained are described below.

1. Select levelling benchmarks

As discussed in chap. 2, levelling data from the Netherlands, Belgium, and Germany is available. For the integration of the levelling data with the PSI data sets, a first selection of benchmarks with a minimum of two levelling measurements is made. The selected benchmarks are shown in Fig. A 53.

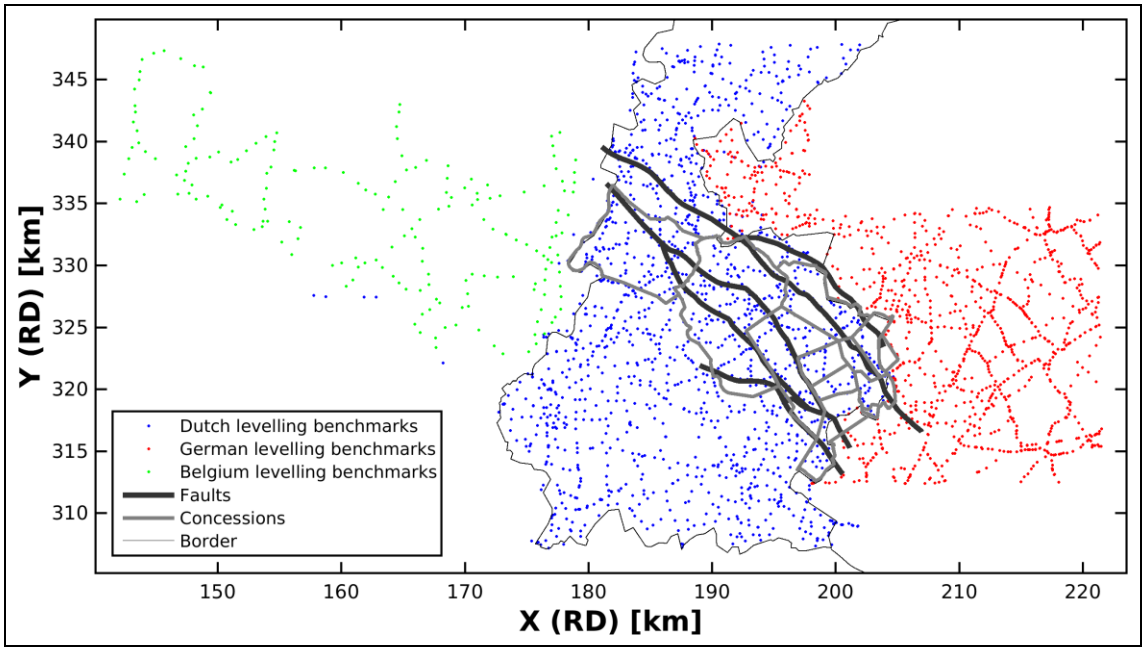

Fig. A 53: Levelling benchmarks with two or more measurements

2. Predict time series

For each benchmark, a PSI time series is predicted based on Kriging. Here, PS within a 400 m radius around the levelling benchmark are used. In case a fault is crossing the 400 m radial area, only PS on the same side of the fault as the benchmark are used for the prediction, see Fig. A 54. At this stage, the PSI time series are transformed from radar Line-Of-Sight (LOS) direction to the vertical direction, thereby neglecting any possible motion in horizontal direction. As the incidence angles of the data acquisitions used range from 26 to 34 degrees, the measurements are actually sensitive to horizontal motion as well. Because the

main signal in the area is the vertical motion due to the abandoned mining activities, the maximum horizontal motion is expected where the gradients in the ground motion signal are largest (SAMIEI-ESFAHANY et al., 2009). That is, the horizontal motion is expected to be zero at the centre of the ground motion signal, as well as outside the motion area. Because of the elongated shape of the ground heave area (see e.g., Figures A5 – A7), most horizontal motion is expected at the North and South boundaries. However, since InSAR observations are not sensitive to motion perpendicular to the orbit track of the satellite, the observations are almost insensitive for these motions. Only for gradients in East-West direction, a horizontal component in the measurements can be expected, which are neglected by assuming vertical motion only. The variogram used by the Kriging is obtained by estimating a Gaussian variogram with a nugget for 51 selected key levelling benchmarks, for each epoch of the PS time series, based on the PS within the 400 m range of the particular benchmark. Subsequently, the average per epoch of the 51 estimates is taken as the final variogram per epoch, which is applied for all benchmarks. The results are PSI based time series at each benchmark location shown in Fig. A 53.

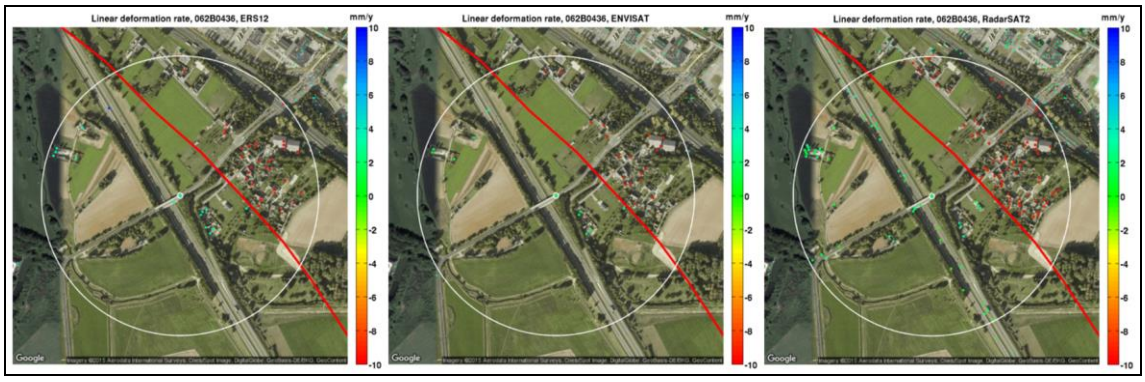

Fig. A 54: PS within a 400 m radius used for the prediction of a PSI time series at the levelling benchmark location. In case the area is crossed by a fault, only PS at the same side of the fault as the levelling benchmark are used.

3. Merge time series

At this stage, levelling time series and PSI time series for three measurement epochs (ERS-1/2 (1992-2000), ENVISAT (2003-2010), and RadarSAT-2 (2010-2014)) are available at the levelling benchmark locations. However, they all have their own reference. The levelling heights are provided in NAP, whereas each PSI time series provides relative deformation values with respect to the first epoch. Hence, each PSI time series starts at zero.

To integrate the levelling and PSI time series, a least-square 3rd-degree polynomial fit is used, according to the approach by CARO CUENCA & HANSSEN (2010), see Fig. A 55. To provide a deformation time series, instead of heights in NAP, the epoch of the last levelling campaign, that is 13.05.2012, is taken as reference time t_0. The mathematical model applied is

$$\begin{bmatrix} y_{\text{lev}} \\ y_{\text{ERS}} \\ y_{\text{ENV}} \\ y_{\text{R2}} \end{bmatrix} = \begin{bmatrix} (t_{\text{lev}}-t_0)^3 & (t_{\text{lev}}-t_0)^2 & (t_{\text{lev}}-t_0) & 1 & 0 & 0 & 0 \\ (t_{\text{ERS}}-t_0)^3 & (t_{\text{ERS}}-t_0)^2 & (t_{\text{ERS}}-t_0) & 1 & 1 & 0 & 0 \\ (t_{\text{ENV}}-t_0)^3 & (t_{\text{ENV}}-t_0)^2 & (t_{\text{ENV}}-t_0) & 1 & 1 & 1 & 0 \\ (t_{\text{R2}}-t_0)^3 & (t_{\text{R2}}-t_0)^2 & (t_{\text{R2}}-t_0) & 1 & 1 & 1 & 1 \end{bmatrix} \begin{bmatrix} a \\ b \\ c \\ d_1 \\ d_2 \\ d_3 \\ d_4 \end{bmatrix},$$

where y are vectors with the time series of the different data sets, t are epochs of the measurements, and the 1 and 0 actually represent vectors of ones and zeros, respectively.

In the inversion, a-priori standard deviations of 5 mm for the levelling measurements, and 5 mm for the PSI measurements are assumed. In chap. 2.3 it was discussed that the precision of C-band PSI measurements typically is 1.1-4.0 mm. Since all three PSI time series are based on C-band acquisitions, the same precision model for all measurements is assumed. To account for an additional

inaccuracy due to the least-square prediction at the levelling benchmarks, the value of 5 mm for the PSI measurements is adopted. For the levelling measurements the same, high-end, value is applied. Furthermore, all observations are assumed to be uncorrelated. Apart from the example in Fig. A 55, Appendix 2 contains the integrated time series of 51 selected key levelling benchmarks.

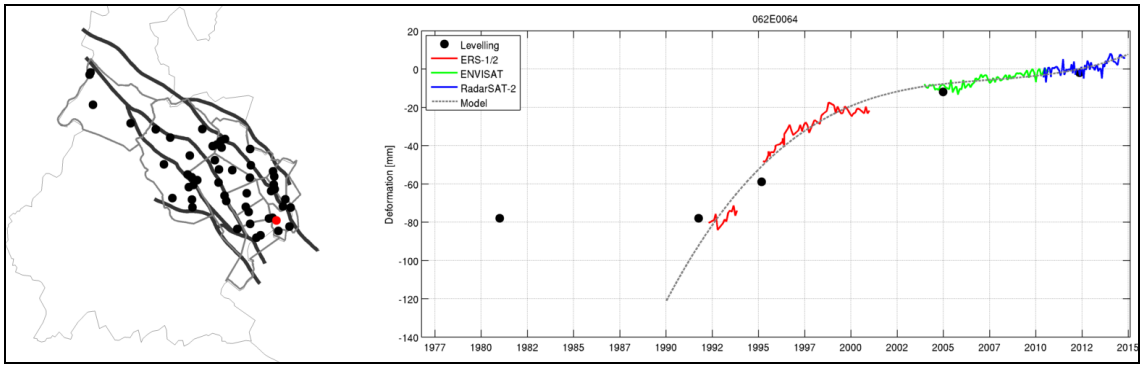

Fig. A 55: Example of an integrated PSI and levelling time series based on a 3rd-degree polynomial. The integrated time series for all 51 selected key levelling benchmarks are provided in Appendix 2

3.3.3 Cross-profiles and contour maps

Based on the GNSS integrated PSI time series, cross-profiles and contour maps are created. Fig. A 56 shows the trajectories of the profiles, which are presented in Appendix 3. Three examples are given in Fig. A 57 to Fig. A 59. To create the profiles, boxes of 250 m (along profile) by 2.000 m (across profile) are created, and the time series of all PS within the box are averaged, separately for the ERS-1/2, ENVISAT, and RadarSAT-2 data sets. Subsequently, the same approach using a 3rd-degee polynomial to integrate the time series as applied at the levelling benchmark locations is applied. However, since the number of levelling benchmarks is limited and the number of boxes with levelling observations will be small, the levelling measurements are not integrated here.

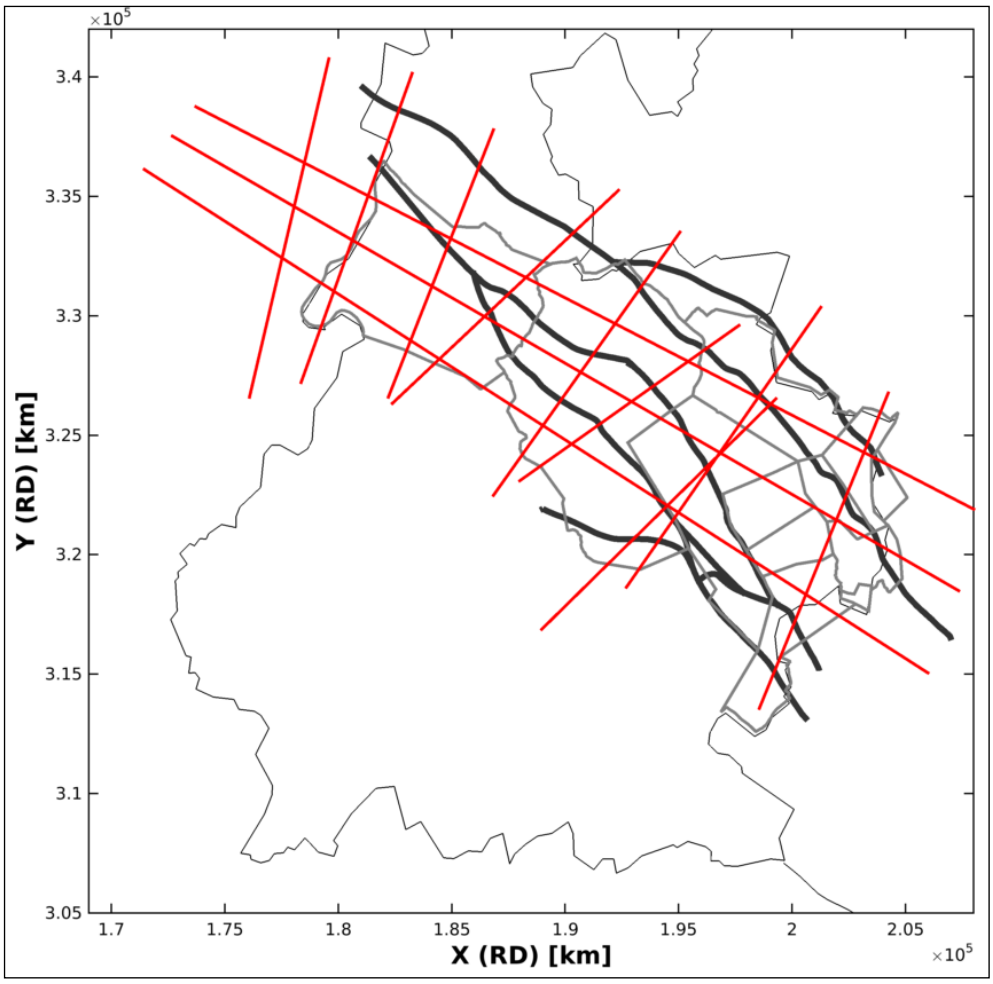

Fig. A 56: Trajectories of cross-profiles (red lines), provided in Appendix 3

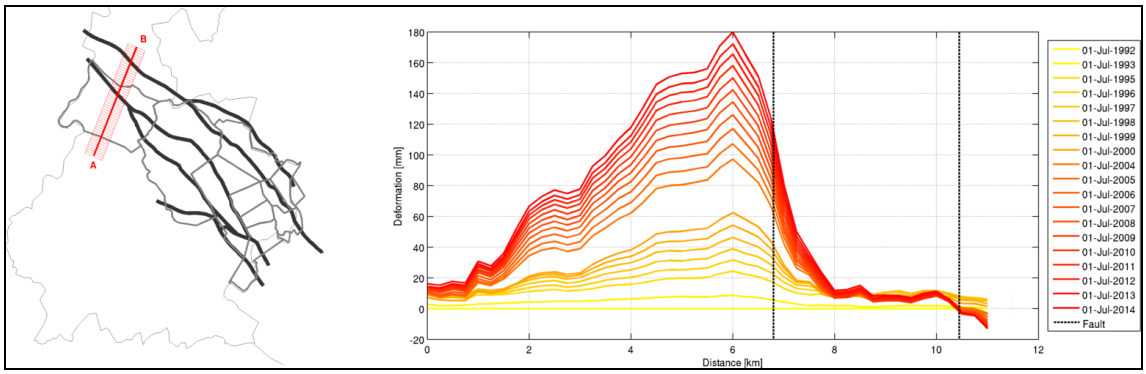

Fig. A 57: Deformation cross-profile across the Maurits mine

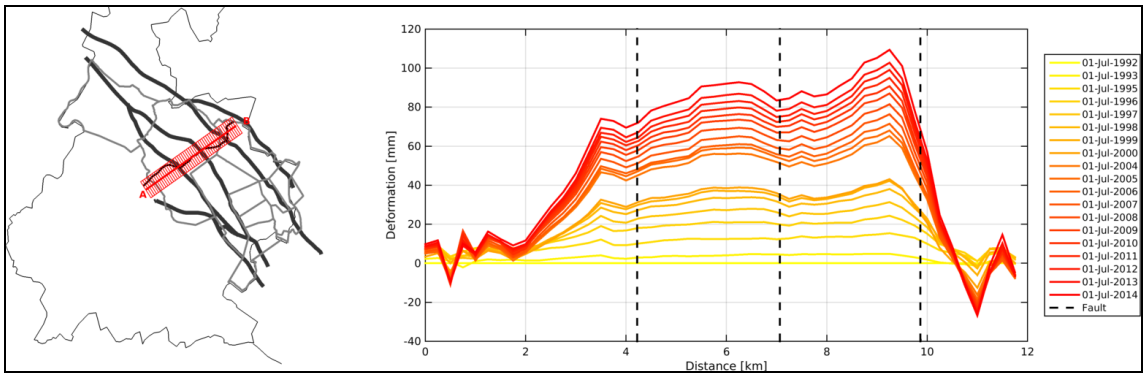

Fig. A 58: Deformation cross-profile along the original levelling-based Aalbeek-Hoensbroek-Schinveld profile by Pöttgens (1985), see Fig. A 33

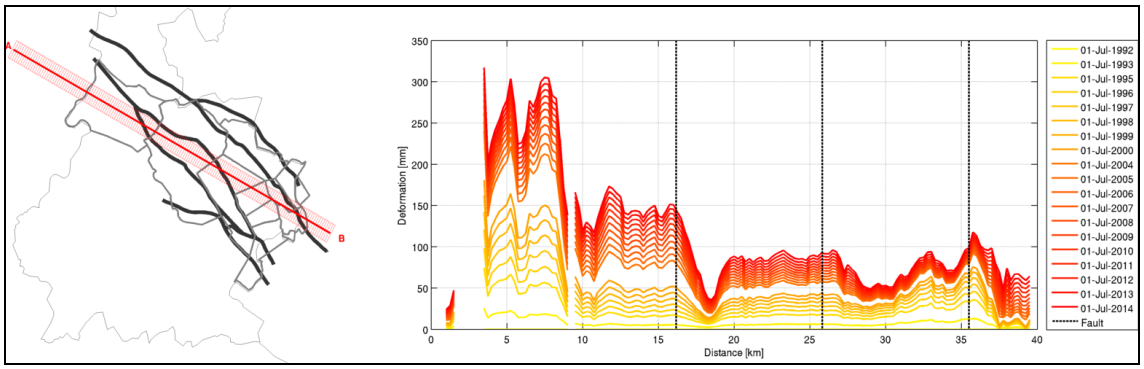

Fig. A 59: Deformation cross-profile across the South Limburg mining region

To obtain a regular sampling of the deformation profiles over time, a Kriging over time is applied to the integrated PSI time series to obtain estimates at the 1st of July of every year. The Kriging is based on a Gaussian variogram with a nugget, which is estimated for each profile separately. Because of the nugget, the Kriging has also a smoothing effect on the time series.

The contour maps are created using a four-step approach. First, the PSI time series are interpolated to a regular grid with a 100 m spacing using inverse squared distance weighting. Here, a maximum distance between the PS and the grid of 1000 m is applied. As a result, if no PS are available in the vicinity of a grid cell, a NoValue is obtained. Next, the 3rd-degree polynomial based

integration of the time series is applied. Again, the levelling observations are not used here. As a final step, the same Kriging operation is applied as was done for the cross-profiles. Hereby, both values at certain regular time intervals are obtained, and the time series are smoothened. Finally, contour maps are made with a 20 mm contour interval. An example of the resulting contour map for the full InSAR time span is shown in Fig. A 60.

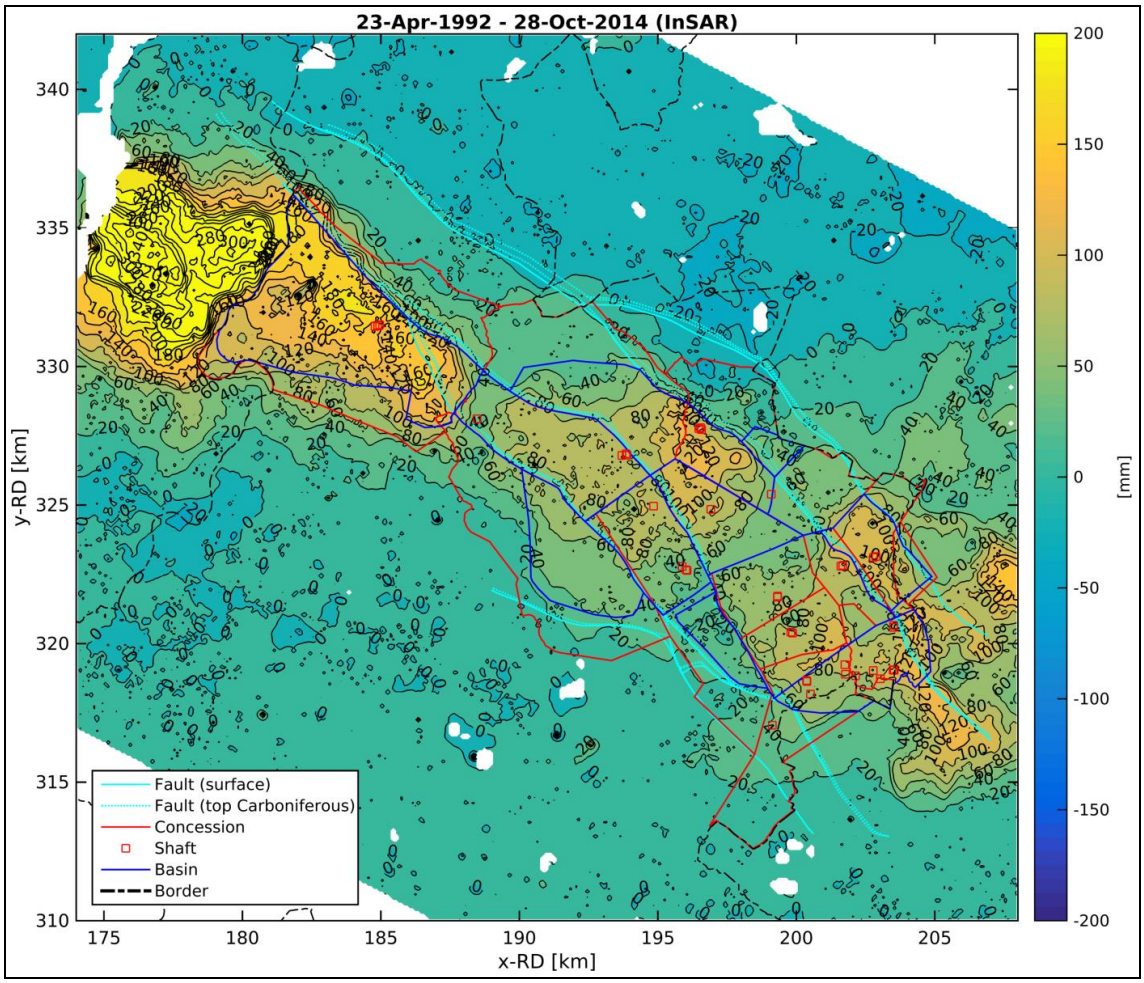

Fig. A 60: Total deformation over the full period for which PSI data is available (23.04.1992 to 28.10.2014)

Additional maps for certain dedicated time spans are provided in Appendix 4. By combining the InSAR-based estimates with the levelling-based estimates in the 1974 - 1992 period, a total levelling-InSAR contour map of the 1974 - 2014

period is created, see Fig. A 61. This contour plot is computed from levelling data over the period 01.01.1974 until 23.04.1992, and InSAR data from 23.04.1992 until 28.10.2014. Note that the maximum ground heave (more than 300 mm) and subsidence strongly exceeds the colour bar used. However, this colour bar is kept to enable a direct comparison with the other figures.

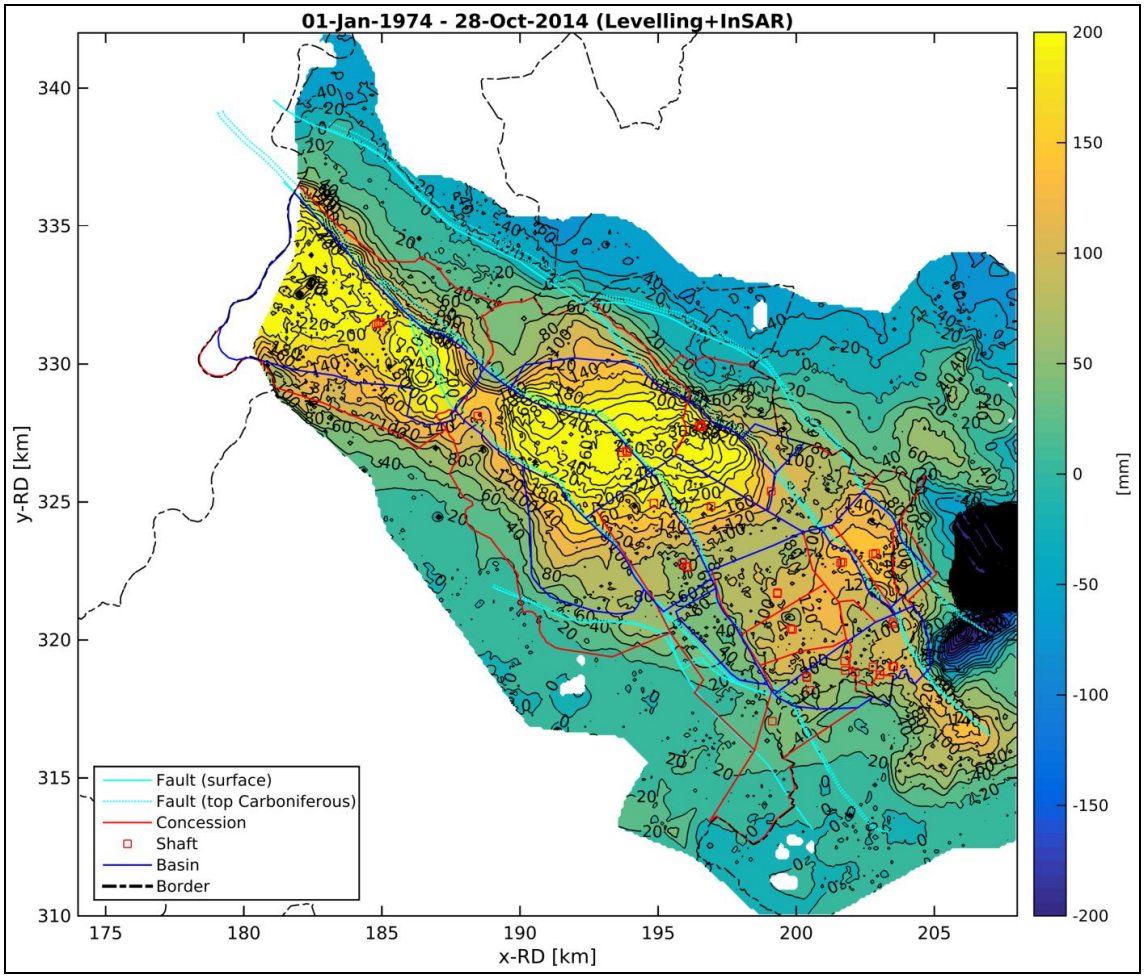

Fig. A 61: Contour plot showing the vertical displacement [in mm] for the South Limburg mining area between 01.01.1974 and 28.10.2014

3.3.4 Comparison levelling - InSAR

Since the levelling and InSAR measurements both cover a large part of the 1992 to 2014 period, a comparison can be made between the results. The estimated ground movement by both techniques repeated in Fig. A 62. The difference between the results is visualised in Fig. A 63. Differences of more than 6 cm in the total deformation values can be observed.

These differences are caused by a combination of

1) inherit differences between the measurement techniques (benchmarks versus radar reflection points),

2) measurement inaccuracies,

3) spatial interpolation (especially of the sparse levelling benchmarks),

4) extrapolation of the levelling time series (last epoch in 2012), and

5) inaccuracies due to the integration of the PSI time series using a 3rd-degree polynomial. This comparison shows that although the different techniques each are characterised by a high level of precision, derived products, such as contour maps, should be interpreted with care.

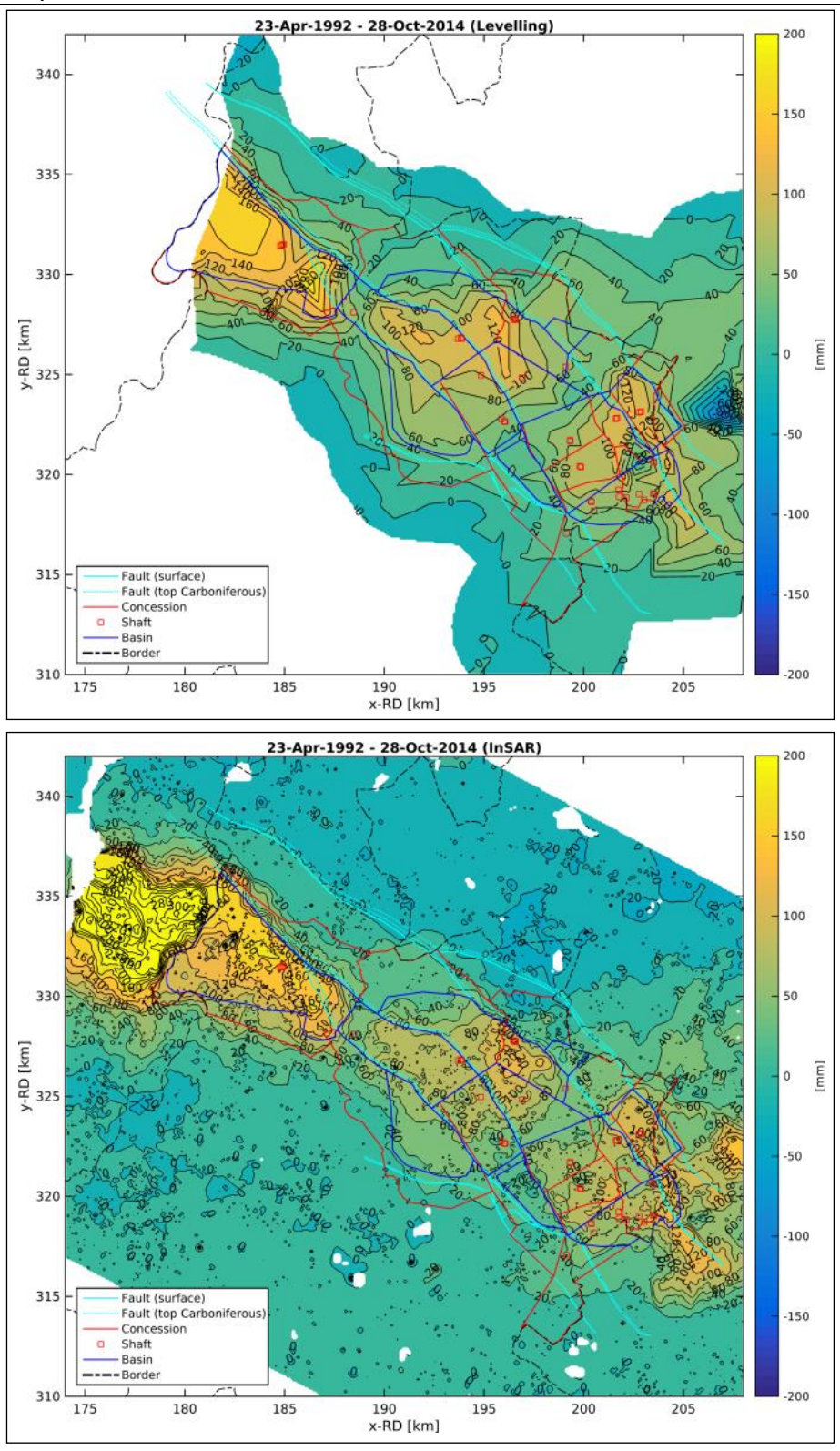

Fig. A 62: Ground movement over the period 1992 - 2014. Above) levelling, below) InSAR

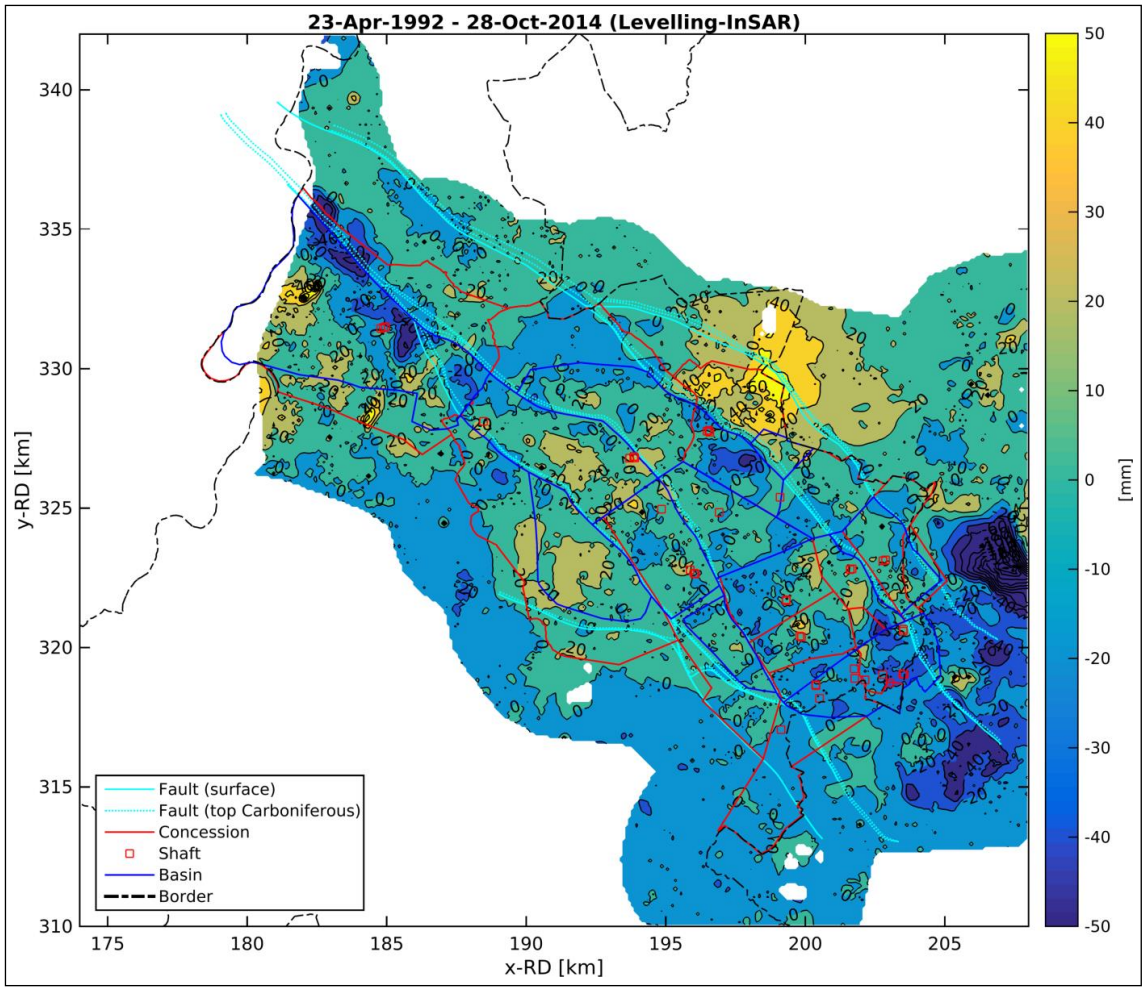

Fig. A 63: Difference in estimated ground movement between levelling and InSAR, over the period 1992 - 2014

References

BLESS, M.J.M., BOSUM, W., BOUCKAERT, J., DURHAUM, H.J., KOCKEL, F., PAPROTH, E., QUERFURTH H. & VAN ROOYEN, P. (1980): Geophysikalische Untersuchungen am Ost-Rand des Brabanter Massivs in Belgien, den Niederlanden und der Bundesrepublik Deutschland.- Mededelingen Rijksgeologische Dienst, Volume 32-17, pp.313-343.

DE BRUIJNE, A., VAN BUREN, J., KÖSTERS , A. & VAN DER MAREL, H. (2005): Geodetic reference frames in the Netherlands.- Netherlands Geodetic Commission, 43, Delft.

CARO CUENCA, M. & HANSSEN, R. (2010): A Least-square Approach for Joining Persistent Scatterer InSAR Time Series Acquired by Different Satellites.- Living Planet Symposium, Bergen, Norway, 28 June – 2 July 2010, pp. 7.

CROSETTO, M., MONSERRAT, O., BREMMER, C., HANSSEN, R., CAPES, R. & MARSH, S. (2009): Ground motion monitoring using SAR interferometry: quality assessment.- European Geologist, 26(2009), pp. 12-15.

CROSETTO, M., MONSERRAT, O., CUEVAS, M., DEVANTHERY, N. & CRIPPA, B. (2016): Persistent Scatterer Interferometry: A review.- ISPRS Journal of Photogrammetry and Remote Sensing, 115(May 2016), 78-89..

FERRETTI, A., PRATI, C. & ROCCA, F. (2001): Permanent Scatterers in SAR Interferometry.- IEEE Transactions on Geoscience and Remote Sensing, 39(1), 8-20.

MAHAPATRA, P.S., SAMIEI ESFAHANY, S., VAN DER MAREL, H. & HANSSEN, R.F. (2013): On the use of transponders as coherent radar targets for SAR interferometry.- IEEE Transactions on Geoscience and Remote Sensing, 52(3), 1869-1878.

MARINKOVIC, P., KETELAAR, G., VAN LEIJEN, F. & HANSSEN, R. (2007). InSAR quality control: analysis of five years of corner reflector time series.- Proceedings of FRINGE 2007, Frascati, Italy.

NOHLMANS, R.A.M. (1990): Gravity measurements, processing and evaluation; test cases de Peel and South-Limburg.- Afstudeerscriptie Faculteit der Geodesie, Technische Universiteit Delft.

PÖTTGENS, J.J.E. (1985): Bodenhebung durch ansteigendes Grubenwasser.- The Development of Science and Art of Minerals Surveying, Proceedings 6th International Congress, International Society of Mine Surveying, vol. 2, p. 928 - 938; Harrogate (GB).

SAMIEI ESFAHANY, S., HANSSEN, R., VAN THIENEN-VISSER, K. & MUNTENDAM-BOS, A. (2009). On the effect of horizontal deformation on InSAR subsidence estimates.- Proceedings of FRINGE 2009, Frascati, Italy.

VAN DER ZON, N. (2013): Kwaliteitsdocument AHN-2, Technical report, Actueel Hoogtebestand Nederland, version 1.3, in Dutch.

VAN LEIJEN, F.J. (2014): Persistent Scatterer Interferometry based on Geodetic Estimation Theory. NCG, Amersfoort, The Netherlands.

Part B - Calculation and prognosis

1 Objectives

Due to the rising mine water decompaction occurs of the broken rock above coal panels. This results in ground heave at the surface. When the mine water head starts to rise above the top of the Carboniferous, hydraulic heads of individual units of the sediment cover rise as well, bringing about additional decompaction. As a result, additional ground heave at the surface is generated. The total ground heave due to decompaction of the broken rock above the coal panels and the sediment cover can increase to some dm and is distributed gradually over a relatively large area. In most cases no damage to houses and other surface structures is to be expected. Only for special configurations, where the presence of tectonic faults is one of the key factors, differential ground heave may occur. Predictions of future differential ground heave can only be made if a prognosis of ground heave is established in general.

The objective of this report is to develop a method to predict future (differential) ground heave due to decompaction of broken rock above the coal panels and the sediment cover in the coal mining area of South Limburg.

To achieve this, first existing methods to predict ground heave over abandoned coal mines are analysed, and a method is selected for this project (chap. 2). In chap. 3 the ground heave at five key points is calculated according to the selected method, using mine maps, mine water- and groundwater data. The results are compared with the measured ground heave, in order to check the validity of the method, and to assess the parameters of the ground heave calculation. This analysis also provides the opportunity to assess the ground heave due to decompaction of the sediment cover. In chap. 4 predictions are made of the final

ground heave at the end of the mine water rise, corresponding to final values of the mine water level. In chap. 5 the ground heave is calculated for a number of benchmarks across the Feldbiß fault and the results are compared with the measured values at the benchmarks and InSAR data. This analysis serves to study the ground heave behaviour across a major fault zone and to verify whether differential movements occur. Conclusions are drawn in chap. 6.

2 Review of concepts of ground heave over abandoned coal mines

2.1 General characteristics of observed ground heave

At present it is generally recognised that a rise of the mine water level brings about ground heave at the surface. Examples of the relation between mine water rise and ground heave are shown in Fig. B 1 and Fig. B 2. Clearly a correlation exists between mine water rise and ground heave. However, after the beginning of the mine water rise, ground heave may start with a delay of up to 5 years. Fig. B 2 reveals that at benchmarks 062E037 and 062E034 ground heave starts at least 3 years after the onset of the mine water rise.

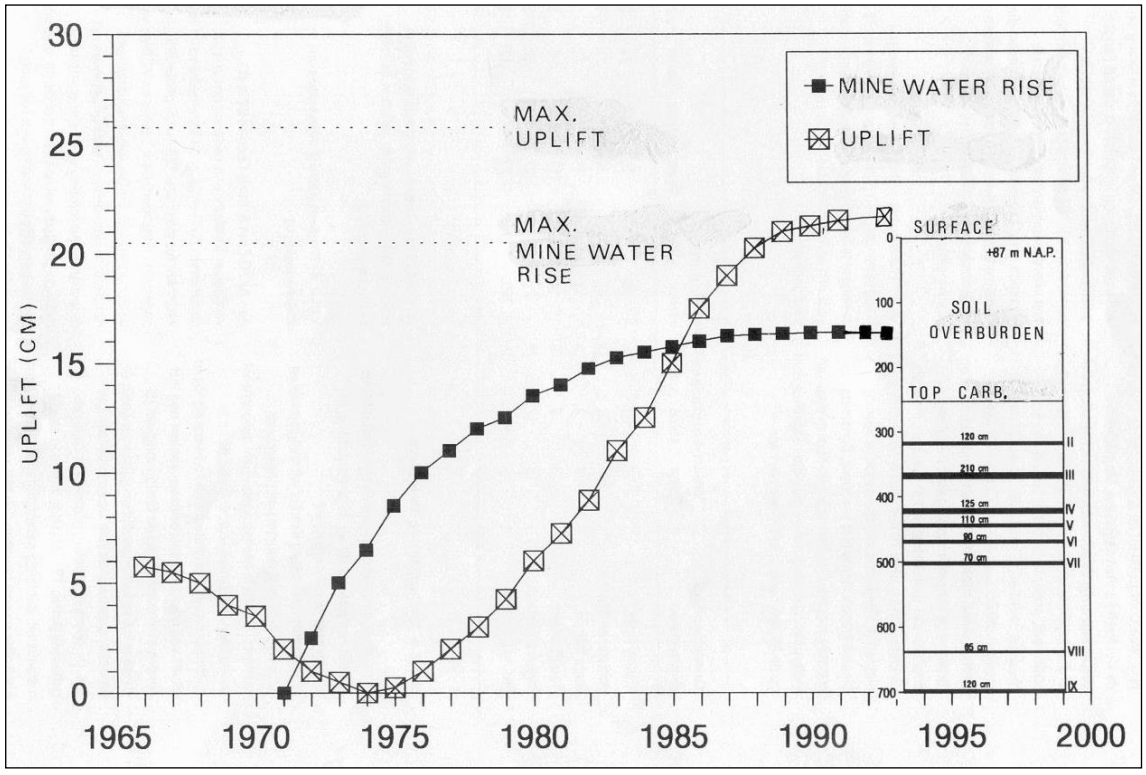

Fig. B 1: Time series of mine water level and ground movement at benchmark 060D0099 over the mine Emma-Hendrik (BEKENDAM & PÖTTGENS, 1995)

Fig. B 1 however, does not necessarily show a delayed response by upward ground movement to flooding. The flooding started in 1971, but there is an

overlapping period with subsidence during the latest coal extraction till 1973 and the first reactions of flooding. It should also be mentioned that, according to HEITFELD et al. (2014), flooding could even induce some subsidence initially, before the onset of ground heave.

Both figures also show that ground heave does not increase when the mine water has stopped to rise. After renewed mine water rise ground heave resumes without significant delay (Fig. B 2).

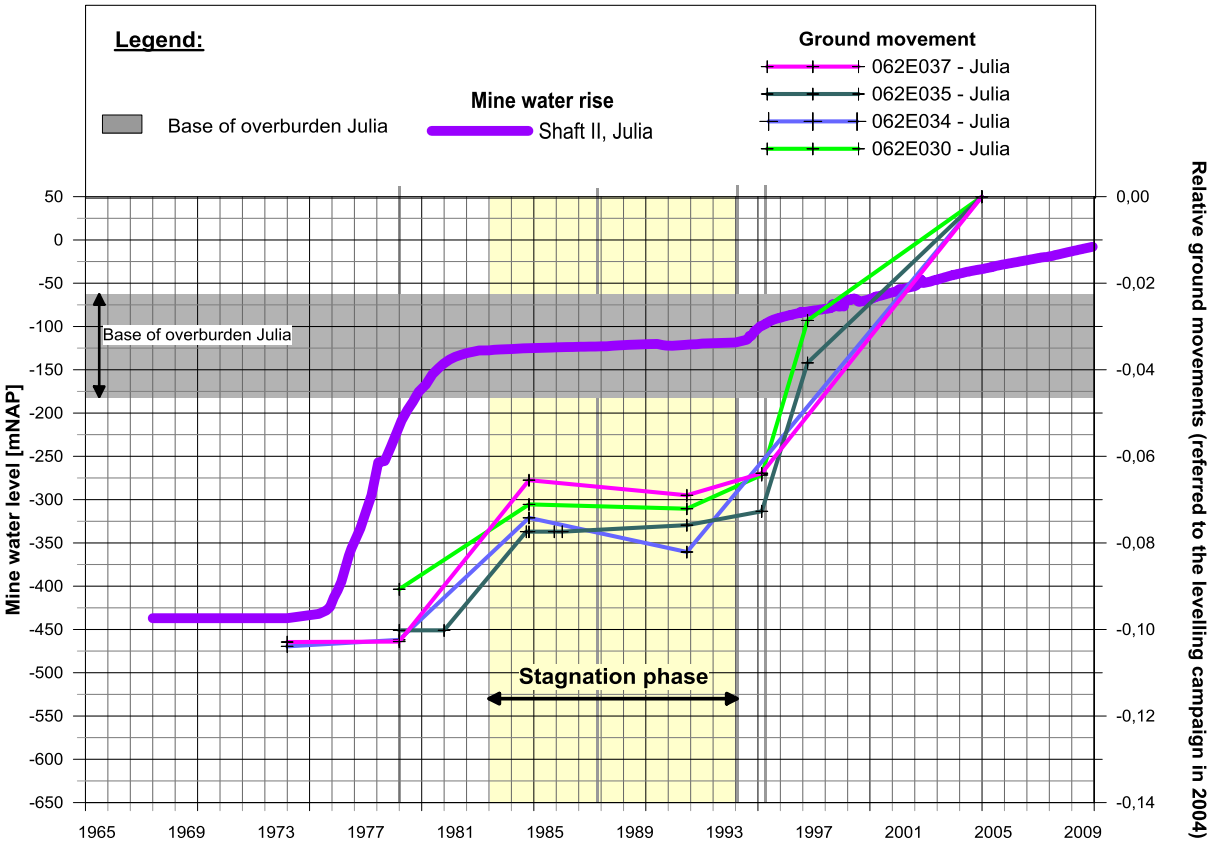

Fig. B 2: Time series of mine water level and ground movement at various benchmarks over the mine Julia (ROSNER, 2011)

2.2 Ground heave due to swelling clay minerals

The first publication on the ground heave over abandoned coal mines is written by OBERSTE-BRINK (1940). He suggested that the ground heave is caused by swelling of clay minerals in the flooded zone of disturbed rock above the coal extractions. According to this mechanism the amount of ground heave is independent of the mine water level, once the zone of disturbed rock is completely flooded. Since it is generally observed that ground heave increases with a rise of the mine water level, swelling clay minerals must play a minor role in the development of ground heave.

SPICKERNAGEL (1975) acknowledged that swelling of clay minerals will promote ground heave, but he did not exclude that an increasing pore pressure in the zone of disturbed rock could be important.

2.3 Ground heave due to decompaction

PÖTTGENS (1985) and other authors explained the ground heave as a result of an increase in pore pressure in the disturbed rock over a longwall coal panel. The subsiding overburden over a coal panel can be divided into 4 zones on the basis of the characteristic deformation behaviour. These zones are described below, from bottom to top (KRATZSCH, 2013; HOLLMANN, 1995). The lowest two zones are shown in Fig B 3.

1. the immediate roof layer, which separates from the rock mass above and collapses either on top of the stowing material, or, if no stowing has been applied, on the floor. As a result, the mine opening is filled with rock debris. This zone is also known as the zone of “Verbandsauflösung” (HOLLMANN & NÜRENBERG, 1972). Its thickness is estimated at up to 3 times the seam thickness (PÖTTGENS, 1985; HOLLMANN, 1995).

2. the main roof, which deflects gradually downwards over the disintegrated rock. Deformation is characterised by movements along discontinuities, mainly near-vertical joints, at a cm- to dm- scale, accompanied by some rotation and extension. This zone corresponds to the zone of "Verbandszerrüttung" of HOLLMANN & NÜRENBERG, and its thickness is up to 9 times the seam thickness (HOLLMANN, 1995).

3. the intermediate zone, which deflects downwards more or less elastically, with only minor shear movements along bedding planes and near-vertical discontinuities at a mm- to cm-scale. This zone of "Verbandsauflockerung" of HOLLMANN & NÜRENBERG has a thickness of up to 15 times the seam thickness (HOLLMANN, 1995).

4. the surface zone, characterised by gradual deflection without discontinuous deformation of significance.

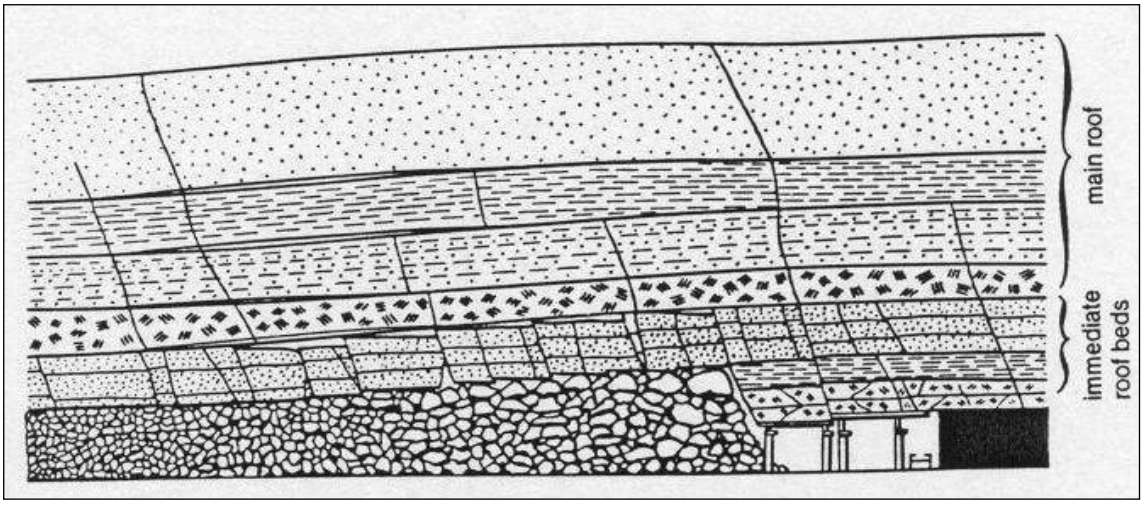

Fig. B 3: Deformation zones directly over an undermined rock mass (after KRATZSCH, 2013)

Especially the immediate roof layer, and to a lesser extent the main roof, show a porosity and permeability which exceed considerably the original values before mining. This disturbed rock mass is prone to the ingress of mine water. Once a

zone of disturbed rock is flooded, the pore pressure increases when the mine water continues to rise. Since the total stress σ remains more or less the same, apart from a small increase due a slightly higher unit weight of the newly saturated part of the overburden, the effective stress σ' inside the disturbed rock will decrease as much as the pore pressure p increases, according to Eq. 1. As a result, the zone of disturbed rock expands, and at the surface ground heave develops.

$$\sigma = \sigma' + p \quad (1)$$

The (vertical) decompaction of the disturbed zone above a coal panel is analysed with the help of the theory of poro-elasticity, which considers a linear relation between the decompaction of the disturbed zone of infinite horizontal extent and the increase in pore pressure:

$$\Delta h = h \cdot D_m \cdot \Delta p \quad (2)$$

where:

h = thickness (m) of the zone of disturbed rock

D_m = decompaction coefficient of the zone of disturbed rock (m^2/N)

Δp = increase in pore pressure (N/m^2)

Actually, decompaction due to rising mine water can be considered as the opposite of compaction due to the withdrawal of oil or gas from a reservoir. The ground heave at the surface is not equal to the decompaction in the subsurface generally. In order to determine the ground heave at the surface, the application of influence functions are necessary. An influence function $k_z = du_z/dA$ relates the infinitesimal ground heave du_z at a surface point due to decompaction of an infinitesimal element with an area dA in the subsurface. The total ground heave

at a surface point due to decompaction of the whole zone of disturbed rock equals:

$u_z = \Delta h \cdot \int k_z \cdot dA$ (3)

For several mined coal panels the contribution of each panel has to be added to achieve the total ground heave.

2.4 The Pöttgens-Geertsma model

In order to determine the ground heave over a decompacting zone of disturbed rock, PÖTTGENS (1985) proposed to apply the theory of subsidence of GEERTSMA (1973), which was developed for the assessment of subsidence over compacting gas and oil reservoirs and is still used at present. The influence function of Geertsma is described by:

$$k_z = \frac{1-\nu}{\pi} \cdot \frac{D}{(r^2+D^2)^{\frac{3}{2}}} \quad (4)$$

where ν is the Poisson's ratio. The maximum ground heave at the surface, over the centre of a circular zone of disturbed rock of radius R, depth D and thickness h is equal to:

$$u_z(0,0) = 2 \cdot (1-\nu) \cdot \left[1 - \frac{\frac{D}{R}}{\sqrt{1+\frac{D^2}{R}}}\right] \cdot \Delta h \quad (5)$$

Profiles of ground heave u_z at the surface, normalised by the decompaction Δh of the disturbed rock in the subsurface, are shown in Fig. B 4. The horizontal distance from the centre of the zone of disturbed rock r is normalised by radius R. The Poisson's ratio is 0,25. The curves apply to a circular zone of disturbed rock with various D/R ratios. For disturbed rock zones of a relatively small

horizontal extent at a relatively great depth, ground heave is limited and fairly evenly distributed over a wide area. In the opposite case ground heave is considerable and concentrated in the centre. Subsidence over coal extractions, using the influence function of Knothe (see chap. 2.5) generally does not extend beyond r = D from the edge of the extraction. Fig. B 4 shows that ground heave extends beyond r = 3 R, measured from the centre, or beyond r = 2 R, measured from the edge of the zone. This corresponds to an extension of ground heave of r = 10 D outside the edge of the zone of disturbed rock of a D/R ratio of 0,2 and an extension of r = D for a D/R ratio of 2,0. Thus, for many configurations the ground heave extends over a larger area than the subsidence developed before.

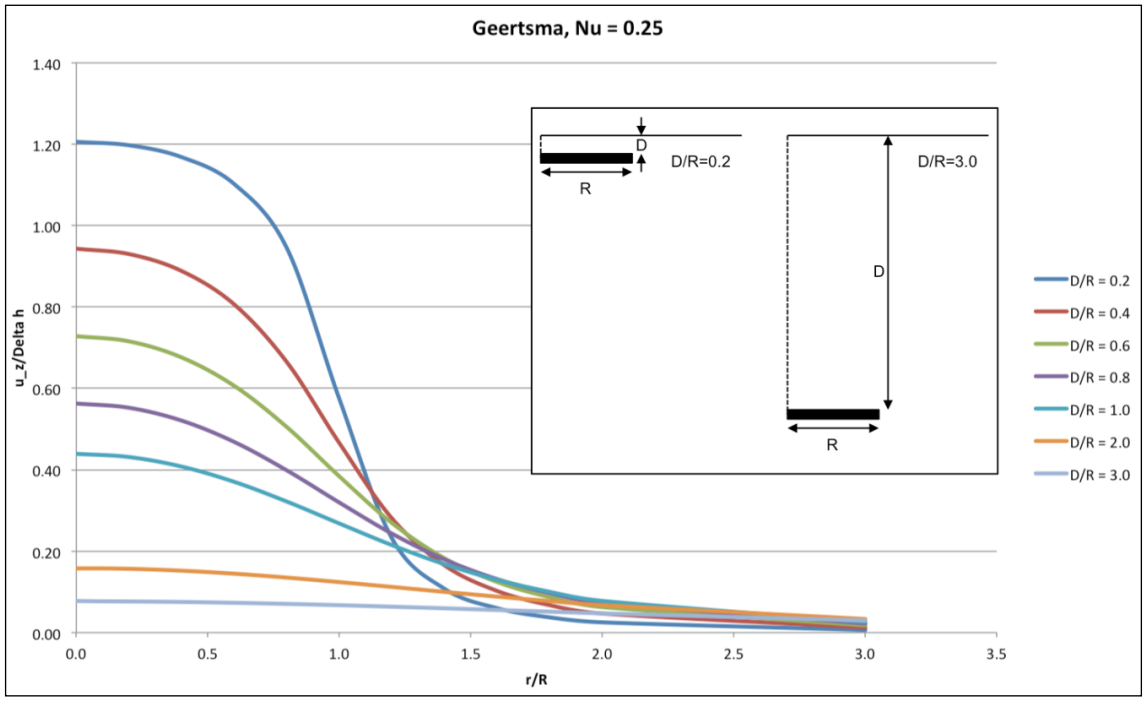

Fig. B 4: Profiles of surface ground heave, normalised by the decompaction in the subsurface, over a circular zone of disturbed rock with a radius R at a depth D (r denotes the horizontal distance from the centre of the zone)

PÖTTGENS considered a thickness h of the zone of disturbed rock of 4 times the seam thickness, and calculated a value for the decompaction coefficient D_m of $3{,}5 \cdot 10^{-9}$ m^2/N, by comparing measured and calculated ground heave for

benchmark 060D0099. SROKA (2005) criticised Pöttgens' choice to employ 4 times the seam thickness as the thickness of the zone of disturbed rock, stating that research has showed that this zone varies between 3 and 20 times the seam thickness. However, it should be noted that decompaction and ground heave are linearly related to both h and D_m (Eq. 2). If h is estimated too small, then measured and calculated ground heave still fit if D_m is increased.

Fig. B 5 depicts the subsidence from 1915 to 1974 and the ground heave from 1974 to 1984. A rough correlation can be recognised between both curves, but the ratio between ground heave and subsidence varies along the profile. The location of maximum ground heave, at benchmark 060D0099, does not coincide with the location of maximum subsidence, at benchmark 060D0108. This is an indication that the influence functions for ground heave and subsidence are different. Generally the ground heave is 2 to 4 % of the subsidence.

2.5 The Sroka-Preusse model, comparison with the Pöttgens model

SROKA and PREUSSE (2006, 2015) chose more or less the same approach as PÖTTGENS. However, they did not use the influence function of GEERTSMA, but that of KNOTHE:

$$k_z = \frac{1}{R_d^2} exp\left[-\pi \cdot \frac{r^2}{R^2}\right] \quad (6)$$

where $R_d = D \cdot \tan \gamma$, with R_d as the radius of influence and γ as the angle of draw, measured from the vertical (Fig. B 6). Only coal extractions inside the area of influence can affect the surface, whether it is subsidence or ground heave. The affected area at the surface expands at an increase of the angle of draw.

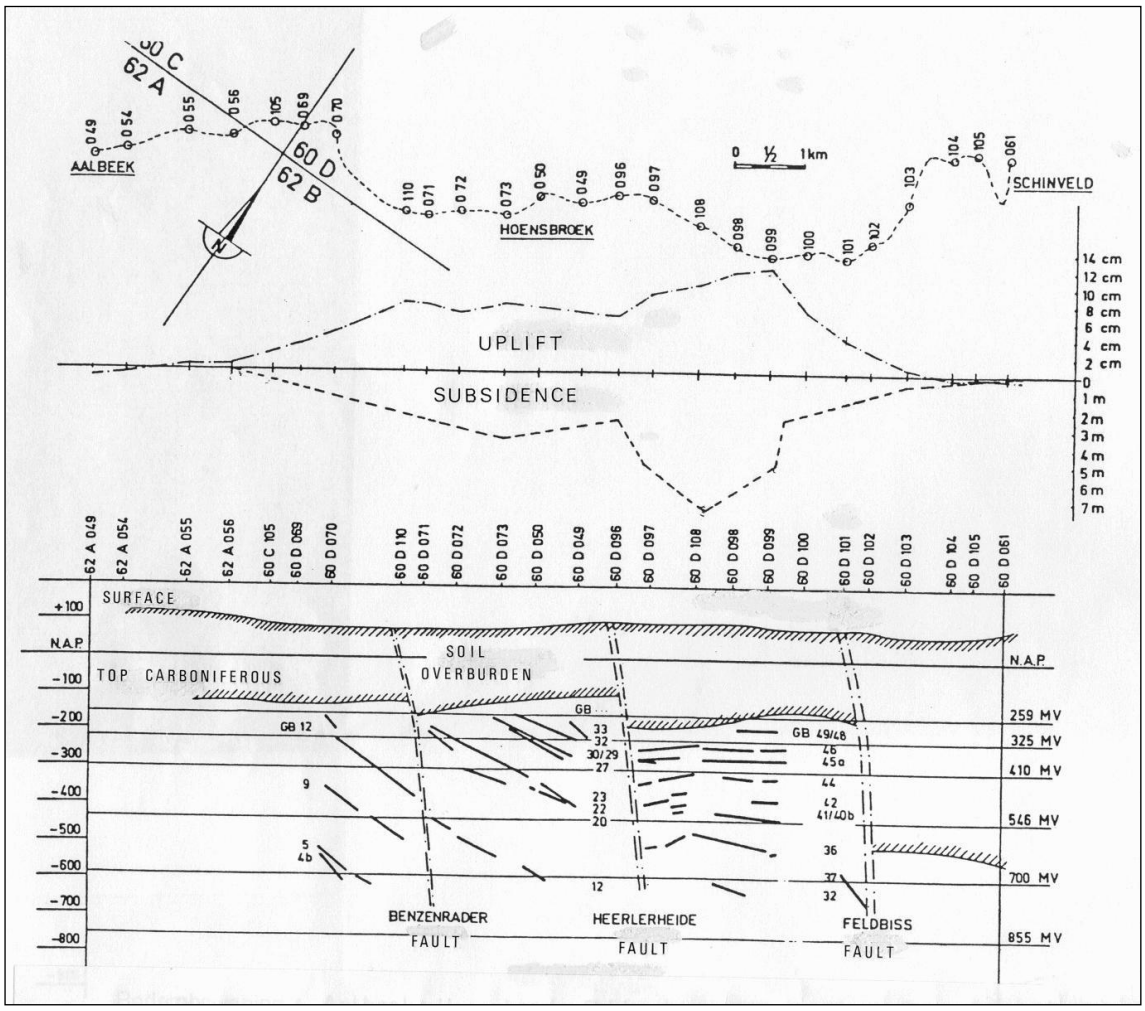

Fig. B 5: The profile Aalbeek-Hoensbroek-Schinveld (Emma-Hendrik mines) showing the measured subsidence (1915-1974) and the ground heave (1974-1984), with mined coal layers and fault zones below (PÖTTGENS, 1985)

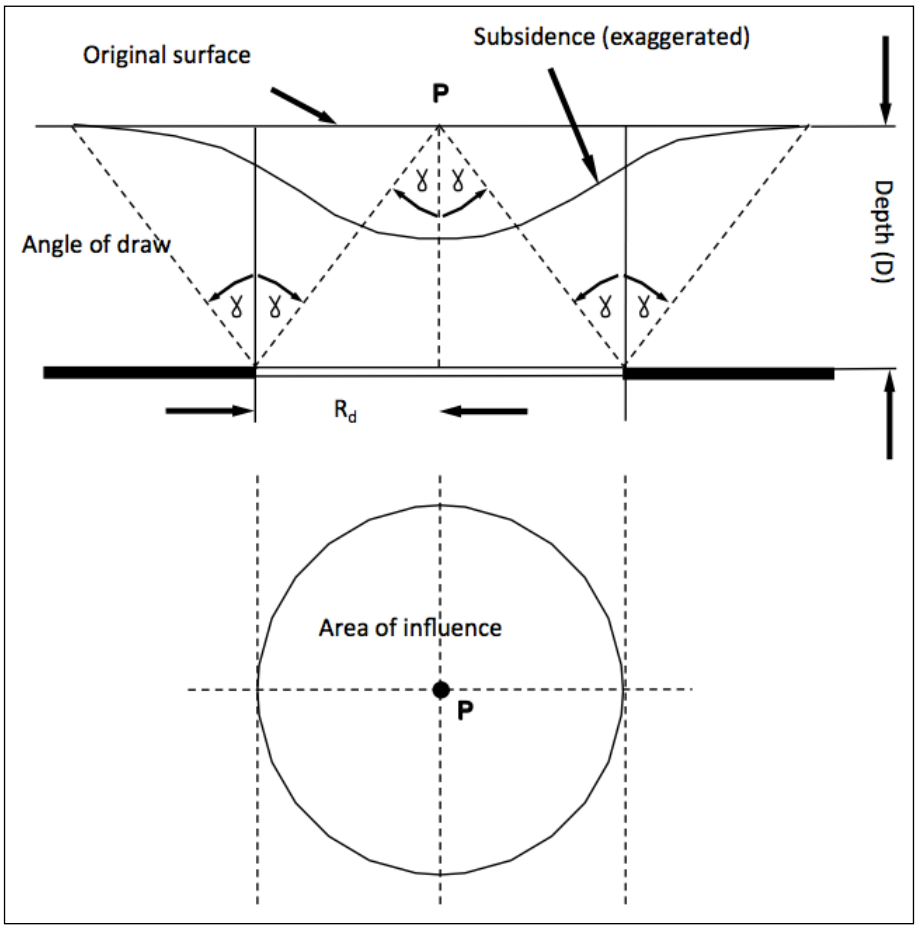

Fig. B 6: Area of influence, angle of draw, and subsidence/ground heave area

Subsidence in the South Limburg coal district was calculated using an integration net, based on the influence function of KNOTHE, with an angle of draw of 45°.

In Fig. B 7 and Fig. B 8 the ground heave profiles according to the influence functions of GEERTSMA and KNOTHE are compared. In Fig. B 7 the ground heave profiles for a circular zone of disturbed rock with a D/R ratio of 1,0 are calculated, using the influence functions of GEERTSMA and KNOTHE. The Poisson's ratio is 0,25. Obviously the GEERTSMA profile does not match that of KNOTHE with an angle of draw γ of 45°. Then it is unsuccessfully tried to fit the KNOTHE profile by increasing the angle of draw. Only by applying a correction factor as well, the KNOTHE profile reasonably matches that of GEERTSMA. This is possible for an angle of draw of 74° and a correction factor of 1,94.

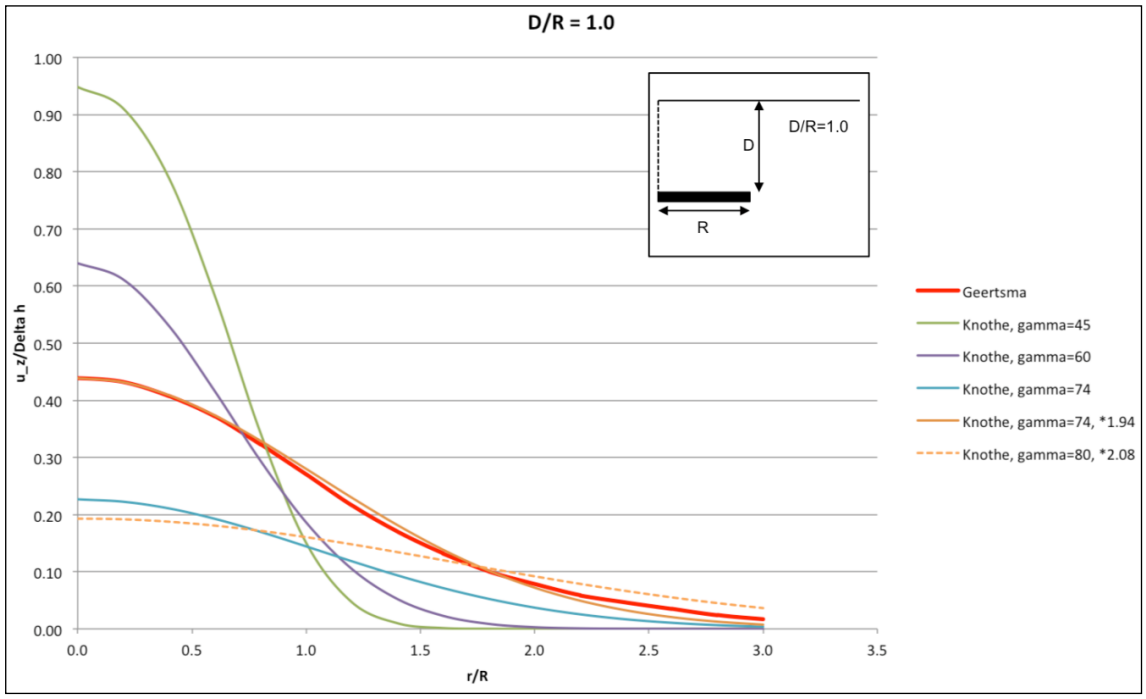

Fig. B 7: Profiles of surface ground heave, normalised by the decompaction in the subsurface, over a circular zone of disturbed rock of a D/R ratio of 1.0, according to the GEERTSMA influence function and several variants of the KNOTHE influence function (r denotes the horizontal distance from the centre of the zone

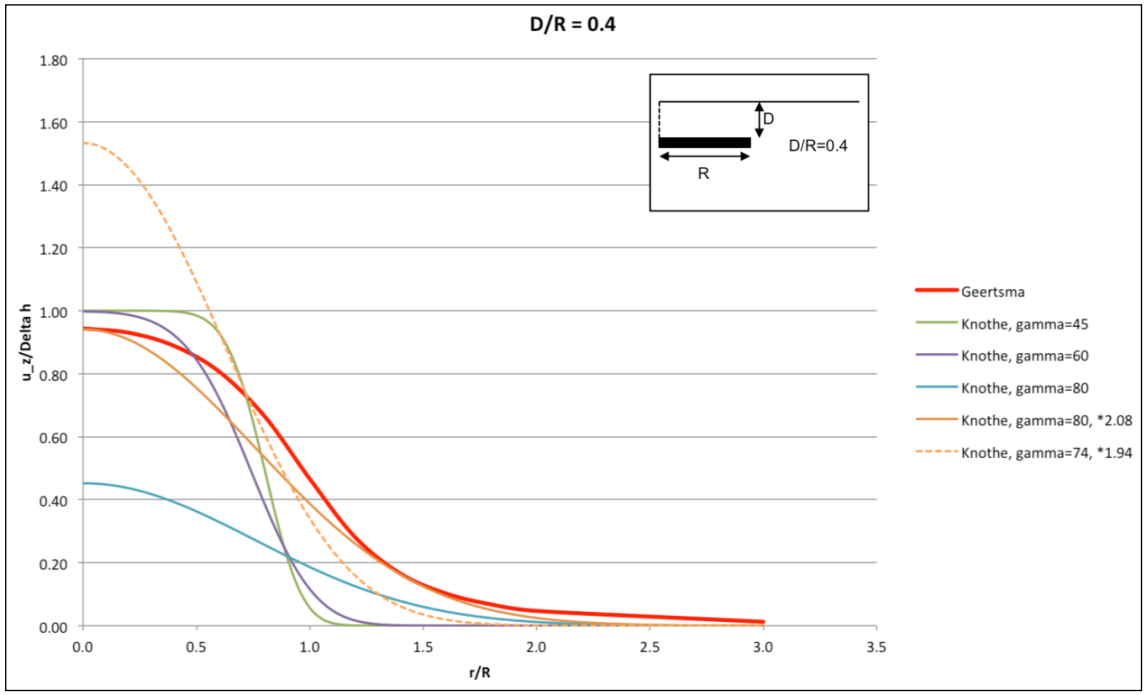

Fig. B 8: Profiles of surface ground heave, normalised by the decompaction in the subsurface, over a circular zone of disturbed rock of a D/R ratio of 0,4, according to the GEERTSMA influence function and several variants of the KNOTHE influence function (r denotes the horizontal distance from the centre of the zone)

This analysis was repeated for a D/R ratio of 0,4 (Fig. B 8). Now the KNOTHE profile fits more or less that of GEERTSMA if an angle of draw of 80° and a correction factor of 2,08 is applied. The KNOTHE profile, which fits for D/R = 1,0, clearly does not match the GEERTSMA profile at all for D/R = 0,4. Fig. B 7 shows that the KNOTHE profile, which fits for D/R = 0,4, does not match the GEERTSMA profile for D/R = 1,0.

SROKA (2005) reported that for subsidence calculations over oil and gas fields the KNOTHE influence function was applied, and that an angle of draw of 82° resulted, much larger than the 45° for subsidence over coal extractions. This result supports the validity of the GEERTSMA influence function, which is characterised by a large affected area at the surface. The mechanism of ground heave over decompacting zones of disturbed rock above coal panels is comparable with that of subsidence over oil and gas fields. Therefore the GEERTSMA influence function is appropriate for the calculation of ground heave over flooded coal panels. The KNOTHE influence function gives different results as that of GEERTSMA, at least for one combination of the angle of draw and correction factor.

2.6 The FENK model

FENK (1998, 2000, 2006) also considered the ground heave as a result of decompaction. In his model the surface subsidence s_e due to coal extraction equals the compaction Δm of the zone of broken rock, with an initial thickness m (Fig. B 9). The vertical stress on the zone of broken rock is $\sigma = D\,\gamma_o$, the product of depth D and unit weight γ_o of the overburden. According to Hooke's Law:

$$s_e = \Delta m = m \cdot D \cdot \gamma_o / E_s \qquad (7)$$

where E_s is the "Steifezahl", the constrained modulus of the zone of broken rock. After compaction, the thickness of the zone of broken rock is reduced to:

$$m - s_e = [(E_s/D \cdot \gamma_o) - 1] \cdot s_e \quad (8)$$

After flooding the zone decompacts, and the resulting ground heave u_z equals the decompaction Δh, according to FENK:

$$u_z = \Delta h = D_m \cdot (m - s_e) \cdot W \cdot \gamma_w \quad (9)$$

W is the height of the column of mine water above the extraction, γ_w is the unit weight of water.

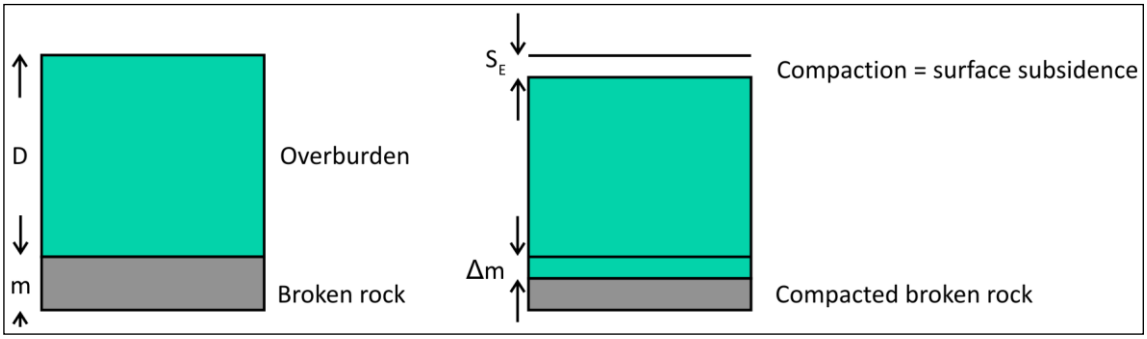

Fig. B 9: Compaction, subsidence and the zone of broken rock according to FENK (1998)

Combining Eqs. (8) and (9) gives:

$$u_z = D_m \cdot W \cdot \gamma_w \cdot [(E_s/D\ \gamma_o) - 1] \cdot s_e \quad (10)$$

If the mine water rises up to the surface, W = D, and this equation can be simplified to:

$$u_z = D_m \cdot \gamma_w \cdot [(E_s/\gamma_o) - D] \cdot s_e \quad (11)$$

FENK (2000) applied this formula in the Zwickauer coal district, and the result of a linear regression on 26 benchmarks was:

$u_z = 0{,}024\ (2024 - D)\ s_e$ (12)

From this result it can be derived that:

$E_s = 46{,}6\ MN/m^2$

$D_m = 2{,}4 \cdot 10^{-9}\ m^2/N$

The advantage of the model of FENK is that ground heave can be calculated with relatively little effort, without knowing the thickness of the zone of broken rock and the size and shape of the coal panels.

However, the model has some serious drawbacks, especially for the South Limburg coal district:

- If the mine water has not reached the surface, the linear regression is more complex.
- In Zwickau several coal seams were mined. FENK's model takes just one seam into account. In his analysis FENK considered only the deepest layer. Essentially the model is not adequate for a multi-seam situation.
- The constrained modulus E_s of the broken rock (during the compaction phase) must equal the reciprocal of the compaction coefficient. This $D_m = 1/E_s = 2{,}15 \cdot 10^{-8}\ m^2/N$, which is about 10 times as large as the decompaction coefficient D_m during decompaction. The difference can be explained as follows. During compaction certain processes occur, i.e. significant rearrangement of rock fragments, which do hardly play a role during decompaction, when the volume of the broken rock has already considerably reduced.
- The subsidence must be known, which is not true everywhere in the South Limburg coal district.

– In the model the ratio of surface subsidence and compaction in the subsurface is the same as that of ground heave and decompaction. This is only true if the influence functions for subsidence and ground heave are the same, which is most probably not correct.
– Decompaction of a sediment cover is not included in the model. Since a sediment cover is present in a considerable part of the South Limburg coal district, the model is not adequate there.

2.7 Decompaction of the sediment cover

The Carboniferous is covered by Mesozoic, Tertiary, and Quaternary sediments. Piezometer data of the sediment cover show that, once the sediment cover becomes flooded, the hydraulic heads in the sediment layers start to rise (ROSNER, 2011). Flooding of the sediment cover means that the hydraulic head of the mine water emerges above the interface between the Carboniferous and the sediment cover. Flooding is not necessarily accompanied by flow of mine water into the sediments.

The rise of the hydraulic heads in the sediment layers can be explained as follows. Due to flooding of the sediment cover, water from the sediments cannot freely trickle downwards into the Carboniferous anymore. During a further rise of the mine water level, the difference between hydraulic heads in the sediment layers and that of the mine water is reduced. As a result, the influx of water from the sediment layers into the Carboniferous decreases (ROSNER, 2011).

A rise of the hydraulic head in the sediment layers brings about decompaction, analogous to decompaction of the zone of disturbed rock above coal extractions in the Carboniferous. An important difference is that sediment layers have a lateral extent which is much greater than that of coal extractions. In practice, the lateral extent is that large that no influence function has to be applied for the

determination of ground heave, i.e. for sediment layers the ground heave at the surface equals the decompaction in the subsurface. Exceptions occur when sediment layers are intersected by tectonic faults which are sealing and/or show a considerable offset.

It should also be noted that the sediment layers in the South Limburg coal district are not indurated, except the limestones of the Maastricht formation. Accordingly, most sediment layers show a much larger decompaction coefficient than the disturbed Carboniferous rock. The thickness of the sediment layers can attain several tens of metres, which is much more than the thickness of 8 m at most of the disturbed rock zone over a coal panel. Therefore, the ground heave per metre rise of the hydraulic head is expected to be greater for the sediment layers than for the disturbed Carboniferous rock. On the other hand, the rise of the hydraulic head is 20 m at most in the sediment layers, and several hundreds of metres in the zones of disturbed rock.

Ground heave u_z due to decompaction of sediment layers can be determined with Eq. 2:

$$u_z = \Delta h = h \cdot D_m \cdot \Delta p$$

Two complications exist:

- A method has to be found to separate the ground heave contributions from the decompaction of the Carboniferous disturbed rock and that of the sediment layers.
- The sediment cover comprises several layers, each with its own D_m. If the ground heave of the sediment cover is known, it applies to the cover as a whole. It will be difficult to assess the decompaction coefficients for each sediment layer separately.

GIESE (2010) extensively studied the compaction and decompaction of sediment layers around the lignite open pit mines in Germany, some tens of km from the South Limburg coal district. It will be attempted to apply the parameters, measured for some of the same layers as in South Limburg, in the ground heave calculations.

2.8 Selected methods for the study

It is generally recognised that ground heave over abandoned coal mines is brought about by decompaction of the zone of disturbed rock above coal panels. The mechanism of ground heave is comparable with that of subsidence over oil and gas fields, where the GEERTSMA influence function applies. Therefore, this influence function is chosen to calculate the ground heave at the surface. The KNOTHE influence function is not used because it gives different results. Moreover, it is not clear which angle of draw applies. The method of FENK has several limitations for the South Limburg coal district and is not used as well.

When the sediment cover is flooded by the mine water, it decompacts as well. Since the sediment layers are generally horizontally extensive, no influence function is needed. In chap. 3.4 it will be attempted to overcome the complications described in chap. 2.7.

3 Analysis of ground heave developed up to recently

3.1 Outline of the method

3.1.1 Key points requirements

For the analysis five key points were selected. The requirements for these key points were:

- Regular levelling data are available over the major part of the period from the beginning of the mine water rise until recently.
- The mine water level is known over the period mentioned above.
- The key points relate to different thicknesses of the sediment cover, depths of the coal extractions, and the amount of coal extraction.

3.1.2 Data acquisition and selection of key points

Several key points were initially selected by IHS. For these key points IHS provided georeferenced mine maps, which include all coal extractions possibly affecting the surface at the key points due to rising mine water. The levelling data were provided by the Technical University Delft, Department of Geoscience and Remote Sensing, Delft. The NAP heights were converted into the system before the revision in 2005. The mine water level data were given by WG 5.2.4/5.2.5. However, levelling data meeting the requirement above proved not to be available for all key points. From the initially selected key points, five key points, which meet all requirements above, were finally chosen for this study.

The five key points, corresponding with benchmarks, are shown in Fig. B 10. Keypoint 1 is situated over the central part, key point 2 over the northern part, and keypoint 3 over the southern part of the Emma concession. Key points 4 and 5 are located over the Julia concession.

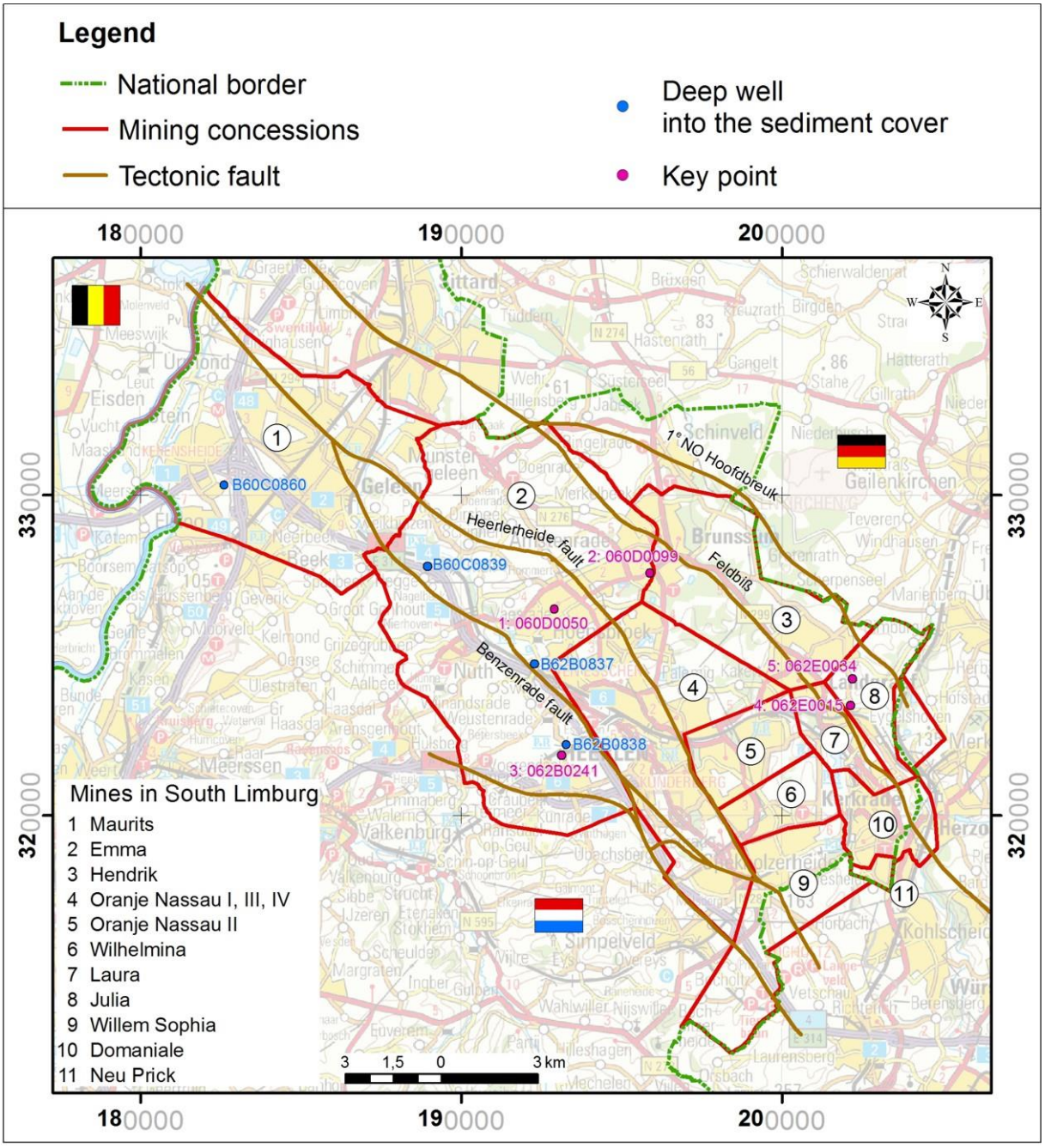

Fig. B 10: Key points (in purple), deep wells into the sediment cover (in blue), concession areas and main tectonic faults

The characteristics of the key points are listed in Tab. B 1. Levelling data are available from 01.01.1974 onwards, except for keypoint 4, where levelling began in 01.01.1979. For key points 3 and 5 data were acquired since the beginning of

the mine water rise, and for the remaining key points levelling began 4 to 5 years after the start of the mine water rise. The most recent levelling data date from 2012. The number of coal extractions, and their depth, which contribute to ground heave at the key points are much greater for key points 1 and 2 than for key points 3-5.

Tab. B 1: Key point characteristics

Key point	Benchmark	X	Y	Elevation NAP (m)	Concession	Main basin	Period levelling data From	To	Number of extractions	Depth extractions (m) Minimum	Maximum	NAP Top Carb. key point	Thickness sediment cover (m)
1	060D0050	192900	326440	93	Emma/Hendrik	North	01-01-74	13-05-12	65	243	793	-123	216
2	060D0099	195880	327570	87	Emma/Hendrik	North	01-01-74	13-05-12	47	237	697	-139	226
3	062B0241	193130	321880	85	Emma	North	01-01-74	13-05-12	4	245	555	-87	172
4	062E0015	202130	323440	112	Julia/Laura	Central	01-01-79	13-05-12	14	157	492	-113	225
5	062E0034	202190	324270	135	Julia/Laura	Central	01-01-74	13-05-12	14	180	515	-110	245

3.1.3 Calculation of decompaction in the Carboniferous

The decompaction Δh of the zone of disturbed rock above a coal extraction was calculated with Eq. 2 (chap. 2.3):

$$\Delta h = h \cdot D_m \cdot \Delta p \quad (2)$$

The thickness h of the zone of disturbed rock was taken as 4 times the seam thickness, in analogy to PÖTTGENS (1985). The seam thickness is defined here as the total thickness of the extracted rock, comprising coal beds and interlayered shale beds. In the STANDAARD LEGENDA (1973) this total thickness is known as the "laagopening". The seam thickness could be obtained by adding the thickness of shale- and coal beds, indicated in cm, with "l" and "k" respectively, on the mine maps (Fig. B 11). For each coal extraction an average value was estimated.

For some extractions the thickness is not indicated on the mine maps. In this case the values from the STANDAARD LEGENDA were used.

The decompaction coefficient D_m was yet to be established. As a first estimation, the value of $3{,}5 \cdot 10^{-9}$ m^2/N of PÖTTGENS (1985) has been applied.

Fig. B 11: Detail of mine map with NAP levels of the coal layer (in blue), tables of excavated coal (k), and shale beds (l)

The pore pressure Δp at any given time depends on the NAP level of the coal extraction and the NAP level of the mine water at that time. The mine water levels were provided by WG 5.2.4/5.2.5, as mentioned above. The NAP level of the coal extraction is indicated in blue letters or blue underlined letters on the mine maps (Fig. B 11). For each extraction an average value was established.

The coal layers are often offset by tectonic faults (Fig. B 12). For example, the mean NAP level of the coal extraction GB36 is -300 m west of the Heerlerheide fault and southeast of the 70 m fault. Northwest of the 70 m fault the mean NAP level is -540 m. Since the NAP level is an important parameter when calculating the pore pressure and the ground heave (see below), the coal extractions were

subdivided into separate extractions when these are intersected by important tectonic faults.

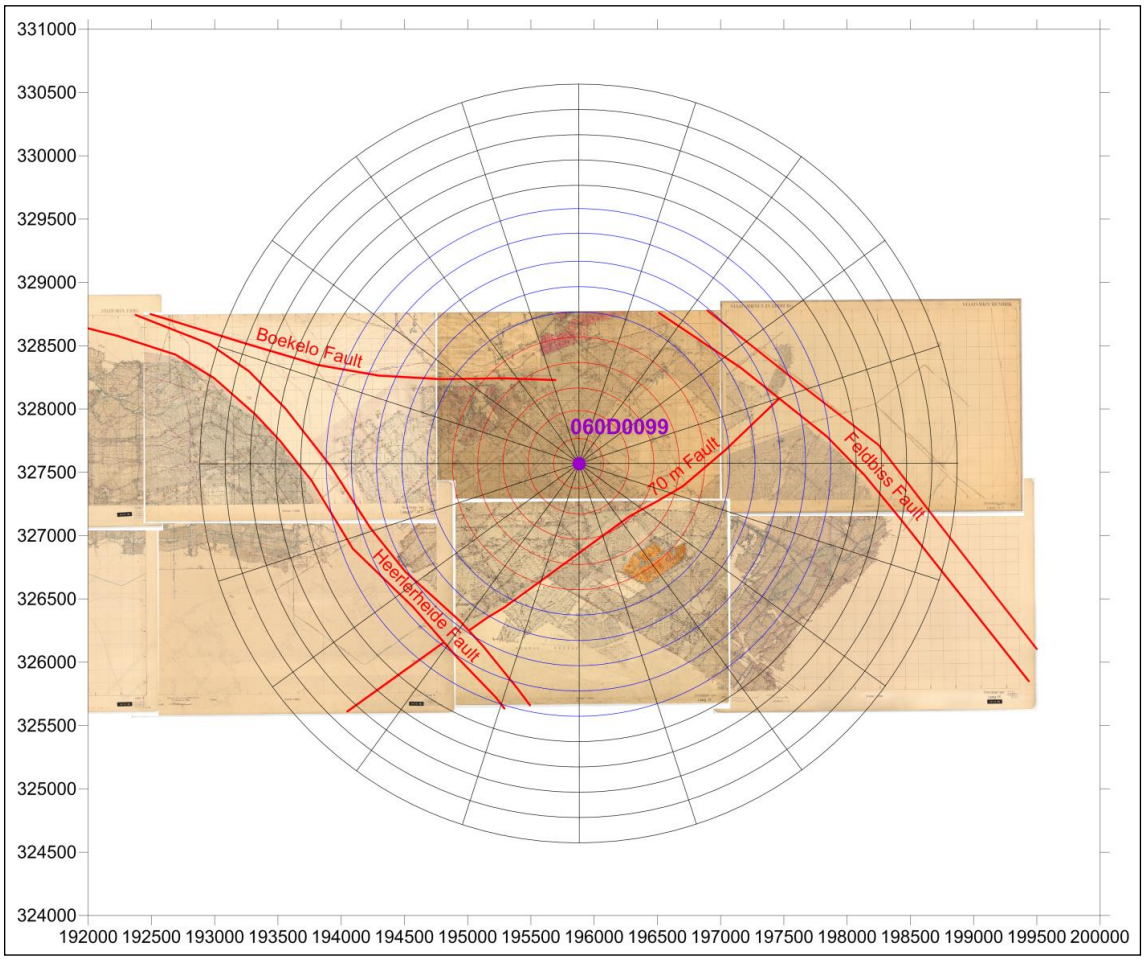

Fig. B 12: The integration net, based on GEERTSMA's influence function, applied for key point 2 (benchmark 060D0099) and coal layer GB36

3.1.4 Calculation of ground heave due to decompaction in the Carboniferous

The ground heave at a key point, due to decompaction of the disturbed rock over a given coal extraction, was determined by means of an integration net, which is based on GEERTSMA's influence function. A Poissons' ratio of 0,25 was applied. In Fig. B 12 an example is given for the ground heave at key point 2 (benchmark

060D0099) as a result of decompaction of the disturbed rock over coal layer GB36. A radius of the integration net of 995 m was chosen for all calculations. Each of the 15 rings was subdivided into 20 elements. The contribution to ground heave due to decompaction inside an element decreases from the inner - to the outer ring. The contribution to ground heave per element depends on the depth of the coal extraction. The ground heave was calculated by locating the centre of the integration net over the key point, and by counting per ring the number of elements which are situated inside the coal extraction. Sometimes extractions were locally stowed, pneumatically, hydraulically, by hand or using packs. In this case the seam thickness was reduced per element, according to the manual drafted by PÖTTGENS (2002). In Tab. B 2 the calculation of ground heave at key point 2 due to decompaction of the disturbed rock over coal extraction GB36 northwest of the 70 m fault is shown as an example. Here the ground heave u_z is 47,86 % of the decompaction Δh. The calculation of ground heave was repeated for each extraction separately.

All determined parameters were finally listed in a table. As an example, Tab. B 3 shows the parameters for keypoint 2 for all coal extractions and for the ground heave which developed from 01.01.1974 till 01.01.1976. The mean thickness of the coal seam is indicated in red if no data were depicted on the mine maps, and the value of the STANDAARD LEGENDA was used. Several extractions were not flooded yet at the beginning of 1976, which is indicated in the table by the absence of pressure, decompaction Δh and ground heave. The total ground heave, due to the decompaction of disturbed rock over all extractions, was obtained by adding the separate contributions. This calculation was repeated for 15 to 20 periods per key point.

Tab. B 2: Results of the ground heave (u_z) calculation due to decompaction (Δh) of the disturbed rock over the extraction to the NW of the 70 m fault in coal layer GB36

Layer:	**GB36_NW of 70 m fault**
Depth D (m):	**627**
Radius R (m):	**995**
Nu:	**0.25**
Δh (mm):	**102.14**

Ring	From r/R	To r/R	Term r_i-1	Term r_i	K_z(ring)	Sum 5 rings	Elements (N)	K_z * N
1	0	0.2	1.0000	0.9531	0.0703		15	0.0527
2	0.2	0.4	0.9531	0.8443	0.1633		14.5	0.1184
3	0.4	0.6	0.8443	0.7242	0.1801		11.5	0.1035
4	0.6	0.8	0.7242	0.6188	0.1582		9	0.0712
5	0.8	1	0.6188	0.5331	0.1285	0.7003	7	0.0450
6	1	1.2	0.5331	0.4649	0.1023		8.5	0.0435
7	1.2	1.4	0.4649	0.4104	0.0817		7.5	0.0306
8	1.4	1.6	0.4104	0.3664	0.0660		3	0.0099
9	1.6	1.8	0.3664	0.3304	0.0540		1	0.0027
10	1.8	2	0.3304	0.3005	0.0449	0.3489	0.5	0.0011
11	2	2.2	0.3005	0.2754	0.0377		0	0.0000
12	2.2	2.4	0.2754	0.2540	0.0321		0	0.0000
13	2.4	2.6	0.2540	0.2355	0.0276		0	0.0000
14	2.6	2.8	0.2355	0.2196	0.0240		0	0.0000
15	2.8	3	0.2196	0.2056	0.0210	0.1424	0	0.0000
							u_z/Δh	**0.4786**
							u_z (mm)	**48.8905**

3.2 Expected time series of ground heave

Ground heave begins when the disturbed rock over the lowest coal extraction is flooded and starts to expand, and increases upon flooding of shallower extractions and an increase of the mine water pressure in the disturbed rock over all extractions already under water. The ground heave accelerates when more and more extractions are flooded. Such acceleration is shown in Fig. B 13 for an imaginary configuration of several coal extractions. The initially relatively slow increase of the ground heave could mistakenly be seen as a delay. To keep it simple, the rate of the mine water rise is taken to be constant, which is usually not true in reality. The ground heave due to decompaction of the disturbed rock over the coal extractions, shown in red in Fig. B13, increases linearly over time when all zones of disturbed rock 1 to 8 have been flooded (mine water level 8).

Tab. B 3: Parameters for keypoint 2 for all coal extractions and for the ground heave which developed from 01.01.1974 till 01.01.1976

Layer (GB nr.)	Map	Area calculation	Mine	Basin	Field Standaard Legenda	NAP Coal layer [m]	Mean NAP Coal layer [m]	NAP 060D099 [m]	Depth Coal layer [m]	Thickness St. Leg. [cm]	Mean thickness Coal layer [cm]	NAP Mine water 01-01-74	NAP Mine water 01-01-76	Raise Mine water [m]	increase pressure [N/m²]	Δh [mm]	ground heave [mm]
54	41	N of Boekelo-fault	Emma/Hendrik	Central/South	Oostveld/Zuidveld	-350/-490	-420	87	507	130	180	-438	-325	95	950000	19.15	0.05
53	41_49_50	N of Boekelo-fault	Emma/Hendrik	Central/South	Oostveld/Zuidveld	-240/ -520	-320	87	407	116/--	100	-438	-325	0	0	0.00	0.00
53	41	S of Boekelo-fault	Emma/Hendrik	Central/South	Oostveld/Zuidveld	-200/-250	-220	87	307	116/--	100	-438	-325	0	0	0.00	0.00
52	41_48_49_50	N of Boekelo-fault	Emma/Hendrik	Central/South	Oostveld/Zuidveld	-250/-420	-330	87	417	82/--	82	-438	-325	5	50000	0.46	0.01
52	49	S of Boekelo-fault	Emma/Hendrik	Central/South	Oostveld/Zuidveld	-220	-220	87	307	82/--	82	-438	-325	0	0	0.00	0.00
51	41_48_49_50	N of Boekelo-fault	Emma/Hendrik	Central/South	Oostveld/Zuidveld	-240/-470	-350	87	437	101/--	110	-438	-325	25	250000	3.08	0.10
51	49	S of Boekelo-fault	Emma/Hendrik	Central/South	Oostveld/Zuidveld	-200/-230	-230	87	317	101/--	100	-438	-325	0	0	0.00	0.00
50	41_49_50	W and N	Emma/Hendrik	Central/South	Oostveld/Zuidveld	-210/-330	-260	87	347	110/--	120	-438	-325	0	0	0.00	0.00
50	57_50	SE	Emma/Hendrik	Central/South	Oostveld/Zuidveld	-140/-160	-150	87	237	110/--	110	-438	-325	0	0	0.00	0.00
48_49	41_48_49_50	N of Boekelo-fault	Emma/Hendrik	Central/South	Oostveld/Zuidveld	-220/-560	-400	87	487	118	118	-438	-325	75	750000	9.91	0.94
48_49	50	S of Boekelo-fault	Emma/Hendrik	Central/South	Oostveld/Zuidveld	-180/-210	-200	87	287	118	118	-438	-325	0	0	0.00	0.00
46	41_49_50	N of Boekelo-fault	Emma/Hendrik	Central/South	Oostveld/Zuidveld	-310/-610	-450	87	537	98/--	120	-438	-325	113	1130000	15.19	1.75
46	49_50_56_57	S of Boekelo-fault	Emma/Hendrik	Central/South	Oostveld/Zuidveld	-130/-400	-250	87	337	98/--	120	-438	-325	0	0	0.00	0.00
45b	49_50_56	S of Boekelo-fault	Emma/Hendrik	Central/South	Oostveld/Zuidveld	-230/-360	-300	87	387	211/152	200	-438	-325	0	0	0.00	0.00
45a	41_49_50	N of Boekelo-fault	Emma/Hendrik	Central/South	Oostveld/Zuidveld	-300/-690	-450	87	537	211/149	150	-438	-325	113	1130000	18.98	1.23
45a	49_50_56_57	S of Boekelo-fault	Emma/Hendrik	Central/South	Oostveld/Zuidveld	-180/-370	-250	87	337	211/149	150	-438	-325	0	0	0.00	0.00
44	41_49_50	N of Boekelo-fault	Emma/Hendrik	Central/South	Oostveld/Zuidveld	-350/-550	-450	87	537	87/107	100	-438	-325	113	1130000	12.66	0.62
44	49_50_51_56_57	S of Boekelo-fault	Emma/Hendrik	Central/South	Oostveld/Zuidveld	-200/-420	-300	87	387	87/107	100	-438	-325	0	0	0.00	0.00
42	48_49	W of Heerlerheide fault	Emma	Central	Westveld	-160/-370	-240	87	327	118	118	-438	-325	0	0	0.00	0.00
42	41_49_50	N of Boekelo-fault	Hendrik	South	Zuidveld	-560/-660	-610	87	697	104	120	-438	-325	113	1130000	15.19	0.08
42	49_50_56	S of Boekelo-fault	Hendrik	South	Zuidveld	-320/-490	-380	87	467	104	104	-438	-325	55	550000	6.41	1.50
42	50_51_57_58	SE of 70 m fault	Hendrik	South	Zuidveld	-120/-370	-220	87	307	104	104	-438	-325	0	0	0.00	0.00
41	48_49_56	W of Heerlerheide fault	Emma	Central	Westveld	-130/-410	-260	87	347	150	150	-438	-325	0	0	0.00	0.00
41	49_50_56	E of Heerlerheide fault	Hendrik	South	Zuidveld	-370/-530	-400	87	487	72	160	-438	-325	75	750000	13.44	0.29
40	48_49	W of Heerlerheide fault	Emma	Central	Westveld	-130/-260	-210	87	297	104	104	-438	-325	0	0	0.00	0.00
40	49_50_56_57	NW of 70 m fault	Hendrik	South	Zuidveld	-320/-530	-470	87	557	86	86	-438	-325	113	1130000	10.88	3.06
40	50_51_57_58	SE of 70 m fault	Hendrik	South	Zuidveld	-110/-440	-280	87	367	86	86	-438	-325	0	0	0.00	0.00
39	48_49_56	W of Heerlerheide fault	Emma	Central	Westveld	-150/-430	-270	87	357	164	164	-438	-325	0	0	0.00	0.00
38	49_56	W of Heerlerheide fault	Emma	Central	Westveld	-180/-220	-200	87	287	46	46	-438	-325	0	0	0.00	0.00
38	50	S of Boekelo-fault	Hendrik	South	Zuidveld	-480/-550	-510	87	597	67	100	-438	-325	113	1130000	12.66	0.06
38	41_50	North	Hendrik	South	Zuidveld	-600/-660	-630	87	717	67	100	-438	-325	113	1130000	12.66	0.07
38	57	South	Hendrik	South	Zuidveld	-310/-390	-350	87	437	67	100	-438	-325	25	250000	2.80	0.02
37	48_49_55_56	W of Heerlerheide fault	Emma	Central	Westveld	-130/-500	-300	87	387	138	138	-438	-325	0	0	0.00	0.00
37	41_50	NW of 70 m fault	Hendrik	South	Zuidveld	-400/-720	-600	87	687	66	66	-438	-325	113	1130000	8.35	0.80
37	51_57_58	SE of 70 m fault	Hendrik	South	Zuidveld	-250/-510	-400	87	487	66	66	-438	-325	75	750000	5.54	0.14
36	48_49_55_56	W of Heerlerheide fault	Emma	Central	Westveld	-140/-500	-300	87	387	117	200	-438	-325	0	0	0.00	0.00
36	49_50_51_56_57	NW of 70 m fault	Hendrik	South	Zuidveld	-410/-680	-540	87	627	122	200	-438	-325	113	1130000	25.31	12.12
36	50_51_57_58	SE of 70 m fault	Hendrik	South	Zuidveld	-100/-530	-300	87	387	122	150	-438	-325	0	0	0.00	0.00
35	48_49_55_56	W of Heerlerheide fault	Emma	Central	Westveld	-160/-550	-330	87	417	98	110	-438	-325	5	50000	0.62	0.00
35	56_57	NW of 70 m fault	Hendrik	South	Zuidveld	-500/-540	-510	87	597	146	140	-438	-325	113	1130000	17.72	0.32
35	57_58	SE of 70 m fault	Hendrik	South	Zuidveld	-220/-340	-260	87	347	146	140	-438	-325	0	0	0.00	0.00
32	55_56	W of Heerlerheide fault	Emma	Central	Westveld	-110/-360	-240	87	327	135	135	-438	-325	0	0	0.00	0.00
32	41_50_57	NW of 70 m fault	Hendrik	South	Zuidveld	-580/-810	-670	87	757	165	170	-438	-325	113	1130000	21.52	2.25
32	50_51_57_58	SE of 70 m fault	Hendrik	South	Zuidveld	-250/-660	-500	87	587	165	170	-438	-325	113	1130000	21.52	2.09
27	48_49_54_55_56	W of Heerlerheide fault	Emma	Central	Westveld	-150/-600	-350	87	437	107	110	-438	-325	25	250000	3.08	0.01
27	57	SE of 70 m fault_I	Hendrik	South	Zuidveld	-680/-720	-700	87	787	136	140	-438	-325	113	1130000	17.72	0.43
27	51_57_58	SE of 70 m fault_II	Hendrik	South	Zuidveld	-110/-620	-340	87	427	136	150	-438	-325	15	150000	2.52	0.04
																Total	27.97

When the sediment cover is flooded (mine water level 10 and higher), additional decompaction of the sediment occurs. The total resulting ground heave, due to the decompaction of the disturbed rock in the Carboniferous and that in the sediment cover, is shown in blue. As stated above, in practice the rate of the mine water rise is variable, with periods of stagnation, acceleration and deceleration. Therefore, in reality the time series of ground heave will be slightly more complex.

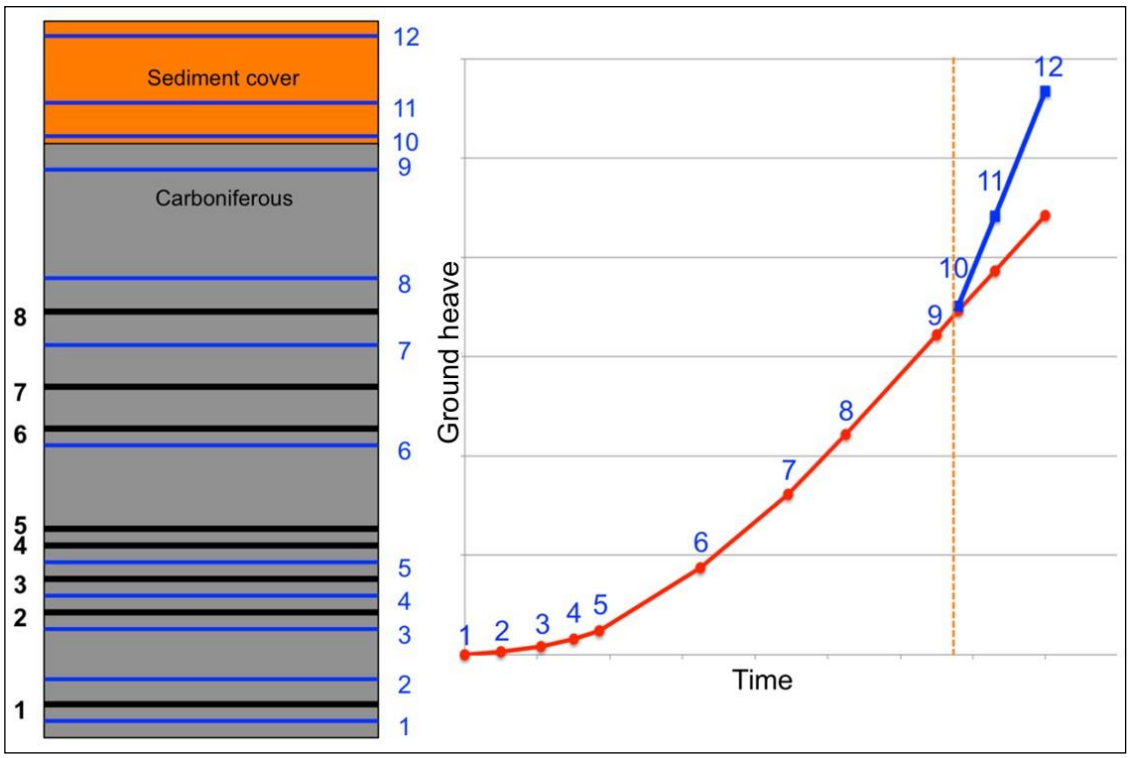

Fig. B 13: Schematic development of ground heave at a constant rate of the mine water rise. See text for explanation

3.3 Results and interpretation

The results for key points 1-5 are shown in Fig. B 14 to Fig. B 18; in these figures the mine water level is represented by a brown graph line, the calculated ground heave due to decompaction in the Carboniferous is shown in red, and the ground heave, measured at the benchmark, is shown in blue. Additionally the NAP level of the base of the sediment cover at the key point is shown.

A common feature is that, if the right decompaction factor is applied, the calculated and measured curves match initially, but then diverge when the sediment cover is flooded. The difference between the measured and calculated ground heave is attributed to the ground heave due to decompaction of the sediment cover, and is indicated in yellow in Fig. B 14 to Fig. B 18.

The applied decompaction coefficients are shown in Tab. B 4. The values vary from $2{,}5 \cdot 10^{-9}$ to $3{,}5 \cdot 10^{-9}$ m^2/N, and fit within the range of previously established data (Tab. B 5).

Tab. B 4: Decompaction coefficients applied for key points 1 to 5

Key point	Benchmark	D_m [m²/N]
1	060D0050	$2{,}80 \cdot 10^{-9}$
2	060D0099	$2{,}80 \cdot 10^{-9}$
3	062B0241	$3{,}50 \cdot 10^{-9}$
4	062E0015	$2{,}50 \cdot 10^{-9}$
5	062E0034	$2{,}50 \cdot 10^{-9}$

For key point 2 the decompaction coefficient of $2{,}8 \cdot 10^{-9}$ m^2/N proved to be less than the value of $3{,}5 \cdot 10^{-9}$ m^2/N, derived by PÖTTGENS.

For key points 1, 2, and 3 the divergence seems to have occurred about 2 years before the mine water reached the sediment cover. This can be explained by the slope of the top of the Carboniferous. Downdip from the key point the mine water reached the sediment cover earlier than directly under the key point itself. Decompaction of the lower part of the sediment cover downdip from the key point could have brought about ground heave already at the key point, because the ground movement is distributed laterally (chap. 2.4 and chap. 2.5).

Tab. B 5: Measured decompaction coefficients for disturbed rock over coal extractions

	D_m broken rock [m²/N]	
Caved goaf South Limburg	$3{,}50 \cdot 10^{-9}$	PÖTTGENS (1985)
Well packed shale goaf	$4{,}00 \cdot 10^{-9}$	MUKHERJEE et al. (1993)
Normally packed shale goaf	$5{,}70 \cdot 10^{-9}$	MUKHERJEE et al. (1993)
Loosely packed shale goaf	$7{,}20 \cdot 10^{-9}$	MUKHERJEE et al. (1993)
Caved goaf Zwickau	$2{,}40 \cdot 10^{-9}$	FENK (1998, 2006)
Caved goaf Ibbenbüren	$4{,}60 \cdot 10^{-9}$	GOERKE-MALLET (2000)
Fractured rock	$3 \cdot 10^{-10}$ to $7 \cdot 10^{-9}$	DOMENICO & MIFFLIN (1965)

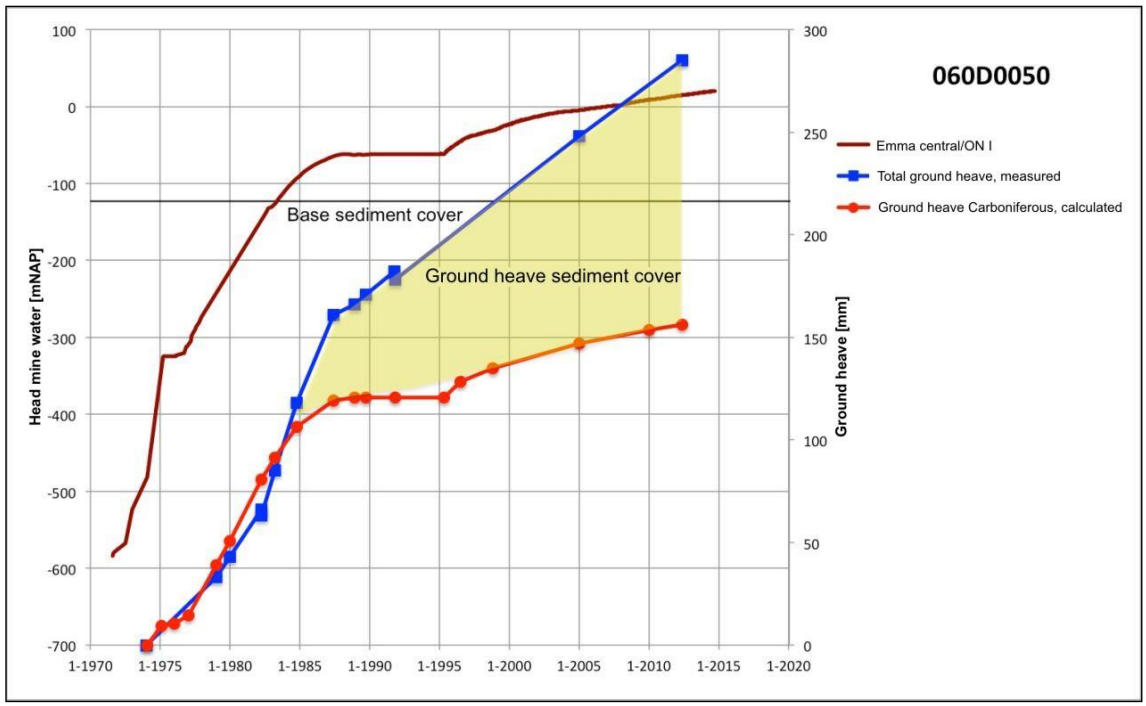

Fig. B 14: Time series for key point 1 of calculated ground heave due to decompaction in the Carboniferous, and of measured ground heave, including ground heave due to decompaction in the sediment cover

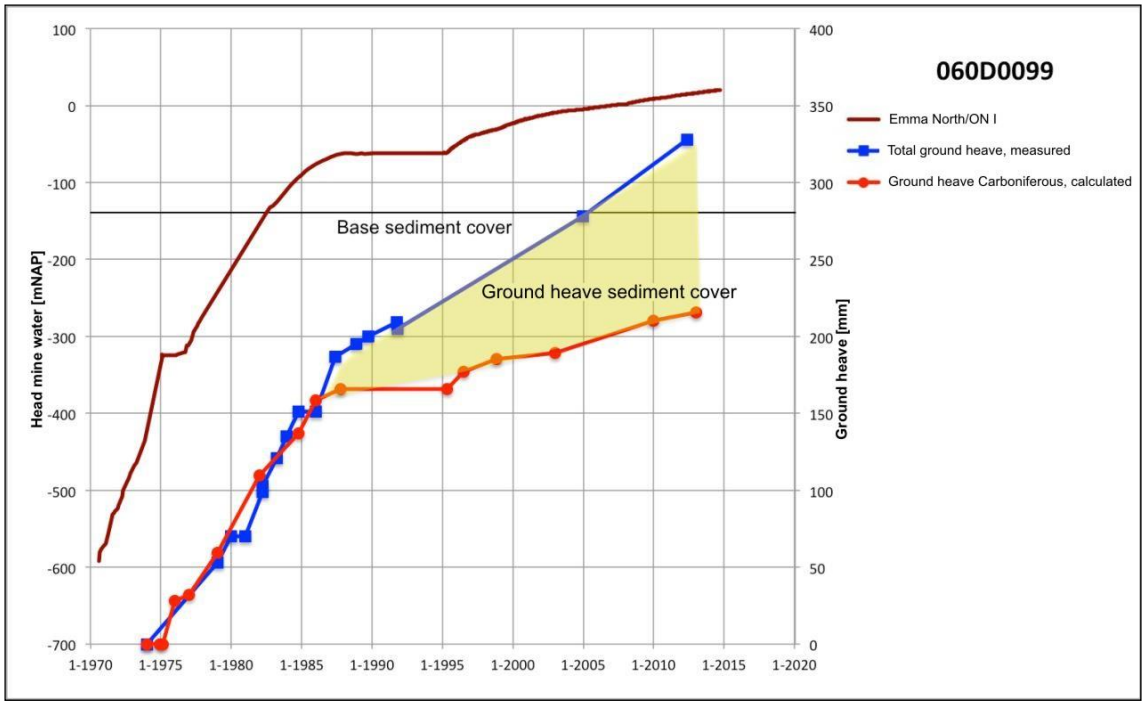

Fig. B 15: Time series for key point 2 of calculated ground heave due to decompaction in the Carboniferous, and of measured ground heave, including ground heave due to decompaction in the sediment cover

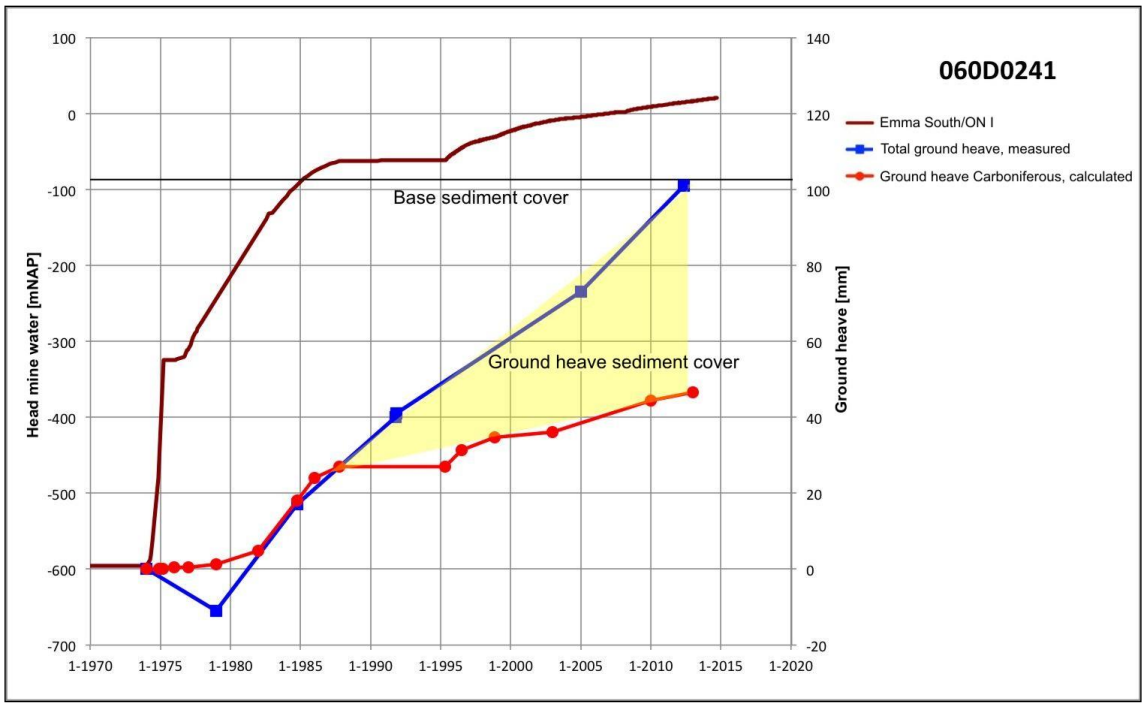

Fig. B 16: Time series for key point 3 of calculated ground heave due to decompaction in the Carboniferous, and of measured ground heave, including ground heave due to decompaction in the sediment cover

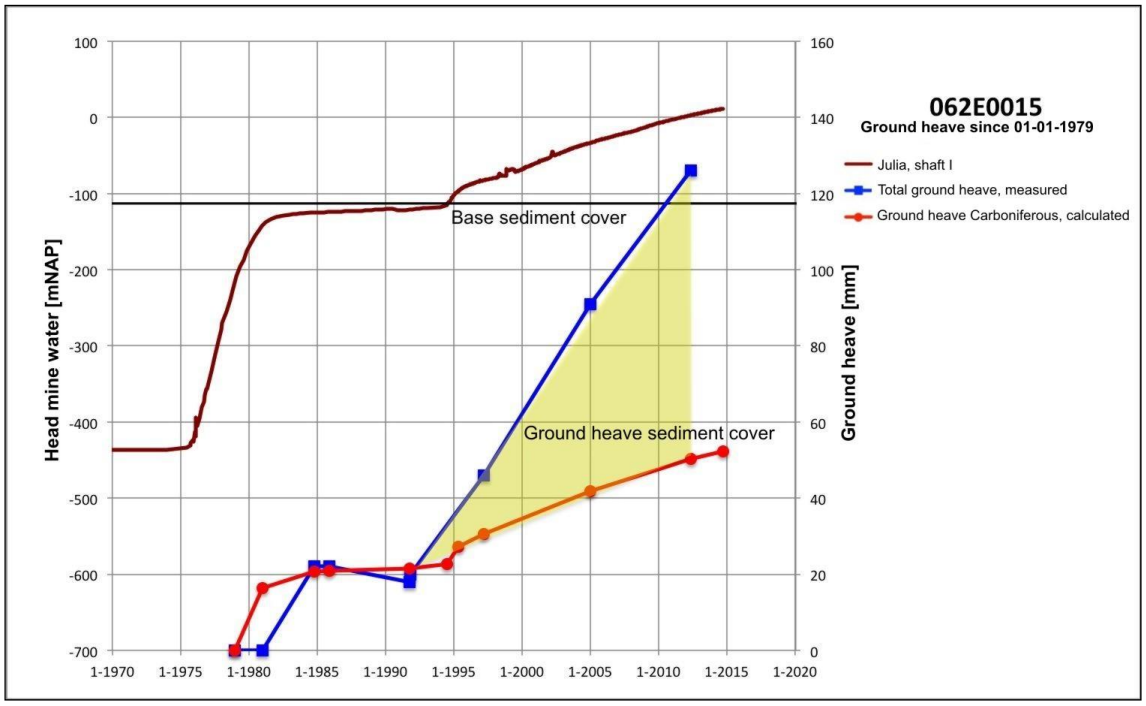

Fig. B 17: Time series for key point 4 of calculated ground heave due to decompaction in the Carboniferous, and of measured ground heave, including ground heave due to decompaction in the sediment cover

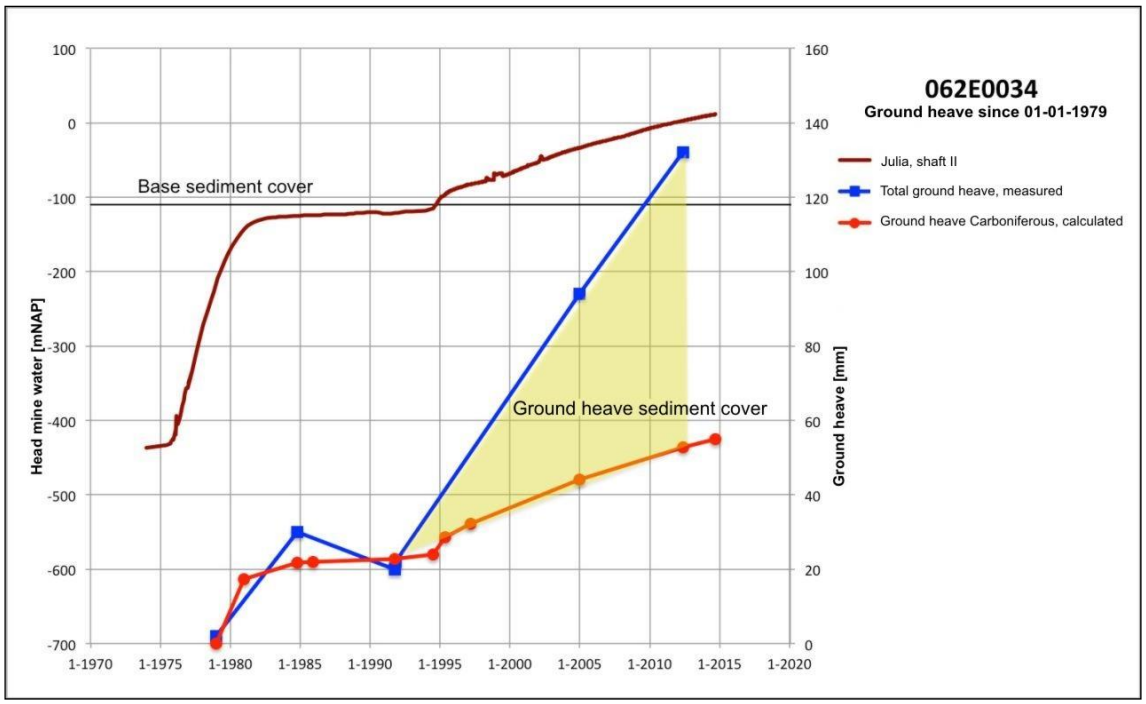

Fig. B 18: Time series for key point 5 of calculated ground heave due to decompaction in the Carboniferous, and of measured ground heave, including ground heave due to decompaction in the sediment cover

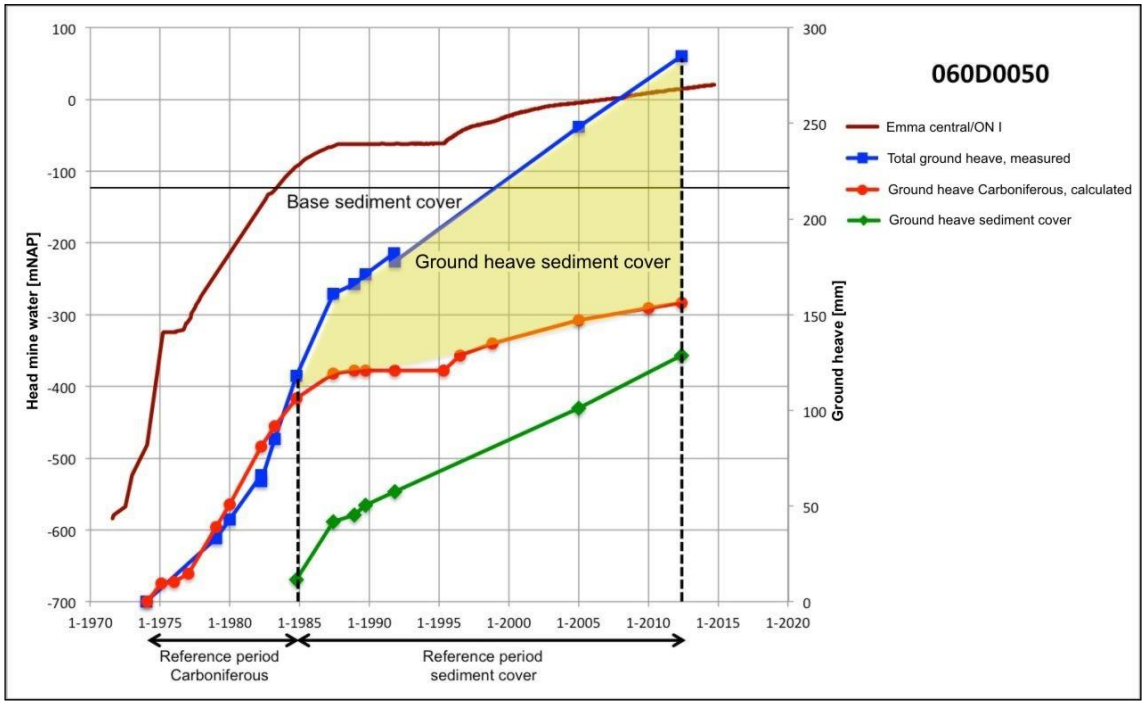

Fig. B 19: Reference periods for the assessment of decompaction parameters of the disturbed rock in the Carboniferous and of the sediment cover

3.4 Calculation of ground heave due to decompaction of the sediment cover

In chap. 3.3 it was shown that the ground heave due to decompaction of the sediment cover equals the difference between the measured (total) ground heave and the calculated ground heave due to decompaction in the Carboniferous, from the moment both time curves began to diverge. In the time series of ground heave two reference periods can be defined (Fig. B 19):

- A reference period 1 from the beginning of the ground heave until such time that decompaction in the sediment cover begins, and both curves mentioned above start to diverge. This reference period is related to ground heave, caused by decompaction in the Carboniferous, and serves to determine the decompaction coefficient of the disturbed rock over the coal extractions.
- A subsequent reference period 2, which starts at the moment both time curves begin to diverge. This reference period is related to ground heave, caused by both decompaction in the Carboniferous and the sediment cover. This period is to be used for the assessment of the decompaction coefficients of the layers in the sediment cover, knowing already the decompaction coefficient of disturbed rock over the coal extractions.

3.4.1 Method 1: using decompaction coefficients and hydraulic heads

In chap. 2.7 it was explained how, once the mine water reaches the top of the Carboniferous, the hydraulic heads in the layers of the sediment cover start to rise as well. The decompaction coefficients of the layers in the sediment cover can be assessed as follows:

- Simplify the stratigraphy, derived from REGIS v2.1.
- Construct time curves of the measured heads for the different sediment layers during the reference period for the sediment cover.

- Assess the decompaction coefficient D_m for each layer, considering the range of literature values, and calculate the ground heave. Contrary to ground heave due to decompaction of broken rock over coal extractions, for the sediment cover the ground heave equals the decompaction. Thus, no influence function has to be applied (chap. 2.7).
- Repeat the calculation until the values of D_m are such that the calculated and measured ground heave due to decompaction of the whole sediment cover matches.

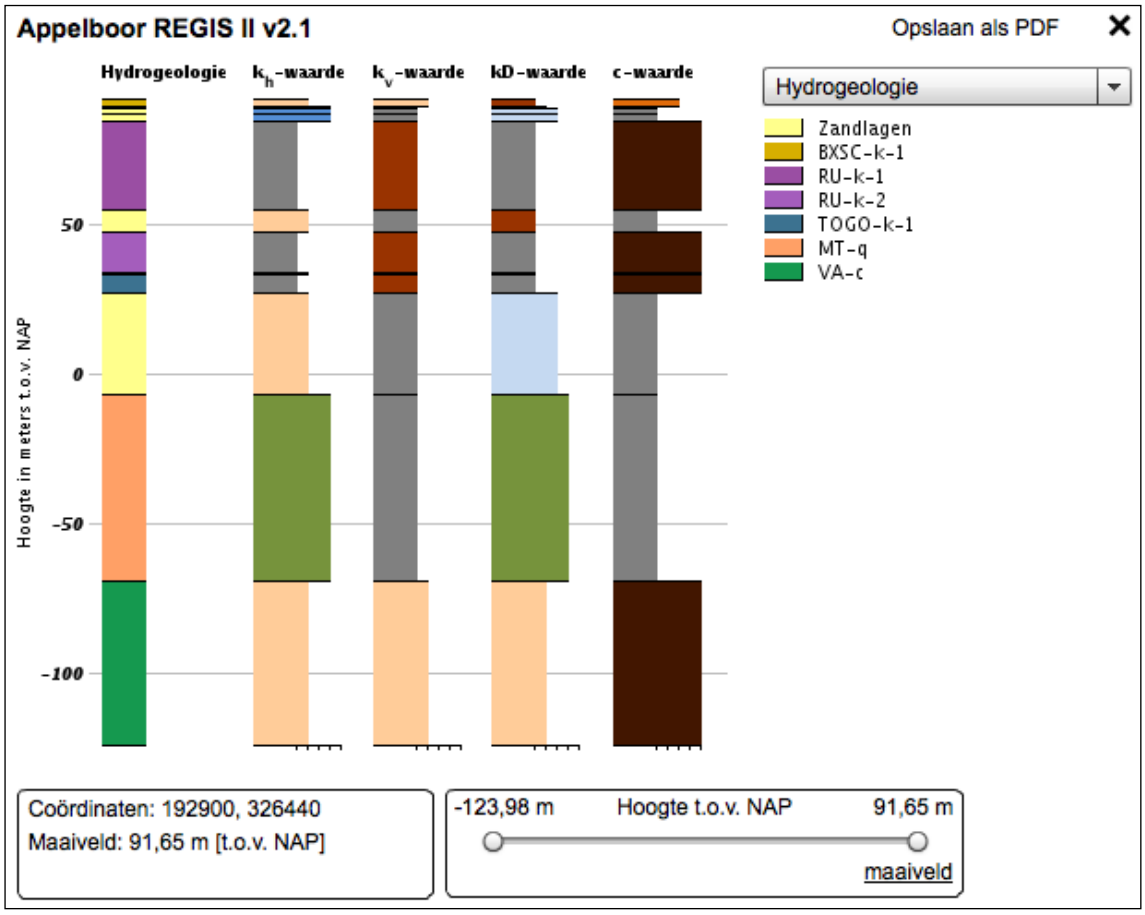

Fig. B 20: Stratigraphy at key point 1 (benchmark 060D0050)

Unfortunately, hydraulic heads in deep layers of the sediment cover have been measured in just 4 wells (Fig. B 10). Therefore the method can only be applied at key points 1 (060D0050) and 3 (060B0241), where hydraulic heads in a large part of the sediment cover are available.

Fig. B 20 and Fig. B 21, and Tab. B 6 and Tab. B 7 show the stratigraphy and the conductivities of the individual layers for both key points, according to REGIS v2.1. The sediment cover comprises the clayey Vaals formation of a low conductivity and the limestones of the Maastricht formation of a moderate conductivity. The upper part of the sediment cover of key point 1 contains more layers of low conductivity (clayey units of the Rupel and Tongeren formations) than key point 3.

Tab. B 6: Stratigraphy and conductivities at key point 1 (benchmark 060D0050)

NAP [m]		Depth [m]						
From	to	From	to	Formation	Subunit	Lithology	k_v [m/day]	k_d [m/day]
"Appelboor" 060D0050								
91.65	89.03	0	2.62	Boxtel Formation	Schimmert	clay, sandy clay, clayey sand	0.001 to 1	<1
89.03	88.99	2.62	2.66	Boxtel Formation	3e sandy unit	sand (fine to coarse), gravel		1 to 10
88.99	88.43	2.66	3.22	Breda Formation	2e sandy unit	sand (fine to coarse), gravel		1 to 10
88.43	86.81	3.22	4.84	Breda Formation	3e sandy unit	sand (fine to coarse), gravel		10 to 100
86.81	84.12	4.84	7.53	Breda Formation	4e sandy unit	sand (fine to coarse), gravel		10 to 100
84.12	54.55	7.53	37.1	Rupel Formation	1e clayey unit	clay, sandy clay, clayey sand	< 0.001	
54.55	47.18	37.1	44.47	Rupel Formation	2e sandy unit	sand (fine to coarse), gravel		<1
47.18	33.9	44.47	57.75	Rupel Formation	2e clayey unit	clay, sandy clay, clayey sand	< 0.001	
33.9	32.94	57.75	58.71	Rupel Formation	3e sandy unit	sand (fine to coarse), gravel		<1
32.94	26.89	58.71	64.76	Tongeren Formation	Goudsberg	clay, sandy clay, clayey sand	< 0.001	
26.89	-6.75	64.76	98.4	Tongeren Formation	2e sandy unit	sand (fine to coarse), gravel		10 to 100
-6.75	-69.24	98.4	160.89	Maastricht Formation		limestone		100 to 1000
-69.24	-123.24	160.89	214.89	Vaals Formation		altern. sandy and clayey layers	0.001 to 1	1 to 10

Tab. B 7: Stratigraphy and conductivities at key point 3 (benchmark 060B0241).

NAP [m]		Depth [m]						
From	to	From	to	Formation	Subunit	Lithology	k_v [m/day]	k_d [m/day]
"Appelboor" 060D0241								
86.83	79.15	0	7.68	Boxtel Formation	Schimmert	clay, sandy clay, clayey sand		<1
79.15	78.98	7.68	7.85	Boxtel Formation	2e sandy unit	sand (fine to coarse), gravel		10 to 100
78.98	77.89	7.85	8.94	Boxtel Formation	3e sandy unit	sand (fine to coarse), gravel		10 to 100
77.89	75.86	8.94	10.97	Tongeren Formation	1e sandy unit	sand (fine to coarse), gravel		1 to 10
75.86	54.08	10.97	32.75	Tongeren Formation	2e sandy unit	sand (fine to coarse), gravel		10 to 100
54.08	-1.45	32.75	88.28	Maastricht Formation		limestone		100 to 1000
-1.45	-80.69	88.28	167.52	Vaals Formation		altern. sandy and clayey layers		1 to 10
-80.69	-85.24	167.52	172.07	Aken Formation		clay, sandy clay, clayey sand	0.001 to 1	10 to 100

At well B62B0837, at about 175 m distance from key point 1, the hydraulic heads in the Maastricht and Boxtel-Breda formations show a fairly strong correlation with the development of the mine water level (Fig. B 22). This also applies to the Vaals formation, apart from a decrease in head from 1985 to 1995. From 1995 onwards the increase in head was clearly largest in the deepest level (Vaals formation) and diminished to the shallower levels of the Maastricht and Boxtel-Breda formations. Of course the hydraulic heads are affected by variations in precipitation and groundwater withdrawal as well.

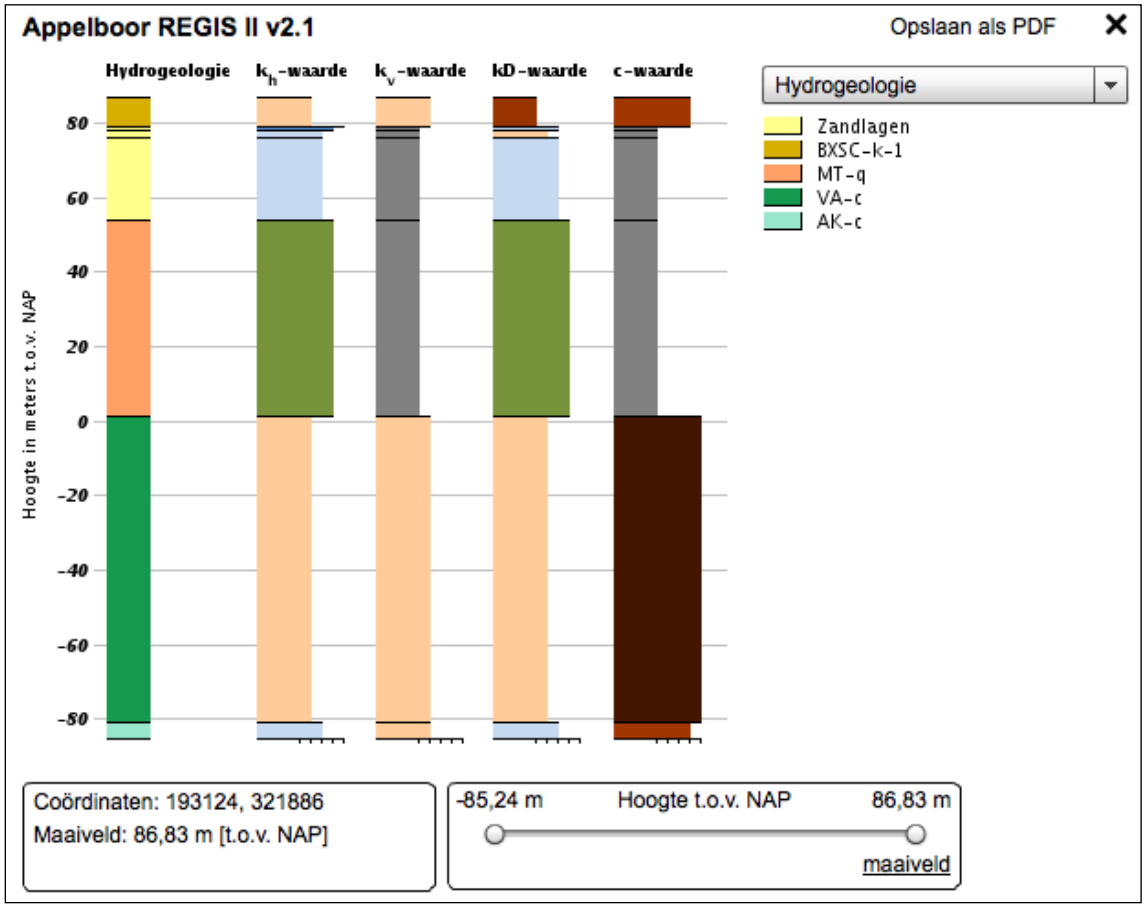

Fig. B 21: Stratigraphy at key point 3 (benchmark 060B0241)

Also at well B62B0838, at about 65 m distance from key point 3, a strong correlation exists between the hydraulic heads in the sediment cover and the mine water level (Fig. B 23). The graph also depicts time curves for the Beegden (a shallow unit) and Maastricht formations which were determined by the IBRAHYM model, and delivered by WG 5.2.4/5.2.5. Because the IBRAHYM model contains only the sediment cover, and does not take the Carboniferous into account, the curves show a development which is opposite what has been measured, and cannot be used for the calibration of the ground heave calculations.

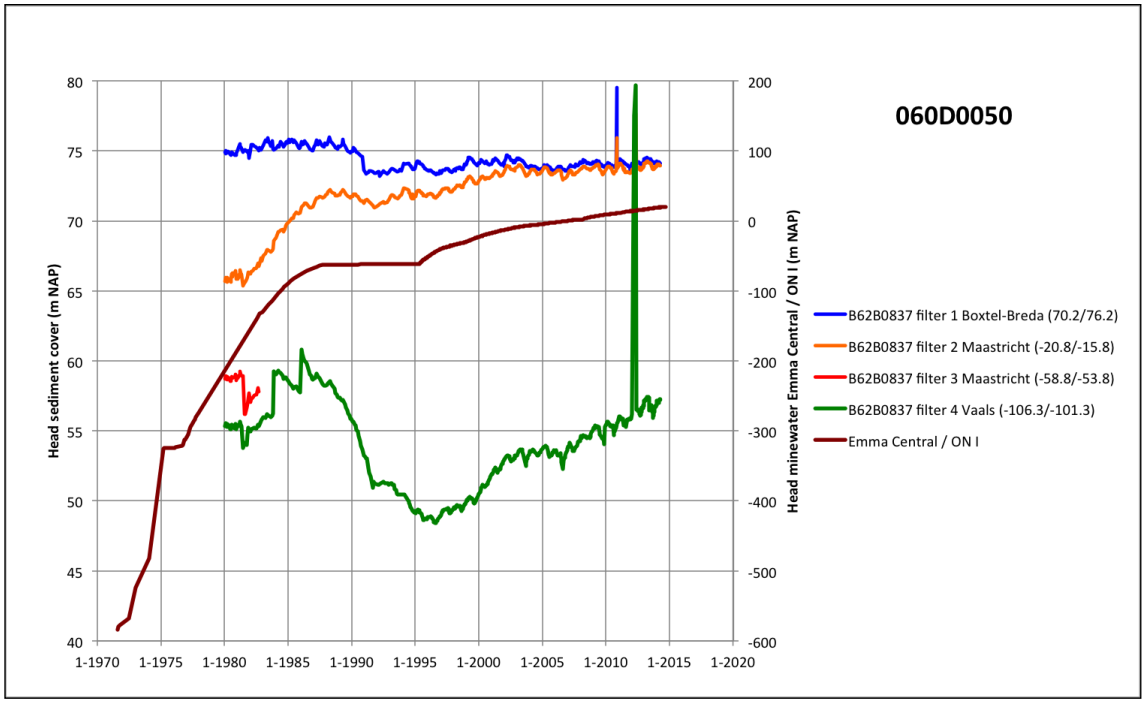

Fig. B 22: Time series of hydraulic heads in the sediment cover, measured at well B620837

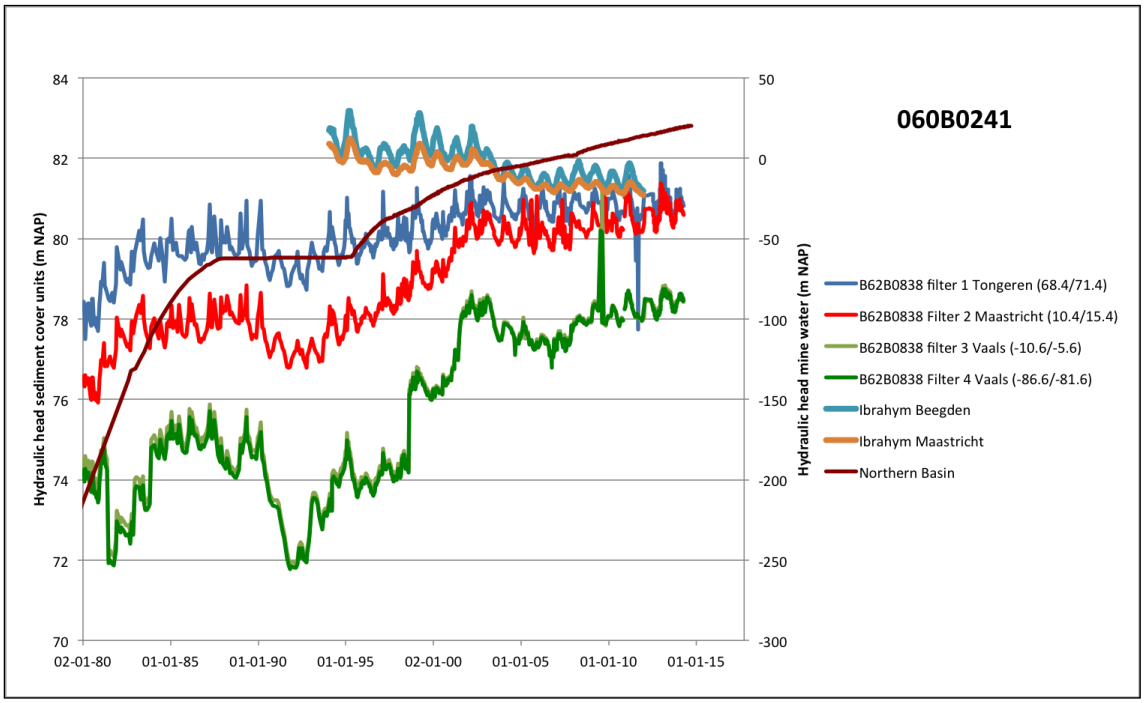

Fig. B 23: Time series of hydraulic heads in the sediment cover, measured at well B62B0838

The decompaction coefficients were estimated using literature values, as listed in Tab. B 8. GIESE (2010) studied in great detail the (de)compaction behaviour of soil units, which also occur at key points 1 and 3, near lignite open pit mines within 25 km distance of South Limburg coal district.

Tab. B 8: Literature data of decompaction coefficients for various soil types

Typical values of D_m for other rock and soil types [m²/N]	Min	max	
Soft clay	3.00E-07	2.00E-06	Domenico and Mifflin (1965)
Stiff clay	7.00E-08	3.00E-07	Domenico and Mifflin (1965)
Loose sand	5.00E-08	1.00E-07	Domenico and Mifflin (1965)
Dense sand, gravel	5.00E-09	2.00E-08	Domenico and Mifflin (1965)
Sound rock		< 3E-10	Domenico and Mifflin (1965)
Sandstone Groningen gasfield	4.50E-11	7.50E-11	NAM (2000)
Clayey soil (min/max at 25/200 m depth)	6.2E-10	1.8E-07	Giese (2010)
Sandy soil (min/max at 25/200 m depth)	3.1E-10	2.9E-09	Giese (2010)

However, he established the (de)compaction parameters only for the relatively shallow soil units, and not for the Vaals, Maastricht, and Tongeren formations. The shallow part was subdivided in a detailed way into small units, which often

cannot be distinguished in the description from REGIS v2.1. Furthermore, the assessment of decompaction coefficients for soil is more complicated than that for rock, because (de)compaction soil is strongly non-linear (VERRUIJT, 1999):

$$\varepsilon = -\frac{1}{C} \cdot \ln\left(\frac{\sigma}{\sigma_1}\right) \quad (13)$$

where ε is the vertical deformation, σ the stress and σ_1 the initial stress. C is the dimensionless (de)compaction constant. From Eq. 13 it can be concluded that the amount of (de)compaction depends on the depth of the soil layer. GIESE related his (de)compaction constant C_c to the void ratio e, instead of the strain. The decompaction coefficient for a given void ratio and stress (related to depth) can be written as follows:

$$D_m = \frac{C_C}{1+e} \cdot \frac{1}{\sigma_1} \quad (14)$$

The decompaction coefficients from GIESE in Tab. B 8 represent the minimum and maximum values which result from the application of Eq. 14 to his results.

As outlined in chap. 2.7, it is difficult to assess the decompaction coefficients for each sediment layer separately, when the ground heave is only known of the sediment as a whole. GIESE did not experience this problem because extensometer measurements at various levels in the subsurface were available. Therefore the stratigraphy of Tab. B 6 and Tab. B 7 were simplified, and compaction coefficients from Tab. B 8 were adjusted such that the calculated ground heave matched the measured value. The hydraulic head has not been measured in all layers. For the Aken and Tongeren formations a raise in head is estimated, based on the principle that the increase in head becomes less from deep to shallow layers. The decompaction coefficient for the Maastricht formation was derived from measured values of the unloading E-modulus (BEKENDAM, 1998). The results are listed in Tab. B 9 and Tab. B 10.

3.4.2 Method 2: using the relation between ground heave and mine water head

During a further rise of the mine water level, the difference between hydraulic heads in the sediment layers and that of the mine water is reduced (chap. 2.7). As a result, the influx of water from the sediment layers into the Carboniferous decreases, and the heads in the sediment layers is raised. It can be reasoned that a more or less linear relation exists between the rise of the mine water head and the rise of the heads in the sediment layers. This means that ground heave due to decompaction of the sediment cover is linearly related to the change in mine water head.

Tab. B 9: Results of the ground heave calculation due to decompaction of the sediment cover for key point 3

NAP From [m]	to [m]	Thickness [m]	Formation	1-7-87 to 13-5-2012: Raise head [m]	Increase pressure [N/m²]	D_m Proposed [m²/N]	Δh Calc. [mm]	Δh Meas. [mm]
86.83	77.89	8.94	Boxtel Formation	0	0.00E+00	1.00E-08	0.00	
77.89	54.08	23.81	Tongeren Formation	1	1.00E+04	1.00E-07	23.81	
54.08	-1.45	55.53	Maastricht Formation	2.5	2.50E+04	4.0E-10	0.56	
-1.45	-80.69	79.24	Vaals Formation	3.5	3.50E+04	1.00E-08	27.73	
-80.69	-85.24	4.55	Aken Formation	3.5	3.50E+04	1.00E-08	1.59	
Total decompaction sediment cover							**53.69**	**55.5**

Tab. B 10: Results of the ground heave calculation due to decompaction of the sediment cover for key point 1

NAP From [m]	to [m]	Thickness [m]	Formation	15-10-1984 to 13-5-2012: Raise head [m]	Increase pressure [N/m²]	D_m Proposed [m²/N]	Δh Calc. [mm]	Δh Meas. [mm]
91.65	84.12	7.53	Boxtel-Bredal Formation	-1.5	-1.50E+04	1.00E-08	-1.13	
84.12	32.94	51.18	Rupel Formation	0	0.00E+00	1.00E-07	0.00	
32.94	-6.75	39.69	Tongeren Formation	3.4	3.40E+04	1.00E-07	134.95	
-6.75	-69.24	62.49	Maastricht Formation	3.8	3.80E+04	4.0E-10	0.95	
-69.24	-123.24	54.00	Vaals Formation	-0.9	-9.00E+03	1.00E-08	-4.86	
Total decompaction sediment cover							**129.91**	**129**

This method does not require the assessment of the decompaction coefficients of the sediment cover. Just the mine water heads have to be considered from the beginning of the decompaction of the sediment cover till the last measurement of the ground heave.

To verify this concept the ground heave due to decompaction in the Carboniferous was calculated for each levelling measurement in the second reference period. The ground heave due to decompaction of the sediment cover was obtained by subtracting this calculated value from the measured total ground heave. Then for each key point the ground heave due to decompaction in the sediment cover was depicted in Fig. B 24 versus the head of the mine water.

Clearly a correlation exists between this ground heave and the mine water head for all key points. For key points 1 (060D0050) and 2 (060D0099) the ground heave slightly increases during stagnation of the mine water level, but this could be explained by time-dependent groundwater flow.

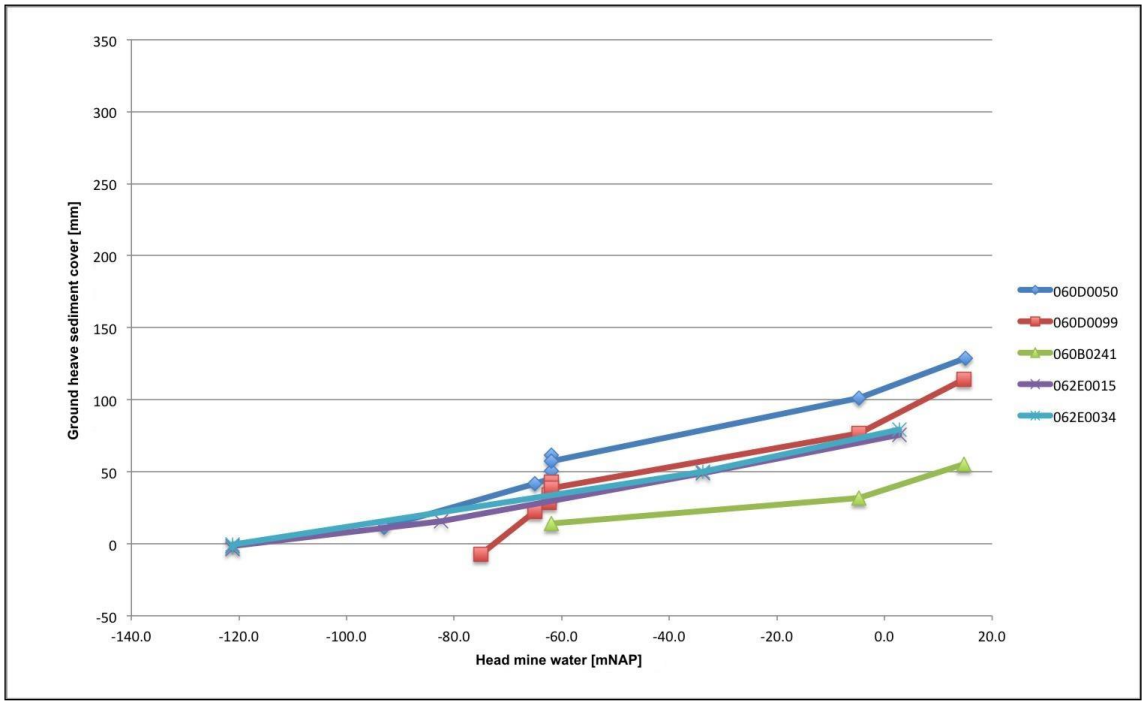

Fig. B 24: Ground heave due to decompaction of the sediment cover versus mine water head for the 5 key points

It can be reasoned that such a correlation applies to the ground heave due to decompaction in the Carboniferous as well, from the moment all extractions are flooded. Indeed, the correlation is obvious (Fig. B 25).

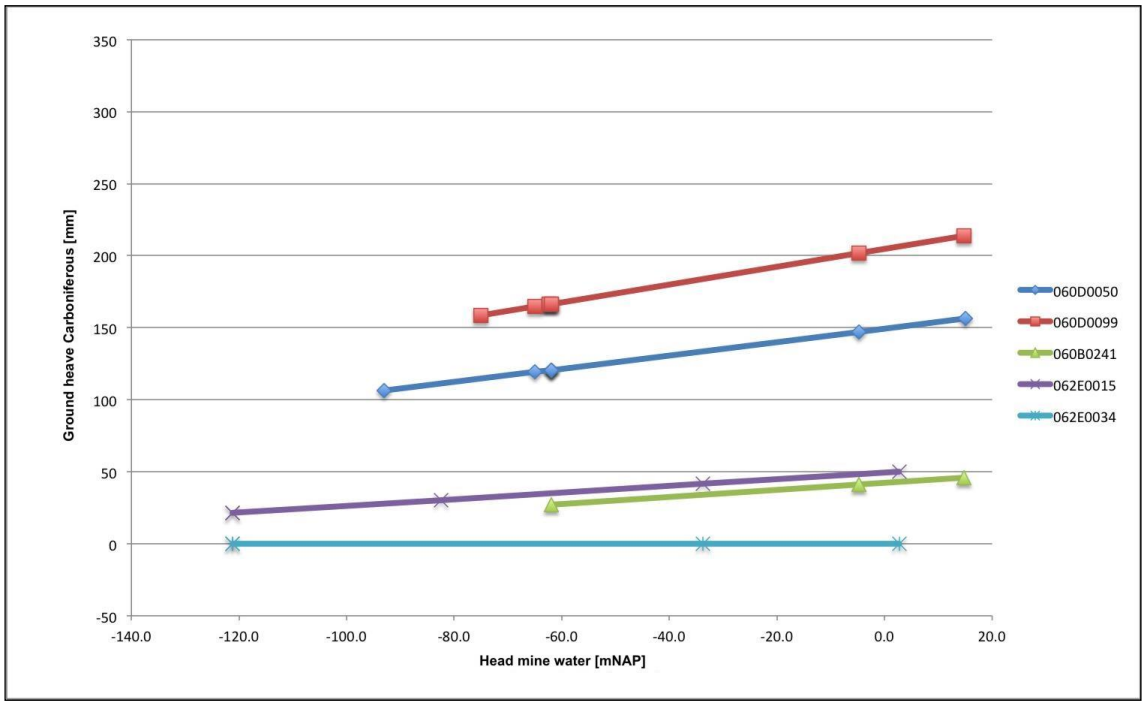

Fig. B 25: Ground heave due to decompaction in the Carboniferous versus mine water head for the 5 key points

Because both the ground heave due to decompaction in the Carboniferous and the ground heave due to decompaction in the sediment cover are correlated to the mine water head, the total ground heave must be correlated to the mine water head as well. This reasoning can be expressed in the following equation:

$$u_{z,\,total} = u_{z,\,Carb} + u_{z,\,sed} = A \cdot h_{mw} + B \cdot h_{mw} = (A + B) \cdot h_{mw} = C \cdot h_{mw} \qquad (15)$$

where $u_{z,total}$, $u_{z,Carb}$ and $u_{z,sed}$ signify the total ground heave, the ground heave due to decompaction in the Carboniferous and the ground heave due to decompaction in the sediment cover. A, B, and C are constants, and h_{mw} is the head of the mine

water. The constants A, B, and C are unique for each surface point. The validity of Eq. 15 is shown in Fig. B 26.

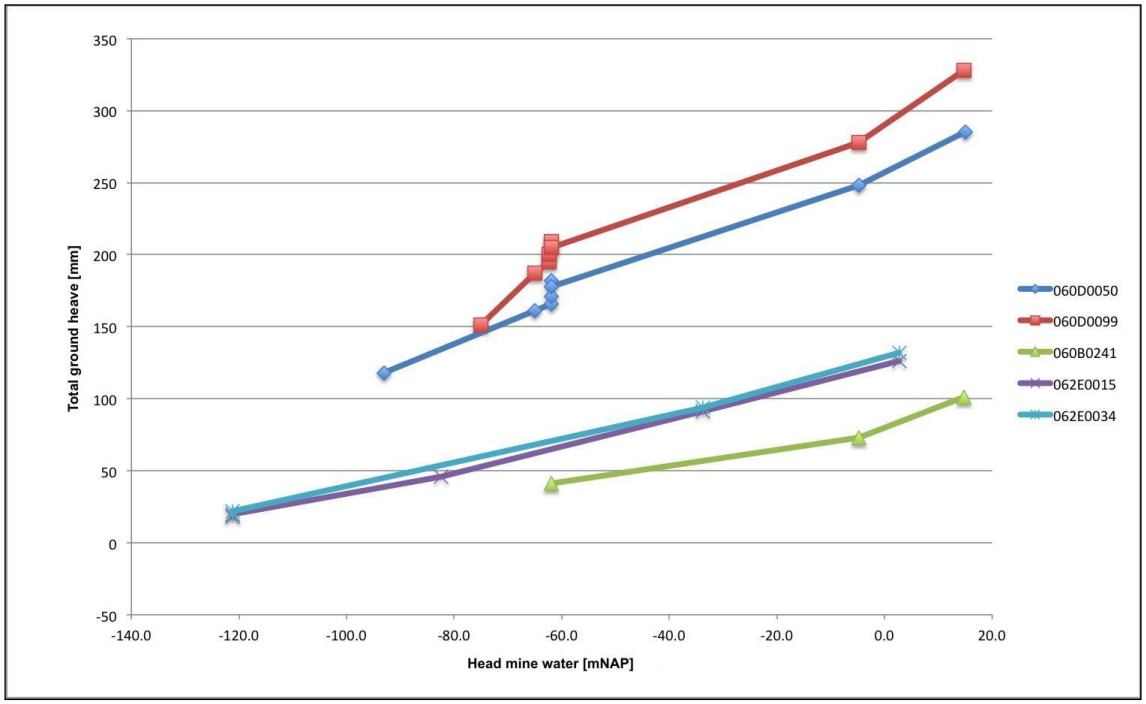

Fig. B 26: Total ground heave versus mine water head for the 5 key points

This is a useful result, because this formula enables to make a prognosis of future ground heave, for a given mine water head, quickly and efficiently for each surface point, where the sediment cover is flooded. In Part 1 of this working group detailed maps of vertical displacements were constructed on the basis of InSAR data for various periods. It is useful to verify the correlation using the several InSAR data points. If the verification is successful, it could be attempted to make a detailed ground heave prognosis for final mine water levels, using the concept outlined above.

3.5 Advantages and disadvantages of methods 1 and 2

The advantages (+) and disadvantages (-) of the different methods can be summarised as follows:

Method 1:

- Heads for the different sediment layers, calculated with the IBRAHYM model, differ significantly from the measured heads, since the mine water rise is not included in the model. Therefore the IBRAHYM results cannot be used to calculate the values of D_m for the reference period.
- In most wells only hydraulic heads have been measured in sediments at shallow levels. In the mining area only 4 wells exist where the hydraulic heads have been measured in deeper sediment layers. Therefore, method 1 can be applied in a very limited part of the mining area.
- Even if hydraulic heads are also available for deeper sediment layers for the reference period, these data were measured for a limited number of layers. For other layers the time series of heads must be interpreted.
- For most sediment layers no reliable values of D_m exist, and general literature values must be used.
- When time series of measured and calculated ground heave are compared, D_m cannot be established for layers separately. It is only possible to assess a combination of D_m for the various layers which fit best.
- This combination of D_m values fit for one location, but will probably not always fit at other locations where the composition of the sediment cover is different.

\+ Theoretically the method is the most correct one.

Method 2:

- During the reference period groundwater extraction and variations in precipitation may have affected the heads of several sediment layers, and, as

a consequence, also the amount of ground heave. This effect is not taken into account, because the extrapolation is based on just the change of the mine water level.

\+ Method 2 is much less time consuming than method 1, and can be applied at any location of the mining area.

It must be concluded that method 1 is highly unpractical and not accurate in practice, because most parameters are not known exactly. Apart from one disadvantage, method 2 is more reliable, and can be applied relatively quickly at any location. Therefore method 2 is preferred.

4 Prognosis of final ground heave

4.1 Input parameters

A prognosis of the final ground heave was made, using, at key points 1 and 3, both methods for the determination of the ground heave due to decompaction of the sediment cover. For key points 2, 4, and 5 only method 2 was applied.

The final hydraulic heads of the mine water and the individual layers of the sediment cover were provided by WG 5.2.4/5.2.5. Three scenarios were distinguished, and these heads increase from best case, to average case to worst case scenario. The previously derived decompaction coefficients of Tab. B 4 were used to calculate the ground heave due to decompaction in the Carboniferous. The decompaction coefficients of Tab. B 9 and Tab. B 10 were applied for the calculation of the ground heave due to decompaction of the sediment cover according to method 1.

4.2 Results

The results for methods 1 and 2 are summarised in Tab. B 11 and Tab. B 13 respectively. In Tab. B 12 the results for methods 1 and 2 are compared.

The final ground heave, using both methods, is graphically presented in Fig. B 27 to Fig. B 30 for key points 1 and 3. The final ground heave for the remaining key points is depicted in Fig. B 31 to Fig. B 33. Method 2 extrapolates the ground heave due to decompaction of the sediment cover which developed during the second reference period, according to the ratio of the mine water rise during the reference period and that from the end of the reference period to the final situation.

Tab. B 11: Prognosis of final ground heave for the best, average, and worst case scenario, according to method 1

1	060D0050			Best	Average	Worst
	date	15-10-84	13-05-12		Final	
	Head mine water [mNAP]	-93.0	14.8	73.1	79.8	106.8
	Ground heave sediment cover [mm]	0.0	129.0	621.4	655.8	685.9
	Ground heave Carboniferous [mm]	106.3	156.2	183.1	186.2	198.7
	Total ground heave [mm]	106.3	285.2	804.5	842.0	884.5
3	062B0241			Best	Average	Worst
	Date	01-07-87	13-05-12		Final	
	Head mine water [mNAP]	-64.06	14.8	73.1	79.8	106.8
	Ground heave sediment cover [mm]	0	55.5	144.7	144.7	145.5
	Ground heave Carboniferous [mm]	27.0	45.7	59.8	61.4	68.0
	Total ground heave [mm]	27.0	101.2	204.5	206.1	213.5

Tab. B 12: Comparison of the ground heave due to decompaction of the sediment cover, calculated with methods 1 and 2

1	060D0050		Best	Average	Worst
Ground heave sediment cover [mm]		Method 1	621.4	655.8	685.9
Ground heave sediment cover [mm]		Method 2	198.8	206.8	239.1
3	062B0241		Best	Average	Worst
Ground heave sediment cover [mm]		Method 1	144.7	144.7	145.5
Ground heave sediment cover [mm]		Method 2	96.5	101.2	120.2

Method 1 predicts an ground heave, due to decompaction of the sediment cover, which exceeds the result according to method 2. For key point 1 the ground heave according to method 1 is even almost 3 times as large as that according to method 2. In chap. 3.5 it is already explained that method 1 is not reliable. Therefore only the results using method 2 are considered in this report from now on.

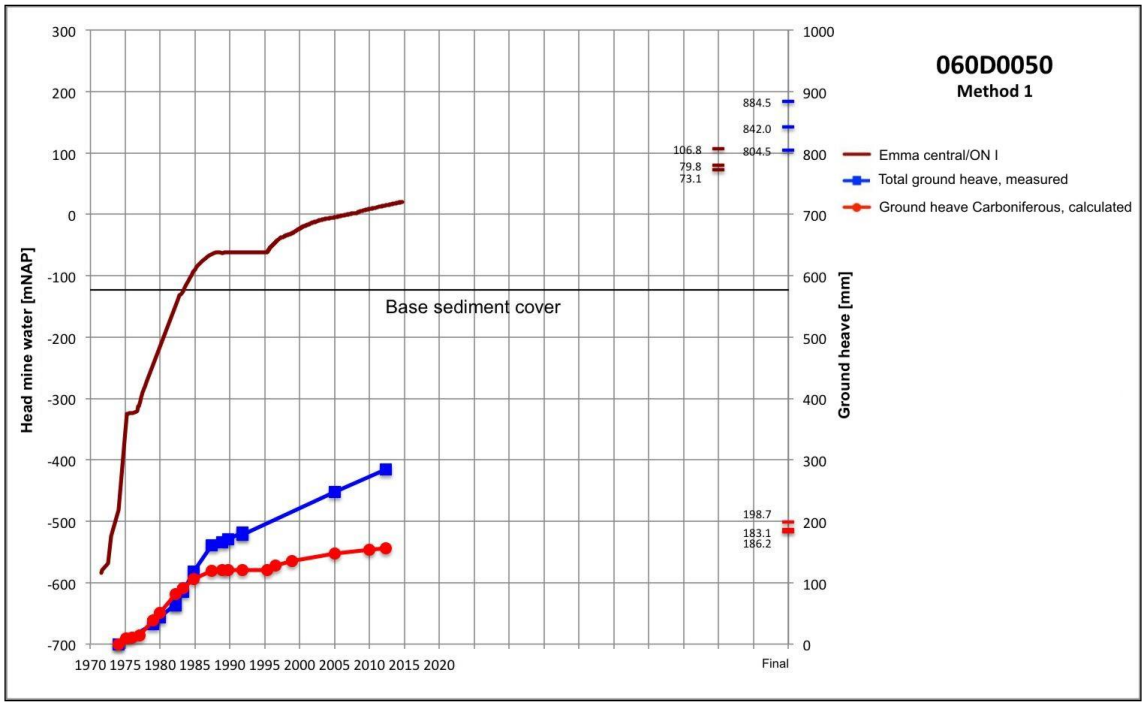

Fig. B 27:Prognosis of the total ground heave and the ground heave due to decompaction in the Carboniferous for key point 1, using method 1

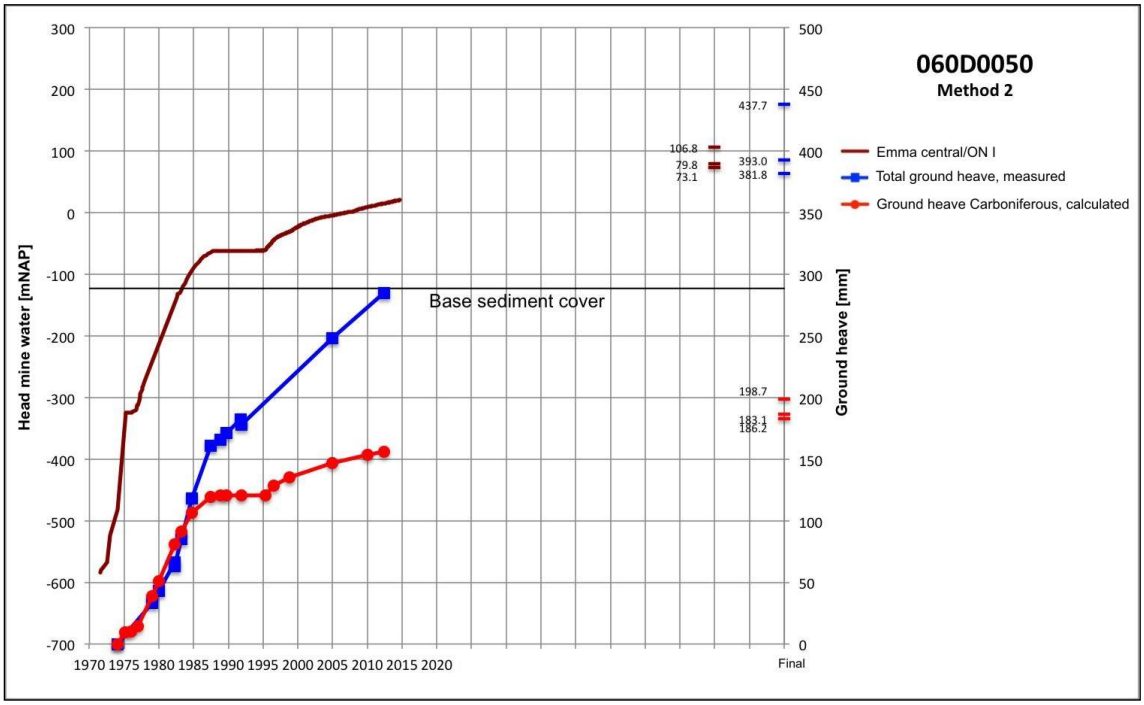

Fig. B 28: Prognosis of the total ground heave and the ground heave due to decompaction in the Carboniferous for key point 1, using method 2

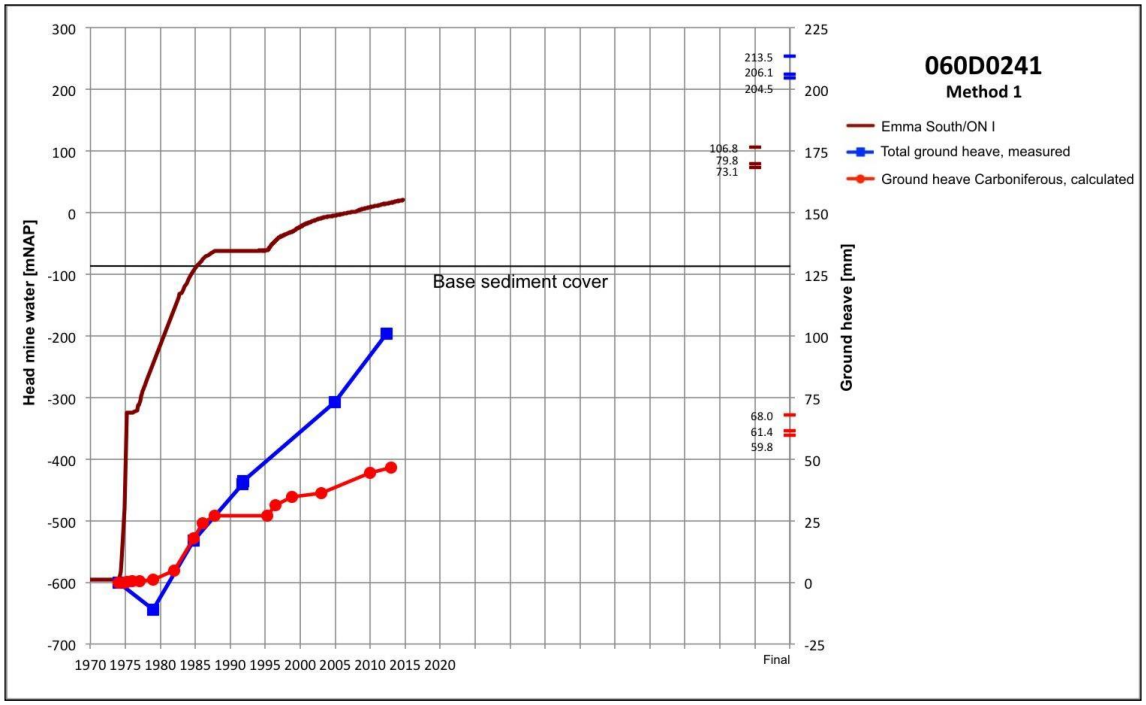

Fig. B 29: Prognosis of the total ground heave and the ground heave due to decompaction in the Carboniferous for key point 3, using method 1

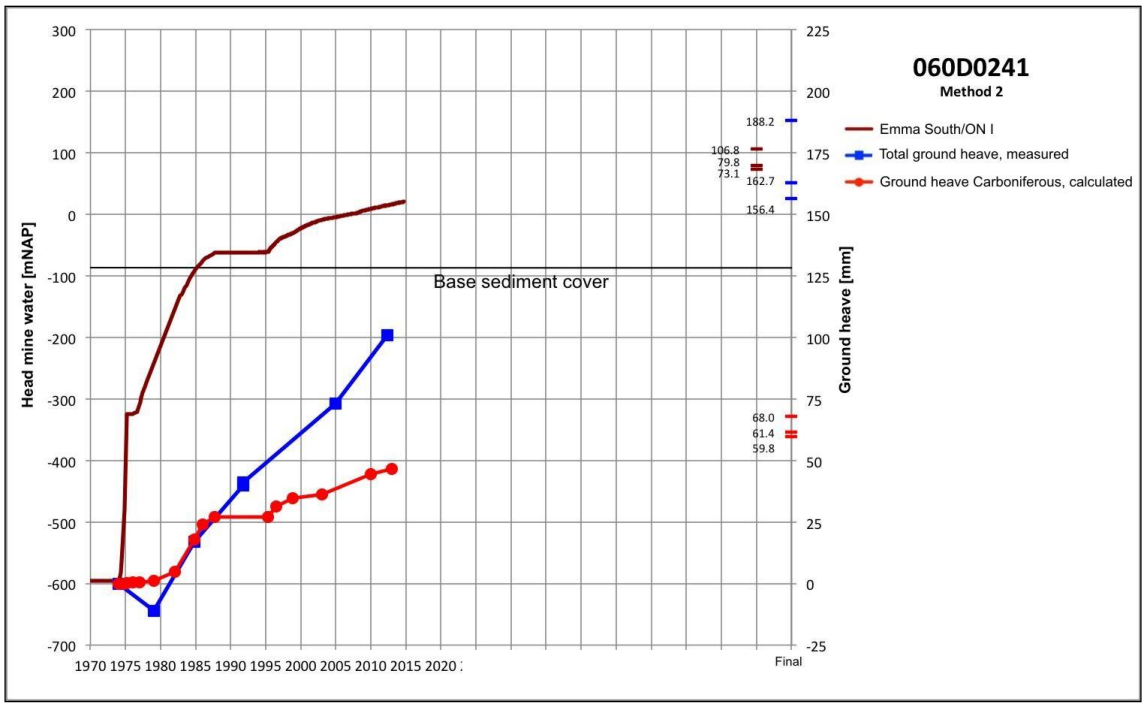

Fig. B 30: Prognosis of the total ground heave and the ground heave due to decompaction in the Carboniferous for key point 3, using method 2

Tab. B 13: Prognosis of final ground heave for the best, average, and worst case scenario, according to method 2

1	060D0050			Best	Average	Worst
	Date	15-10-84	13-05-12		Final	
	Head mine water [mNAP]	-93.0	14.8	73.1	79.8	106.8
	Ground heave sediment cover [mm]	0.0	129.0	198.8	206.8	239.1
	Ground heave Carboniferous [mm]	106.3	156.2	183.1	186.2	198.7
	Total ground heave [mm]	106.3	285.2	381.8	393.0	437.7
2	**060D0099**			**Best**	**Average**	**Worst**
	Date	01-01-86	13-05-12		Final	
	Head mine water [mNAP]	-75.0	14.8	73.1	79.8	106.8
	Ground heave sediment cover [mm]	0.0	114.4	188.7	197.2	231.6
	Ground heave Carboniferous [mm]	158.6	213.6	249.3	253.4	270.0
	Total ground heave [mm]	158.6	328.0	438.0	450.6	501.6
3	**062B0241**			**Best**	**Average**	**Worst**
	Date	01-07-87	13-05-12		Final	
	Head mine water [mNAP]	-64.06	14.8	73.1	79.8	106.8
	Ground heave sediment cover [mm]	0	55.5	96.5	101.2	120.2
	Ground heave Carboniferous [mm]	27.0	45.7	59.8	61.4	68.0
	Total ground heave [mm]	27.0	101.2	156.4	162.7	188.2
4	**062E0015**			**Best**	**Average**	**Worst**
	Date	06-10-91	13-05-12		Final	
	Head mine water [mNAP]	-121.2	2.6	73.2	79.9	105.3
	Ground heave sediment cover [mm]	0.0	75.8	118.9	123.0	138.6
	Ground heave Carboniferous [mm]	21.5	50.3	78.3	79.8	85.7
	Total ground heave [mm]	21.5	126.0	197.2	202.9	224.3
5	**062E0034**			**Best**	**Average**	**Worst**
		06-10-91	13-05-12		Final	
	Head mine water [mNAP]	-121.2	2.6	73.2	79.9	105.3
	Ground heave sediment cover [mm]	0.0	79.2	124.4	128.7	144.9
	Ground heave Carboniferous [mm]	22.7	52.8	69.9	71.6	77.7
	Total ground heave [mm]	22.7	132.0	194.3	200.2	222.6

In Tab. B 14, derived from Tab. B 13, the ratios between the final ground heave and the ground heave developed in 2012/2013 are shown. In the worst case scenario the total ground heave will increase with another 53 to 86 %. The contribution to the ground heave is largely by the sediment cover, which will increase with another 83 to 117 %. For most key points the increase of the ground heave due to decompaction in the Carboniferous, of 26 to 49 %, is smaller. Only key point 4 shows a considerable increase of another 71 %.

Tab. B 14: Ratios of final ground heave to ground heave in 2012/2013, using method 2

Ratio final ground heave / ground heave in 2012-2013

		Final Best	Final Average	Final Worst
1	**060D0050**			
Ground heave sediment cover [%]		1.54	1.60	1.85
Ground heave Carboniferous [%]		1.17	1.19	1.27
Total ground heave [%]		1.34	1.38	1.53
2	**060D0099**			
Ground heave sediment cover [%]		1.65	1.72	2.02
Ground heave Carboniferous [%]		1.17	1.19	1.26
Total ground heave [%]		1.34	1.37	1.53
3	**062B0241**			
Ground heave sediment cover [%]		1.74	1.82	2.17
Ground heave Carboniferous [%]		1.31	1.34	1.49
Total ground heave [%]		1.54	1.61	1.86
4	**062E0015**			
Ground heave sediment cover [%]		1.57	1.62	1.83
Ground heave Carboniferous [%]		1.56	1.59	1.71
Total ground heave [%]		1.57	1.61	1.78
5	**062E0034**			
Ground heave sediment cover [%]		1.57	1.62	1.83
Ground heave Carboniferous [%]		1.32	1.36	1.47
Total ground heave [%]		1.47	1.52	1.69

Tab. B 15: Ratios of the ground heave due to decompaction in the sediment cover and in the Carboniferous on the one hand and the total ground heave on the other hand, using method 2

Ratio ground heave sediment cover / total ground heave and ratio ground heave Carboniferous / total ground heave

		2012/2013	Final Best	Final Average	Final Worst
1	**060D0050**				
Ground heave sediment cover [%]		0.45	0.52	0.53	0.55
Ground heave Carboniferous [%]		0.55	0.48	0.47	0.45
Total ground heave [%]					
2	**060D0099**				
Ground heave sediment cover [%]		0.35	0.43	0.44	0.46
Ground heave Carboniferous [%]		0.65	0.57	0.56	0.54
Total ground heave [%]					
3	**062B0241**				
Ground heave sediment cover [%]		0.55	0.62	0.62	0.64
Ground heave Carboniferous [%]		0.45	0.38	0.38	0.36
Total ground heave [%]					
4	**062E0015**				
Ground heave sediment cover [%]		0.60	0.60	0.61	0.62
Ground heave Carboniferous [%]		0.40	0.40	0.39	0.38
Total ground heave [%]					
5	**062E0034**				
Ground heave sediment cover [%]		0.60	0.64	0.64	0.65
Ground heave Carboniferous [%]		0.40	0.36	0.36	0.35
Total ground heave [%]					

In Tab. B 15 it can be observed for key points 1 and 2 that in 2012/2013 the contribution to ground heave by the Carboniferous exceeds that by the sediment cover. For key points 3 to 5 the contributions are the other way around. This is not surprising since the number of coal extractions is much greater at key points 1 and 2 than at the other ones. The final ground heave results largely from decompaction of the sediment cover (55 to 65 % in the worst case scenario), except for key point 2.

In Tab. B 16 the ratios of the ground heave by the sediment cover and the Carboniferous on the one hand and the total ground heave on the other hand is listed for the period between 2012/2013 and the final situation. These ratios correspond more or less with the ground heave which is still to develop. For all key points the larger part of the future ground heave will result from decompaction of the sediment cover, i.e. 64 to 74 % in the worst case scenario.

Tab. B 16: Ratios of the ground heave due to decompaction in the sediment cover and in the Carboniferous on the one hand and the total ground heave on the other hand, for the period from 2012/2013 till the final situation, using method 2

Ratio ground heave sediment cover / total ground heave and ratio ground heave Carboniferous / total ground heave for the period 2012-2013 to final

		Best	Average	Worst
1	**060D0050**			
Ground heave sediment cover [%]		0.72	0.72	0.72
Ground heave Carboniferous [%]		0.28	0.28	0.28
Total ground heave [%]				
2	**060D0099**			
Ground heave sediment cover [%]		0.68	0.68	0.68
Ground heave Carboniferous [%]		0.32	0.32	0.32
Total ground heave [%]				
3	**062B0241**			
Ground heave sediment cover [%]		0.74	0.74	0.74
Ground heave Carboniferous [%]		0.26	0.26	0.26
Total ground heave [%]				
4	**062E0015**			
Ground heave sediment cover [%]		0.61	0.62	0.64
Ground heave Carboniferous [%]		0.39	0.38	0.36
Total ground heave [%]				
5	**062E0034**			
Ground heave sediment cover [%]		0.73	0.72	0.72
Ground heave Carboniferous [%]		0.27	0.28	0.28
Total ground heave [%]				

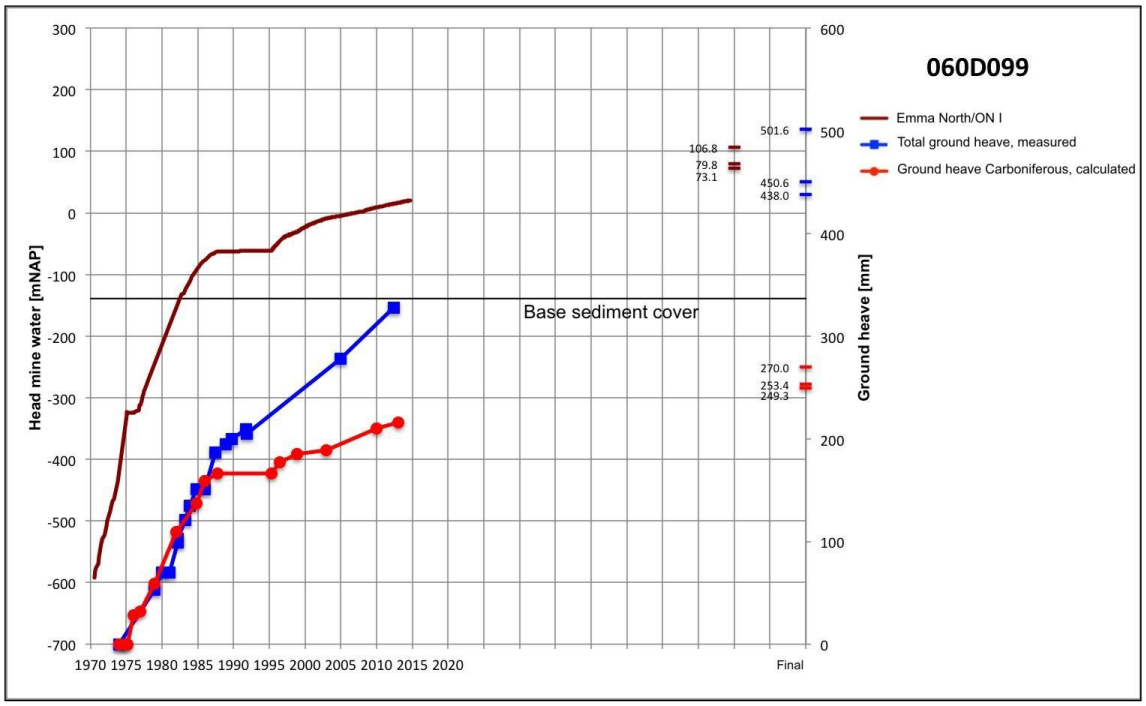

Fig. B 31: Prognosis of the total ground heave and the ground heave due to decompaction in the Carboniferous for key point 2, using method 2

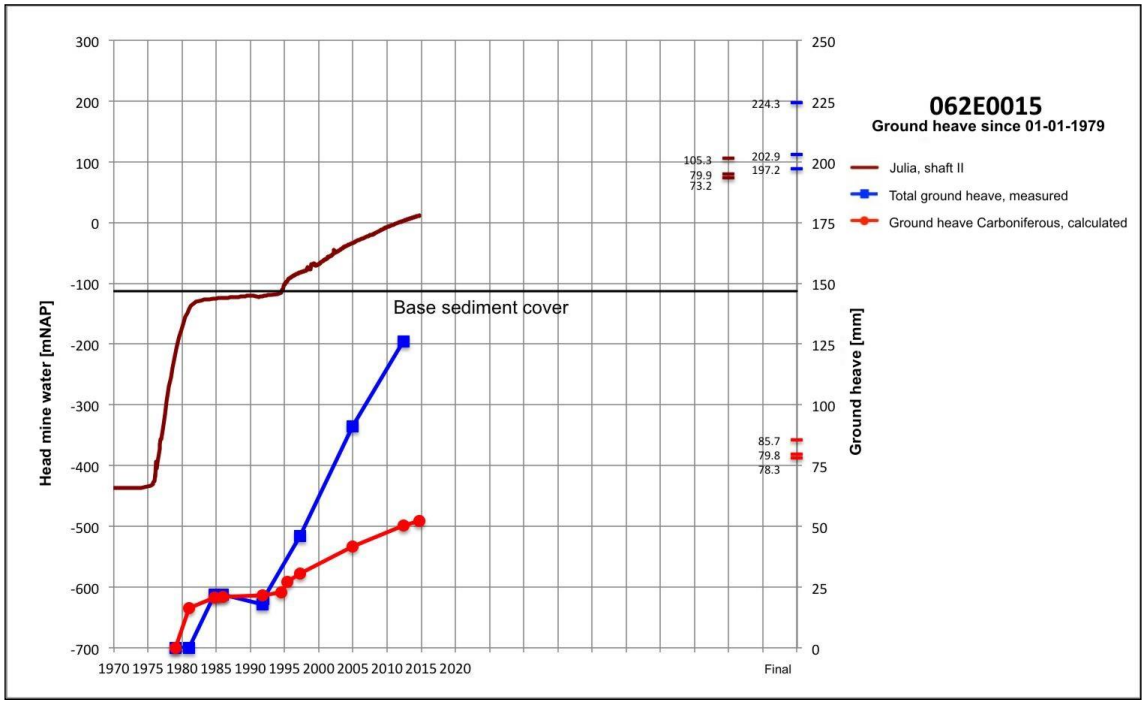

Fig. B 32: Prognosis of the total ground heave and the ground heave due to decompaction in the Carboniferous for key point 4, using method 2

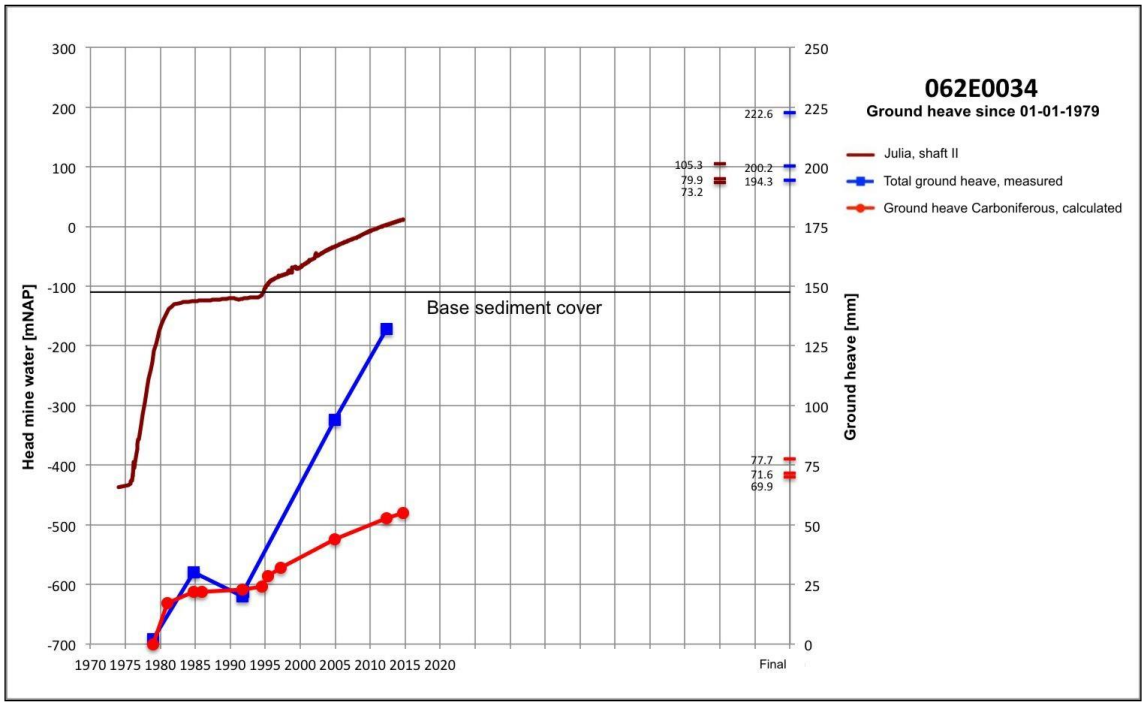

Fig. B 33: Prognosis of the total ground heave and the ground heave due to decompaction in the Carboniferous for key point 5, using method 2

Key points 1 and 2 are representative for the areas which show the largest ground heave in the coal district from 1974 to 2014 (part A). Key points 3, 4, and 5 are located closer to the boundary of the mined area, which is characterised by less ground heave. Large amounts of ground heave, which are comparable to the area of key points 1 and 2, have also been measured in the Maurits concession area, in the most north-western part of the coal district. Unfortunately the mine water level has not been measured in this basin since 1968. Therefore, neither analysis of the existing ground heave nor prognosis of the final ground heave in the future is possible here. However, on the basis of the already developed ground heave, the mine configuration, the composition of the sediment cover and the predicted heads for the mine water and overlying aquifers (Report WG 5.2.4/5.2.5), the final ground heave in the area of the Maurits concession can be expected to be comparable with that of the area of key points 1 and 2. An accurate prognosis of final ground heave is only possible if one or more observation wells are

constructed with filters in the Carboniferous and in the overlying aquifers, as proposed in Report WG 5.2.4/5.2.5.

All in all, key points 1 and 2 can be considered as representative for the areas with the largest final ground heave, and key points 3, 4, and 5 can be regarded as characteristic for areas where final ground heave is moderate.

5 Ground heave profile across the Feldbiß fault

To assess the ground heave across a major fault zone, the vertical movements along the eastern part of the "PÖTTGENS profile" (1985) were analysed from benchmark 060D0099 (key point 2) to 060D0061 (Fig. B 34).

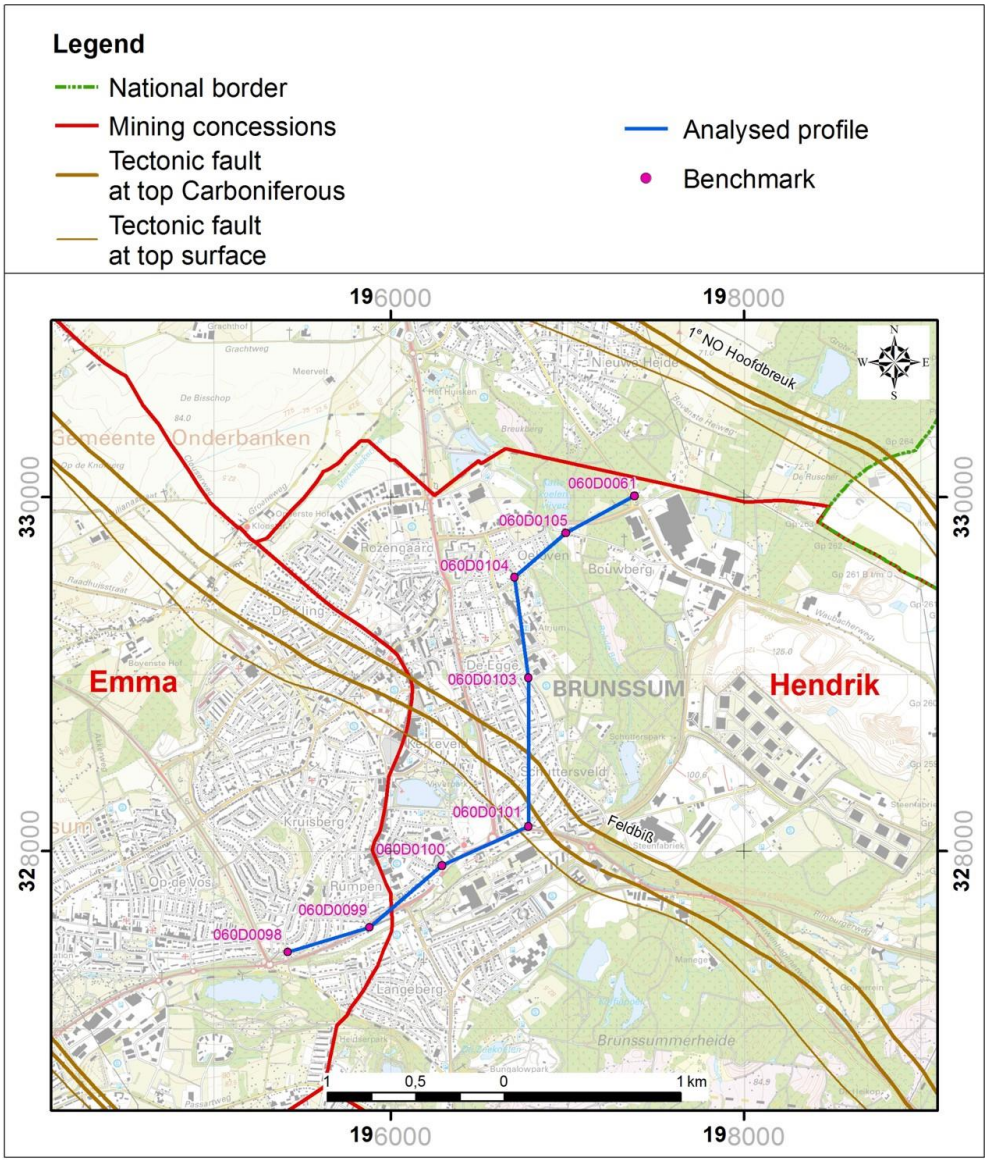

Fig. B 34: Analysed profile across the Feldbiß fault zone. The solid lines represent the margins of the fault zone at the top of the Carboniferous. The dashed line indicate the approximate location of the fault zone at the surface

Southwest of the fault zone, several coal extractions occur, but to the northeast the area is unmined. For all surface points the same decompaction coefficient of $2{,}8 \cdot 10^{-9}$ m^2/N, established for benchmark 060D0099, was applied. The ground heave due to decompaction in the Carboniferous is calculated according to the method outlined in chap. 3.1.3 and chap. 3.1.4. The time series of the total measured ground heave and the calculated ground heave due to decompaction in the Carboniferous are depicted in Fig. B 35 to Fig. B 41. In the calculation of the ground heave a possible influence of the fault zone on the ground heave profile is obviously not incorporated.

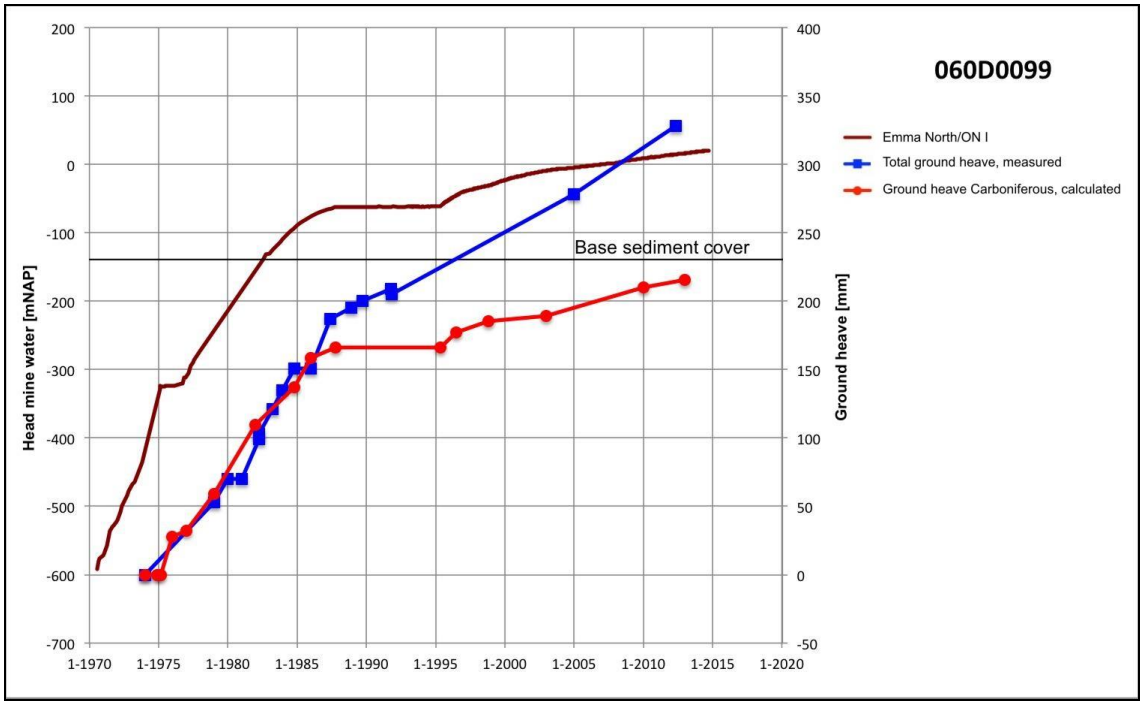

Fig. B 35: Time curves of calculated ground heave due to decompaction in the Carboniferous and of total measured ground heave at benchmark 060D0099

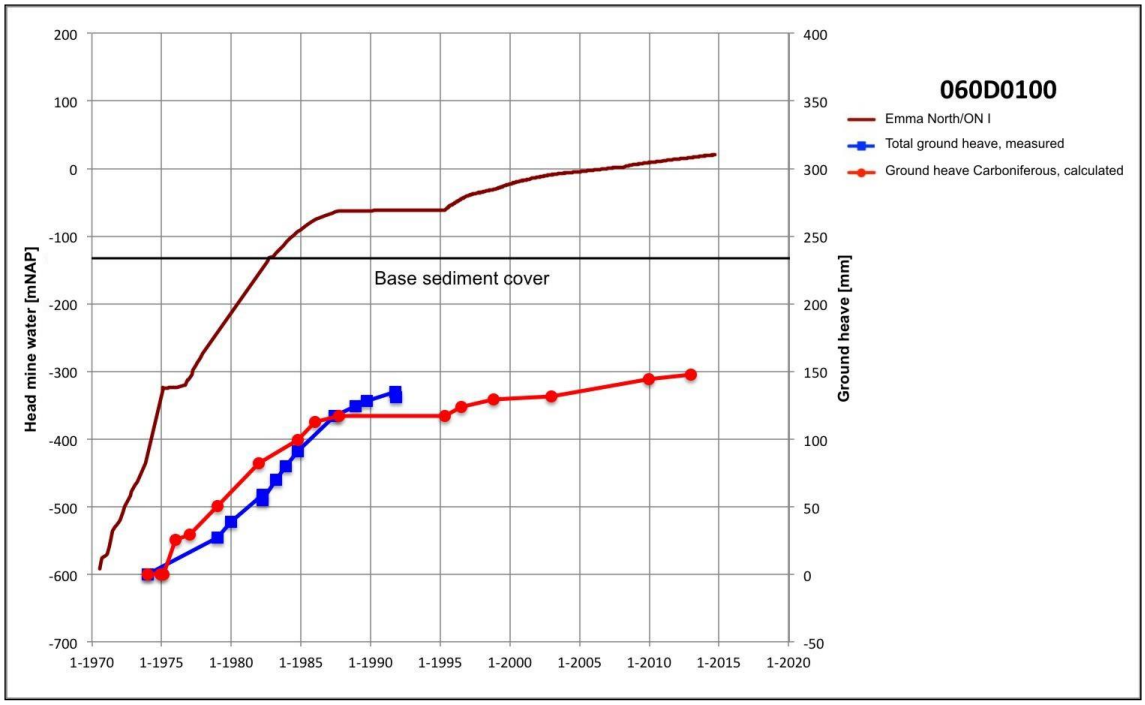

Fig. B 36: Time curves of calculated ground heave due to decompaction in the Carboniferous and of total measured ground heave at benchmark 060D0100

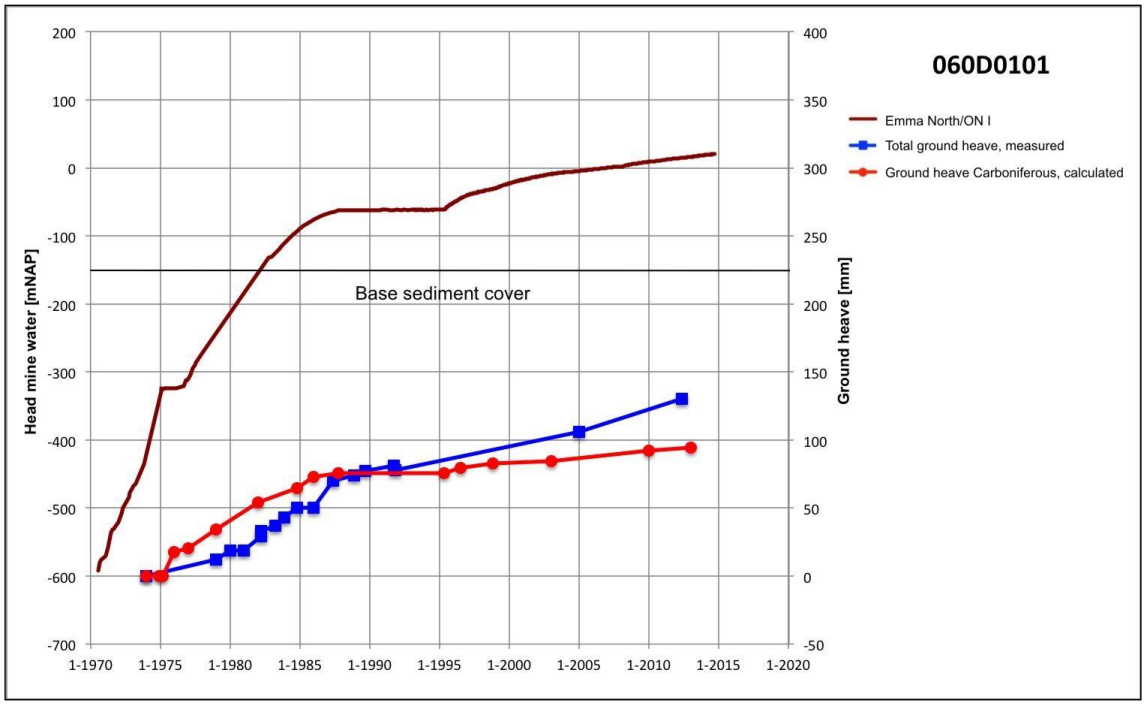

Fig. B 37: Time curves of calculated ground heave due to decompaction in the Carboniferous and of total measured ground heave at benchmark 060D0101

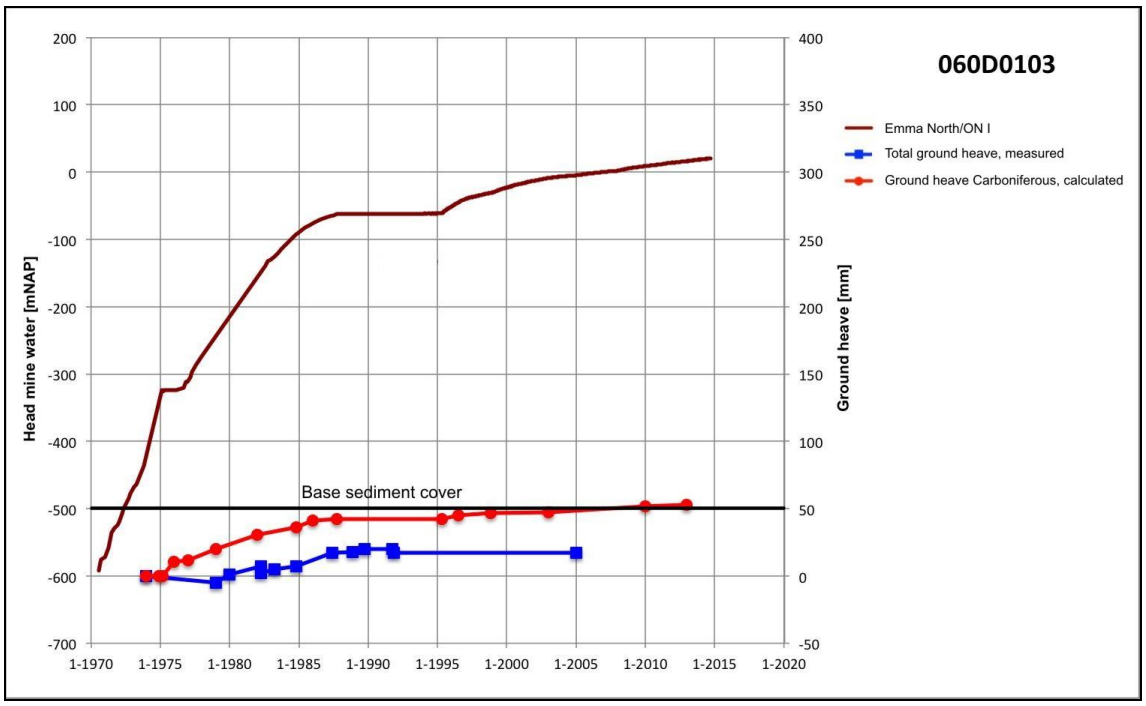

Fig. B 38: Time curves of calculated ground heave due to decompaction in the Carboniferous and of total measured ground heave at benchmark 060D0103

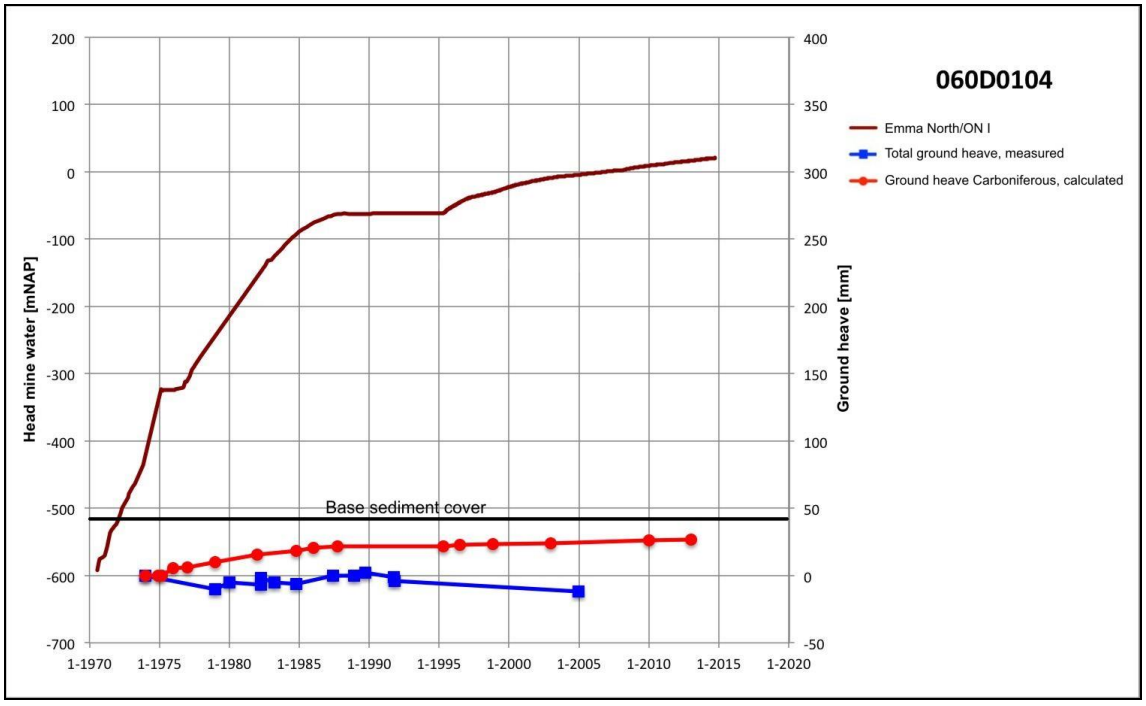

Fig. B 39: Time curves of calculated ground heave due to decompaction in the Carboniferous and of total measured ground heave at benchmark 060D0104

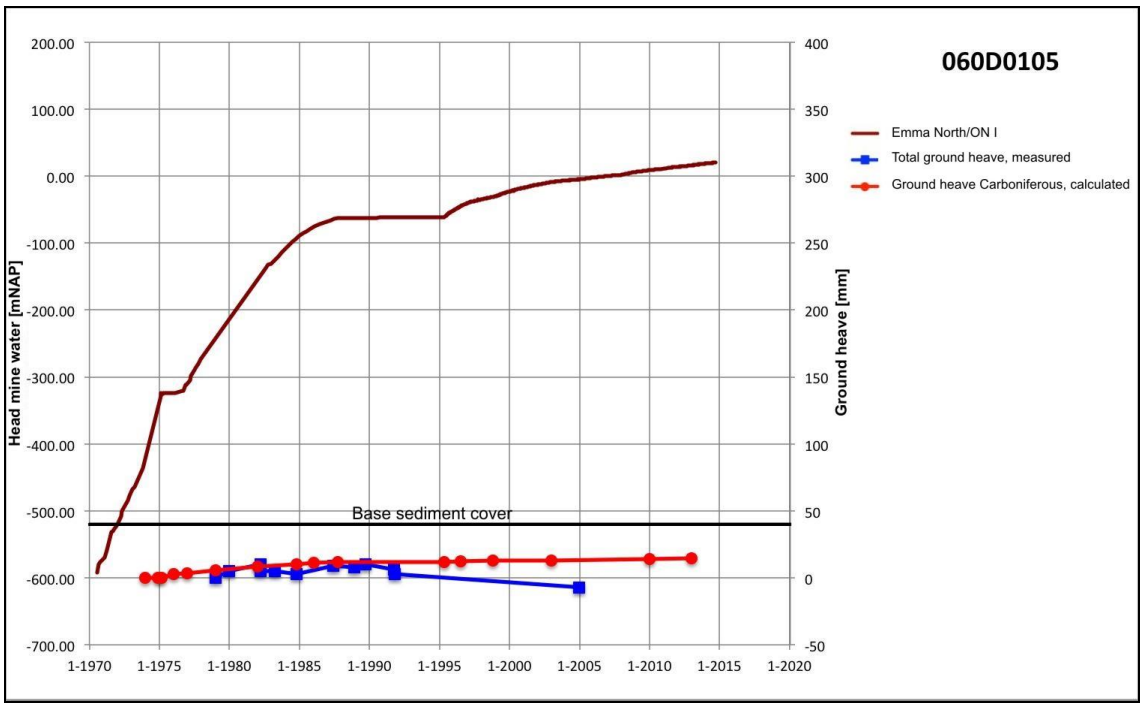

Fig. B 40: Time curves of calculated ground heave due to decompaction in the Carboniferous and of total measured ground heave at benchmark 060D0105

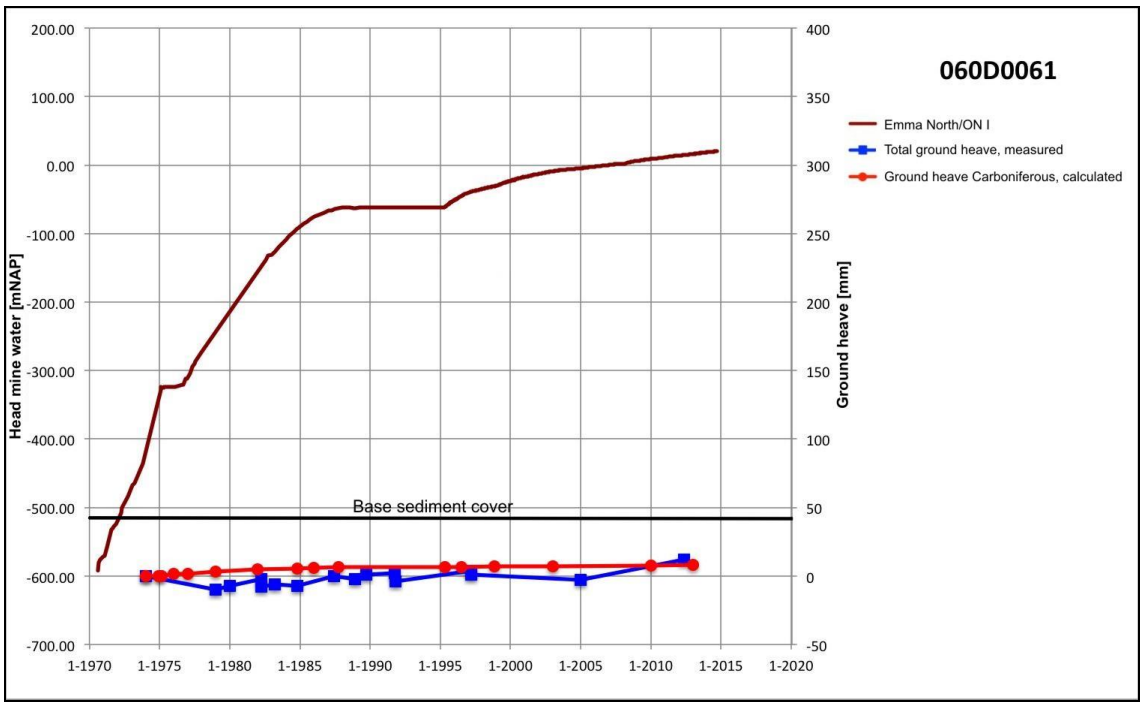

Fig. B 41: Time curves of calculated ground heave due to decompaction in the Carboniferous and of total measured ground heave at benchmark 060D0061

At benchmarks 060D0099 and 060D0100, which are situated to the southwest of the fault zone, the measured and calculated ground heave match until the flooding of the sediment cover. Thence the curves diverge as usually, because the sediment cover decompacts as well. At benchmark 060D0101, which is situated in or in the direct vicinity of the fault zone, the ground heave curves show more or less the same development. However, at the benchmarks to the northeast of the fault zone the calculated ground heave exceeds the measured ground heave. This difference decreases from benchmark 060D0103 to 060D0061. At benchmark 060D0103 still a small amount of ground heave was measured, but with greater distance from the fault zone hardly any ground heave has developed (Fig. B 42). Meanwhile the calculated ground heave is reduced as well towards the northeast, because the influence of the decompaction of the disturbed rock over the coal extractions to the southwest of the fault zone becomes weaker, according to the applied influence function (Fig. B 43).

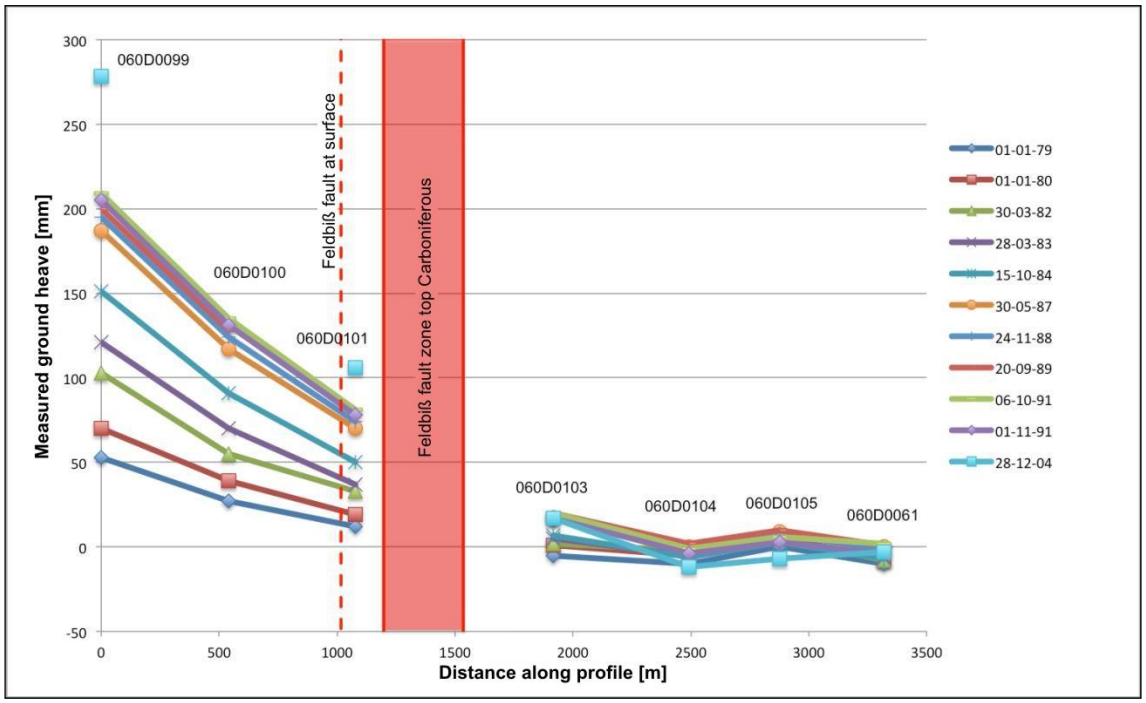

Fig. B 42: Profile of measured ground heave across the Feldbiß fault zone

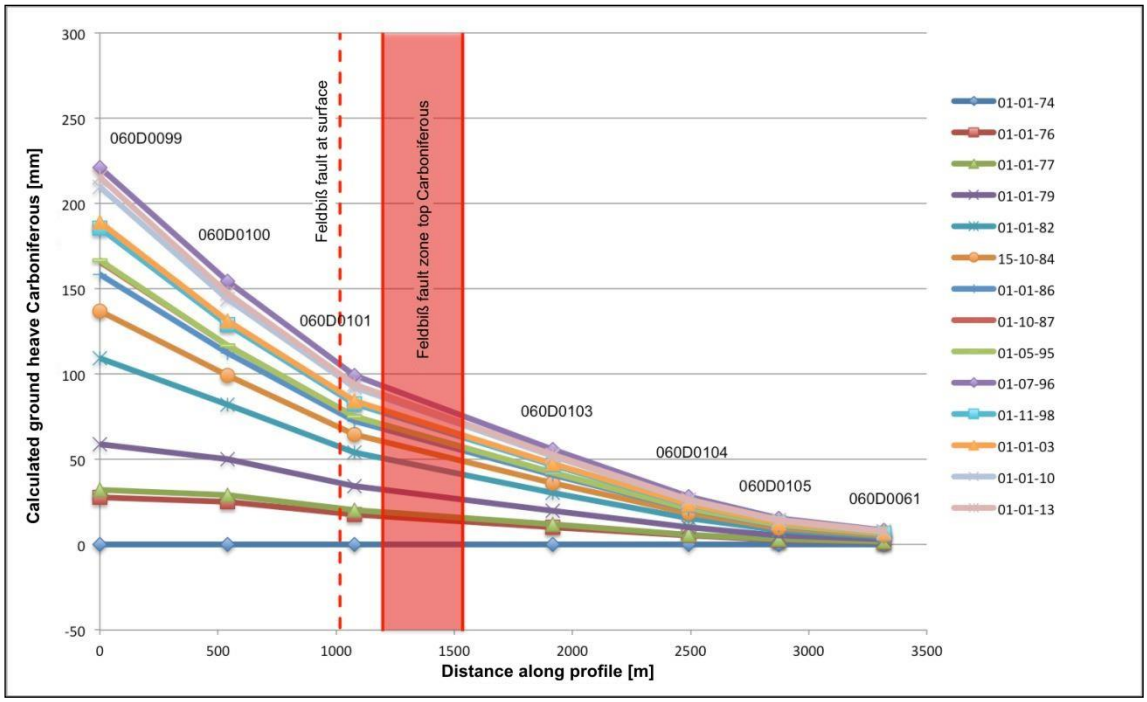

Fig. B 43: Profile of calculated ground heave due to decompaction in the Carboniferous across the Feldbiß fault zone

It is possible that the Feldbiß fault zone acts as a barrier for vertical motion in the subsurface. The fault zone is about 170 m wide. The more detailed profile, based on InSAR data and provided by the Delft University of Technology, shows that, if differential ground heave exists, it is accommodated gradually across the zone (Fig. B 44). In the investigated area near the Feldbiß fault zone no damage to houses or structures have been reported up to now.

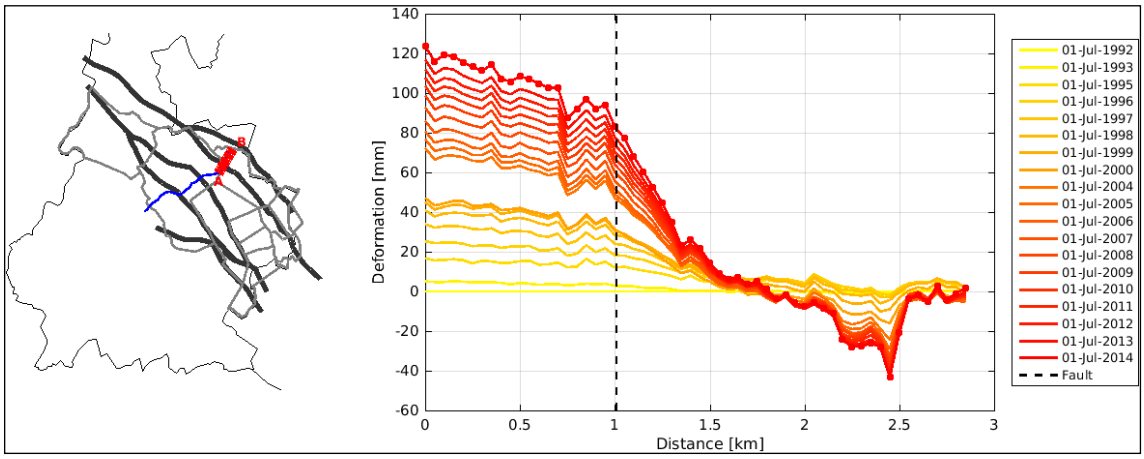

Fig. B 44: Profile of ground heave, based on InSAR data across the Feldbiß fault zone (Delft University of Technology)

In Fig. B 45 the measured (total) ground heave is shown versus the mine water head. Also for the benchmarks across the fault zone, ground heave and mine water head are correlated. To the northeast of the fault zone there is hardly any ground heave upon a rise of the mine water level.

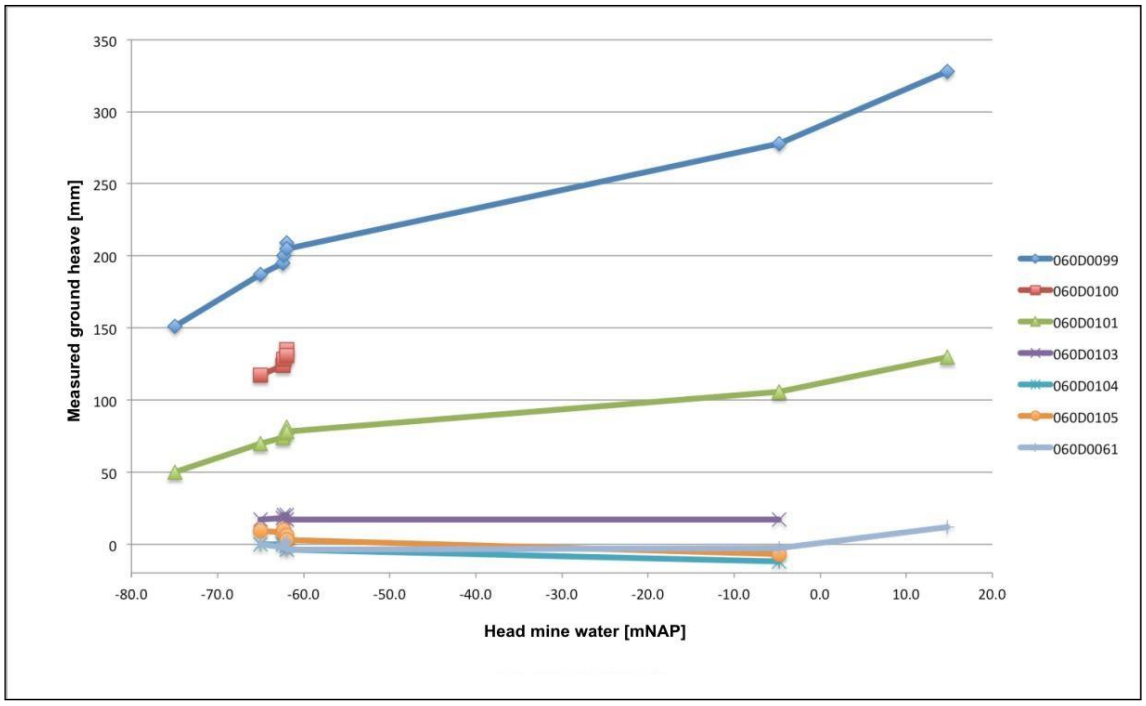

Fig. B 45: Total ground heave versus mine water head for the 7 benchmarks across the Feldbiß fault zone

6 Conclusions

1) The GEERSTMA influence function adequately describes surface ground heave due to decompaction of disturbed rock over mined coal panels.

2) The decompaction coefficient proved to be $2{,}5 \cdot 10^{-9}$ to $3{,}5 \cdot 10^{-9}$ m^2/N, assuming a thickness of the zone of disturbed rock of 4 times the seam thickness.

3) For the ground heave calculations an integration net was applied to determine the contributions to the surface ground heave for each coal extraction. This method is accurate, but also time consuming.

4) Initially the calculated and measured time curves match if the right decompaction factor is applied, but diverge when the sediment cover is flooded. The difference between the measured and calculated ground heave is attributed to the ground heave due to decompaction of the sediment cover.

5) In general, for a given mine water head, a prognosis of surface ground heave due to decompaction of disturbed rock in the Carboniferous can be well established, using GEERTSMA's Influence function.

6) For each of the five studied key points a separate correlation exists between the (total) measured ground heave and the mine water head, from the moment the sediment cover is flooded by the mine water. Such a correlation was also observed for the separate contributions by the disturbed rock in the Carboniferous and by the sediment cover.

7) It is useful to verify the correlation, for instance by using the several InSAR data points. If the verification is successful, it could be attempted to make a detailed ground heave prognosis for final mine water levels on the basis of this correlation. In this way it would be possible to make a prognosis of future ground heave, for a given mine water head, with relatively little

effort for each surface point, where the sediment cover is flooded. Time consuming calculations, using mine maps and influence functions, can then be avoided.

8) For the five investigated key points the final (total) ground heave ranges from 188 to 502 mm (worst case), 163 to 451 mm (average case) or 156 to 438 mm (best case).

9) These values of final ground heave correspond to an additional 87 to 174 mm (worst case), 61 to 123 mm (average case) or 55 to 110 mm (best case) relative to the ground heave developed in 2012/2013 (see Tab. B 17). The contribution to the ground heave is largely by the sediment cover.

10) Evidence exists that differential ground heave could have occurred across the Feldbiß fault zone in Brunssum. However, if so, it is accommodated gradually across the zone.

Tab. B 17: Additional ground heave (calculated with method 2) for the best - average - worst case scenario

Key Point	Actual (2012/2013)	Ground heave [mm]					
		Total ground heave (calculation with method 2)			Additional ground heave (calculation with method 2)		
		Scenario of rise of mine water (s. WG 5.2.4/5.2.5)					
		Best	Average	Worst	Best	Average	Worst
1	285,2	381,8	393,0	437,7	96,6	107,8	152,5
2	328,0	438,0	450,6	501,6	110,0	122,6	173,6
3	101,2	156,4	162,7	188,2	55,2	61,5	87,0
4	126,0	197,2	202,9	224,3	71,2	76,9	98,3
5	132,0	194,3	200,2	222,6	62,3	68,2	90,6

References

Literature

BAGLIKOW, V. (2010): Schadensrelevante Auswirkungen des Grubenwasseranstiegs im Erkelenzer Steinkohlenrevier.- Schriftenreihe Inst. f. Markscheidewesen, Bergschadenkunde und Geophysik im Bergbau an der RWTH Aachen, Heft 1-2010, 121 S., 84 Abb.; Aachen.

BEKENDAM, R.F. (1998): Pillar stability and large-scale collapse of abandoned room and pillar mines in South-Limburg, the Netherlands, PhD thesis Technische Universiteit Delft.

BEKENDAM, R.F. & J.J.E. PÖTTGENS (1995): Ground movements over the coal mines of southern Limburg, The Netherlands, and their relation to rising mine waters, In: Land subsidence, Proc. 5th Int. Symp. On Land Subsidence, The Haque, IAHS Publ. 234, 3-12.

DOMENICO, P.A. & M.D. MIFFLIN (1965): Water from low-permeability sediments and land subsidence, Water Resources Research, 1, 563-576.

FENK, J. (1997): Zeitreihenanalysen für Hebungsprozesse über stillgelegten Steinkohlenbergwerken, Wissenschaftliche Tagung des Deutschen Markscheider-Vereins, Wissenschaftliche Schriftenreihe im Markscheidewesen, Heft 17, 117-122.

FENK, J. (1998): Hebungen der Tagesoberfläche über stillgelegten Steinkohlenbergwerke im Zwickau-Oelsnitzer Revier (Diskussionsbeitrag).

FENK, J. (2000): Eine analytische Lösung zur Berechnung von Hebungen der Tagesoberfläche bei Flutung unterirdischer Bergwerksanlagen, Das Markscheidewesen, 107, 2, 420-422.

FENK, J. (2006): Hebungen nach Einstellung von Wasserhaltungen, ein Diskussionsbeitrag.

GEERTSMA, J. (1973): Land subsidence above compacting oil and gas reservoirs, J. Petroleum Technology, June 1973, 734-744.

GIESE, S., (2010): Bodenbewegungen infolge von Sümpfungsmaßnahmen für tiefe Tagebaue am Beispiel des Rheinischen Braunkohlenreviers.- Diss. RWTH Aachen, Schriftenreihe Geotechnik im Bauwesen, RWTH Aachen, H. 6, 271 S., 140 Abb., 19 Tab.; Aachen (D).
http://darwin.bth.rwth-aachen.de/opus3/volltexte/2010/3381/pdf/3381.pdf (website visited 01.2015)

GOERKE-MALLET, P., A. PREUSSE & W.G. COLDEWEY (2001): Hebungen der Tagesoberflache über betriebenen und gefluteten Bergwerken, In: Tagungsband der 43, Wissenschaftlichen Tagung des Deutschen Markscheider-Vereins Trier 2001 ,126-139.

HEITFELD, M., P. ROSNER, M. MÜHLENKAMP & H. SAHL (2004): Bergschäden im Erkelenzer Steinkohlenrevier. - 4. Altbergbau-Kolloquium, 14 S., 10 Abb.; Leoben (Österreich).

HEITFELD, M., P. ROSNER & M. MÜHLENKAMP (2014): Auswirkungen von Geländehebungen im Zuge des Grubenwasseranstiegs im Ruhrrevier - ein Ansatz zur Bewertung der Risiken.- 14. Altbergbau-Kolloquium, S. 41 - 60, 8 Abb.; Gelsenkirchen.

HOLLMANN, F. (1995): Zur bleibenden Beeinträchtigung der Nutzung von Boden und Baugrund im Senkungstrog nach Einstellung bergbaulicher Tätigkeit bzw. nach Auslaufen bergbaulicher Bodenbewegungen, Bergbau, 46, 76-82.

HOLLMANN, F. & R. NÜRENBERG (1972) Der tagesnahe Bergbau als technisches Problem bei der Durchführung von Baumaßnahmen im Niederrheinisch-Westfälischen Steinkohlengebiet, Mitt. Westphälischen Berggewerkschaftskasse, 30.

HOLZHEIM, M., A. PREUßE & A. SROKA (2006): Auswirkungen des Grubenwasserwiederanstiegs auf die Tagesoberflächen - Stand der Forschung.

8. Aachener Altlasten- und Bergschadenkundliches Kolloquium, RWTH Aachen, 2006.

KRATZSCH, H. (2013): Bergschadenkunde, Deutscher Markscheider Verein e V, Bochum.

MUKHERJEE ET AL. (1993): Caved goaf behaviour, Int.J.R.Mech. Min.Sci & Geomech. Abstr. 1993.

OBERSTE-BRINK, K. (1940): Die Frage der Bodenbewegungen infolge Bergbaus.- Glückauf, 76, S. 249-256; Essen.

PÖTTGENS, J.J.E. (1985): Bodenhebung durch ansteigendes Grubenwasser.- The Development of Science and Art of Minerals Surveying, Proceedings 6th International Congress, International Society of Mine Surveying, vol. 2, p. 928 - 938; Harrogate (GB).

PÖTTGENS, J.J.E. (2002): Handleiding voor het gebruik en lezing van mijnkaarten, Reg. Hist. Centrum voor Limburg, Maastricht.

PREUSSE, A. & M. PAPST (2015): Bodenbewegung in Folge eines Grubenwasseranstiegs, nachbergbau in NRW.

ROSNER, P. (2011): Der Grubenwasseranstieg im Aachener und Südlimburger Steinkohlenrevier - Eine hydrogeologisch-bergbauliche Analyse der Wirkungszusammenhänge.- Diss. RWTH Aachen, 194 S., 67 Abb., 7 Tab., 4 Anh., 7 Anl.; Aachen (D). http://darwin.bth.rwth-aachen.de/opus3/volltexte/2011/3741 (website visited 11.2014)

SPICKERNAGEL, H. (1975): Hebungen des Gebirges als Folgen des Bergbaus unter Tage In : Glückauf Forschungshefte 36, H. 4, 170-176.

SROKA, A. (2005): Ein Beitrag zur Vorausberechnung der durch Grubenwasseranstieg bedingten Hebungen.

VERRUIJT, A. (1999): Grondmechanica, Delft university Press.

ZSCHIESCHICK, D., C. DREBENSTEDT & A. SROKA (2006): Der Kenntnisstand zu vertikalen Bodenbewegungen durch den Grundwasserwiederanstieg, 7. Geokinematischer Tag, Freiberg, 1-12.

Other documents

- Geologisch Bureau Heerlen (1973): Standaard legenda.

Part C - Assessment of impact potential

1 Subject and boundary conditions

1.1 Introduction

The rise of mine water after cessation of mine drainage generates ground heave (OBERSTE-BRINK, 1940). For the South Limburg mining district, PÖTTGENS (1985) firstly published an outline of the dimensions and the possible principles of ground heave induced by rising mine water in a greater area.

For the adjacent German hard coal mining districts of Erkelenz and Aachen, that were abandoned in the 1990s, publications about ground movements are available from HEITFELD et al. (2003), BAGLIKOW (2003), HEITFELD et al. (2004), and BAGLIKOW (2010) among others. For the hard coal mining districts of Aachen and South Limburg, a comprehensive study about the impacts of mine water rise was provided by ROSNER (2011). A differentiated characterisation of differential ground heave caused by mine water rise in the Erkelenz mining district was firstly published by HEITFELD et al. (2004).

The damages at buildings that have emerged in the context of mine water rise in the Erkelenz mining district initiated an extensive public dialogue about the risks by differential ground heave especially in view of the future mine water rise in the Ruhr mining district. Therefore the German RAG Aktiengesellschaft initiated the research project „ABSMon“ („Monitoring of historical mining“) to acquire the fundamentals for a substantiated risk assessment and for a purposive, optimised monitoring system. As part of this research project, IHS elaborated the characteristics of the kinematic of ground heave induced by rising mine water; furthermore risk factors for the development of significant differential ground

heave have been defined. The results are based on a comprehensive study of ground heave in other coal mining districts already flooded.

Today the risk factors elaborated within the research project „ABSMon“ built the basis for the risk assessment of the permit procedures for the mine water rises in the German hard coal districts. This procedure is adopted to the South Limburg mining district within this project.

1.2 State of knowledge about the development of ground heave

1.2.1 Causes for ground heave

Basically, the causes for ground heave can be outlined as follows:

- During the course of mine water rise, ground heave is mainly caused by buoyancy; the alternated stress conditions within the loosened bedrock initiate strain events.

- Strain events emerge in the course of flooding the coal-bearing bedrock that was loosened by mining activity; they also emerge due to altering hydraulic heads in the overlaying overburden.
  The kinematic of mining induced ground movements (subsidence and ground heave) that are caused by altered hydraulic heads is well known from the large-scale dewatering regions around the lignite opencast mines in the Lower Rhenish Basin, Germany.

The physical basics of this kinematic are also applicable to the conditions in the South Limburg mining district.

1.2.2 Temporal progression of ground heave during the course of mine water rise

The principles of the temporal progression of ground movements/ground heave during the course of mine water rise can be described as follows:

- In a first phase of the mine water rise within the level of the bedrock commonly no significant ground heave is to be expected. In North Rhine-Westphalia, depending on the rate of mine water rise, ground heave occurred about 3 to 5 years after the cessation of mine drainage.

  In the early stage of mine water rise, first of all, residual subsidence has to be compensated and the loosened rock has to be compressed. Only after an appropriate stress has built up strain events can lead to ground heave at the surface. For this to happen, a certain pressure head and an appropriate flooding-/strain-volume is required, which varies with depth and intensity of mining.

  In the flooded areas of the mining districts in North Rhine-Westphalia and South Limburg, the average mined depth is about 700 to 1.000 m; initial ground heave was observed after the rock volume was submerged by approx. 300 to 400 m.

- If mining related subsidence has already abated by the time mine dewatering was ceased, flooding can cause a temporary increase of subsidence before ground heave starts. Suchlike events are known from some areas in the mining districts of North Rhine-Westphalia (i.a. in the Erkelenz mining district). The developments can be ascribed to the subsidence due to saturation; the shear strength at the borders of the single grains is reduced by wetting the grain boundary.

- Once induced ground heave develops more or less parallel to the progression of mine water rise. Hence, ground movement can be regulated by controlling the mine water level (e.g. through dewatering measures).

- Strain events in the coal-bearing bedrock and in the overburden overlap when mine water rise also causes a rise of the hydraulic heads in the aquifers of the overburden. As a consequence, ground heave might increase if the mine water level reaches the overburden subsequent to the complete flooding of a coal mine.

- The highest amount of ground heave can be observed in the areas where the mining induced subsidence was most intensive.
  In the abandoned mining districts evaluated by now maximum amounts of ground heave have emerged in a range between 0,2 and 0,3 m; therewith, the maximum amounts of ground heave are within an average magnitude of 2 to 3 % of the mining induced subsidence.

1.2.3 Risk factors for the development of discontinuities relevant for damages

Considering the occurrence of differential ground heave that might lead to damages at the surface, the following fundamental facts have to be regarded:

- In North Rhine-Westphalia damages at buildings due to differential ground movements induced by mine water have only be recorded from the area along the tectonic Rurrand fault zone in the Erkelenz mining district (cities of Wassenberg and Hückelhoven).

- In other abandoned mining districts neither such damages nor comparable discontinuities have been observed.

- Therefore the conditions for the development of damage-relevant discontinuities induced by rising mine water are highly specific and, overall, the probability of occurrence is low.

The characteristics of the progression of damages at the Rurrand fault in the Erkelenz mining district can be summarised as follows:

- The „line of damages“ that developed in the Erkelenz mining district is orientated after a predetermined main tectonic trajectory in the bedrock and in the overburden rather than after purely mining related discontinuities (e.g. border of mine workings).

- The mining related discontinuities outside of tectonic fault zones create a less pronounced trajectory in the underground. Furthermore, these discontinuities often get overprinted by the multiple impacts of mining at different depths.
  According to the previous findings these non-tectonic trajectories will not be reactivated by ground heave, which is only a percentage of the mining induced subsidence that formed these trajectories.

- The characteristic of the reactivated tectonic trajectory that caused a „line of damage“ in the Erkelenz mining district (Rurrand fault) is its recent tectonic activity (e.g. earthquakes of Roermond and Düren, Germany). The tectonic fault disrupts the bedrock as well as the overburden with a system of joints up to the level of the Quaternary cover. The presence of clay selvages within the fault makes it easier to induce a movement along a distinct trajectory.

- Therefore such a distinct tectonic trajectory is a main requirement for the development of a sharp discontinuity due to comparable low amounts of ground heave.

- The increased activation potential as well as the hydraulic potential of such tectonic trajectory favour the delimitation of ground heave to the tectonic block which is affected by mining; consequently, damage-relevant discontinuities can develop at such fault zone.

- The characteristics of mine water rise in the Erkelenz mining district were both the relatively rapid flooding of the coal mine and the early inclusion of the overburden in the increase of pressure heads.
  Consequently, on one hand, an increased impulse (buoyancy) was induced; on the other hand, an early overlap with strain events in the overburden occurred which overall lead to an increased ground heave.
  The overlap of these different kinematics favoured the activation of the predetermined tectonic trajectory in the underground.

With respect to the identification of areas with high potential for the development of damage-relevant discontinuities by ground heave, the following essential factors can be concluded:

An increased impact potential caused by the development of discontinuities due to differential ground heave has to be expected at hydraulic active main tectonic fault zones where

- **mining only took place on one site of the hydraulic active fault zone**

- **in the course of mine water rise, a single-sided increase of groundwater level/pressure heads occurs in the overburden or where, for other reasons, a contrary development of the groundwater heads takes place in the overburden on both sides of the fault zone.**

Furthermore, the specific stress and deformation behaviour of the overburden layers that are affected by rising pressure heads as well as the shear strength of the potential trajectory have to be regarded.

1.2.4 Approach for the identification of potential impact areas

For the identification of areas where significant differences in ground heave may develop in the course of mine water rise, the geologic and hydraulic conditions as well as the mining conditions have to be analysed and evaluated in respect of the aforementioned risk factors. For this project the following workflow can be derived from this:

- Compilation of mine workings and the areas with mining induced subsidence
- Compilation of mining induced discontinuities (drempels/verzakkingen)
- Classification of areas with different characteristics of ground movements due to both their mining history and the progression of mine water rise
- Compilation of the tectonical faults which have been relevant for the mining activities
- Assessment of the mechanical characteristics of the relevant tectonic fault zones
- Assessment of the potential for ground movements for each flooding area in respect to the level of the already flooded mine workings, the thickness of the rock to be flooded, and the rate of mine water rise
- Identification of marginal areas of ground heave and assessment of the potential impact of differential ground heave on the surface during a further mine water rise

- Identification of risk areas within the potential impact areas of differential ground heave (i.e. urbanised areas).

In the following, the facts on these risk factors are compiled and evaluated for the project area.

2 Geographical and geological framework

2.1 Geographical outline of the study area

The project area is situated between the cities of Aachen/Herzogenrath, Germany, in the southeast and Geleen in the northwest. The area is densely populated due to its industrial history; the centres of settlement are located around the former operational plants of the coal mines (Fig. C 1)

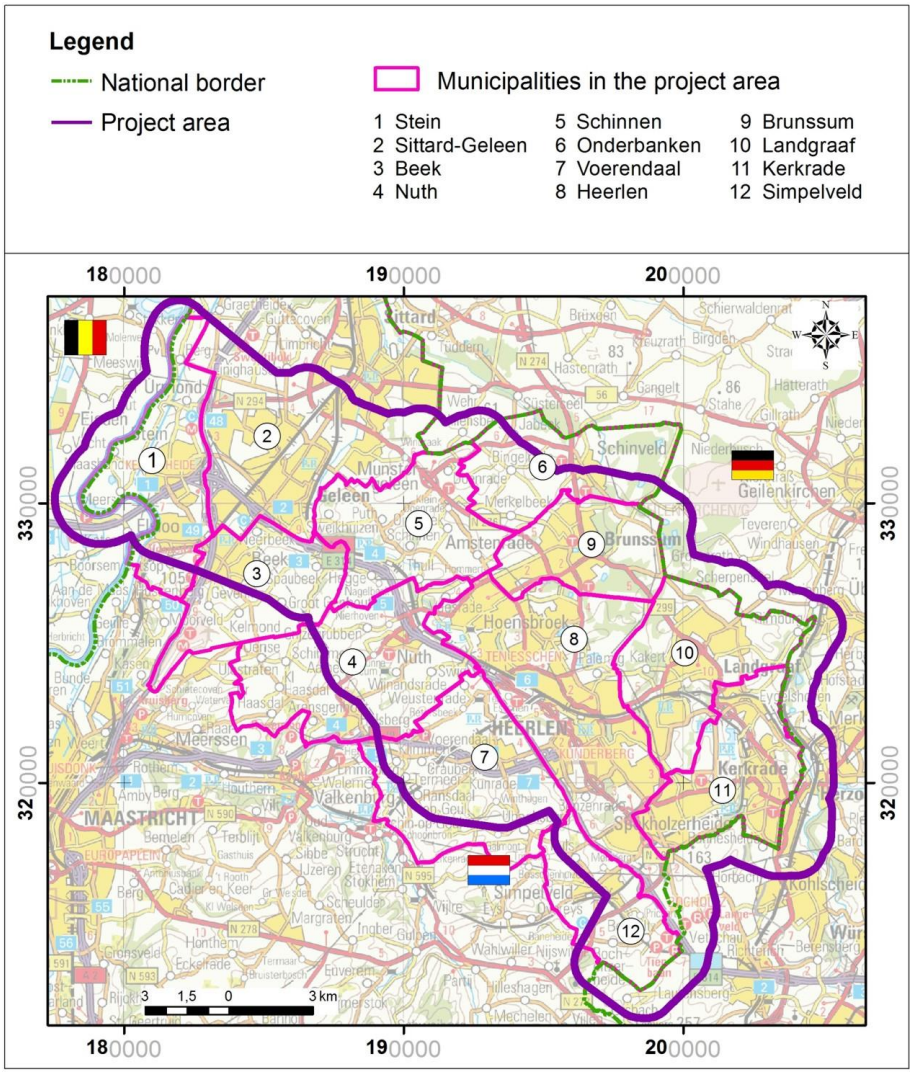

Fig. C 1: Spatial outline and land use in the project area

The Belgian mining district (Eisden coal mine) is located in the northwest of the project area, the German mining district to the southeast. The final abandonment of these mining districts took place in the early 1990s; mine water is still rising in these areas as well. Hence, ground heave also occurs in the mining districts that are adjacent to the South Limburg mining district.

In addition the influence of the drainage measures of the German lignite opencast mines has to be considered; this also affects the northeastern part of the South Limburg mining district (see chap. 2.3). The regional lowering of the groundwater level by the huge brown coal pits lead to a regional subsidence of the surface. A further alteration of groundwater heads is induced by groundwater plants that are situated within the study area (see report WG 5.2.4./5.2.5). Due to these groundwater extractions, additional ground movements possibly interfering with the impacts from mine water rise have to be expected. This complex situation has to be considered within the evaluation of the impacts of mine water rise as well.

2.2 Structure of the coal-bearing bedrock

In the northeastern part of South Limburg, the coal-bearing layers of the Upper Carboniferous are located right beneath the overburden. In general, the Upper Carboniferous layers are dipping northwest and northeast. Therefore, the coal-bearing layers are cropping out in the southeast; to both the northeast and the northwest, the Upper Carboniferous layers submerge under an overburden that successively increases in thickness (Fig. C 2). At the southwestern edge of the mining district, the coal-bearing layers are cropping out at the base of the overburden. In the southeast of the mining district, in the area of the cities Kerkrade/Herzogenrath the coal-bearing layer are cropping out at the surface

(Wurm-valley and Amstelbach-valley) or are to be found beneath a thin sedimentary cover (see chap. 2.3).

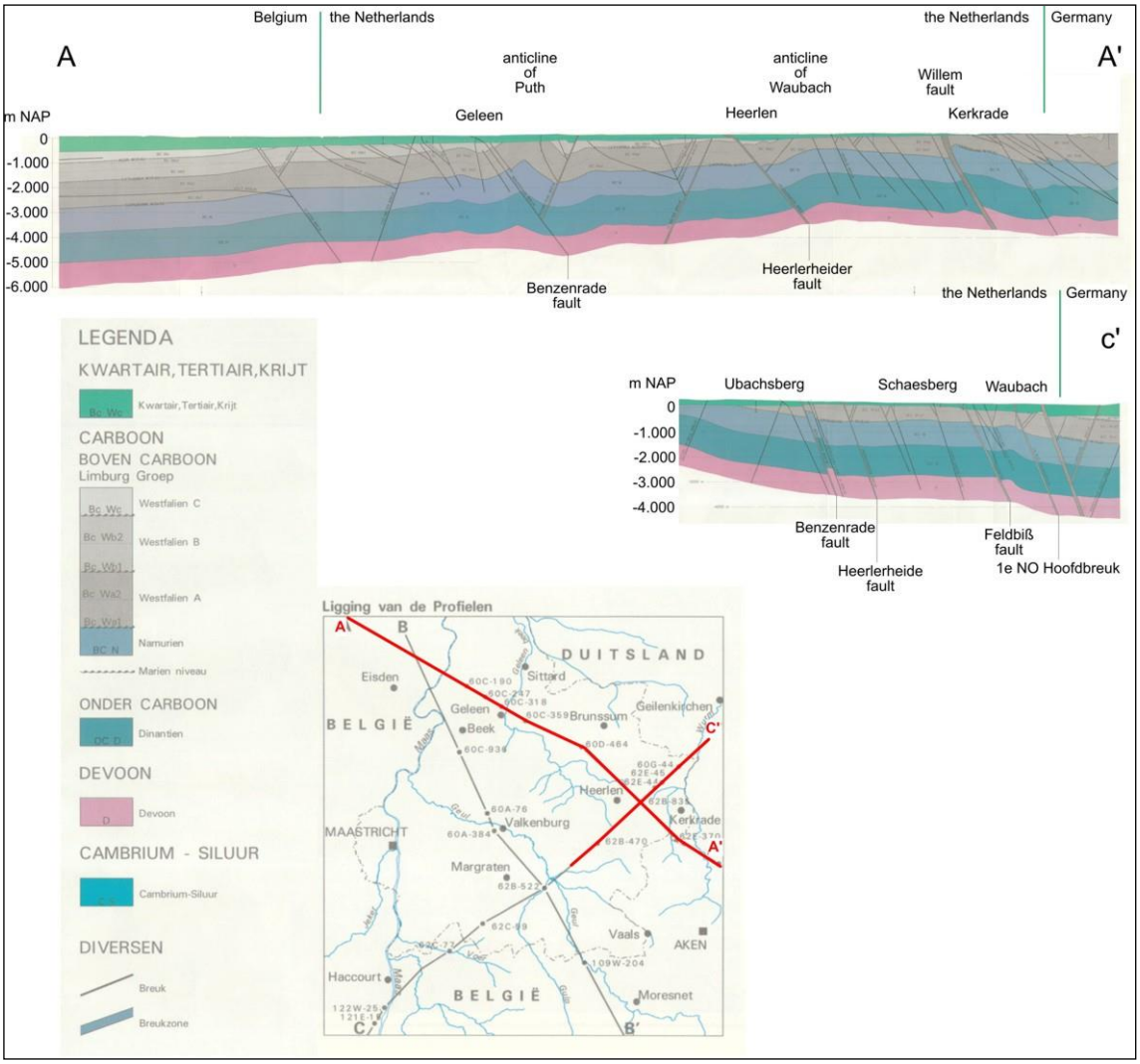

Fig. C 2: Geological structure of the Carboniferous underground (source: Geologische Kaart van South Limburg en omgeving – Paleozoikum; scale 1:50.000)

In the southeastern part of the mining district, in the Kerkrade area, the Carboniferous is characterised by tight folding; however, the intensity of that folding decreases to the northwest. Hence, the coal-bearing layers are mainly flat dipping in the central and northern parts of the mining district.

At the Puth and Waubach anticlines (Schinnen area and area of Heerlen/Landgraaf, respectively), the coal-bearing layers are locally folded (Fig. C 2, section A-A‘). Here, on a local basis, only few coal seams occur; therefore, little to no mining operation was carried out (see chap. 3.1).

The broad Willem fault in the area of the Willem Sophia and Domaniale mining concessions is a further remarkable SW-NE-striking structure; mining was omitted in the vicinity of this structure.

2.3 Structure of the overburden

In the northwestern part of the Maurits and Emma coal mining concessions (Stein region and Schinnen region, respectively), the overburden thickness extends to about 350 m. In the eastern part of the South Limburg mining district, east of the Feldbiß fault zone (Hendrik and Julia concessions), the overburden covers about 250 m. In the Kerkrade region, the overburden thickness decreases to about 10 to 20 m. In the adjacent German Wurm-valley, the coal-bearing layers are cropping out at ground surface level (Fig. C 3).

The hydraulic interactions between the coal-bearing bedrock and the overburden are discussed in more detail in the report of WG 5.2.4/5.2.5. With respect to the work in hand, the following aspects are of importance:

- The main tectonic faults - the Heerlerheide fault and the Feldbiß fault zone - subdivide the South Limburg mining district into three hydrogeological independent blocks; each block is characterised by an individual composition of the overburden and hence a different hydrogeological regime (“hydrogeological homogeneous areas”; Fig. C 3).

- According to ROSNER (2011), the hydrogeological homogeneous area I is characterised by a basal Cretaceous aquifer (Maastricht limestone).
  Close to the ground surface, a further aquifer is situated in the sandy, locally gravelly Tertiary and Quaternary sediments.

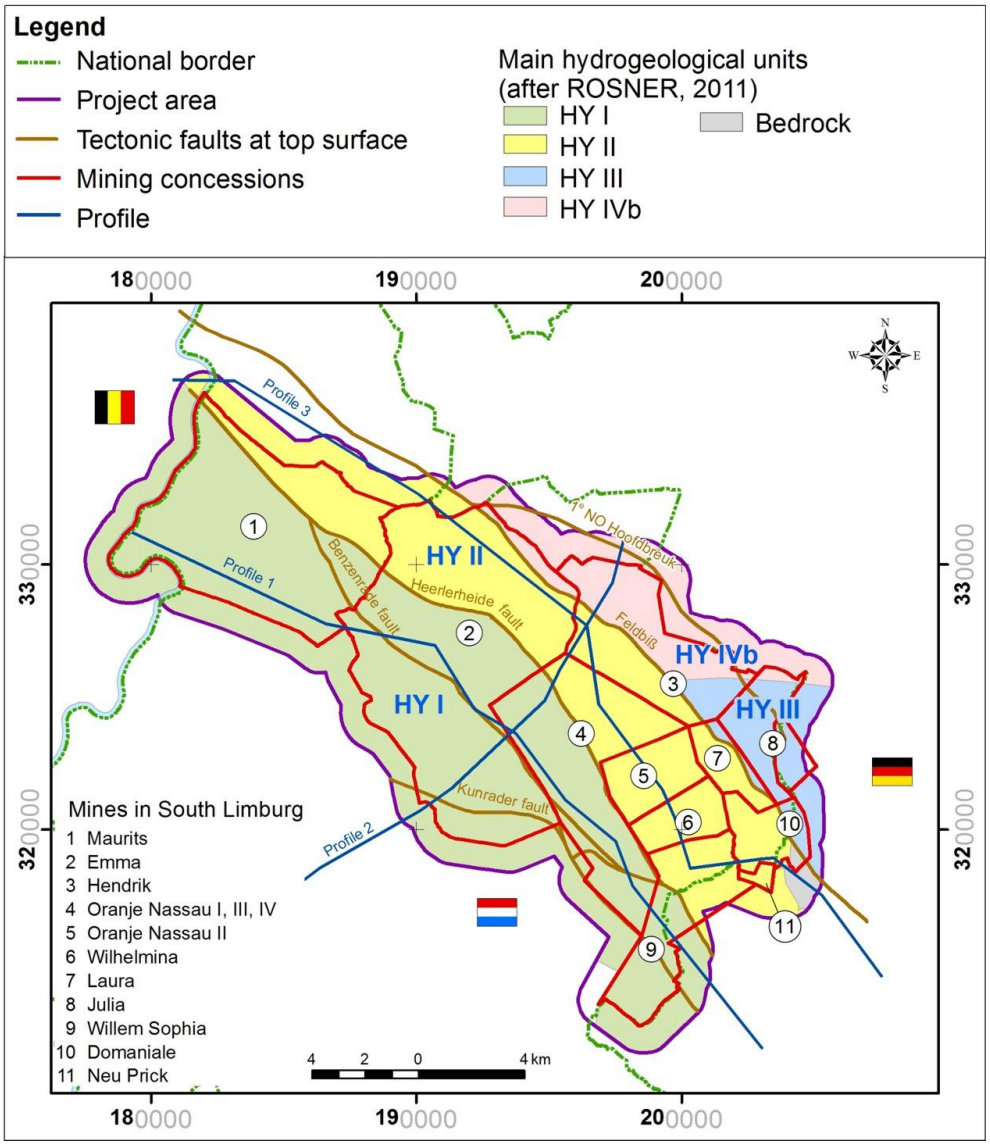

Fig. C 3: Hydrogeological structure of the overburden (after ROSNER, 2011)

- In contrast, the hydrological homogeneous areas II and III are characterised by Tertiary strata mainly, with silt- and clay layers interbedding with sand- and gravel-aquifers as well as brown coal seams.

- In the hydrogeological homogeneous areas III and IV, the groundwater conditions in the South Limburg mining district are interfering with the impacts of groundwater extractions from the German lignite opencast mines as well as the impacts of mine water rise in the Aachen mining district.

- As can be shown by data from piezometers, the groundwater heads in the Cretaceous limestones (hydrogeological homogeneous area I) rise parallel to the mine water heads.

- For the hydrogeological homogeneous areas II, III, and IV in the South Limburg mining district, there is no definite data available that prove the rise of pressure heads in the overburden.
  However, for the hydrogeological homogeneous area IV, corresponding interactions are known from the adjacent Aachen mining district.
  Based on the knowledge gained from inflow of water into the mines that occurred during the operational period, corresponding interactions have to be expected in the hydrogeological homogeneous area II (Fig. C 3).

In the context of differential ground heave at major tectonic faults another crucial question arises in respect of the permeability of fault zones in the overburden.

According to the results from WG 5.2.4/5.2.5 it can be assumed that the major tectonic faults are semi-permeable to impermeable. Owing to this fact, in some aquifers, groundwater levels may develop different on both sides of such a fault zone.

3 Mining conditions

3.1 Location and structure of mine workings

Mining was carried out extensively across the whole area of the South Limburg mining district; however, mining intensity varied with the natural development of coal seams (Fig. C 4). An inventory of the mined area was conducted by WG 5.2.2/5.2.3. An outline of the mined area is given by Fig. C 4. Information about the overall mined thickness is not available.

The mined area is delimited to the southwest by the outcrop of coal seams: To the northeast the successive vertical displacement of the coal-bearing bedrock to greater depth along the major fault zones builds a delimiting factor for the mining: in the Maurits concession by the Heerlerheide fault, in the Emma/Hendrik concessions by the Feldbiß fault zone and in the Julia concession by the 1^{e} NO Hoofdbreuk. Accordingly, these delimiting tectonical structures have to be examined concerning the development of differential ground heave.

Furthermore there are two SW-NE-striking features within the broad mine workings where, owing to the tectonic structure in the underground, little to no mining has taken place: the Puth Anticline, situated between the coal mines of Maurits and Emma and the Waubach Anticline, situated between the coal mines of Julia and Hendrik and between Oranje Nassau II and Oranje Nassau IV, respectively. In a wider sense, the same holds true for the Willem fault in the border area between the coal mines of Willem Sophia/Domaniale and Wilhelmina. Therefore, in these areas, minor mining-related ground movements (subsidence) and ground movements related to the rise of mine water (ground heave) have to be expected as well.

Meanwhile, in the course of the mine water rise, the northwestern part of the South Limburg mining district has been completely flooded to the coal mines of Oranje Nassau I, III, and IV and to Julia. In these areas, the pressure heads in the coal-bearing bedrock have already reached the overburden level. In parts of the southeastern mine district, some mine workings are still situated above the current mine water level (status 12.2014) (Oranje Nassau I, Oranje Nassau II, Wilhelmina, Laura, Willem Sophia, Domaniale, Fig. C 4). In these areas the mine water level currently lies below the base of the overburden.

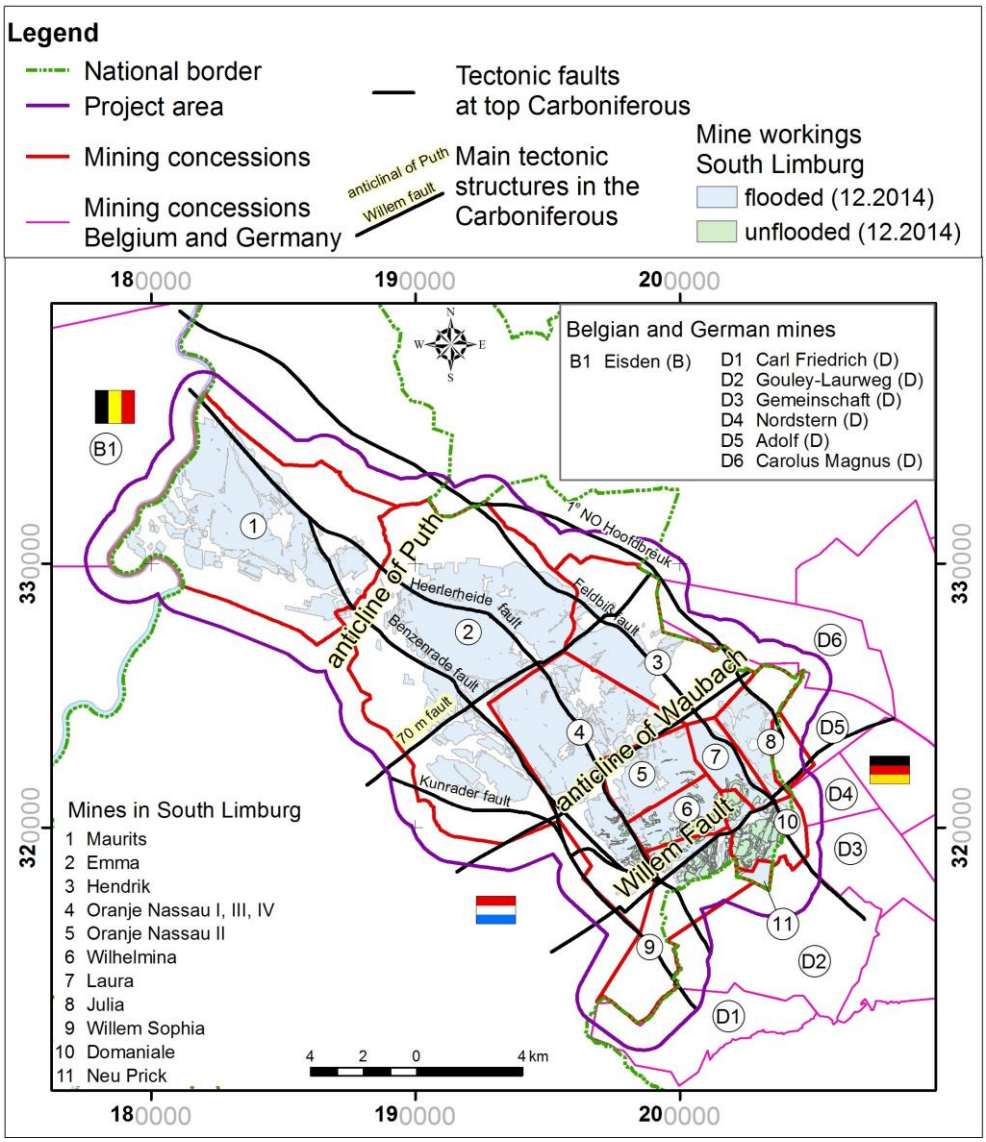

Fig. C 4: Structure of the mined areas

In the course of the further rise of mine water, the mine water level is expected not to reach the base of the overburden in parts of the Willem Sophia and Domaniale coal mining concessions. Regarding the „average case“ that is discussed in the report of WG 5.2.4/5.2.5, mine water will locally rise to a maximum level of about 80 mNAP. This fact is important for the evaluation of the ground heave potential as in these areas no significant changes of the groundwater levels in the overburden are expected (see chap. 3.5).

Regarding the „worst case“ (mine water rise to a level of 110 mNAP), only some single mine workings in the Domaniale concession will lie above the mine water level. In this case, the mine water level will reach the base of the overburden more or less in the complete mining area.

3.2 Mining-induced subsidence

Information about subsidence from the active mining period is available from an inventory that was conducted by the mining authority (published by PÖTTGENS, 1985). Herein, only the findings from the area of the „Staatsmijnen“ (Maurits, Emma, Hendrik, Wilhelmina) as well as from „Laura en Vereeniging“ are presented. Respective information for the coal mines Oranje Nassau, Willem Sophia, and Domaniale is not available.

Fig. C 5 illustrates the location of the areas with most extensive mining within the Maurits, Emma, and Wilhelmina concessions. In the area of the Maurits coal mine, maximum subsidence of about 5,0 to 7,5 m was observed. Within the Emma and Wilhelmina concessions, maximum subsidence of 7,5 to 10,0 m occurred. Similar subsidence values (7,5 to 10 m) have also to be expected for the centres of mining within the Oranje Nassau and Domaniale concessions.

In general, the amounts of subsidence decrease noticeably when approaching the margins of the mined area. Only in the Brunssum area significant subsidence of about 5,0 to 7,5 m was documented up to the Feldbiß fault zone. Hence, this area has to be assessed in particular regarding possible differential ground heave at the Feldbiß fault zone.

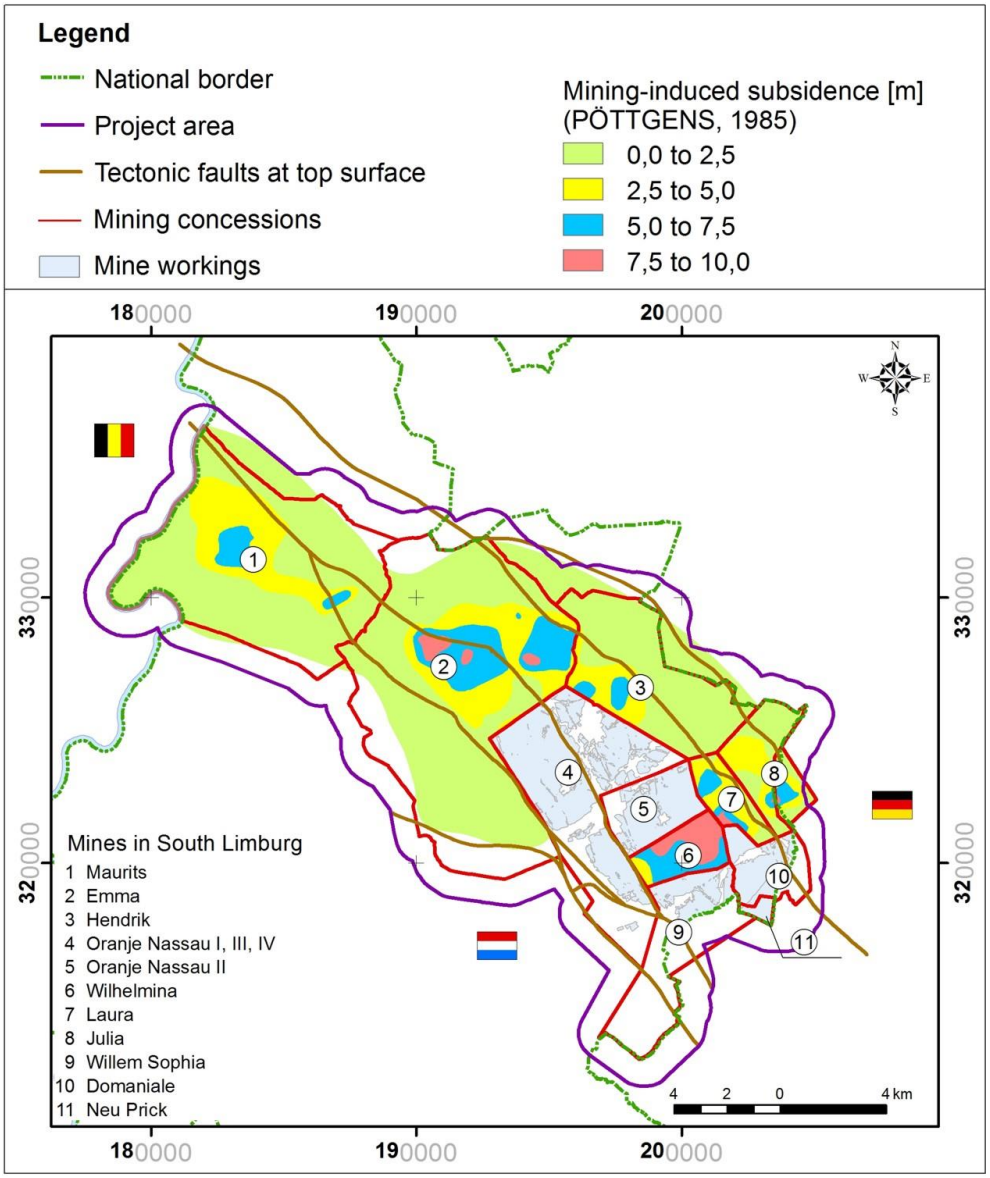

Fig. C 5: Mining-induced subsidence according to PÖTTGENS (1985)

3.3 Drempels and Verzakkingen from the active mining period

Along the major tectonic fault zones at the margins of the mine workings Drempels and Verzakkingen from the active mining period might constitute an additional risk factor for the development of significant differential ground heave respectively discontinuities. An inventory of Drempels and Verzakkingen was conducted by WG 5.2.2/5.2.3 using the information that is available in mine maps (Fig. C 6). There is no respective documentation for the Willem Sophia mine but it is for sure that Drempels and Verzakkingen have also occurred there during the active mining period.

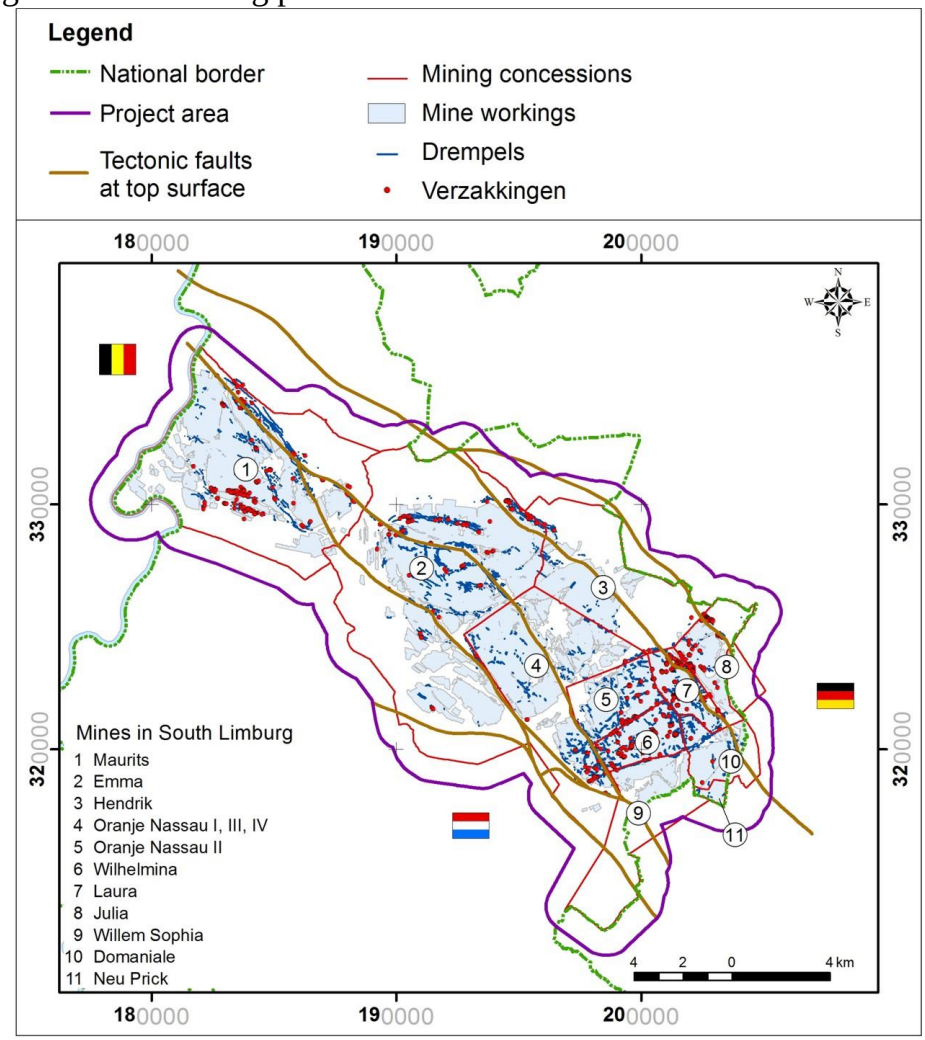

Fig. C 6: "Drempels" and "Verzakkingen" from active mining documented in the mining maps (no documentation for Willem Sophia available)

Among the numerous Drempels and Verzakkingen that are documented in the areas of the mine workings, the Drempels and Verzakkingen located in the vicinity of major tectonic faults (Heerlerheide fault/Maurits coal mine in the Geelen area and Feldbiß fault zone/coal mines Emma and Hendrik in the Brunssum area) are of particular interest in the context of the work in hand. Furthermore, numerous Drempels and Verzakkingen are documented at the eastern margin of the Julia coal mine along the 1^{e} NO Hoofdbreuk spreading on both the Dutch and the German territory.

There is a further noticeable accumulation of Drempels and Verzakkingen at the Feldbiß fault zone in the Eygelshoven area. This accumulation, however, is situated within the major mine workings between the Laura and the Julia coal mine rather than in a marginal mining situation. Therefore, in the context of the potential development of differential ground heave, this accumulation of Drempels and Verzakkingen is of minor relevance according to the experiences from other mining regions (see chap. 1).

3.4 Hydraulic basins and trends of mine water levels

Ground heave generally develops parallel to the rise of mine water; therefore, in the first place, the development of ground heave depends on the date dewatering measures are ceased and the rate of mine water rise. In intervening periods of stagnating mine water level ground heave abates as well.

Furthermore the decompaction of the overburden layers owing to the increase of pressure heads in the overburden is of particular importance for the amount of ground heave (see report WG 5.2.1 - part 2). Especially in the areas of thicker overburden in the northwestern part of the South Limburg mining district, the

mine water level reached the overburden at an early stage and, thus, an increase of pressure heads was induced in the overburden.

Hence, the understanding of the hydraulic structure of the mining district as well as of the temporal progression of the mine water rise in the different parts of the mining district are of particular importance for the understanding and for the interpretation of the ground movements that have been observed in the course of mine water rise till now (see part A). An outline of the hydrogeological structure in the mining district is given by Fig. C 7.

The hydraulic interactions between the coal mines are determined by the lowermost galleries that are connecting the mines. Until the level of these galleries is reached, the rise of mine water takes place in isolated basins. Once these galleries are flooded, the isolated basins merge gradually to a larger basin with a uniform mine water level.

Only the Maurits coal mine (Basin 1) and parts of the mine workings of the Hendrik coal mine (east of Feldbiß fault zone, Basin 4) are not hydraulically connected to the other coal mines of the South Limburg mining district; the connecting galleries were sealed by dams during the abandonment of the coal mines. In the 1970s, the connecting galleries between the coal mines of Laura and Julia were also sealed by dams. The progression of mine water rise, nevertheless, indicates a hydraulic connection between these both coal mines.

Today, there are still five shafts available for monitoring the mine water rise in the South Limburg mining district (Fig. C 7, see report WG 5.2.4/5.2.5). By means of these shafts, the mine water level in the major water provinces (Northern Main Basin, Central Main Basin, Southern Main Basin; see report WG 5.2.4/5.2.5) can be observed. There are no measuring possibilities

for the hydraulically isolated basins 1 and 4 anymore; hence, the mine water level in these areas is unknown.

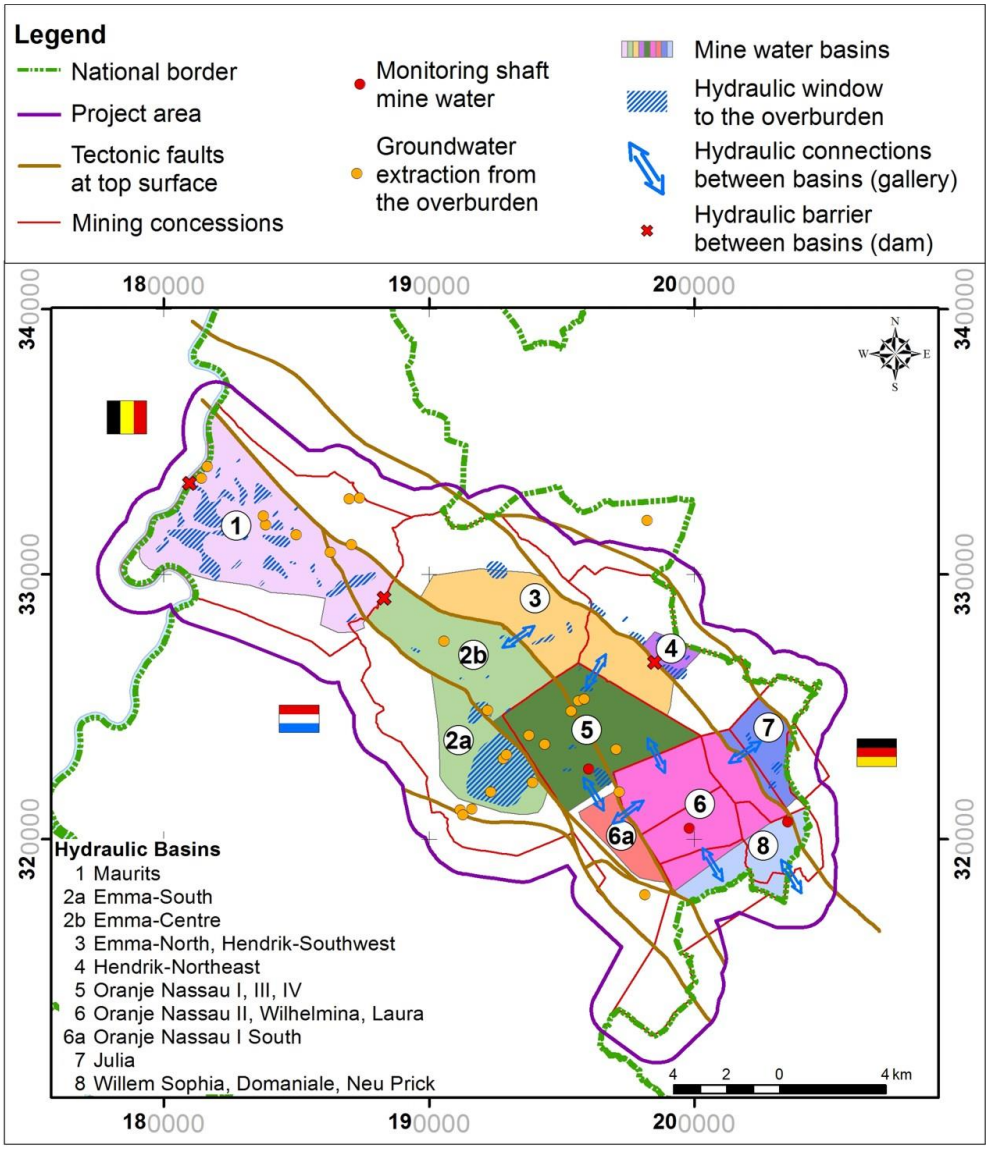

Fig. C 7: Hydraulic structure of the mining district showing documented hydraulic windows to the overburden

The progression of mine water rise is illustrated by Fig. C 8. In principle, three phases of mine water rise can be distinguished:

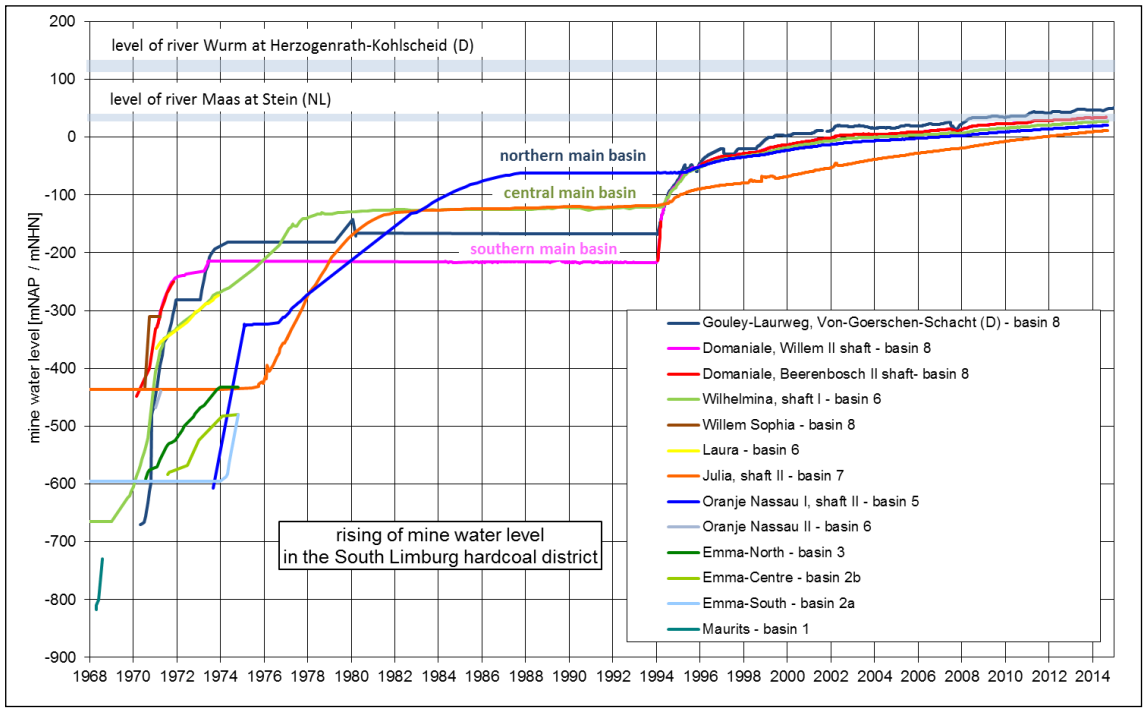

Fig. C 8: Progression of mine water levels since the abandonment of coal mines

- In the first phase, mine water rose to different levels in parts of the separate basins due to the successive abandonment of coal mines in South Limburg (1967 - 1974).

- In the second phase, mine drainage at the Beerenbosch II shaft (Domaniale coal mine) was resumed in 1973 at a level of -241 mNAP in order to protect the coal mines of the Aachen mining district. Until 1988, the mine water levels in the different basins of the South Limburg mining district rose independently until they reached the level of a connecting gallery to a neighbouring basin. Then, all the mine water flowed to the Domaniale mine via the system of interconnected basins. The mine water remained at these levels in the whole area, and all mine water was pumped from the Beerenbosch II shaft to the Wurm river.

  In this second phase, three main basins developed, each characterised by a homogeneous mine water level at levels around -61 mNAP (northern main

basin with basins 2, 3 and 5, as shown in Fig. 4), -120 mNAP (central main basin with basins 6a, 6 and 7) and -214 mNAP (southern main basin, basin 8).

- The third phase started with the terminal cessation of the dewatering measures at the Beerenbosch II shaft (and the Von-Goerschen-shaft in Würselen, Germany) in January 1994. Within one year, a more or less unique mine water level developed in each of the three main basins. Since then, the mine water level has been rising at a more or less uniform level throughout the whole area of the South Limburg mining district (except basins 1 and 4).
- Due to the limited hydraulic connection, a slightly greater difference of the mine water levels developed between the Julia coal mine and the rest of the mining district; however, the difference continues to decrease.
- Thus far, there is no definite knowledge about the mine water levels within both the Maurits coal mine (basin 1) and the Hendrik NE basin (basin 4).
  For the Maurits coal mine (basin 1), the continuing rise of groundwater levels in the overburden (Maastricht limestone) is shown by data from a deep piezometer in the city of Stein. These data indicate that also in this area the rise of mine water is still continuing.

3.5 Influence of mine water rise on the groundwater levels in the overburden

The hydraulic conditions in the overburden as well as the hydraulic interactions with the mining level in the Carboniferous rock are described in detail in the report of WG 5.2.4/5.2.5. Areas of increased inflow of groundwater from the overburden during the mining period (hydraulic windows) are depicted in Fig. C 7.

In assessing the impact potential of ground heave, the areal extension and the amount of rising pressure heads in the overburden with the induced decompaction of the overburden layers are of importance. The following facts have to be stated in this context:

- In the hydrogeological homogeneous area I within the South Limburg mining district (Fig. C 3), the rise of mine water induces an areal increase of the pressure heads in the Cretaceous limestones (Maastricht limestone).

- In the Cretaceous limestones, the documented amounts of rising pressure heads add up to about 25 m in the Maurits mine (deep piezometer B60C0860 in the city of Stein, period 1986 - 2014 only); in Emma-Centre, the amounts add up to approx. 12 m (piezometer B60C0839 in the city of Schinnen) and in Emma-South, the amounts add up to about 4 m (piezometer B62B0838 in the city of Voerendaal).

  For the future, the pressure heads in the Cretaceous limestones are expected to rise between 3 and 10 m within the Maurits concession; for the Emma concession, a further rise of 1 to 2 m is predicted.

- This rise, in the main, is delimited to an area southwest of the Heerlerheide fault.

  As a consequence, especially within the Maurits concession where mining is restricted to the southwest of the Heerlerheide fault, the influence of the mine water rise on the pressure heads in the overburden will be significantly different on both sides of the fault.

  The actual development depends on the permeability of the fault zone.

- Due to the absence of an appropriate deep groundwater piezometer, there is no definite knowledge about significant alterations of the pressure heads in the overburden due to rising mine water in the hydrogeological homogeneous

areas II, III, and IV.

According to WG 5.2.4/5.2.5, a prevailing aquifer system in the Tertiary sediments has to be considered there. The near-surface groundwater piezometers do not indicate any significant evidence for an impact of mine water rise.

Basing on the knowledge gained from evaluations in the adjacent Aachen mining district, it has to be assumed that, in the area of the Julia coal mine, pressure heads are rising within the basal Tertiary sands (see ROSNER, 2011).

- Regarding the whole area of this Tertiary aquifer system, a further minor rise of pressure heads in decimetre range is predicted (report WG 5.2.4/5.2.5). In the „worst case“ scenario, the occurrence of slightly greater rises of pressure heads (about 2 to 3 m) is expected to take place in the area of the Laura and Domaniale coal mining concessions only. Hence, overall, the alterations of pressure heads in the Tertiary aquifer system are expected not to cause any further significant decompaction; consequently, they are expected not to contribute significantly to further ground heave in this area.

- Therefore, in the marginal area of mining within the hydrogeological homogeneous areas II (Emma/Hendrik) and IV (Julia), on both sides of the major tectonic fault zones that margin the mine workings (Feldbiß fault zone and 1^{e} NO Hoofdbreuk), no significant additional impact potential from different developments of pressure heads in the overburden has to be expected.

4 Experiences with the previous development of ground heave

For the South Limburg mining district decades of experiences with the development of ground heave during the course of mine water rise are already available. These experiences gained from the observations of the previous developed kinematics provide an essential basis for the assessment of possible future impacts to the ground surface. Furthermore the already observed ground movements along the major tectonic faults give important information whether ground heave decreases gradually at these margins of the mine workings or indications for the development of discontinuities are visible.

The basis for the assessment of the previous ground movement that has taken place during the rise of mine water was established by TU Delft (see part A). For the period starting from 1992, in addition to the levelling data, there are satellite data available; these data allow for a significantly more differential evaluation of the ground movement. The framework and the data processing are described in part A.

Basing on the evaluation of these data, very detailed insights into the temporal and spatial development of ground movements within the South Limburg mining district could be gained, starting from the 1970s.

4.1 Spatial distribution of ground heave

An outline of the total ground movement that have been detected in the South Limburg mining district since 1974 is given by Fig. C 9.

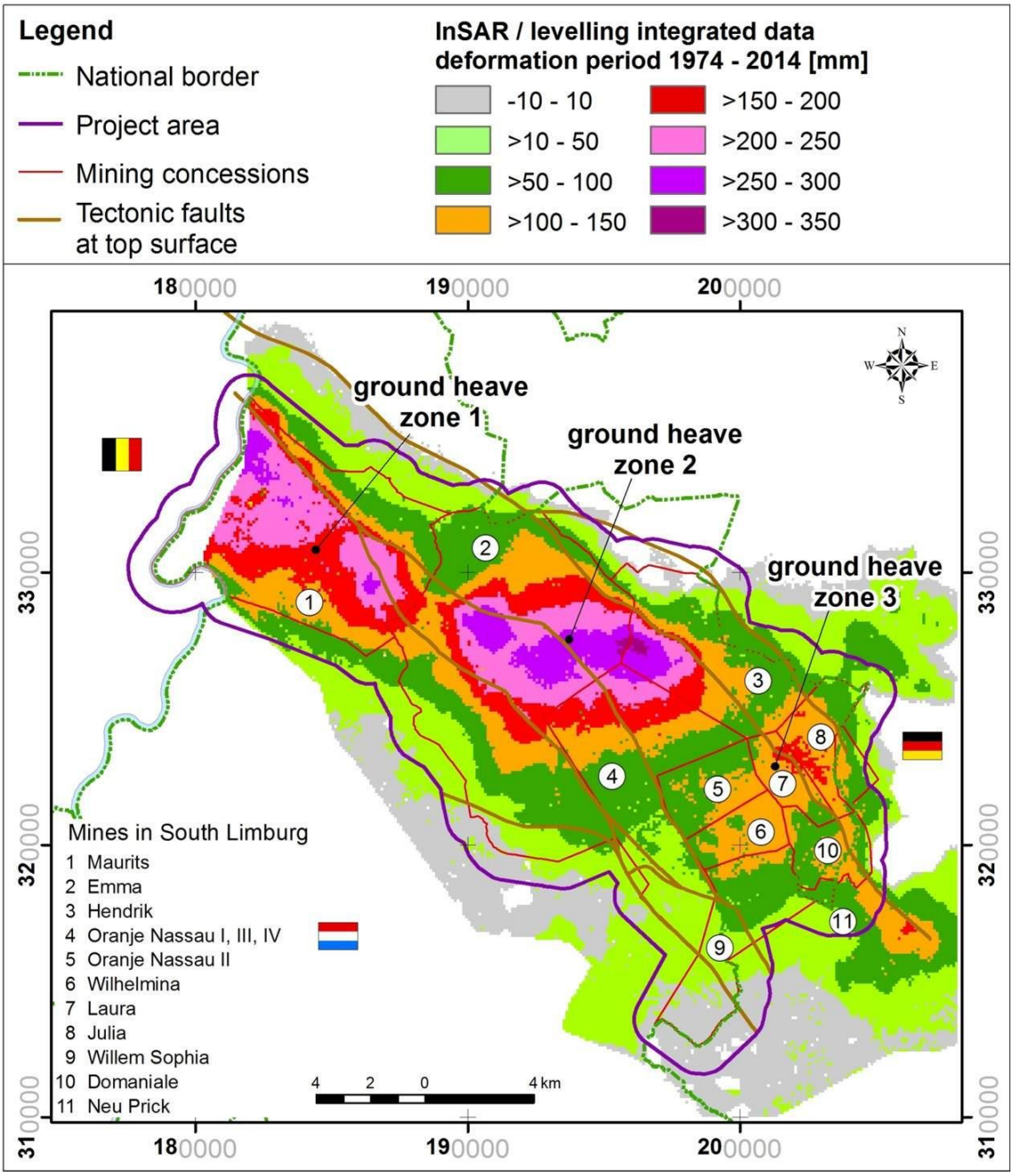

Fig. C 9: Ground movements in the South Limburg mining district from the beginning of mine closure in the 1970s - period 1974 - 2014

The centres of ground heave are situated in the areas of extensive mining in the concessions of the Maurits, Emma, Hendrik and Oranje Nassau III, IV coal mines at Geleen, Stein, and Brunssum. In these areas, ground heave has attained

maximum amounts of 300 to 350 mm until now. The significantly greater amounts of ground heave that, in contrast to the coal mines in the southeastern mining district, prevail in these areas have to be also ascribed to the decompaction of overburden layers in particular; obviously, the impoundage of the basal overburden also induced a spacious rise of pressure heads in the overburden aquifers in these areas.

In the southeastern coal mines of the South Limburg mining district (Wilhelmina, Willem Sophia, and Domaniale), however, significantly smaller amounts of ground heave were observed; the maximum amounts attain around 100 to 150 mm. The overburden has not yet been involved significantly in this area.

In contrast, within the Julia concession, noticeably greater values of ground heave (approx. 150 to 200 mm) have been detected. There the overburden is already involved in changes of pressure heads; consequently, an additional decompaction of the overburden layers has to be expected.

The areas of ground heave are significantly divided by the SW-NE-striking Puth and Waubach anticlines, as well as by the Willem fault (see Fig. C 4). Resulting from the minor mining activity along these structures, ground heave is decreasing gradually in these areas. Hence, there is a spatial tripartition of the areas of ground heave (Fig. C9):

- a northwestern zone of ground heave within the Maurits concession (basin 1) - “ground heave zone 1”,
- a central zone of ground heave within the Emma/Hendrik, Oranje Nassau I, III, and IV concessions - “ground heave zone 2”, as well as a
- southeastern zone of ground heave within the Oranje Nassau II, Wilhelmina, Laura, Julia, Willem Sophia, and Domaniale concessions - “ground heave zone 3”.

Overall, the areas of significant ground heave (> 10 mm) are mainly limited to the study area as well as to the envelope of the mine workings. In the border region between the South Limburg and the Aachen mining district, additional ground heave is taking place that is induced by the flooding of the German coal mines. In the border region between the South Limburg an the Belgian mining district (Eisden mine) additional ground heave resulting from the flooding of the Eisden mine has been taking place since end of the 1980s. This is also particularly reflected in the relatively increased amounts of ground heave in the northwestern periphery of the Maurits coal mine (in the vicinity of the Maas river).

Considering the spatial distribution of significant gradients in the development of ground heave, the following areas are most important:

- the northeastern edge of the mine workings of the Maurits coal mine in Geleen, along the Heerlerheide fault - the northeastern margin of ground heave zone 1;
- the northeastern edge of mine workings of the Emma and Hendrik coal mines in Brunssum, along the Feldbiß fault zone - the northeastern margin of ground heave zone 2.

Apart from these areas with higher gradients of ground heave, in the remainder of the mining district, changes in ground heave are developing over a wider area but with significantly smaller gradients.

4.2 Temporal development of ground heave

Basing on the evaluation of the long-term levelling data, TU Delft elaborated representative time-deformation-diagrams for each basin of the South Limburg mining district (see part A). For the period starting from 1992, more detailed

time-deformation-diagrams are available through the integration of InSAR-data (see part A).

For an overall characterisation of the temporal development of the ground movements in the different basins of the South Limburg mining district, the individual representative graphs of the time-deformation-behaviour are compiled in a diagram in Fig. C 10; the depicted deformations refer to a reference measurement that was carried out in 2012.

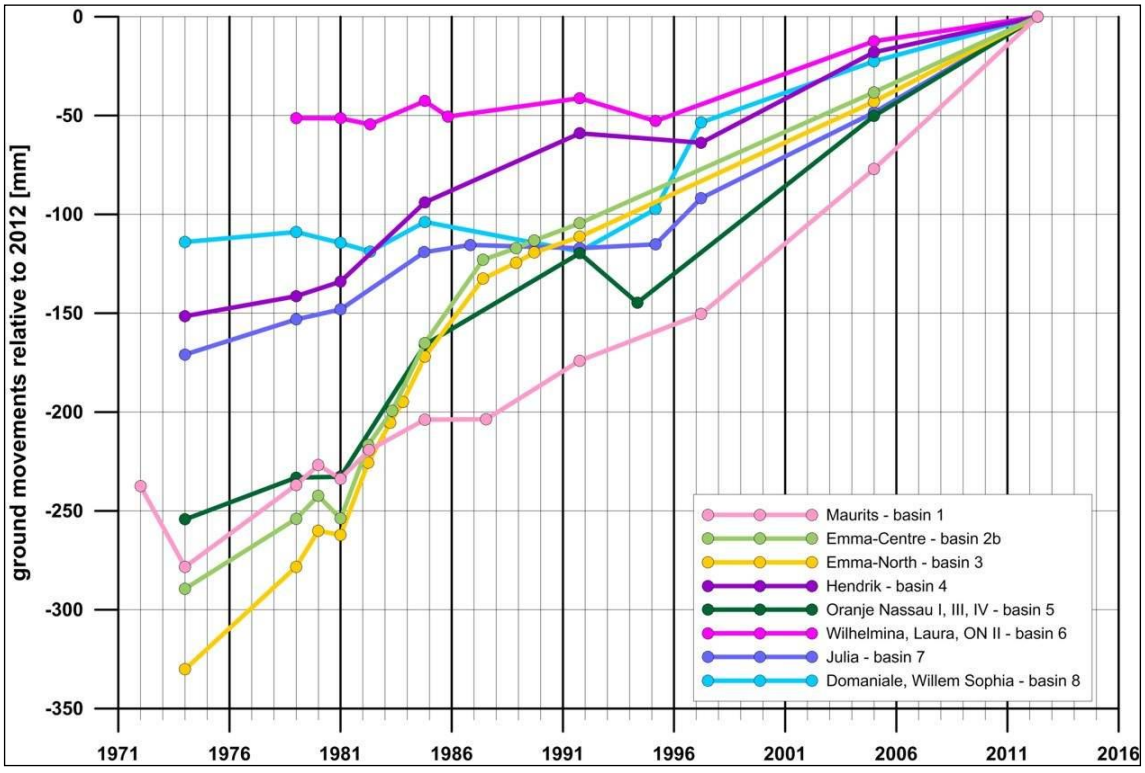

Fig. C 10: Development of the ground movements in the different basins of the South Limburg mining district since the 1970s (see Fig. C 7 for the location of basins)

In principle, the temporal development of ground heave is determined by the course of mine water rise, including the three phases that were discussed in chap. 3.4. In the first phase, major movements occurred in the northwestern basins 1, 2, 3 and 5 (the Maurits, Emma, Oranje Nassau I, Oranje Nassau III, and Oranje Nassau IV concessions). In this phase, the mine workings already got

widely flooded and the basal overburden got involved in decompaction as well. In contrast, in the southeastern basins 6 and 8 (Domaniale, Willem Sophia, Wilhelmina, and Laura concessions), no significant ground heave occurred until 1995; there, the mine workings were not yet entirely flooded. In the basins 7 (Julia coal mine) and 4 (Hendrik coal mine) that are located northeast of the Feldbiß fault zone, at first, only minor ground heave occurred; here, too, the overburden already got involved in decompaction in this phase.

In the second phase, a temporary decrease of the ground heaves became apparent in all basins. In the basins 7 (Julia coal mine) and 4 (Hendrik coal mine) that are located northeast of the Feldbiß fault zone, ground movements were stagnating in the period between 1984 and 1995. In the basins 6 and 8 (Domaniale, Willem Sophia, Wilhelmina, and Laura concessions), still there was no significant ground heave until 1995. In the basins 2, 3, and 5 (Emma/Hendrik, Oranje Nassau I, Oranje Nassau III, and Oranje Nassau IV concessions), a significant decrease of the rate of ground heave was observed.

In contrast, in Basin 1 (Maurtis coal mine) the trend in ground heave that was observed in the first phase seemed to continue at more or less the same rate compared with the first phase. This might due to the fact that, within the Maurits coal mine, mine water rise proceeds independently from the other areas within the South Limburg mining district. The progression of mine water rise within the Maurits coal mine already indicates an additional influence from the Belgian Eisden mine where mine water rises since 1992 and thus gives an additional „movement impulse“.

The spatial distribution of ground heave during the first and the second phase is given by Fig. C 11.

The two-dimensional representation of the ground movements within the South Limburg mining district was constructed on the basis of levelling data and reveals relatively minor values of ground heave (< 50 mm) for the area of the Maurits coal mine. One has to consider, however, that the limited density of measuring points might locally result in misinterpretations with regard to the constructive interpolation.

Basing on both the mining and the hydrogeological conditions, one has to assume that, in this period, ground heave of about 50 to 70 mm, probably up to 90 mm has occurred in the central area of the Maurtis coal mine.

At least since around 1996, in the third phase of water rise, extensive significant ground heave took place in all basins; the spatial distribution of ground heave during this phase is depicted in Fig. C 12.

In both the central and the southeastern zone of ground heave, maximum amounts of ground heave around 110 to 130 mm could be observed in this phase. Despite the minor rise of mine water in the central zone of ground heave (see Northern Main Basin in Fig. C 8), owing to the additional decompaction in the overburden, ground heave takes place in a comparable magnitude in this area.

In contrast, significantly greater values of ground heave (approx. 150 to 180 mm) occur in Basin 1 (Maurits coal mine) during this period. There, in this period, the impact of mine water rise that takes place within the Belgian Eisden coal mine becomes apparent very significantly; in the Eisden coal mine ground heave attains maximum values of > 250 mm (around 300 mm) during this period.

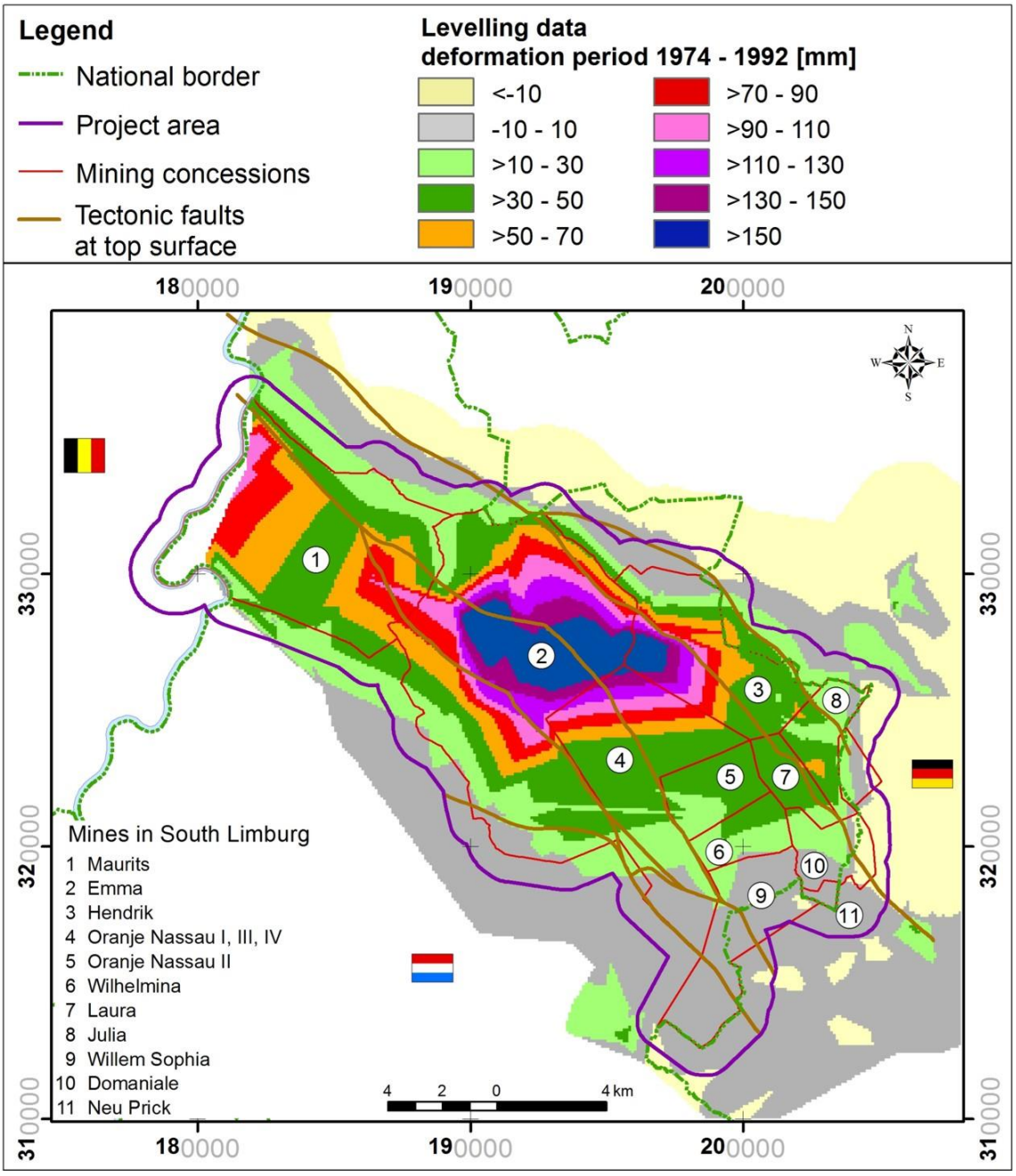

Fig. C 11: Spatial distribution of ground heave in the South Limburg mining district - period 1974 - 1992

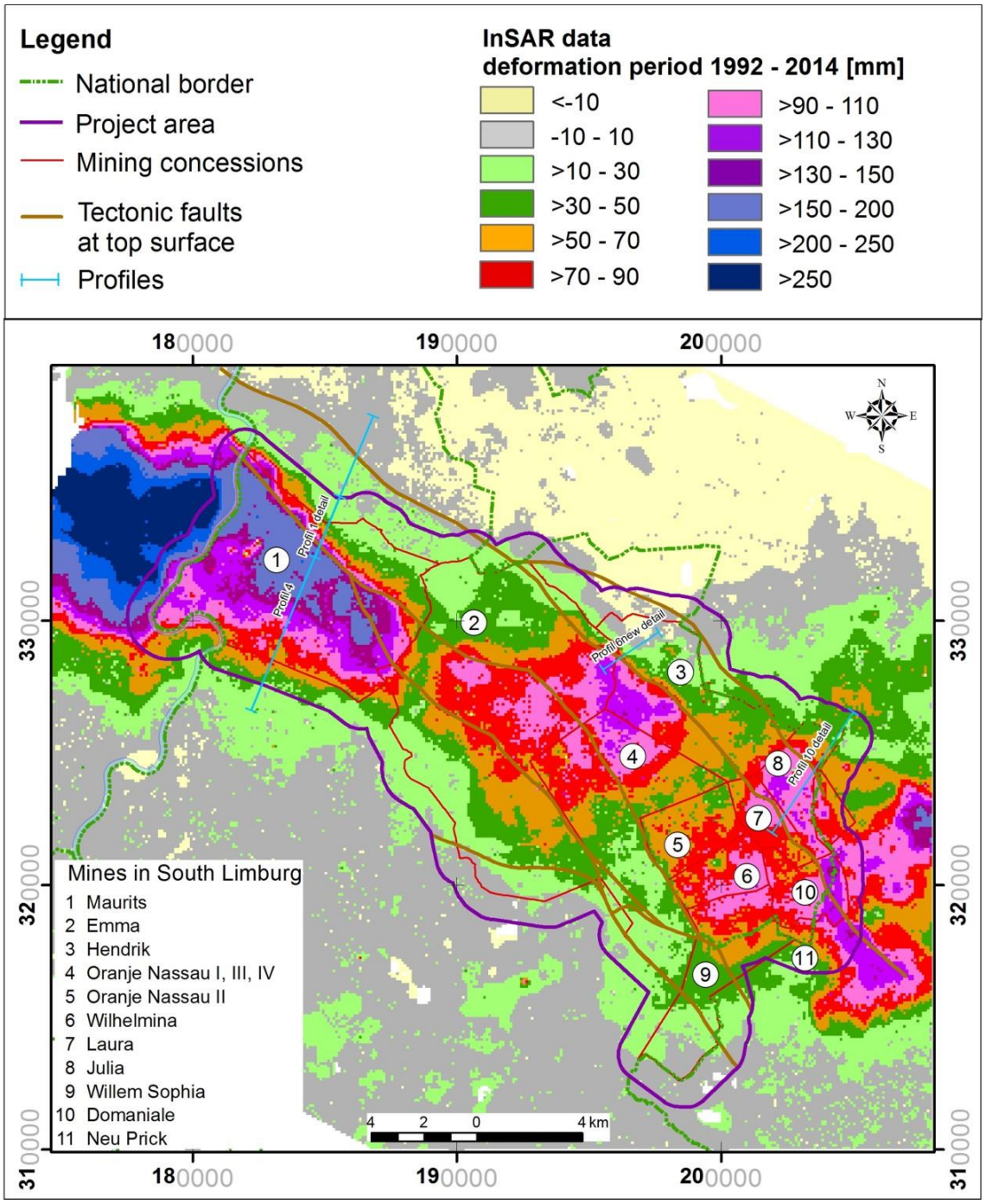

Fig. C 12: Spatial distribution of ground heave in the South Limburg mining district - period 1992 - 2014

The recent development of ground heave (starting in 2009) is illustrated in Fig. C 13. In the meantime, the rate of mine water rise decreased distinctly; mine water rises homogeneously within all basins (except from Basin 1, Maurits coal mine) on a more or less uniform level.

In the southeastern zone of ground heave (ground heave zone 3), only minor amounts of ground heave (< 15 mm) could be observed. More significant ground heave (maximum amounts up to 25 mm) took place in the area of Julia coal mine only. This increased ground heave has to be ascribed to the additional impact of decompaction in the basal overburden layers.

Ground heave continues extensively within the central zone of ground heave (ground heave zone 2); the amounts of ground heave cover about 10 to 20 mm. The focus of ground heave is located within the area of the Hendrik coal mine near the Feldbiß fault zone in the Brunssum area. There, in the period between 2009 and 2014, maximum ground heave covered amounts between 25 and 30 mm while mine water rose about 12 m.

The most marked ground heave is still taking place within the northwestern zone of ground heave (Maurits, ground heave zone 1). There, between 2009 and 2014, ground heave of around 25 to 30 mm has taken place spaciously; within the foci of ground heave, maximum ground heave values of approx. 35 to 40 mm were detected. Approaching the border region between the Maurits and the Belgian Eisden coal mine, the values of ground heave are increasing up to between 40 and 45 mm.

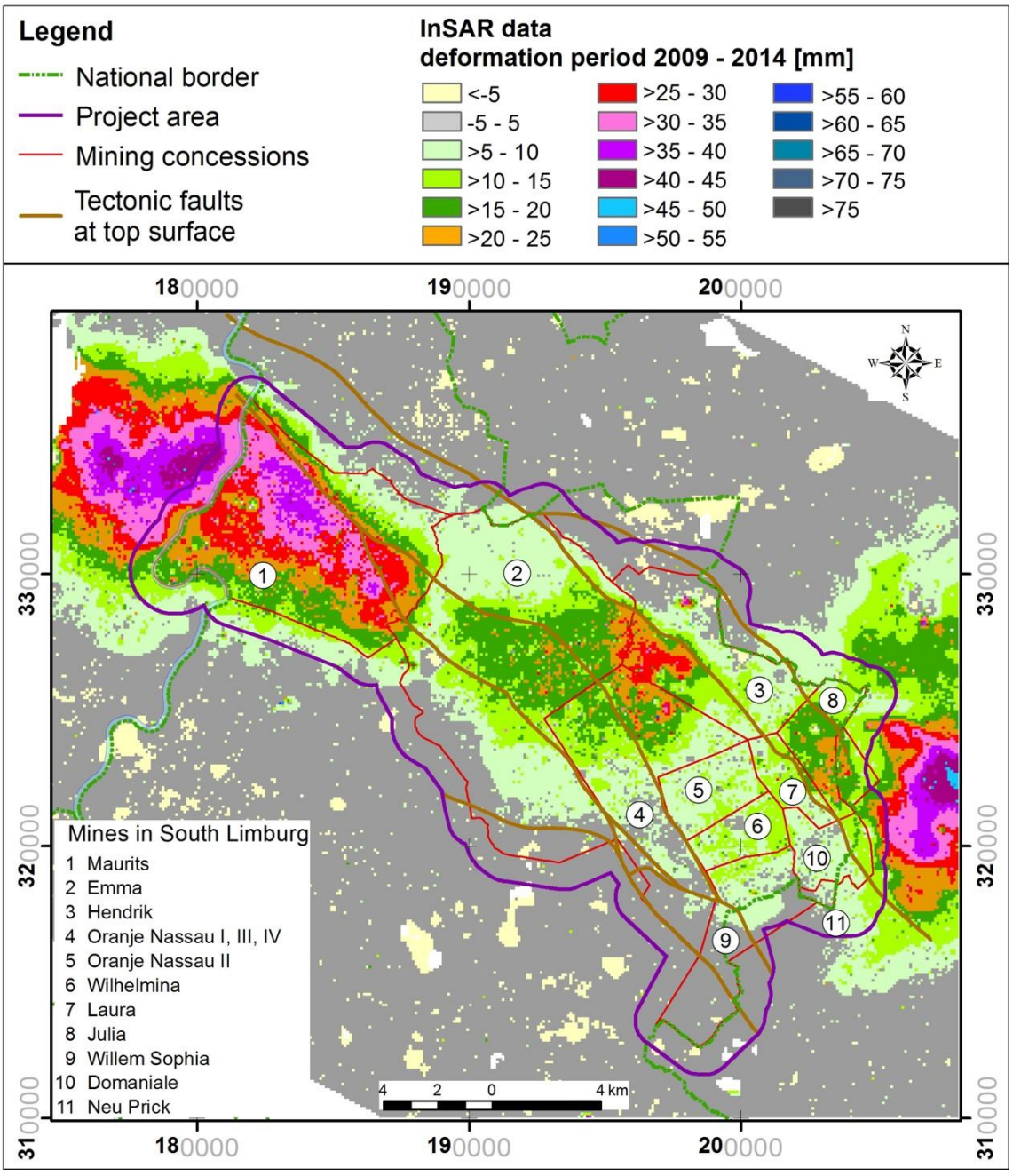

Fig. C 13: Spatial distribution of ground heave in the South Limburg mining district - period 2009 - 2014

The temporal development of ground heave within the most distinct marginal areas of ground heave that are located at the northeastern edge of the Maurits and Emma/Hendrik coal mines (see chap. 4.1) can be outlined as follows:

- Northeastern margin of mine workings within the Maurits coal mine in the Geleen area along the Heerlerheide fault:

  One has to assume that a significant gradient of the ground heave already developed during the first phase of mine water rise along the Heerler-heide fault. During the third phase of the mine water rise, the gradient increases and thus became even more distinct (Fig. C 12). The measurements recorded since 2009 (Fig. C 13) reveal a further significant development of differences in ground heave along the Heerlerheide fault.

- Northeastern edge of mine workings within the Emma and Henrik coal mines in the Brunssum area along the Feldbiß fault zone:

  According to the available measurements a significant gradient already developed during the first phase of water rise along the Feldbiß fault zone (Fig. C 11). This gradient became even more apparent during the third phase (Fig. C 12). Since 2009, the measurements reveal the further increase of differential ground heave along the fault zone. However, the length of the zone that is characterised by significant gradients in ground heave decreases. In this process, the centre of ground heave shifts towards the Brunssumerheide area within the Hendrik concession.

Furthermore, in the third phase of water rise, an additional gradient developed at the northeastern edge of the Julia coal mine at the 1^{e} NO Hoofdbreuk. Ground heave at this edge of mining is continuing since 2009 as well.

4.3 Spatial development of ground heave at the main tectonic faults in the marginal areas of mining

As a basis for a detailed assessment of possible damaging impacts on the surface by differential ground heave in the above described marginal areas of mining with significant gradients in the spatial development of ground heave, the development of ground heave is discussed in detail with the help of cross sections.

For the South Limburg mining district, an appropriate detailed resolution of ground movements is achieved by the evaluation of InSAR-data that are available for the period starting in 1992. As described in part A, TU Delft already constructed numerous representative cross sections for the project area. These cross sections depict the relative development of ground heave referring to the measurement from 1992. Thus the diagrams represent the ground heave that has developed during the third phase of mine water rise.

As discussed in chap. 4.2, locally significant ground heave already developed during the first phase of water rise. This ground heave is not recorded in the diagrams. Nevertheless, the cross sections illustrate the fundamental structural development of ground heave in the marginal areas of mining; this structural development could not have been fundamentally different during the first phase of water rise. By means of these diagrams it is possible to get a strong indication whether the ground heave decreases gradually in the marginal area of mining or ground heave abruptly ends at the major faults and forms a discontinuity. The locations of the cross sections considered in the following are depicted in Fig. C 12.

The cross section in Fig. C 14 impressively illustrates for the ground heave zone 1 (Maurits) the fundamental structural difference between the development

of ground heave that is taking place at the stratigraphy-related southwestern margin of mining and the tectonic-related northeastern margin of mining (Heerlerheide fault).

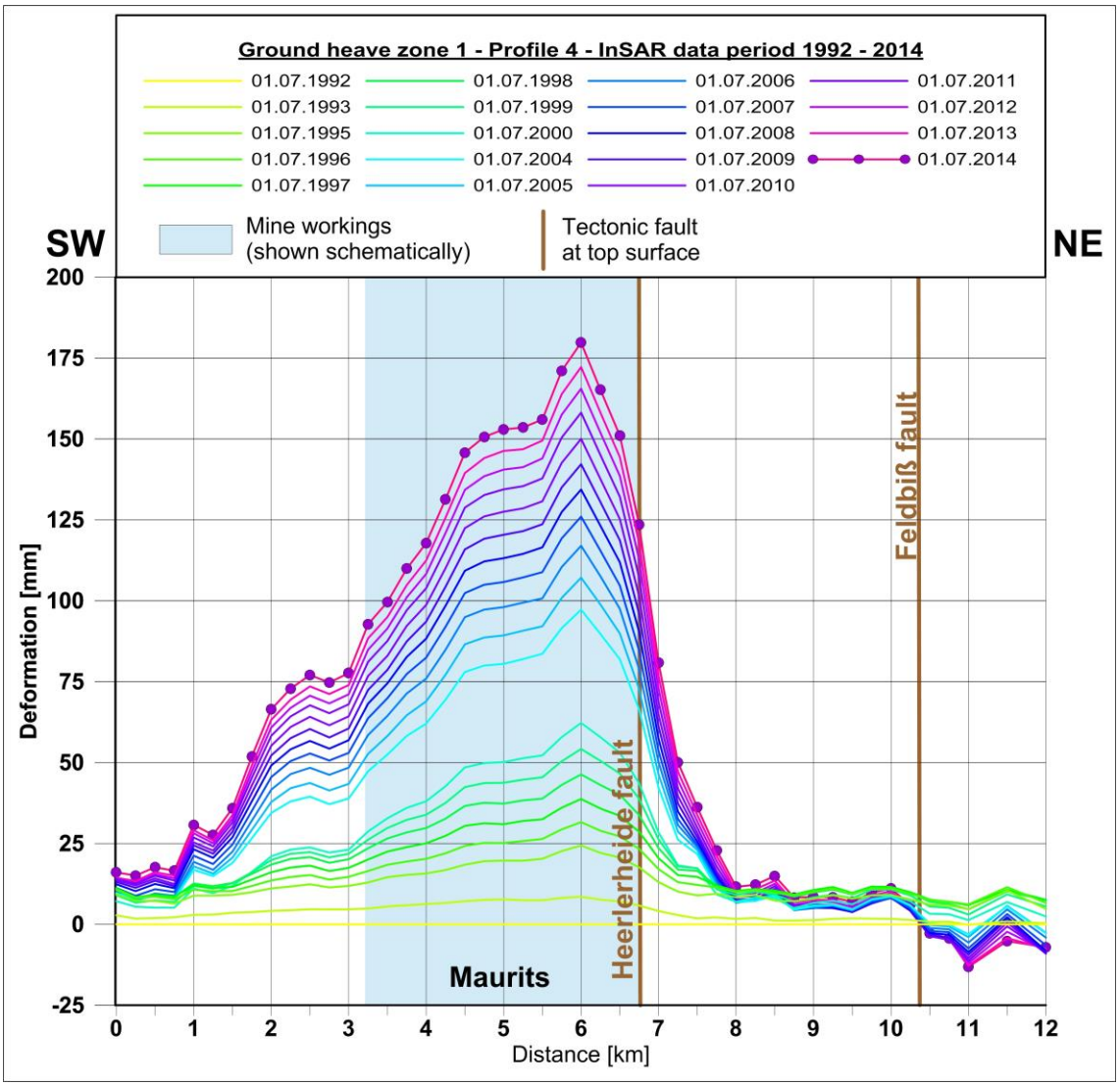

Fig. C 14: Profile 4 SW-NE across the Maurits coal mine (250 m step width)

At the northeastern margin of the Maurits coal mine along the Heerlerheide fault, a comparably steep gradient of ground heave becomes apparent. In contrast, in approaching the southwestern margin of the mined area ground heave decreases gradually with significant smaller gradient and a wider influence area outside the mined area.

Therefore, with regard to possible impacts to the ground surface (discontinuities), one has to consider the tectonic-related northeastern mining margins within the Maurits and Emma coal mines (see chap. 4.2) in particular. In addition to it, the local conditions within the Julia coal mine are discussed.

- Marginal area of ground heave along the Heerlerheide fault in the Geleen area (Maurits coal mine, ground heave zone 1)

As indicated by the cross section across the Heerlerheide fault (Fig. C 15), the amount of ground heave is decreasing gradually from the mined area towards northeast from approx. 160 mm to < 10 mm over a distance of approx. 1,5 km (gradient: about $1 \cdot 10^{-4}$). Even in the most probable location of the Heerlerheide fault (according to TNO), no indication for the development of a significant discontinuity within this marginal transition zone can be identified by the InSAR-data.

This uniform spatial distribution of a gradually decreasing ground heave along the margin of the mined area indicates very strongly, that the Heerlerheide fault has not yet been activated as a primary trajectory in the context of ground heave induced by rising mine water. Furthermore, the kinematic of the ground surface in this marginal ground heave zone indicates that changes in pressure heads within the overburden induced by rising mine water also decrease gradually. Hence the hydraulic effect of the Heerlerheide fault as an impermeable vertical barrier seems to be limited; the results from groundwater modelling performed by WG 5.2.4/5.2.5 hint at a similar interpretation.

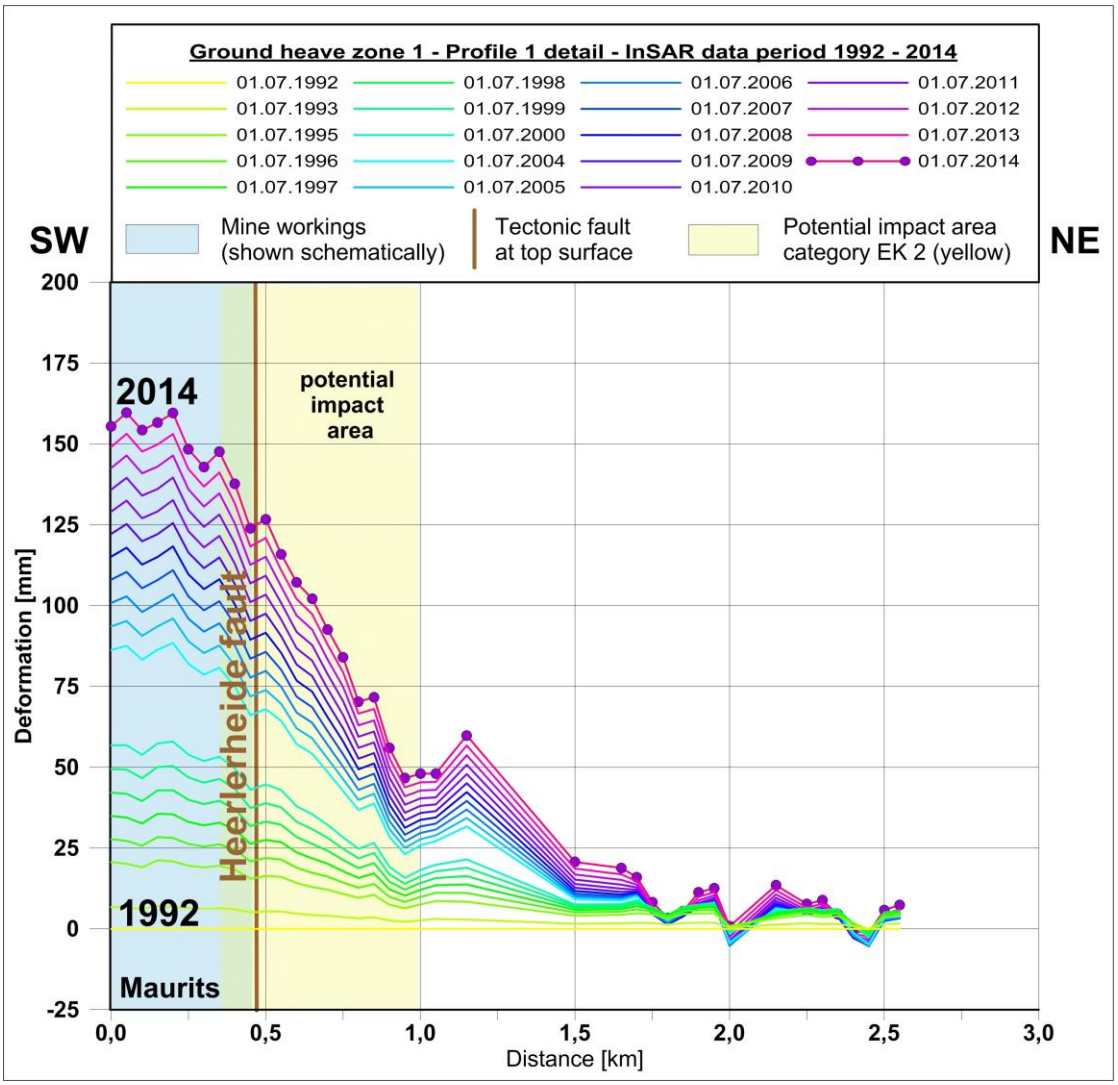

Fig. C 15: Profile 1 detail SW-NE across the Heerlerheide fault zone in Maurits coal mine (50 m step width)

- Marginal area of ground heave along the Feldbiß fault zone in the Brunssum area (Emma and Hendrik coal mines, ground heave zone 2)

The cross section across the Feldbiß fault zone at the eastern margin of the mining area near Brunssum (Fig. C 16) shows a situation very much comparable to the aforementioned situation at the Heerlerheide fault.

Across the Feldbiß fault zone ground heave continuously decreases out of the mined area of Emma to the northeast over a distance of approx. 1,0 km from

values about 120 mm to < 10 mm. Thus, a comparable gradient of $1{,}2 \cdot 10^{-4}$ has developed. The InSAR-data in this marginal transition zone show no significant indication for the development of a discontinuity even in the most probable location of the Feldbiß fault zone, too.

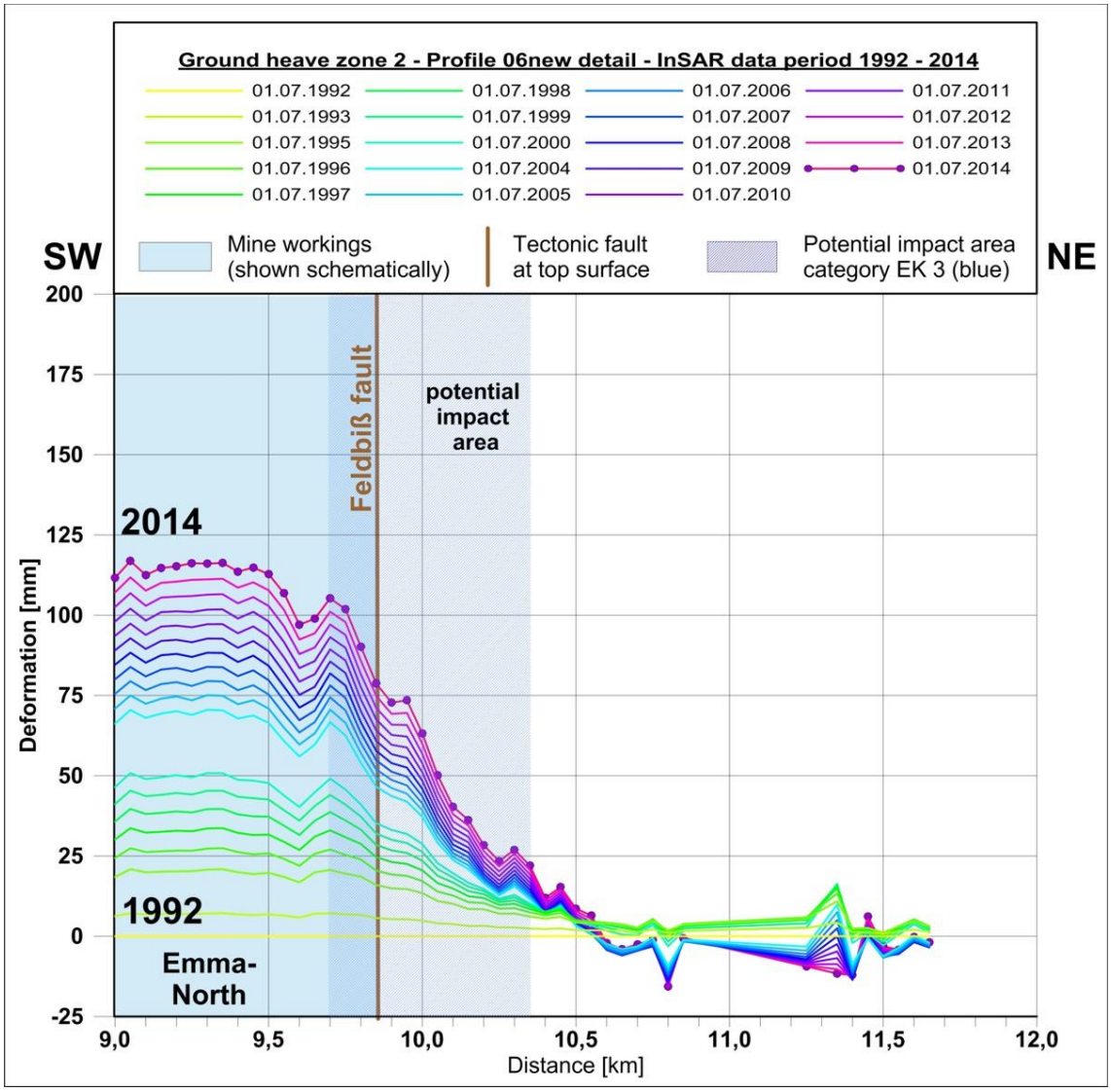

Fig. C 16: Profile 6_{new} SW-NE across the Feldbiß fault zone in Emma coal mine (50 m step width)

Hence the Feldbiß fault zone obviously has not yet been reactivated as a primary trajectory for ground heave due to rising mine water in this area; furthermore no

significant differences in the development of pressure heads in the overburden on both sides of the fault zone have to be expected.

- Marginal area of ground heave along Feldbiß fault zone in the Brunssum area (Zone 3, Laura and Julia coal mines)

Due to the overall minor ground heave that has taken place in ground heave zone 3 since 1974 (see Fig. C 9), initially, there is a minor potential for the development of a significant gradient of ground heave or even discontinuities compared to the margins of the ground heave zones 1 and 2. At the eastern margin of the mined area within the Julia concession a transition zone of ground heave with significant gradient developed. The local situation is illustrated by Fig. C 17.

According to the diagram in Fig. C 17, ground heave continuously decreases out of the mined area of Julia towards northeast over a distance of approx. 0,5 km from values of about 100 to 50 mm. Furthermore east of this area, far beside the mine workings of Julia, significant ground heave can be observed as well. This ground heave can be ascribed to the impact of mine water rise within the Aachen mining district. Due to the significant ground heave that is currently taking place on both sides of the tectonic fault zone and that also has to be expected to take place in the future, the impact potential of differential ground heave at the eastern margin of ground heave zone 3 will not increase significantly in the future.

The ground heave gradient that previously developed at the eastern margin of Julia along 1^{e} NO Hoofdbreuk is approx. $1{,}0 \cdot 10^{-4}$; this matches the conditions at the Heerlerheide fault in the Geleen area and the conditions at the Feldbiß fault zone in the Brunssum area.

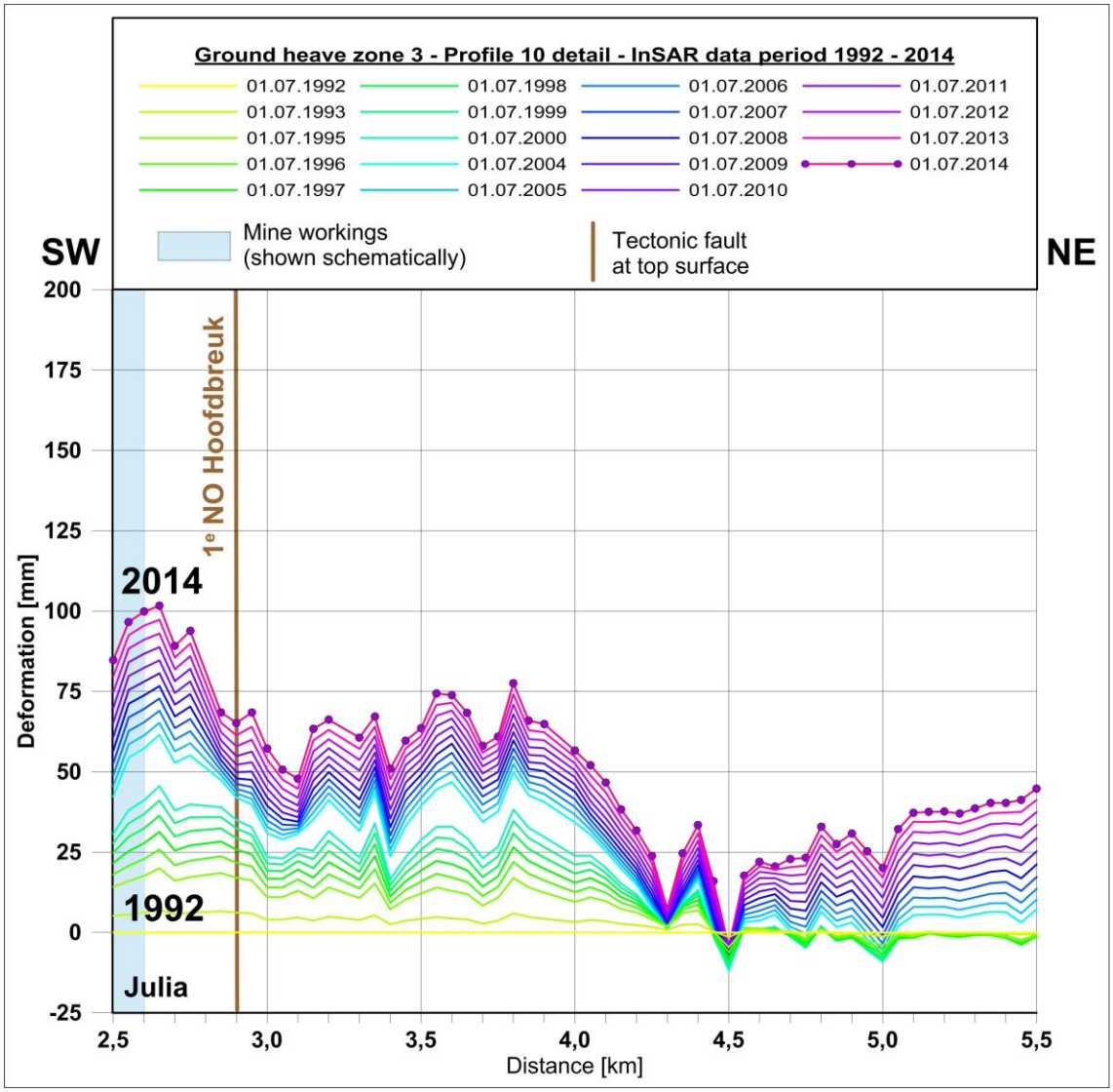

Fig. C 17: Profile 10 detail SW-NE across the 1e NO Hoofdbreuk in Julia coal mine - ground heave zone 3 (50 m step width)

An elongated section in this area, cross section 10 in Fig. C 18, illustrates the different ground heave gradients that developed at the 1e NO Hoofdbreuk as well as at the Feldbiß fault zone within the ground heave zone 3. The diagram reveals that, in the border area between the Laura and the Julia coal mines at the Feldbiß fault zone, ground heave is significantly decreasing towards west. The gradient, however, is considerably shallower than the gradient at the 1e NO Hoofdbreuk; thus, it is considered to be less relevant in the context of possible impacts to the ground surface.

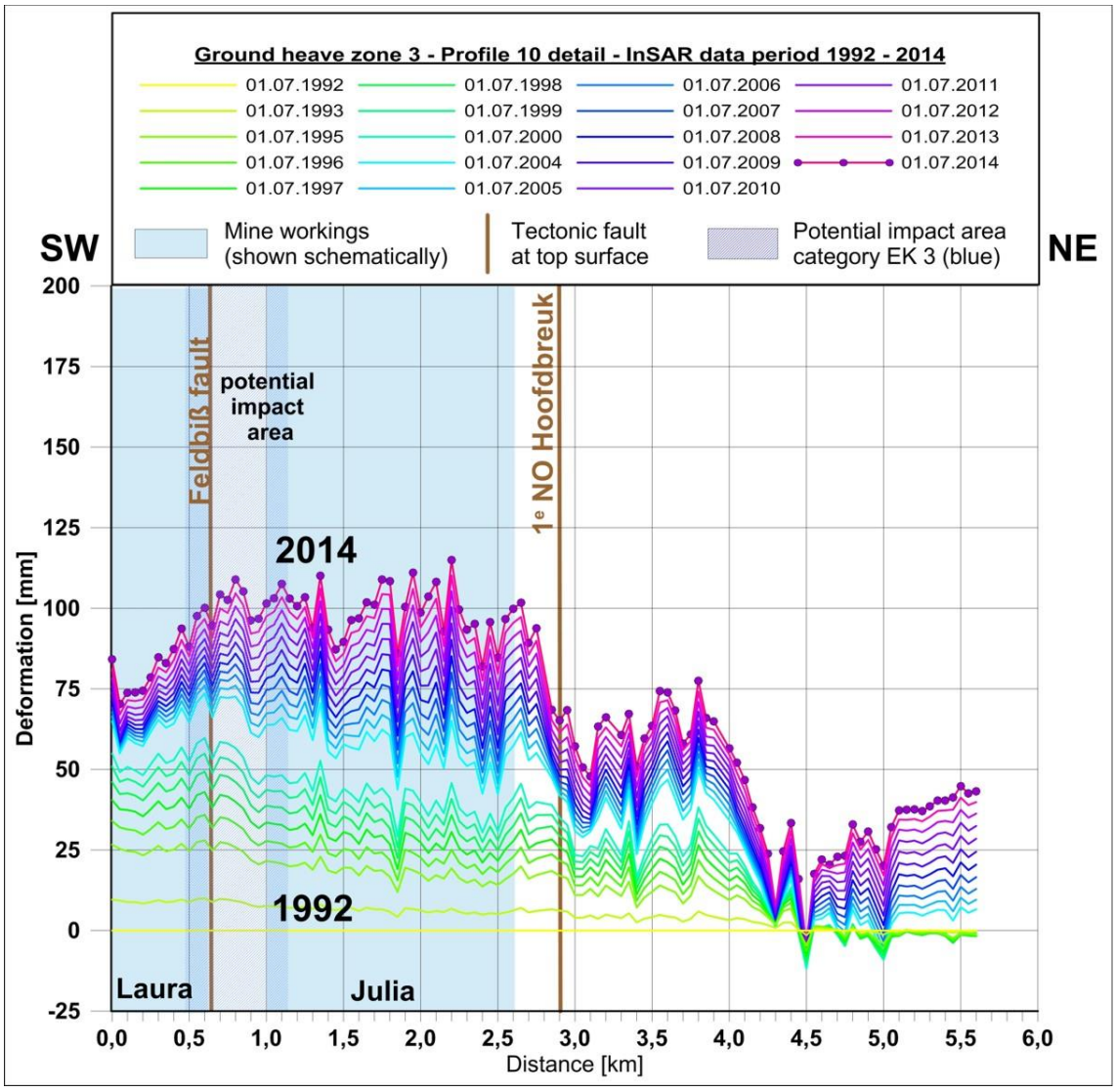

Fig. C 18: Profile 10 SW-NE across the Feldbiß fault zone and 1e NO Hoofdbreuk in Julia coal mine - ground heave zone 3 (50 m step width)

Considering the previous development of ground heave along the distinctive, tectonic-related eastern margins of the mined area in the ground heave zones 1 to 3, the following aspects can be concluded:

- Along the tectonic-related eastern margins of the mined areas transition zones with a gradual decrease of ground heave have developed

- From the centre of the three ground heave zones ground heave decreases in marginal transition zones across the fault zones with a more or less uniform gradient of approx. $1{,}0 \cdot 10^{-4}$.
- The evaluation of the InSAR-data does not provide any distinctive feature that might indicate the development of a significant discontinuity at the fault zones. Furthermore there are no indications for the development of significant differential ground heave along other preferential trajectories.

Regarding the geomechanical and the hydrogeological framework, the following aspects can be concluded from this:

- The tectonic fault zones have not been reactivated as predominant trajectories for differential ground heave due to rising mine water till now.
- The tectonic fault zones are no impermeable hydraulic barriers in the level of the overburden. According to the uniform decompaction behaviour across the fault zones at least a limited hydraulic connection between the separate tectonic blocks has to be assumed. There are no indications for an abrupt change of decompaction ration in the overburden at the tectonic faults due to a differential development of pressure heads in the overburden on both sides of the faults.

  This is also confirmed by the outcomes of groundwater modelling (report WG 5.2.4/5.2.5).

5 Risk assessment

5.1 Setup of an assessment matrix

As a basis for a supraregional applicable differentiated assessment of the risk potential arising from ground heave due to rising mine water in coal mining districts a three-level classification was elaborated within the aforementioned research project "ABSMon" (see chap. 1). The classification provides three impact categories with different probabilities for the occurrence of possibly damage-relevant differential ground heave/discontinuities (HEITFELD, 2015). For that matter the experiences from multiple coal mining districts have been considered (South Limburg-, Aachen-, Erkelenz-, and Ruhr-district). This classification has been applied to the South Limburg mining district within this project. Thereby a supraregional comparison of the risk factors, the impact potentials and actually occurring damage shall be achieved. The approach is transferable to the South Limburg district as the kinematic of the ground heave as well as the geological and mining related framework are comparable. Partially, the evaluations done in the "ABSMon"-project are based on former evaluations of the development of ground heave in the South Limburg mining district (IHS, 2007 and ROSNER, 2011).

Within the discussion about the probability of the development of discontinuities due to differential ground heave and the resulting risk of damage, the conditions in the Erkelenz mining district are an important reference. Yet only there, serious mining induced damages at buildings became apparent (see chap. 1). For the South Limburg mining district, the classification criteria for attributing the above identified zones with most significant gradients of ground heave in the project area to one of the three impact categories have been adjusted to the special tectonic and structural features of the area. This has been done considering the already existing experiences about the development of ground heave in the

project area till now. For the South Limburg mining district, the following classification criteria have been derived from this:

Impact category EK 1 ("red zone") - high probability for the occurrence of significant differences in ground heave and the development of discontinuities:

Scenario 1: Single sided flooding of the mine workings at an impermeable (in the level of the overburden) main tectonic fault zone that disrupts the coal-bearing bedrock as well as the overburden, significant - single sided - rising of the hydraulic pressure heads in the overburden (see city of Wassenberg).

Impact category EK 2 ("yellow zone") - medium probability for the occurrence of significant differences in ground heave and the development of discontinuities:

Scenario 2 a: Single sided flooding of the mine workings at an impermeable (in the level of the overburden) main tectonic fault zone that disrupts the coal-bearing bedrock as well as the overburden, **no** significant - single sided - rising of the hydraulic pressure heads in the overburden.

Scenario 2 b: Single sided flooding of the mine workings at a "permeable" (in the level of the overburden) tectonic fault zone that disrupts the coal-bearing bedrock as well as the overburden with discontinuities (Drempels, Verzakkingen) documented from the active mining period.

Impact category EK 3 ("blue zone") - low probability for the occurrence of significant differences in ground heave and the development of discontinuities:

Scenario 3 a: Flooding of the mine workings at a tectonic fault zone that disrupts the coal-bearing bedrock as well as the overburden with discontinuities (Drempels, Verzakkingen) documented from the active mining period.

Scenario 3 b: Single sided flooding at a tectonic fault zone that disrupts the coal-bearing bedrock as well as the overburden without discontinuities documented from active mining period.

The application of these criteria allows for both the definition of possible zones of discontinuity related to the rising mine water and the differentiation regarding the probability of occurrence.

- fundamental remarks on the probability of occurrence

The three-level classification providing impact categories with different probabilities for the occurrence of an “unfavourable” event is based on the assessment matrix for the classification of risks from sinkholes in areas of near-surface mining relevant for North Rhine-Westphalia. The correspondent assessment matrix was elaborated in collaboration between AK 4.6 “Altbergbau” of the DGGT e.V. (work group on historical mining, German Geotechnical Society) and the DMV e.V. (German Mine Surveyor Association)

Basically, this classification is relatively ranking the probabilities of occurrence based on geotechnical factors; definite, mathematically or empirically derivable probabilities of occurrence cannot be provided. For the impacts from near-surface mining, a definite probability of occurrence can be derived empirically basing on the documented sinkholes.

Related to the flooding of coal mines in North Rhine-Westphalia and in South Limburg serious damages are yet known only in the context of the special geotechnical and hydrological conditions of the Erkelenz mining district that are assigned to impact category EK 1. Hence, in absolute terms according to present experiences a significant probability for the occurrence of damage-relevant discontinuities can only be addressed to areas that are assigned to impact category EK 1.

In contrast, for the underground conditions that are assigned to the impact categories EK 2 and EK 3, there are yet no indications for actual damages that developed in the context of ground heave due to rising mine water from any mining district. Hence, according to present knowledge, the probability for the occurrence of damage-relevant discontinuities in these areas, viewed in absolute terms, has to be regarded to be low.

- fundamental remarks on the risk of damage

Basically, the assignment of possible zones of discontinuity to one of the impact categories does not allow a prediction of the risk of damage or rather the possible severity of damage as it only provides an assignment to a relative probability of occurrence. For the assessment of the risk of damage the actual land use, the type of buildings as well as the actual formation of the discontinuity (e.g. the absolute value of the vertical displacement or the tilting of the ground surface) has to be considered.

- additional assessment criteria

The prementioned impact categories with the assignment of probabilities, in principle, relate to an entire cycle of mine water rise, including the entire flooding of a coal mine and the rising of the mine water level as well as the possibly involved pressure heads in the overburden up to a natural equilibrium.

In the South Limburg mining district the rise of the mine water has progressed quite far till now. Hence, considerable insights about the development of ground heave at potential impact zones along the major tectonic faults already are available. The insights about the development of ground heave in the marginal mining areas till now (gradual transition/discontinuity) provide additional criteria for the assessment of the future impact potential. Furthermore the absolute

amount of the ground heave that is expected in the future has to be considered as a criteria for the assessment of the future impact potential.

In this project these insights have been considered as additional criteria for the assignment of potential impact zones to the above discussed impact categories.

5.2 Assessment of the impact potential

5.2.1 Geological and geotechnical boundary conditions

For the South Limburg mining district the assessment of the impact potential can be based on the following geological and geotechnical boundary conditions:

- The major tectonic faults zones within the South Limburg mining district which disrupt the Carboniferous bedrock as well as the overburden are relatively „young“ fault zones that were active through the Quaternary (especially the Feldbiß fault zone).

- The fault zones can be characterised as broad, complex fracture zones that comprise numerous trajectories. The specific mechanical properties of these tectonic trajectories are unknown. However, owing to the numerous Tertiary clay layers in the overburden, one cannot exclude that clay-smear might has induced a reduced shear strength of the fault zones.

  According to evaluations conducted by the Geological Survey of North Rhine-Westphalia (GD), at the Feldbiß fault zone earthquakes caused vertical ground displacement of 0,8 m at a major trajectory within the fault system (GD NRW, 2008).

  Hence, it cannot be excluded that ground heave caused by rising mine water might concentrate on such a sharp single trajectory characterised by the presence of clay smear and reduced shear strength (similar to the Rurrand fault

in the Erkelenz mining district).

However, comparable conditions have to be expected at the Feldbiß fault zone rather than at the Heerlerheide fault. Along the Heerleheider fault zone a bigger percentage of brittle to plastically reacting limestones is developed.

- In the groundwater model (see report WG 5.2.4/5.2.5) the major tectonic faults in the overburden level are considered to be impermeable and therefore act as hydraulic flow barriers.

  In particular for the Geleen area at the Heerlerheide fault, the groundwater model predicts the rise of pressure heads in the overburden to be in the magnitude of several metres southwest of the fault zone (Maastricht limestone). For the Tertiary layers, on both sides of the fault zone, only minor changes of the pressure heads (< 0,5 m) are predicted.

  Therefore, at least in this area it has to be assumed that the future differences in the changes of pressure heads in the overburden are in the magnitude of several metres to both sides of the fault zone.

  For the other fault zones within the South Limburg mining district, no significant differences in the future development of pressure heads in the overburden are predicted. For the previous mine water rise similar hydraulic conditions have to be assumed.

- From the active mining period discontinuities (Drempels and Verzakkingen) are documented in the mine maps along the major tectonic faults at the margins of the mined areas. This information has to be considered as an additional indication for a possible development of a distinct trajectory due to differential ground heave.

5.2.2 Evaluation of the previous development of ground heave, damage events

- Through 2014 ground heave in the centre of the major ground heave zones added up to amounts up to 300 to 350 mm. Compared to other coal mining districts these are quite high amounts of ground heave, which reach a magnitude of 3 to 4 % of the subsidence induced by the former mining activity.

  One reason for that obviously is the increased influence of decompaction in the overburden due to the changes in pressure heads (see part B).

- The evaluation of the InSAR-data shows that in the project area at the margins of the mined area till now the ground heave decreased gradually along the major fault zones. There are no indications for the development of discontinuities in these transition zones.

  Along the distinct tectonic related margins of the mine workings along the Heerlerheide fault in Geleen as well as along the Feldbiß fault zone in Brunssum and along the 1^{e} NO Hoofdbreuk in Eygelshoven, ground heave decrease in a transition zone across the fault zones with a uniform gradient of about $1{,}0 \cdot 10^{-4}$.

  Therefore, in comparison to the conditions within the damage zone along the Rurrand fault in the Erkelenz mining district, the damage potential is considered to be significantly less.

  At the Rurrand fault in the Erkelenz mining district a distinct discontinuity with a vertical ground displacement of > 100 mm developed at a very short distance of < 10 m within a period of approx. 12 years (see Fig. C 19).

  At the Heerlerheide fault the respective transition zone covers a considerable greater width of approx. 1,5 km.

Along the Rurrand fault, first damages appeared three to four years after the dewatering measures had been ceased in the mine. In the South Limburg mining district through now, approx. 22 years after the terminal cessation of dewatering measures, no comparable damages have been observed.

- Nevertheless for the project area there also are damages announced to the Technische commissie bodembeweging (Tcbb). The accepted damages provided by Tccb for the project have been evaluated by IHS; as these data are confidential there is no documentation in this report. Some of the announced damages have been accepted as mining related by Tccb. Some of these might be related to differential ground heave along major fault zones due to their location. However, a concrete causal connection to differential ground heave could not yet be confirmed.

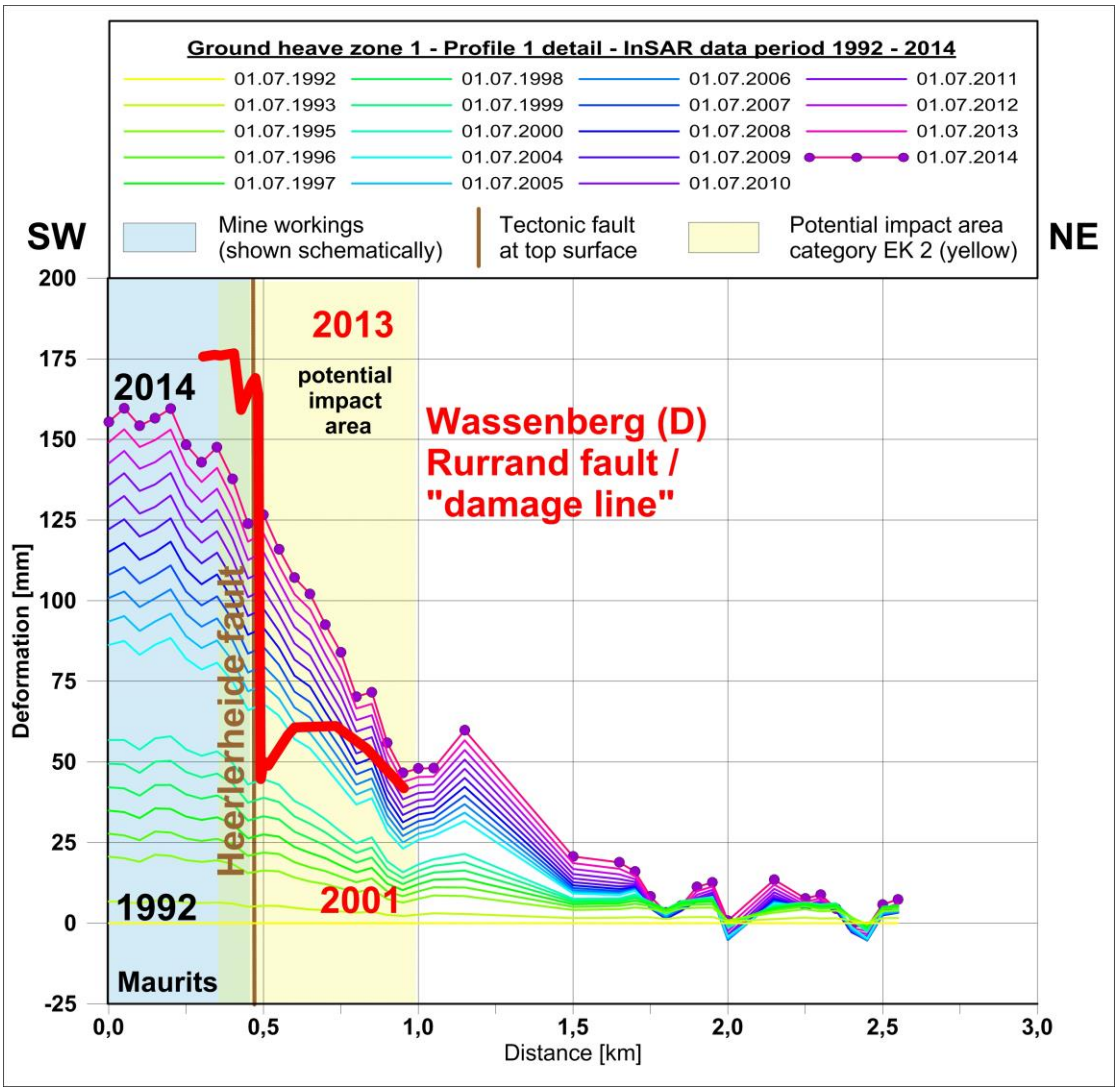

Fig. C 19: Comparison between the ground heave gradients at the Heerlerheide fault in the Geleen area (ground heave zone 1) and the Rurrand fault in the Wassenberg area, Germany

5.2.3 Evaluation of the future ground heave potential

- The overall ground heave potential due to rising mine water in the South Limburg mining district can be estimated to reach max. 440 to 500 mm based on the current prognosis for the centre of ground heave in the ground heave zone 2 („best case“ - „worst case“ for key point 2 (060D009) in ground heave zone 2; see part B)

- The major part of ground heave did already took place. For the future further amounts of ground heave are expected to be about 110 to 170 mm in maximum. Therefore, in principle, impacts related to differential ground heave cannot be excluded.

- For the Maurits coal mine (ground heave zone 1), the mine water level is unknown; hence, a definite prognosis is not possible. From the development of the ground heave till now, by approximation, the amounts of ground heave can be expected to be comparable to those that are expected for ground heave zone 2.

- For ground heave zone 3, significantly minor ground heave has to be expected for the future as well. On the one hand this is indicated by the minor ground heave that took place during the last years (period 2009 - 2014, see Fig. 13). On the other hand, the overburden will be flooded to only a little or no amount („best case“) in this area; hence, there will be no significant additional decompaction of the overburden layers as happened in the other ground heave zones. Even in the „worst case“ the decompaction potential of the overburden layers will not reach a comparable amount to that of the ground heave zones 1 and 2 and is even less than in the area of Julia coal mine.

- The area of the Julia coal mine east of the Feldbiß fault zone represents the main area of ground heave within the ground heave zone 3 during the last years. Presumably, the centre of ground heave will not significantly shift in the future within ground heave zone 3. For the Julia concession additional maximum amounts of ground heave are predicted to be around 60 to 100 mm („best case“ - „worst case“ for key points 4, 5 (062E0015, 062E0034) in ground heave zone 3, see part B).

  Furthermore it has to be considered that significant ground heave also takes place northeast of the mine workings of the Julia concession, caused by mine

water rise in the Aachen mining district.

These areas of ground heave are overlapping. Therefore, the overall potential for the development of significant differences in ground heave is considered to be small in this area.

5.3 Definition of potential impact areas

Based on the results of the work in hand for the future progression of the rising mine water the development of a significant differential ground heave cannot be excluded for the tectonic related marginal areas of mining along the Heerlerheide fault in the Geleen area and along the Feldbiß fault zone in the Brussum and Eygelshoven area (see Plan 1).

For the assignment of impact categories according to Chap. 5.1, the local geological and hydrogeological conditions as well as the mining conditions were appraised in a first step. Subsequently in a second step the positive experiences gained from the evaluation of the previous ground heave kinematic were included. Thereby it is considered that the mine water rise is at a very advanced stage, the biggest part of the ground heave already evolved and the potential impact zones have shown a gradual decrease of ground heave without significant discontinuities till now. This led to a downgrading of the impact categories assigned in step 1.

From this procedure the following assignment of the potential impact areas depicted in Plan 1 to the impact categories defined in chap. 5.1 results:

Impact category EK 2:

Potential impact area 1 at the Heerlerheide fault in the Geleen area:

Criteria:

- single sided flooding at an impermeable tectonic fault zone that disrupts the coal-bearing bedrock as well as the overburden,
- discontinuities from the active mining period documented in the mine maps,
- significant impact on the hydraulic pressure heads in the overburden on one side of the fault zone.

Downgrade from impact category EK 1 (Scenario 1 a), because:

- gradual decrease of ground heave within the transition zone, no indications for discontinuities.

Impact category EK 3:

Potential impact area 2 at the Feldbiß fault in the Brunssum area

Criteria:

- single sided flooding at an impermeable fault zone that disrupts the coal-bearing bedrock as well as the overburden,
- discontinuities from the active mining period documented in the mine maps,
- no significant impact on the pressure heads in the overburden.

Downgrade from impact category EK 2 (Scenario 2 a), because

- gradual decrease of ground heave within the transition zone, no indications for discontinuities.

Potential impact area 3 at the Feldbiß fault in the Eygelshoven area

Criteria:

- flooding of mine workings at a major tectonic fault zone that disrupts the coal-bearing bedrock as well as the overburden
- discontinuities from the active mining period documented in the mine maps

- no significant impact on the pressure heads in the overburden according to the groundwater model; in the level of the basal sands that overlay the Carboniferous bedrock (“Walsumer Sande”) a rise of pressure heads has to be expected to take place only northeast to the fault zone which might produce differential decompaction and has to be taken into account as an additional risk factor.

No downgrade from impact category EK 3 (Scenario 3 a), because:

- There are some damages recorded in the vicinity of impact zone 3.
  However, a concrete causal connection to differential ground heave could not yet be confirmed and the evaluation of the InSAR-data gives no indication for the development of significant discontinuities.
- Nevertheless this area should be taken under detailed control by means of monitoring to provide a sufficient data base for a substantiated assessment of the causes of the reported damages.

The width of the potential impact areas was defined in consideration of both the position accuracy of the tectonic fault zones and the location of discontinuities from the active mining period (Drempels and Verzakkingen). Correspondingly the width of the impact zones was set to 150 m southwest and 500 m northeast of the most probable position of the respective fault zone (see Plans 2 to 4). Thereby also the results from the InSAR-data are considered, which allow a comparably accurate determination of the width of the transition zones of ground heave across the fault zones.

The actual assignment of potential impact areas to the impact categories considers a „worst case“ scenario for the future mine water rise. According to the present knowledge about the development of ground heave within the impact areas, the probability for the development of significant discontinuities by differential ground heave has to be expected to be even lower. But still it also has

to be considered that the assessment is very much based on the results from the InSAR-data, which provide the image for the kinematic of the previous ground heave within the potential impact zones. The maps and profiles shown in part A and C imply some interpolations and inaccuracies that might hide small scale "events" (discontinuities) that can only be detected by a detailed terrestrial monitoring (levelling). Therefore the more unfavourable assignment to the impact categories carried out here also takes this uncertainties into account.

According to the present state of scientific investigations about the occurrence of damages due to differential ground heave no significant differential ground heave which might produce damages to the ground surface has to be expected outside the potential impact zones depicted in plan 1. Within the mined areas ground heave develops uniformly with low gradients to the margins of the mined sections. According to the findings in other coal mining districts in particular no critical differential ground heave has to be expected along discontinuities from the active mining period (Drempels and Verzakkingen), which are located within the mined area.

5.4 Assessment of the damage potential

With regard to the assessment of the future damage potential due to differential ground heave, first of all it has to be stated that ground movements induced by rising mine water (overall ground heave potential in case of complete flooding approx. 0,5 m in maximum) constitutes only a fractional amount of the effects that mining-induced ground movements (up to 10 m of subsidence). Therefore, in principle, the damage potential of ground heave induced by rising mine water is several magnitudes smaller.

As already discussed in chap. 5.1, in any other flooding area of coal mining (e.g. in North Rhine-Westphalia), to date, no serious mining damage has been detected in potential impact zones assigned to impact categories EK 2 and EK 3. Furthermore, one has to consider that mine water rise is already far progressed in the South Limburg mining district, without generating significant discontinuities or serious damages by differential ground heave.

From an absolute point of view, there is only a low probability for the development of damage-relevant discontinuities due to the comparable small amount of ground heave that is expected for the future.

Hence, in principle, the risk of damage caused by the remaining mine water rise in the South Limburg mining district is quite low. Nevertheless, impacts to buildings/infrastructure, cannot be entirely excluded. Serious mining damage (in the sense of a „constructive total loss“) is not expected.

This statement about the risk of damage follows the relevant criteria for the assessment of damage to buildings. Special structures or sensitive infrastructure with special requirements concerning their positional stability have to be estimated on a case-by-case basis.

The actual gradient of ground heave that has been determined for the potential impact areas by $1{,}0 \cdot 10^{-4}$ is compared to the relevant critical value for high-buildings according to civil engineering regulations ($2 \cdot 10^{-3}$, 1/500) smaller by magnitudes. However, the local occurrence of steeper gradients cannot completely be excluded.

References

- Literature

BAGLIKOW, V. (2003): Bergschäden nach Beendigung der Grubenwasserhaltung im tiefen Bergbau.- Das Markscheidewesen 110, Nr. 2, S. 45-49, 7 Abb., Verlag Glückauf; Essen.

BAGLIKOW, V. (2010): Schadensrelevante Auswirkungen des Grubenwasseranstiegs im Erkelenzer Steinkohlenrevier.- Schriftenreihe Inst. f. Markscheidewesen, Bergschadenkunde und Geophysik im Bergbau an der RWTH Aachen, Heft 1-2010, 121 S., 84 Abb.; Aachen.

GD NRW (2008): Paläoseismische Untersuchungen im Bereich der Niederrheinischen Bucht.- scriptum, 17, 72 S., 56 Abb., 6 Tab., 4 Anl.; Krefeld.

HEITFELD, K.-H., M. HEITFELD, P. ROSNER & H. SAHL (2003): Kontrollierter Grubenwasseranstieg im Aachener und Südlimburger Steinkohlenrevier.- 3. Aachener Bergschadenkundliches Kolloquium, H. 97, S. 71-85, 5 Abb.; Aachen.

HEITFELD, M., P. ROSNER, M. MÜHLENKAMP & H. SAHL (2004): Bergschäden im Erkelenzer Steinkohlenrevier. - 4. Altbergbau-Kolloquium, 14 S., 10 Abb.; Leoben (Österreich).

HEITFELD, M., P. ROSNER & M. MÜHLENKAMP (2014): Auswirkungen von Geländehebungen im Zuge des Grubenwasseranstiegs im Ruhrrevier - ein Ansatz zur Bewertung der Risiken.- 14. Altbergbau-Kolloquium, S. 41 - 60, 8 Abb.; Gelsenkirchen.

HEITFELD, M., F. DENYS, I. DE VENT, J. KLÜNKER & P. ROSNER (2015): Bewertung der Risiken durch Spätfolgen des Steinkohlenbergbaus in Südlimburg/Niederlande.- 15. Altbergbau-Kolloquium, S. 130-146, 8 Abb.; Leoben.

IHS - INGENIEURBÜRO HEITFELD-SCHETELIG GMBH (27.02.2007): Bericht zu den möglichen Auswirkungen des Grubenwasseranstiegs im Südlimburger Steinkohlenrevier - Vorstudie.- Unveröffentl. Gutachten im Auftrag des Ministerie van Economische Zaken - Niederlande, 69 S., 1 Anh., 12 Anl.; Aachen (D). http://www.sodm.nl/english/subjects/preliminary study 2007 (website visited 12.2014).

OBERSTE-BRINK, K. (1940): Die Frage der Bodenbewegungen infolge Bergbaus.- Glückauf, 76, S. 249-256; Essen.

PÖTTGENS, J.J.E. (1985): Bodenhebung durch ansteigendes Grubenwasser.- The Development of Science and Art of Minerals Surveying, Proceedings 6th International Congress, International Society of Mine Surveying, vol. 2, p. 928 - 938; Harrogate (GB).

PÖTTGENS, J.J.E. & J.M. VAN HERK (2000): Ground Movements over abandoned Coalmines in relation to rising Mine Waters in Limburg (The Netherlands)..- Lecture French mining Congress, Paris, 14-16 November 2000, 9 p., 8 fig.; Paris (F).

ROSNER, P. (2011): Der Grubenwasseranstieg im Aachener und Südlimburger Steinkohlenrevier - Eine hydrogeologisch-bergbauliche Analyse der Wirkungszusammenhänge.- Diss. RWTH Aachen, 194 S., 67 Abb., 7 Tab., 4 Anh., 7 Anl.; Aachen (D). http://darwin.bth.rwth-aachen.de/opus3/volltexte/2011/3741 (website visited 11.2014).

Part D - Bow-Tie-Analysis and monitoring

1 Bow-Tie-Analysis

1.1 Systematic

In this study the Bow-Tie-Analysis is used as a uniform method to analyse and visualise the risks causes and consequences per after-effect. A schematic representation of a Bow-Tie-Analysis is shown in Fig. D1. The knot of the Bow-Tie, i.e. the centre of the diagram, is formed by the critical incident, or Top Event, which is connected to a certain Hazard. On the left side, the various causes that may trigger the incident are summarised, i.e., the Threats. On the right side, the potential impacts from the top event are listed, i.e. the Consequences.

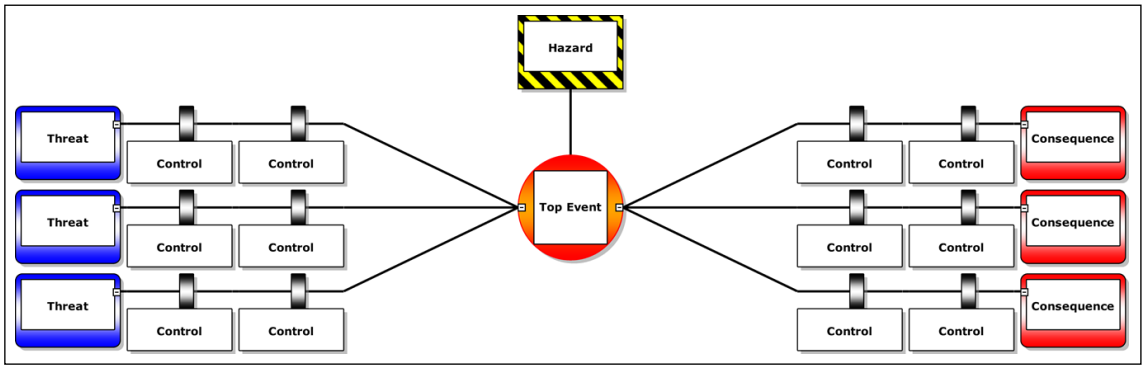

Fig. D 1: Schematic representation of a Bow-Tie-Analysis

Subsequently, Controls can be added in between the Threats, Consequences, and the Top Event. These can be either preventive, i.e., prevent the cause from escalating into a Top Event, or mitigating, i.e. reduce the Consequences once the

Top Event occurred. Also, monitoring controls can be added to detect a Top Event or to direct preventive and/or mitigating controls.

With the results of the investigations in hand the Top Event that has to be regarded for the after-effect/hazard “ground movements” can be described as “differential ground movements”, which might damage buildings or infrastructure on the surface. Within the investigations three potential impact areas have been identified, where the occurrence of this Top Event cannot be excluded (see part C and plan 1).

The Bow-Tie for this Top Event is presented in Fig. D2. In the following the relevant factors of this Bow-Tie are discussed.

1.2 Threats and Consequences

- Threats

Differential ground movements can be induced by rising mine water in areas with specific geological and mining conditions as described in part C (three potential impact areas along the main tectonic faults). A further risk factor is the differential development of groundwater levels in the overburden on the two sides of such a main tectonic fault in these areas. Such differential development of hydraulic heads in the overburden cannot be induced only by rising mine water but as well by groundwater extraction from the overburden.

- Consequences

Differential ground movements can damage buildings or sensitive infrastructure (e.g. pipelines) if the differences in ground movements occur over a very small distance. Furthermore the functionality of infrastructure can be influenced by changing the inclination (e.g. sewers).

Moreover the potential for the development of damaging differential ground movements can cause social unrest in the affected areas. People are afraid that their houses will be damaged and might not able to estimate the actual risk.

1.3 Prevention Controls

In practice, the Threats can only be mitigated by preventing further mine water rise by starting to pump out mine water again. However, such an extensive and perpetual measure is not proportional to the risk potential. The pros and cons of this measure are discussed in detail in the final integrated risk analysis of this project.

The main appropriate prevention controls are monitoring the factors that might lead to differential ground movements which are mine water levels, groundwater levels in the overburden, and ground movements. By monitoring these factors, risk zones might be identified early enough to start appropriate recovery measures. Furthermore, these monitoring measures are necessary to build up an information basis for the assessment of damage at the surface and the identification of rising mine water as the possible cause of damage at the surface.

1.4 Recovery and Escalation Controls

- Recovery Controls

For a better understanding of the processes in the underground of the three potential impact areas and a better base for the assessment of the actual risk, a pilot project in the potential impact area Geleen is proposed. The pilot should provide concrete information about the characteristics of the tectonical shear zones along the main faults near to the surface. For the risk assessment, it is very

important to establish whether a single predominant movement path is developing along the fault zone, or whether several paths with a distance of some metres are developing.

For the detection of locations where significant differential ground movements might occur within the identified three potential impact areas, a detailed monitoring of a representative area is necessary. This information is also basic to be able to initiate further measures in time.

The risk that serious damage occurs to existing buildings is low. Therefore, preventive measures are not required for existing buildings. However, with respect to new building projects and new sensitive infrastructure facilities within the potential impact areas that are defined in the Plans 1 to 4, the following preventive measures are recommended, which can prevent damage in case significant differential ground movements occur:

- Sensitive infrastructure facilities (e.g. gas pipelines) should be reviewed with regard to the tolerance of tilt; if necessary, retrofitting measures are required. This, in particular, pertains for the area around Geleen that is assigned to impact category EK 2.

- For single building projects, a possible tilt should be considered in the planning and the design of the foundation.

- Within the regional development regarding corridors e.g. for pipelines or the location of new settlements the possible influence of differential ground heave should be regarded.

Further important instruments to prevent social unrest in case of the occurrence of differential ground heave or small damage of buildings are awareness-raising and communication. People should be informed about the situation, and should

get an explanation of the things that happen underground, the probability of damage, and the measures that are available to protect or repair their property. People should also know whom they can contact in case of damage, and who will be responsible for repairing the damage. First of all, the people in the administration of the possibly affected municipalities (three potential impact areas) should be informed, because they are the first to whom affected people might announce damages or who recognise such damages during their daily work in the municipality.

- Escalation controls

In case of the occurrence of damages at buildings or infrastructure, immediate measures such as a detailed monitoring of damages and structural analysis of the affected building or infrastructure have to be initiated. If necessary, constructional support work should be carried out to prevent further serious damage, and damage that has already occurred might be repaired. With these measures, a total loss of buildings or infrastructure can be prevented, and the usability restored.

To conclude, the probability that damage occurs due to differential ground movements is, in general, low (see part C). There are measures / instruments to prevent severe damage in case damage occurs. The main instrument to handle this after-effect is the monitoring of the ground movements themselves, as well as other inducing factors such as the rise of mine water and the change of hydraulic heads in the overburden. This is also fundamental for basic evidence insurance.

2 Monitoring

Future ground heave induced by mine water rise should be monitored on a regional basis as well as on a detailed local basis within the identified potential impact areas. The measurements are the fundamental basis for the assessment of potential impacts in the region that is affected by the rise of the mine water.

Each of the monitoring activities require their own spatial and temporal resolution and extent, together a certain precision and detectable range. Moreover, in each case a main parameter of interest is required. An overview of the requirements is provided in Tab. D 1 together with potential techniques that can meet these requirements. Based on the requirements in Tab. D 1, a proposal for a monitoring plan is summarised in Tab. D 2.

In general, it is necessary to have a supplementary monitoring that is based on terrestrial measurements as a reference, on the one hand, and satellite based measurements which deliver a higher density of measurement points and an efficient possibility to have a higher rate of measurement on the other. As an absolute reference for the evaluation of the InSAR data, an adequate net of GNNS-stations is needed in the region. Therefore, the monitoring should comprise the following methods:

1. Extensive areal monitoring of the whole region
   (mining region + 5 km buffer):

- Regional levelling using the existing benchmarks (see Plan 1) as terrestrial reference. Due to the relation between the absolute movements that are expected and the accuracy of the measurements on the one hand and the additional availability of the InSAR-data on the other hand a four to five years interval will be adequate for the terrestrial measurements.

Tab. D 1: Requirements for monitoring activities and potential techniques

Objectives		Spatial resolution	Spatial extent	Temporal resolution	Temporal extent	Parameter	Precision (2σ)	Maximum range	Potential techniques
1	**ground movements whole region**	1000 m	Mining region + 5 km buffer	1 years	40 years	Vertical cumulative displacement	< 1 cm	30 cm	Levelling, InSAR (medium res) +GNSS
2	**ground movements potential impact areas**	10 m	4 to 10 x 3 km	0,5 year	40 years	Vertical and horizontal displacement	< 4 mm	30 cm	Levelling, InSAR (high res)

Note: The temporal resolution concerns the update cycle of the analysis. All available satellite imagery with a repeat cycle of 6 and 24 days will be used.

Tab. D 2: Monitoring plan

	Method	Objective	Where?	When?
1	**GNSS with transponder**	Absolute reference, detrending of InSAR time series	Two stations in each uplift zone (according to Fig. C9) + existing stations.	Continuous
2	**PSI, medium resolution (ascending, descending satellite orbit, Sentinel-1 mission or similar)**	Monitoring whole mining region, fault locations	Mining region + 5 km buffer	yearly updates
3	**PSI, high resolution (ascending, descending satellite orbit, TerraSAR-X mission or similar)**	Monitoring potential impact areas	potential impact areas (Geleen, Brunssum, Eygelshoven) each about 4 to10 x 3 km	0.5 yearly updates
4	**Regional levelling**	Monitoring whole mining region, long term time series	Mining region + 5 km buffer	Every 4 - 5 years
5	**Detailed, local levelling**	Monitoring potential impact areas	potential impact areas (Geleen, Brunssum, Eygelshoven) each with one or two profiles of about 0,75 to 1,5 km length	0.5 yearly updates

Note: Currently existing GNSS stations should continue to operate.

- Periodical evaluation of medium-resolution InSAR-data. These evaluations serve as a basis for the detection of regional trends in between the levelling campaigns. The measurements are a main basis for the assessment of the regional impact on the surface and a verification of the prognosis.
  The evaluation of the data should be done once a year. With this yearly analysis all available satellite imagery with a repeat cycle of 6 and 24 days will be used to get a sufficient resolution of the regional ground movements over time.

  The analysis can be based on Sentinel-1 data, which is an ESA/EU mission with an intended minimum operation time of 20 years, and providing data with a repeat cycle of 6 days (both in ascending and descending orbit). Furthermore, RadarSAT-2 data can be used, with a repeat cycle of 24 days, which is provided via the Dutch satellite data portal.
  As an absolute reference for detrending the INSAR time series GNNS measurements have to be executed. The currently existing GNNS stations should continue to operate. For a higher accuracy two additional GNNS stations should be located in each main ground heave zone according to Fig. C9 as there currently is only one GNNS station within the mine region.

2. Detailed monitoring within the potential impact areas:

- The main basis for a detailed areal monitoring of the potential impact zones is the evaluation of high-resolution InSAR-data. The data are needed to detect possible discontinuities within the whole potential impact zones.
  Maybe specific detailed analysis for representative individual properties/buildings with a suspicious kinematic will be necessary as well.

  To cover the potential impact zones shown in Plan 1 and their surrounding areas of about 4 to 10 km in length and a width of about 3 km should be

evaluated along the critical fault lines. The analysis should be done twice a year to get indications for differential ground heave early enough for further action (e.g. additional terrestrial levelling, looking for damages at buildings).

- As an absolute terrestrial reference a detailed levelling of benchmarks along characteristic profiles across the potential impact areas is necessary to detect discontinuities.

  A proposal for the position of one or two such cross-profiles per potential impact zone is shown in the Plans 2 to 4. The length of the cross-profiles is between 750 and 1.500 m. The distance between the individual benchmarks should not exceed 25 m.

  The benchmarks should be measured twice a year, parallel to the processing of the high-resolution InSAR-data.

The use and combination of the different methods partly is dependent on the accuracy that is needed for the resolution of the ground movements. A higher accuracy will be needed, if e.g. discussions about the interpretation of the measured ground movements develop in the public or damages occur which cannot be interpreted.

The monitoring plan shown in Fig. D2 represents a comprehensive programme for a detailed registration of the ground movements in the mine area. A discussion about the possibilities for a stepwise monitoring plan on base of a cost-benefit analysis will be provided with the integrated Bow-Tie-Analysis in the summary report of the project.

The results of the monitoring should be documented in annual reports. On base of the running monitoring results the monitoring system might have to be optimised according to the proposed priorisation.

Delft, 31. August 2016/Rev. a: 02. December 2016

Dr. ir. Hans van der Marel Dr. ir. Freek van Leijen

Prof. dr. ir. Ramon Hanssen

Maastricht, 31. August 2016/Rev. a: 02. December 2016

Dr. Roland F. Bekendam

Aachen, 31. August 2016/Rev. a: 02. December 2016

Dr. Peter Rosner Dr.-Ing. Michael Heitfeld

Appendix 1

Na-ijlende gevolgen steenkolenwinning Zuid-Limburg

Final report
on the results of the working group
5.2.1 - ground movements

Vertical displacement from 5 year levelling intervals

by

Projectgroup
"Na-ijlende gevolgen van de steenkolenwinning in Zuid-Limburg"
(projectgroup GS-ZL)

on behalf of
Ministerie van Economische Zaken - The Netherlands

Delft, Maastricht and Aachen (D), 31. August 2016

Appendix 1 - Vertical displacement from 5 year levelling intervals

Fig. 1: Contour plot showing the vertical displacement [in mm] for the South Limburg mining area between 01.07.1974 and 01.07.2014 (cumulative from 5 year intervals)

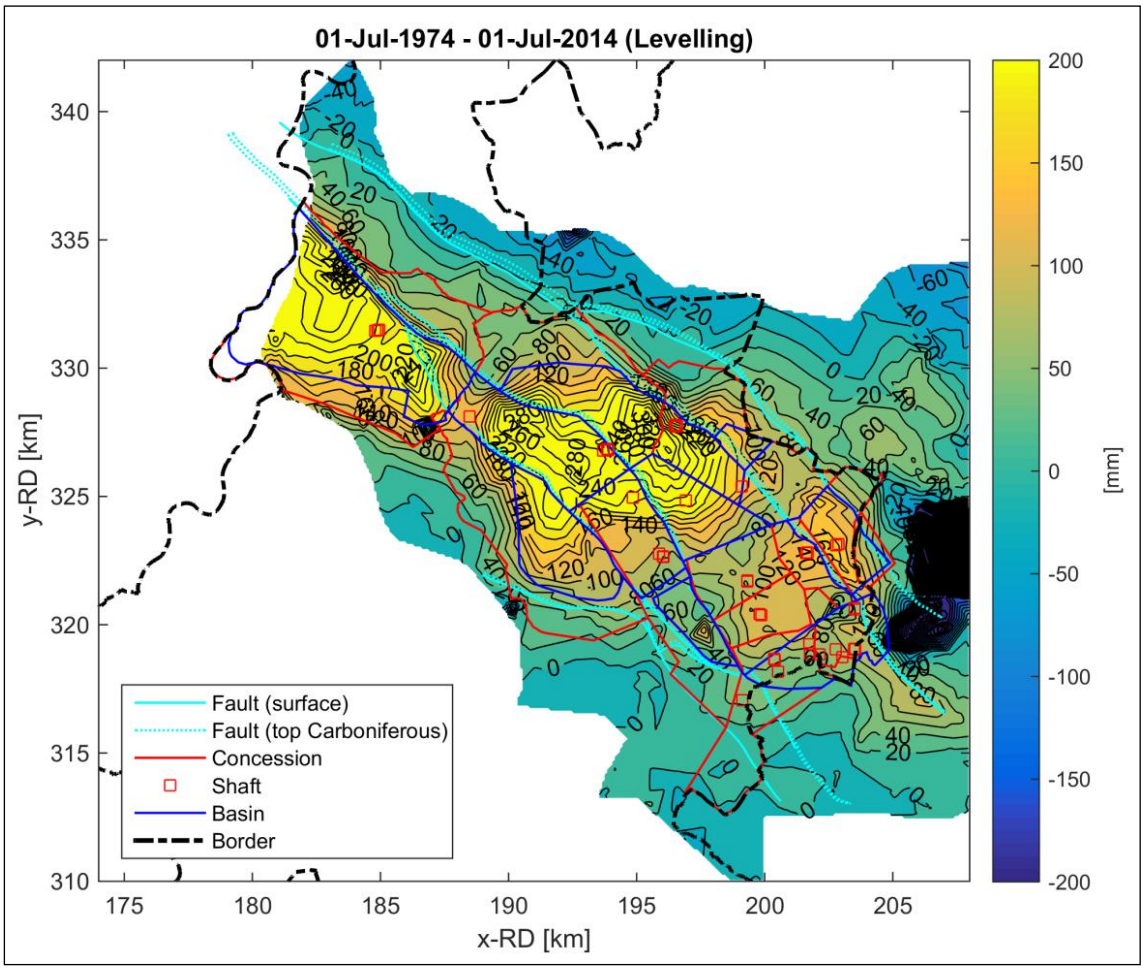

Fig. 2: Contour plot showing the vertical displacement [in mm] for the South Limburg mining area in 5 year intervals

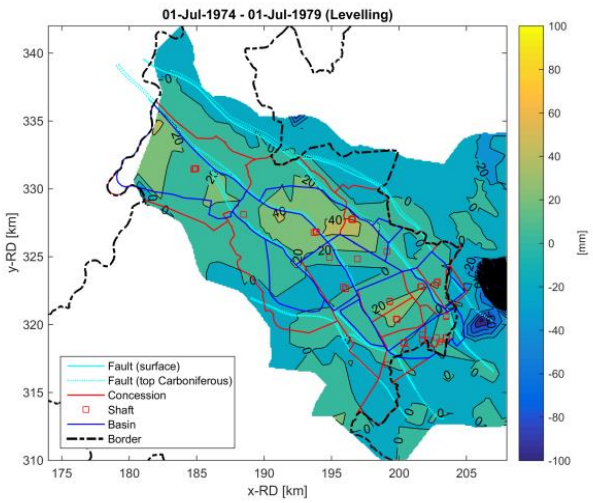

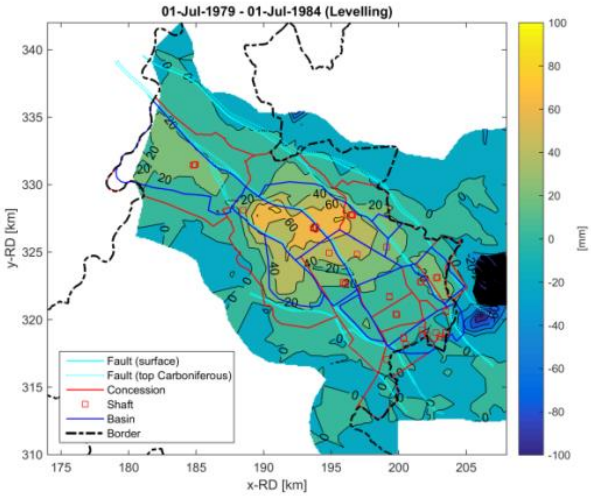

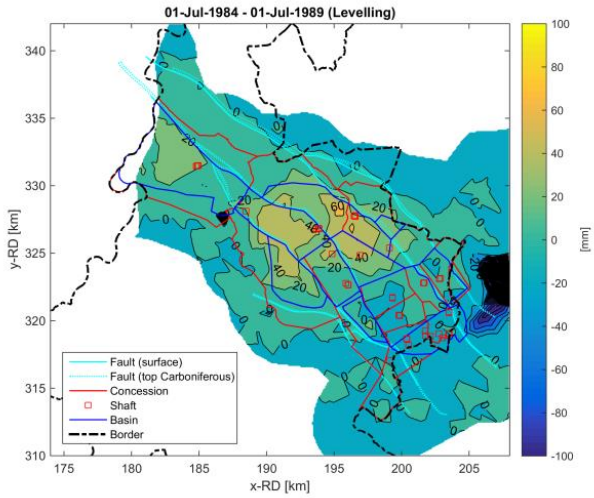

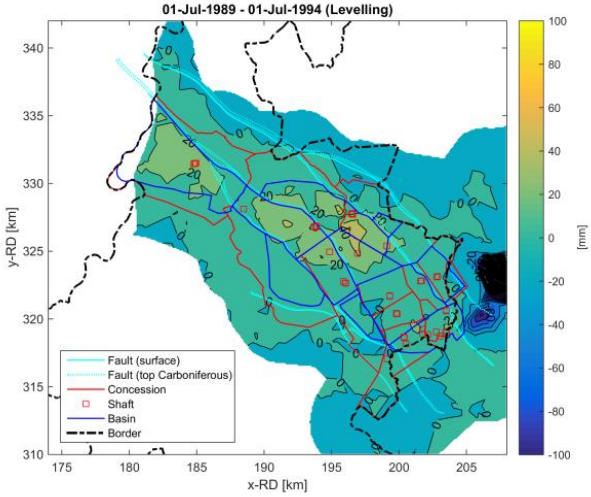

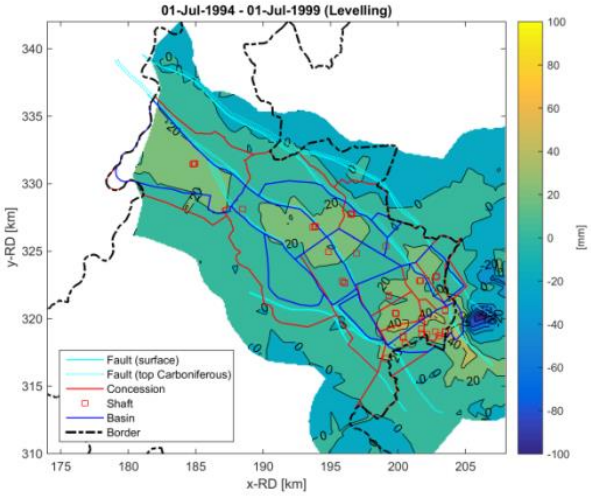
01-Jul-1994 - 01-Jul-1999 (Levelling)
y-RD [km]
x-RD [km]
[mm]
Fault (surface)
Fault (top Carboniferous)
Concession
Shaft
Basin
Border

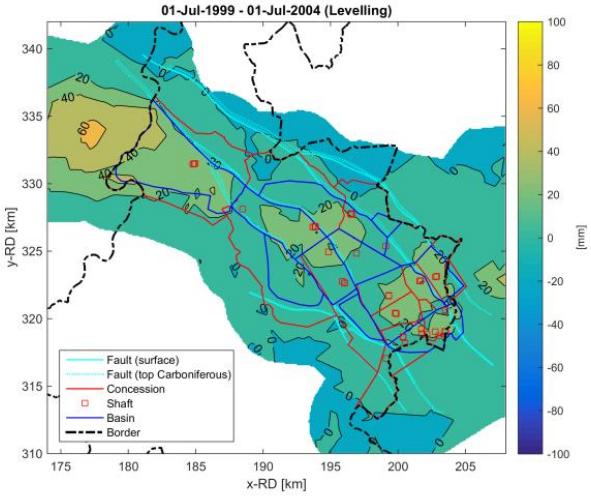
01-Jul-1999 - 01-Jul-2004 (Levelling)
y-RD [km]
x-RD [km]
[mm]
Fault (surface)
Fault (top Carboniferous)
Concession
Shaft
Basin
Border

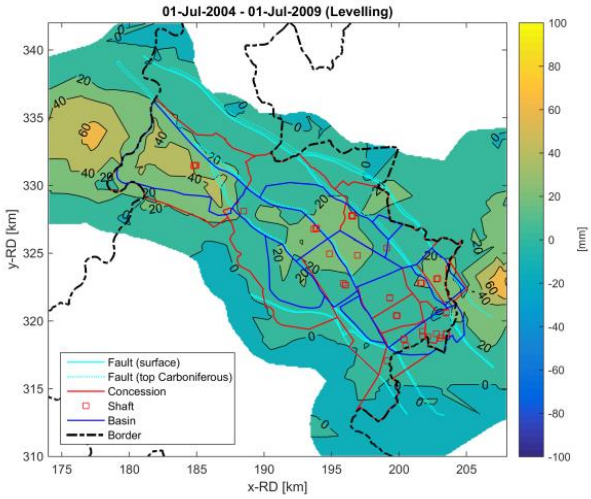
01-Jul-2004 - 01-Jul-2009 (Levelling)
y-RD [km]
x-RD [km]
[mm]
Fault (surface)
Fault (top Carboniferous)
Concession
Shaft
Basin
Border

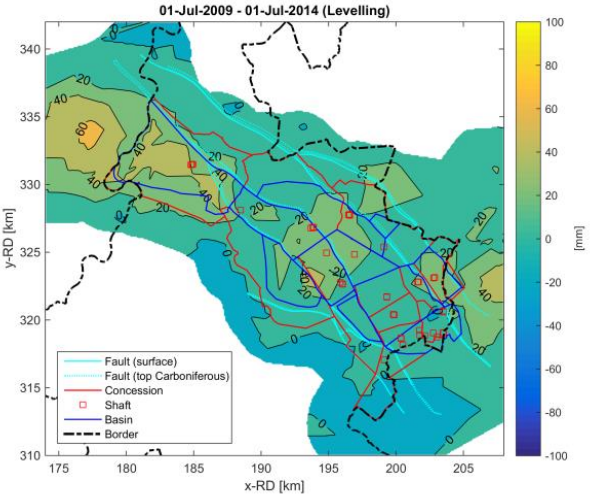
01-Jul-2009 - 01-Jul-2014 (Levelling)
y-RD [km]
x-RD [km]
[mm]
Fault (surface)
Fault (top Carboniferous)
Concession
Shaft
Basin
Border

Appendix 2

Na-ijlende gevolgen steenkolenwinning Zuid-Limburg

Final report
on the results of the working group
5.2.1 - ground movements

Integrated PSI-GNSS-levelling time series at key levelling points

by

Projectgroup
"Na-ijlende gevolgen van de steenkolenwinning in Zuid-Limburg"
(projectgroup GS-ZL)

on behalf of
Ministerie van Economische Zaken - The Netherlands

Delft, Maastricht and Aachen (D), 31. August 2016

Appendix 2 - Integrated PSI-GNSS-levelling time series at key levelling points

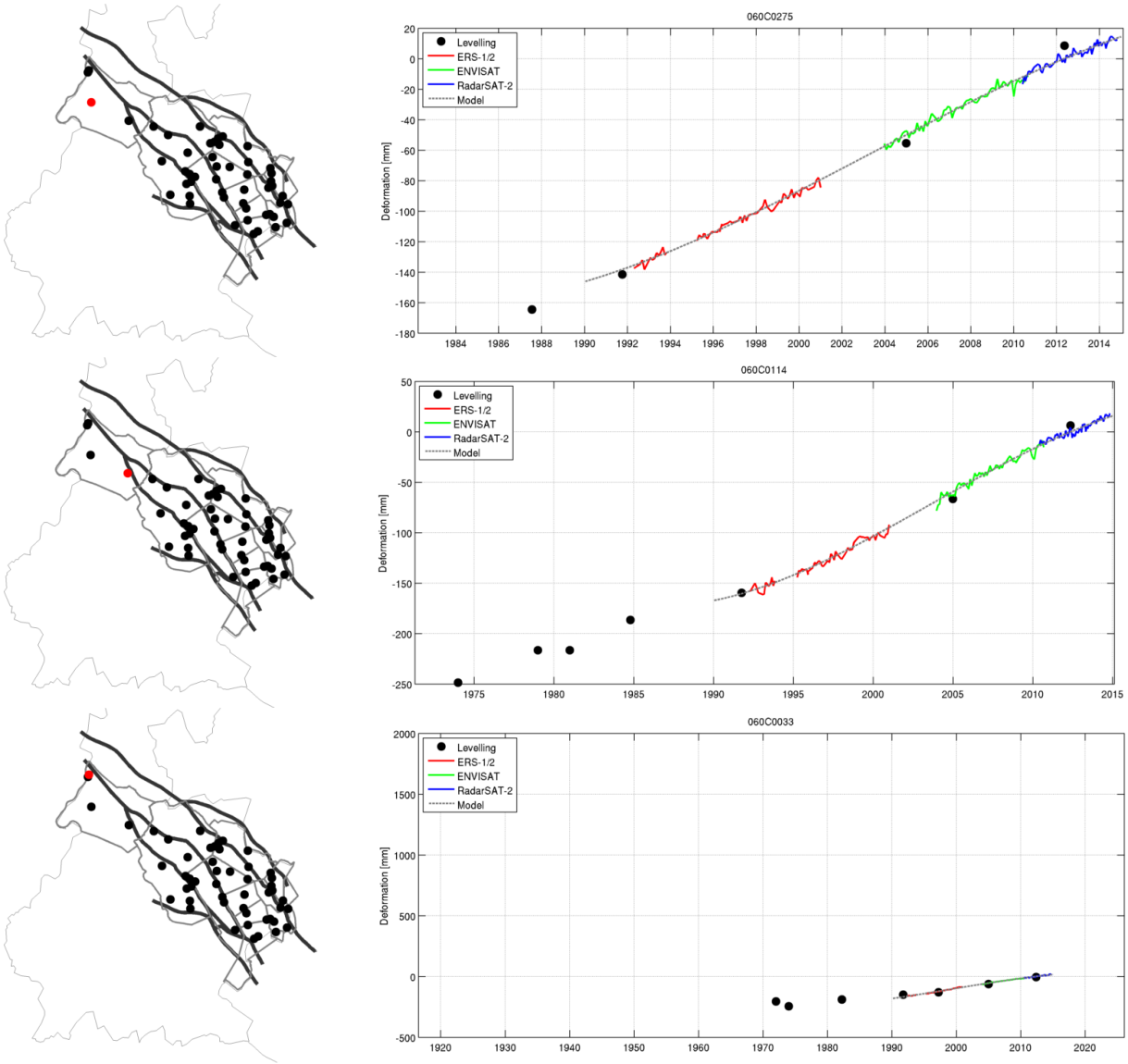

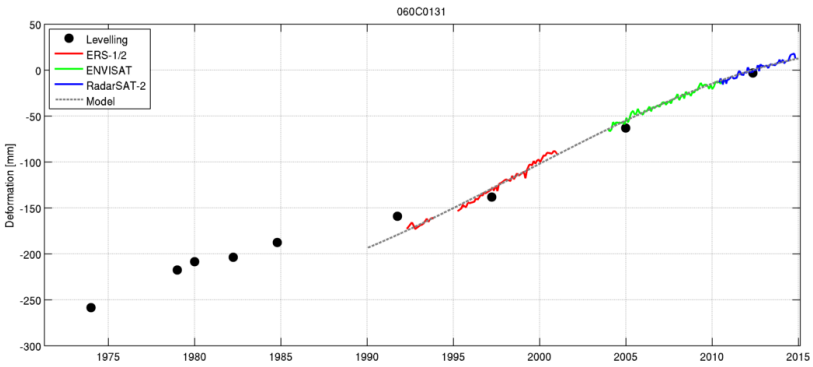
060C0131
Levelling
ERS-1/2
ENVISAT
RadarSAT-2
Model
Deformation [mm]
50
0
-50
-100
-150
-200
-250
-300
1975
1980
1985
1990
1995
2000
2005
2010
2015

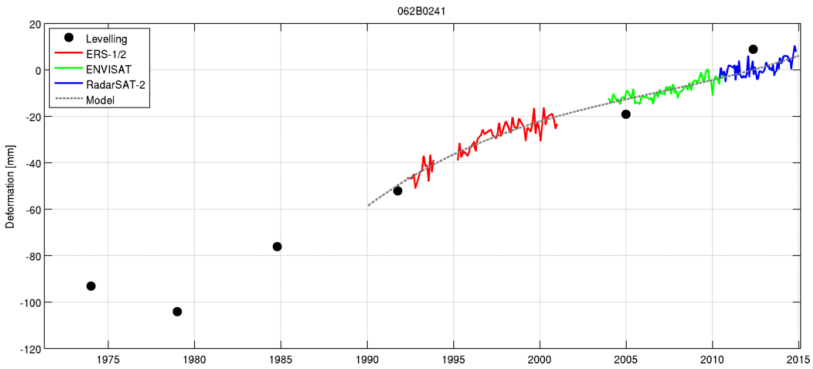
062B0241
Levelling
ERS-1/2
ENVISAT
RadarSAT-2
Model
Deformation [mm]
20
0
-20
-40
-60
-80
-100
-120
1975
1980
1985
1990
1995
2000
2005
2010
2015

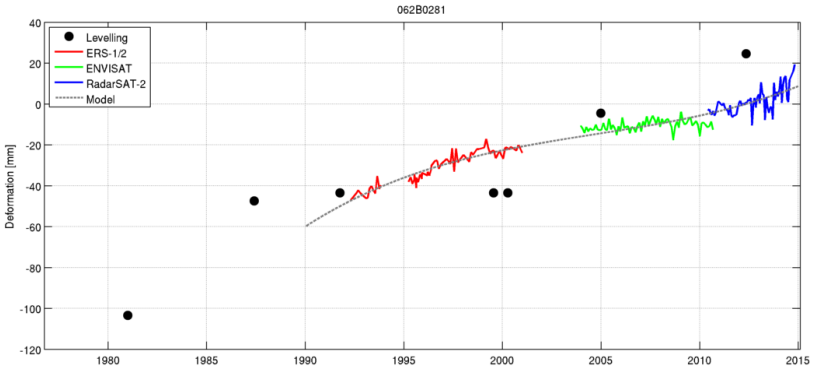
062B0281
Levelling
ERS-1/2
ENVISAT
RadarSAT-2
Model
Deformation [mm]
40
20
0
-20
-40
-60
-80
-100
-120
1980
1985
1990
1995
2000
2005
2010
2015

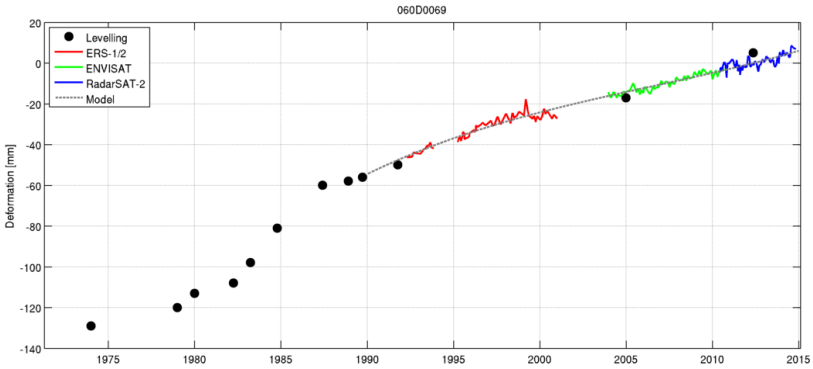
060D0069
Levelling
ERS-1/2
ENVISAT
RadarSAT-2
Model
Deformation [mm]
20
0
-20
-40
-60
-80
-100
-120
-140
1975
1980
1985
1990
1995
2000
2005
2010
2015

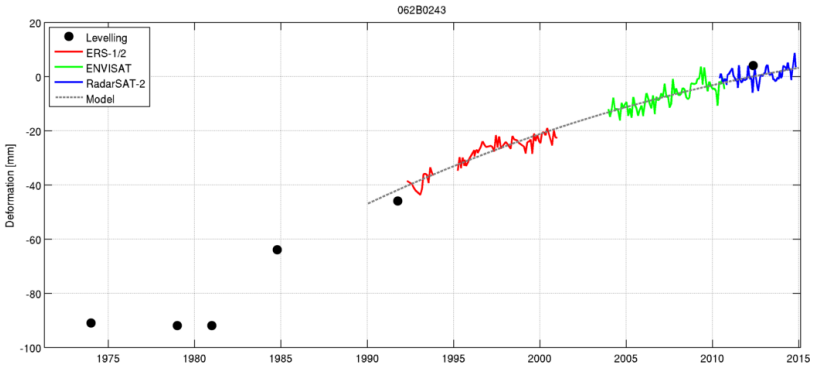
062B0243
Levelling
ERS-1/2
ENVISAT
RadarSAT-2
Model
Deformation [mm]

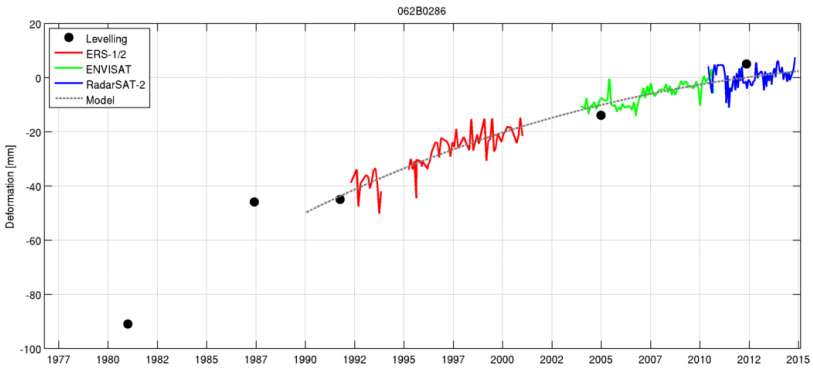
062B0286
Levelling
ERS-1/2
ENVISAT
RadarSAT-2
Model
Deformation [mm]

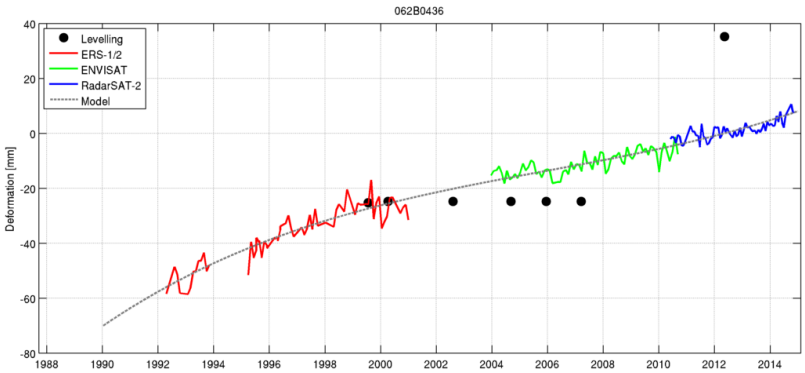
062B0436
Levelling
ERS-1/2
ENVISAT
RadarSAT-2
Model
Deformation [mm]

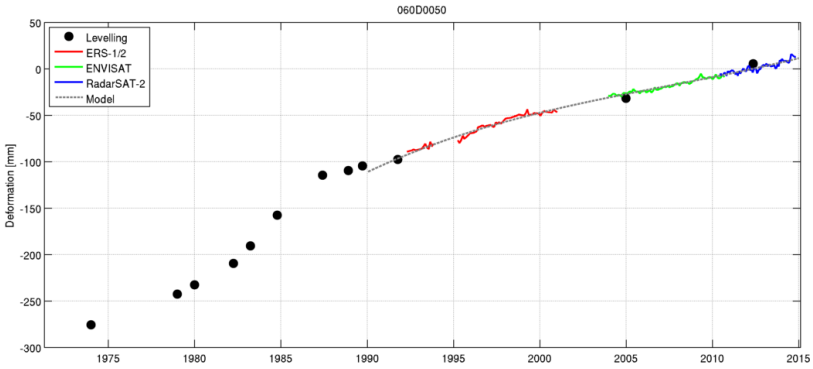
060D0050
Levelling
ERS-1/2
ENVISAT
RadarSAT-2
Model
Deformation [mm]

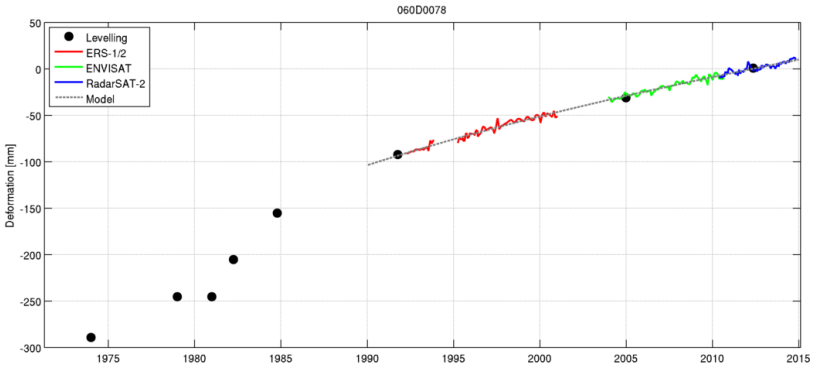
060D0078
Levelling
ERS-1/2
ENVISAT
RadarSAT-2
Model
Deformation [mm]
50
0
-50
-100
-150
-200
-250
-300
1975
1980
1985
1990
1995
2000
2005
2010
2015

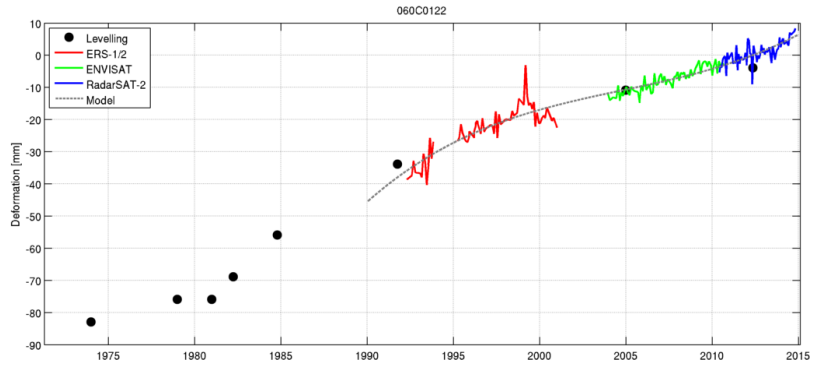
060C0122
Levelling
ERS-1/2
ENVISAT
RadarSAT-2
Model
Deformation [mm]
10
0
-10
-20
-30
-40
-50
-60
-70
-80
-90
1975
1980
1985
1990
1995
2000
2005
2010
2015

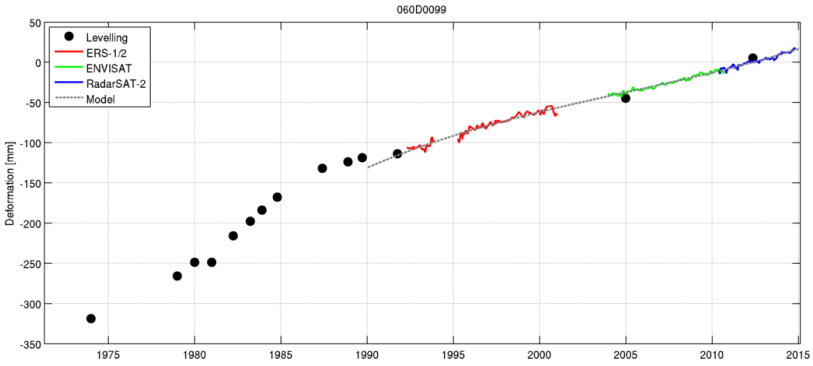
060D0099
Levelling
ERS-1/2
ENVISAT
RadarSAT-2
Model
Deformation [mm]
50
0
-50
-100
-150
-200
-250
-300
-350
1975
1980
1985
1990
1995
2000
2005
2010
2015

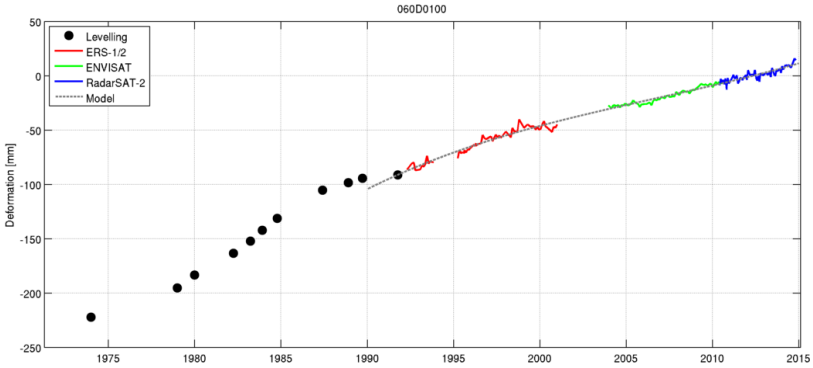
060D0100
Levelling
ERS-1/2
ENVISAT
RadarSAT-2
Model
Deformation [mm]
50
0
-50
-100
-150
-200
-250
1975
1980
1985
1990
1995
2000
2005
2010
2015

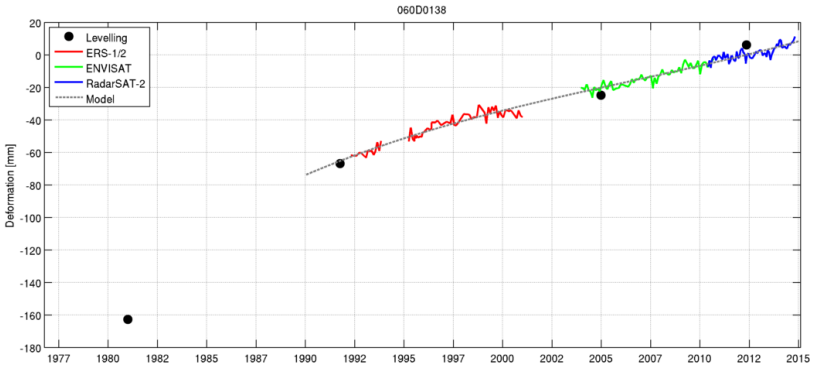
060D0138
Levelling
ERS-1/2
ENVISAT
RadarSAT-2
Model
Deformation [mm]

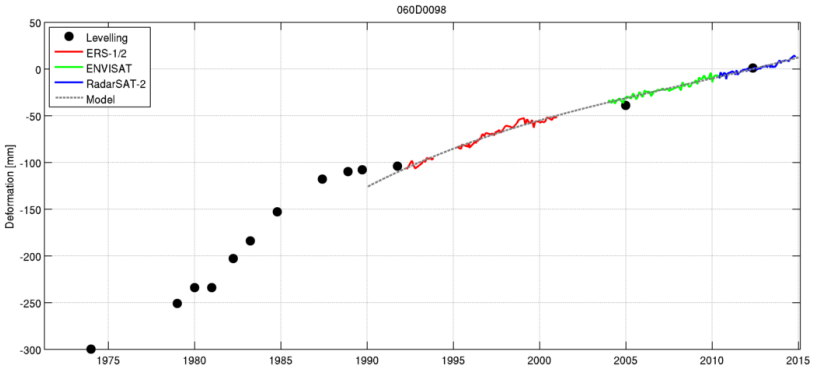
060D0098
Levelling
ERS-1/2
ENVISAT
RadarSAT-2
Model
Deformation [mm]

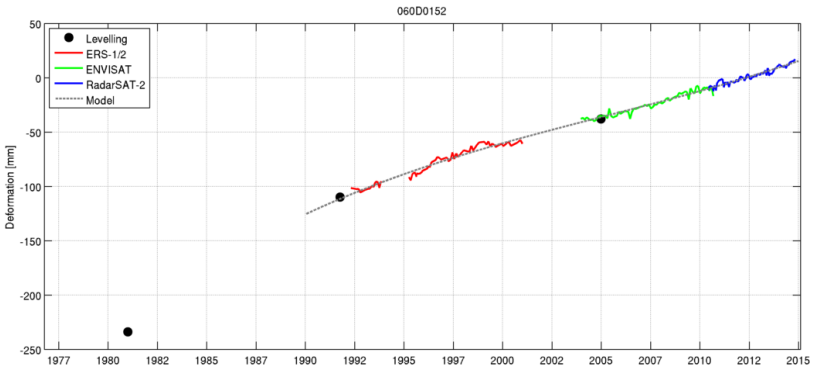
060D0152
Levelling
ERS-1/2
ENVISAT
RadarSAT-2
Model
Deformation [mm]

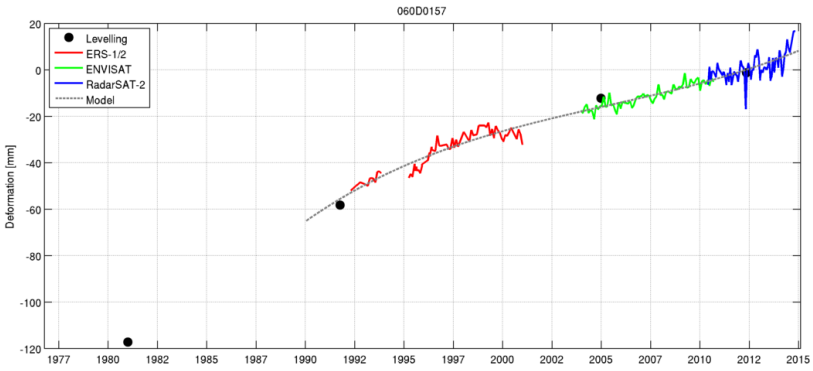
060D0157
Levelling
ERS-1/2
ENVISAT
RadarSAT-2
Model
Deformation [mm]

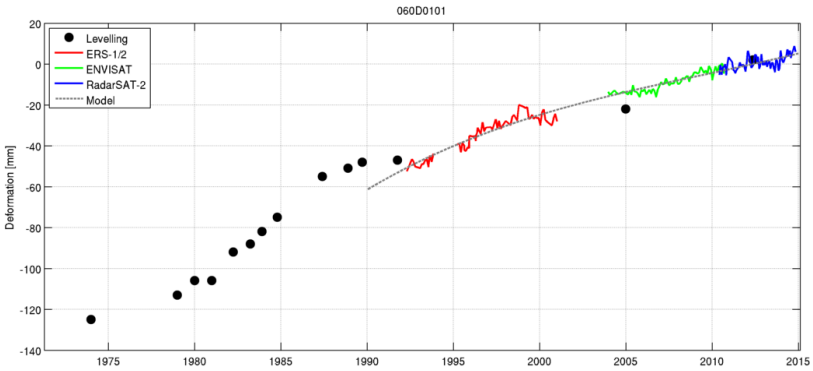
060D0101
Levelling
ERS-1/2
ENVISAT
RadarSAT-2
Model
Deformation [mm]

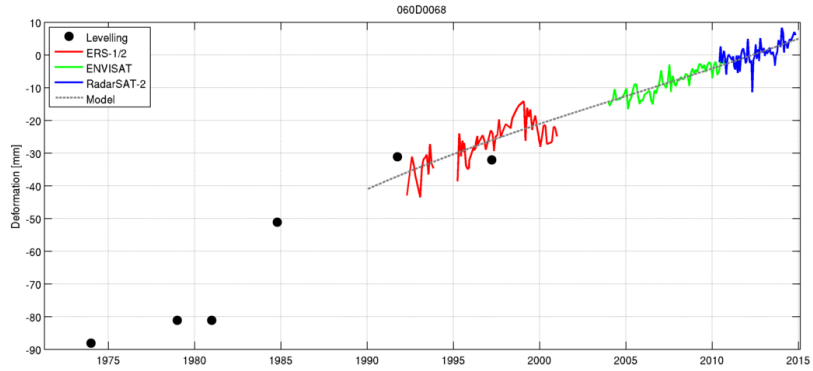
060D0068
Levelling
ERS-1/2
ENVISAT
RadarSAT-2
Model
Deformation [mm]

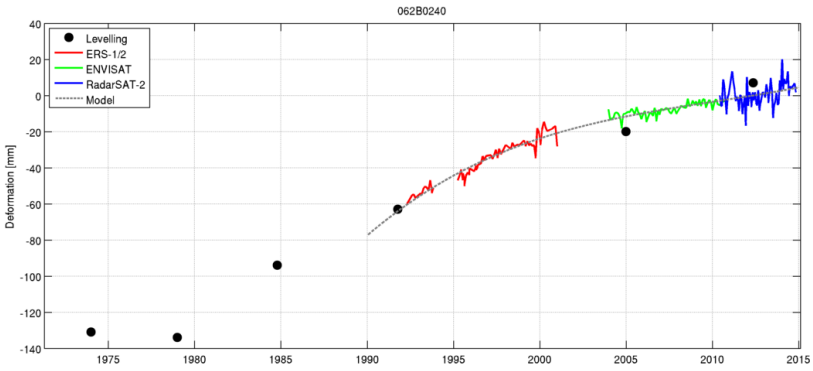
062B0240
Levelling
ERS-1/2
ENVISAT
RadarSAT-2
Model
Deformation [mm]

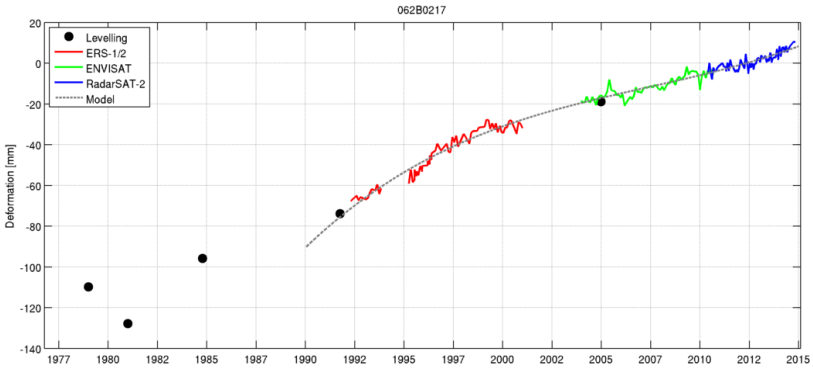
062B0217
Levelling
ERS-1/2
ENVISAT
RadarSAT-2
Model
Deformation [mm]

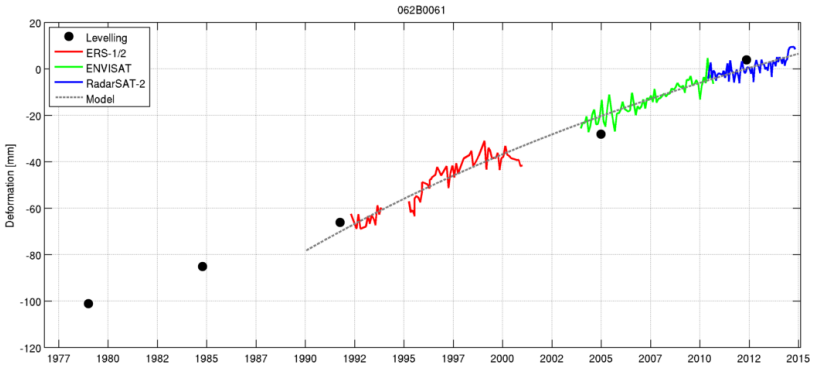
062B0061
Levelling
ERS-1/2
ENVISAT
RadarSAT-2
Model
Deformation [mm]

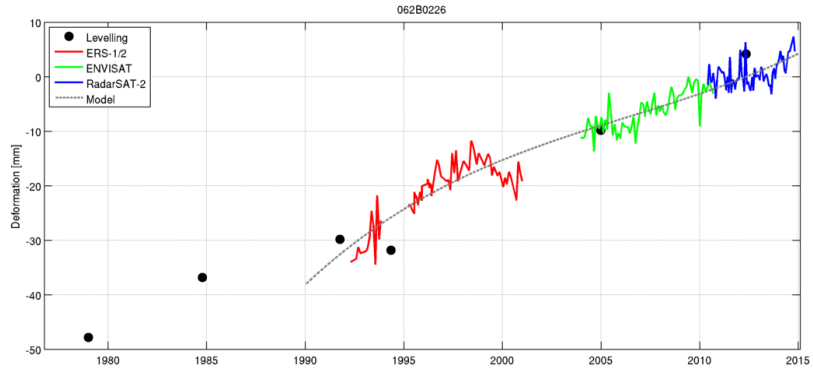
062B0226
Levelling
ERS-1/2
ENVISAT
RadarSAT-2
Model
Deformation [mm]

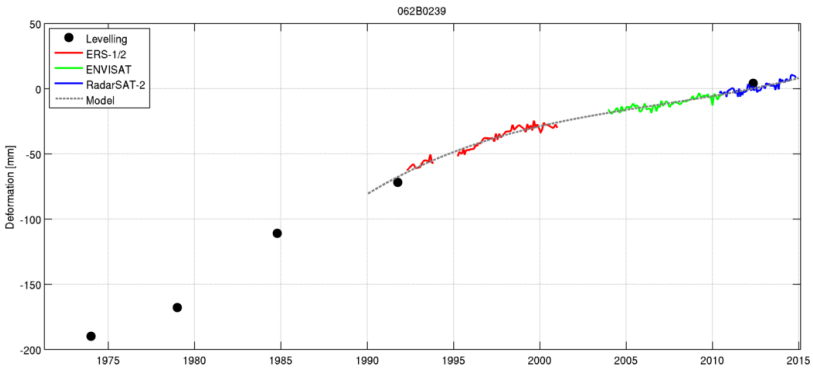
062B0239
Levelling
ERS-1/2
ENVISAT
RadarSAT-2
Model
Deformation [mm]

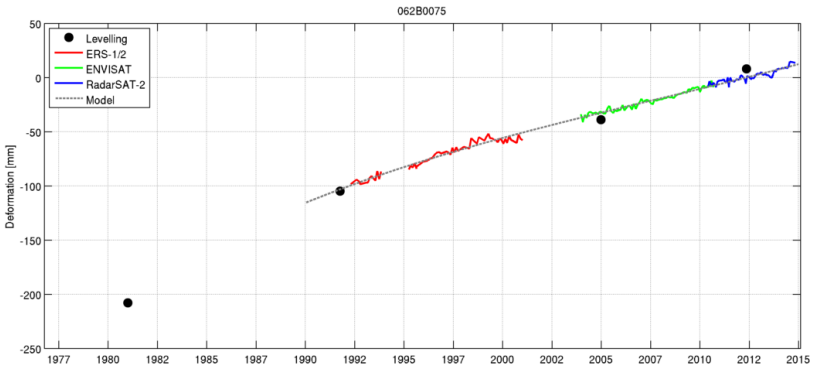
062B0075
Levelling
ERS-1/2
ENVISAT
RadarSAT-2
Model
Deformation [mm]

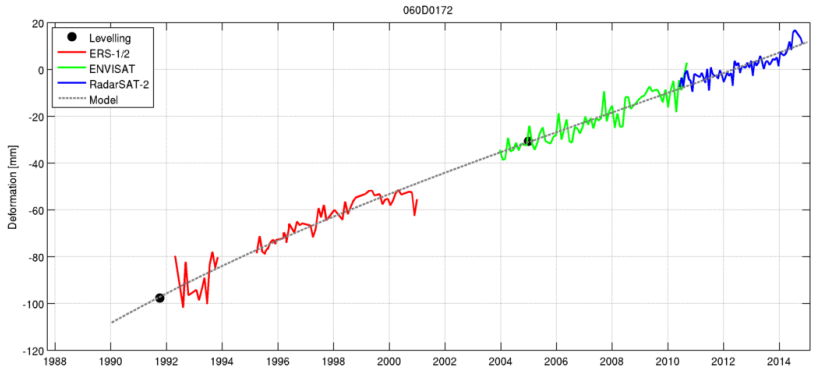
060D0172
Levelling
ERS-1/2
ENVISAT
RadarSAT-2
Model
Deformation [mm]

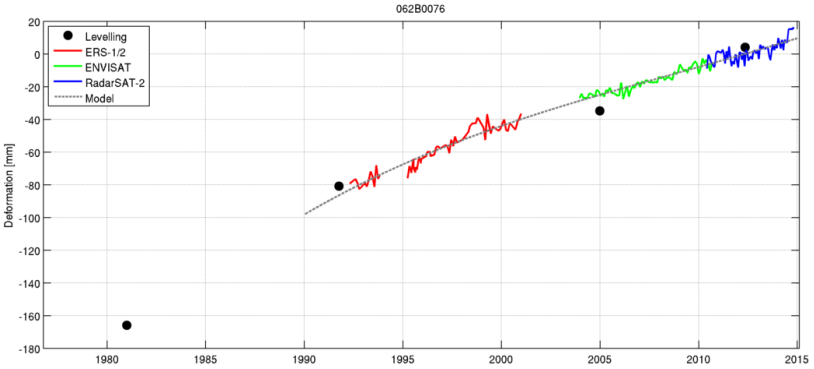
062B0076
Levelling
ERS-1/2
ENVISAT
RadarSAT-2
Model
Deformation [mm]

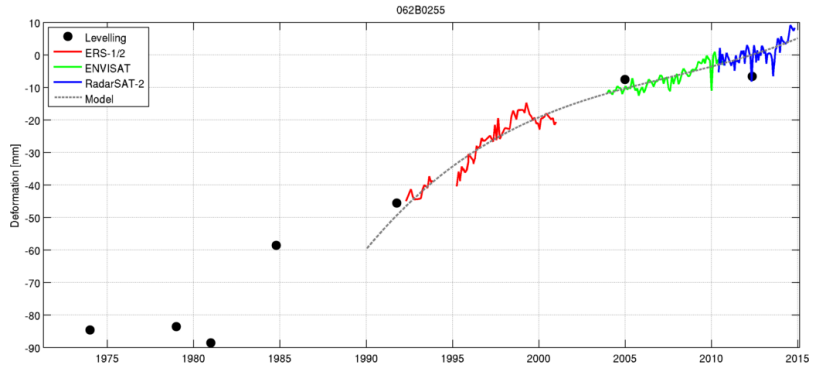
062B0255
Levelling
ERS-1/2
ENVISAT
RadarSAT-2
Model
Deformation [mm]

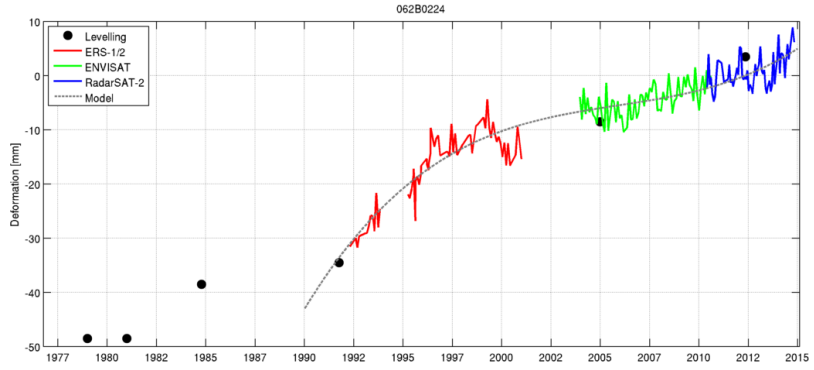
062B0224
Levelling
ERS-1/2
ENVISAT
RadarSAT-2
Model
Deformation [mm]

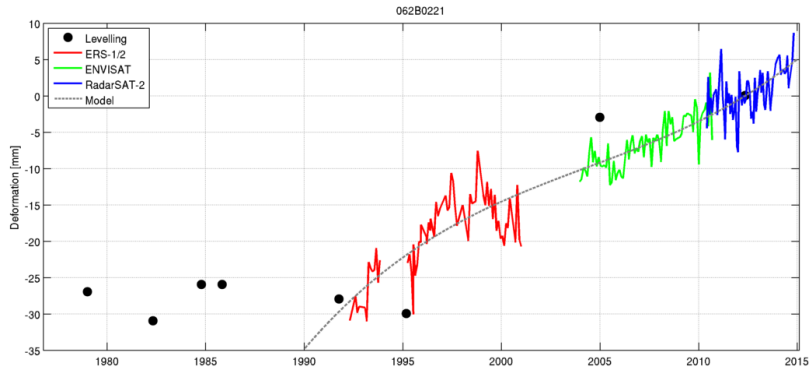
062B0221
Levelling
ERS-1/2
ENVISAT
RadarSAT-2
Model
Deformation [mm]

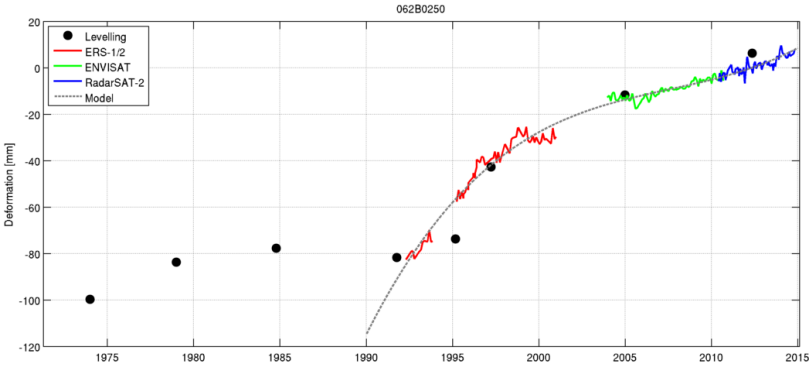
062B0250
Levelling
ERS-1/2
ENVISAT
RadarSAT-2
Model
Deformation [mm]

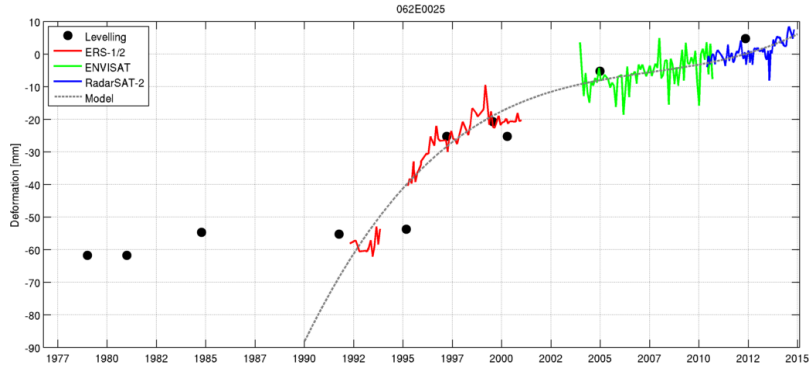
062E0025
Levelling
ERS-1/2
ENVISAT
RadarSAT-2
Model
Deformation [mm]

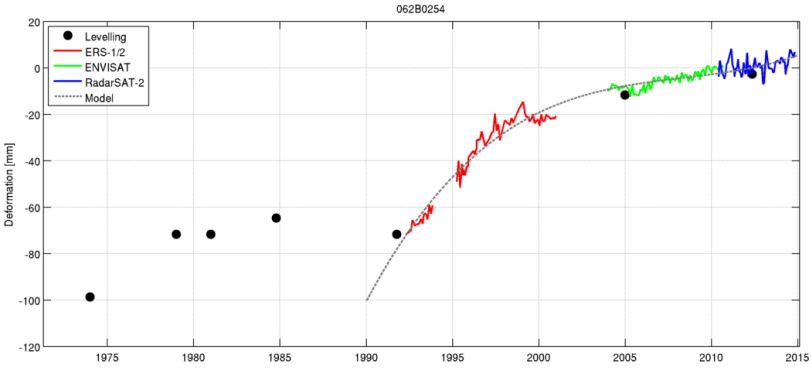
062B0254
Levelling
ERS-1/2
ENVISAT
RadarSAT-2
Model
Deformation [mm]

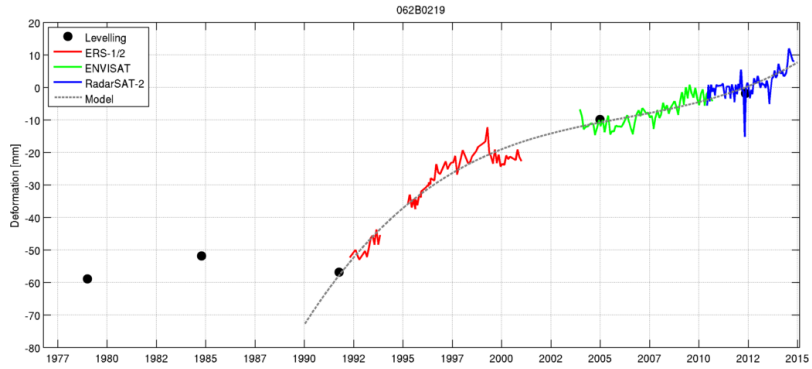
062B0219
Levelling
ERS-1/2
ENVISAT
RadarSAT-2
Model
Deformation [mm]

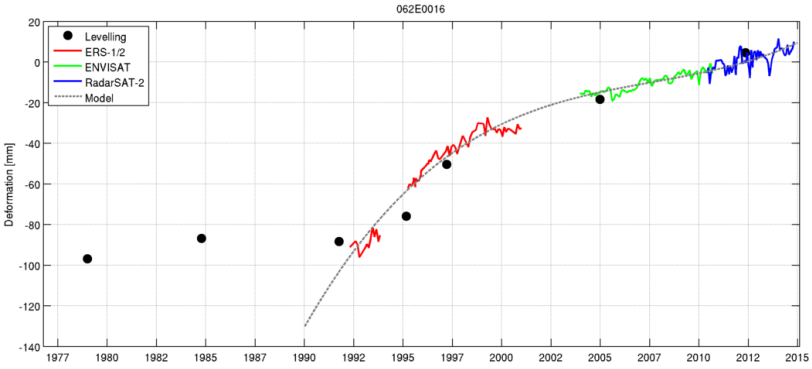
062E0016
Levelling
ERS-1/2
ENVISAT
RadarSAT-2
Model
Deformation [mm]

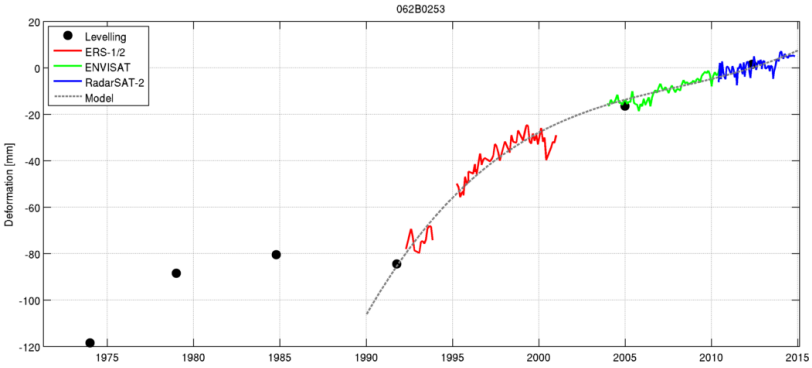
062B0253
Levelling
ERS-1/2
ENVISAT
RadarSAT-2
Model
Deformation [mm]

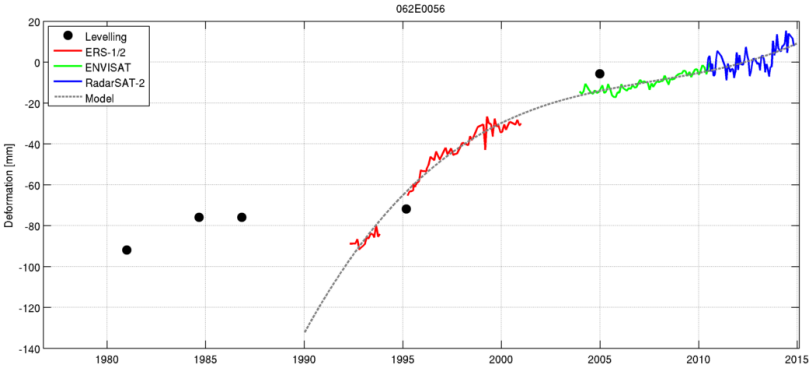
062E0056
Levelling
ERS-1/2
ENVISAT
RadarSAT-2
Model
Deformation [mm]

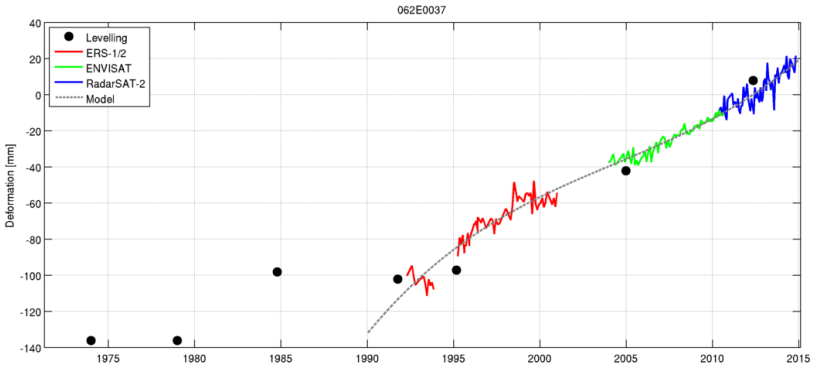
062E0037
Levelling
ERS-1/2
ENVISAT
RadarSAT-2
Model
Deformation [mm]

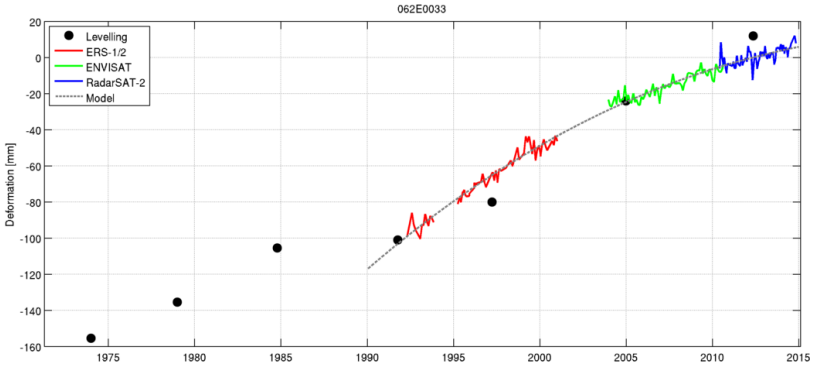
062E0033
Levelling
ERS-1/2
ENVISAT
RadarSAT-2
Model
Deformation [mm]

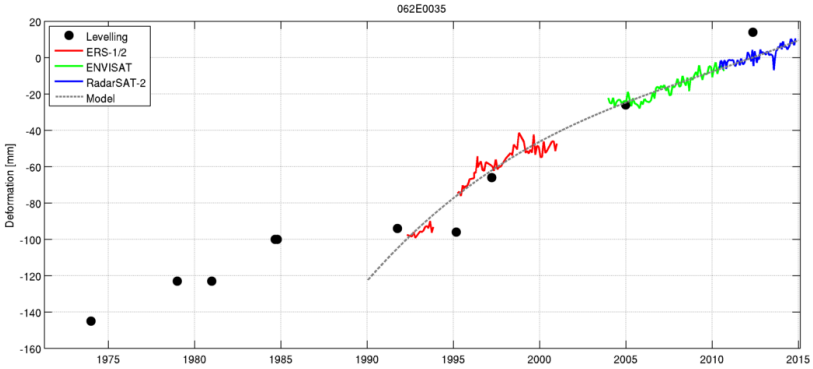
062E0035
Levelling
ERS-1/2
ENVISAT
RadarSAT-2
Model
Deformation [mm]

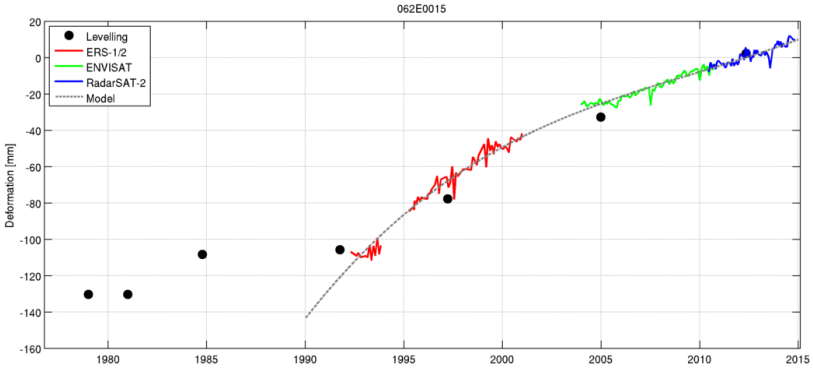
062E0015
Levelling
ERS-1/2
ENVISAT
RadarSAT-2
Model
Deformation [mm]

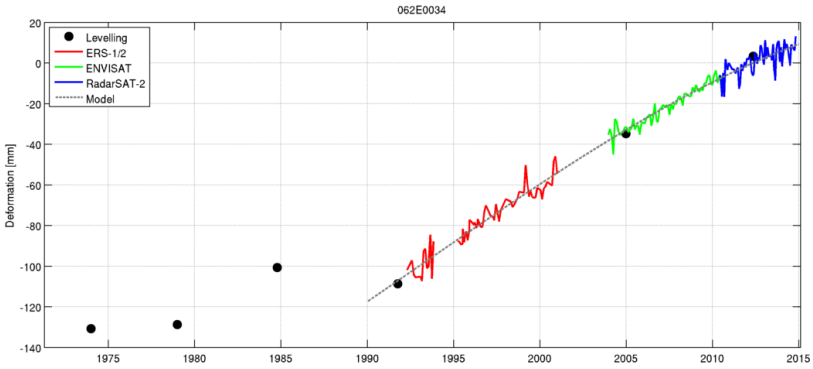
062E0034
Levelling
ERS-1/2
ENVISAT
RadarSAT-2
Model
Deformation [mm]

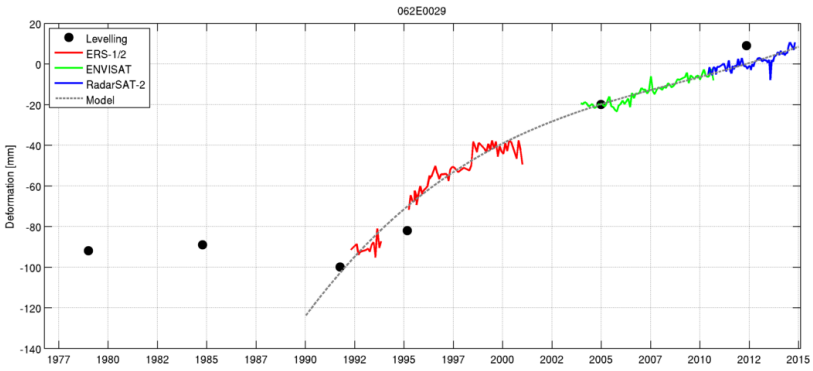
062E0029
Levelling
ERS-1/2
ENVISAT
RadarSAT-2
Model
Deformation [mm]

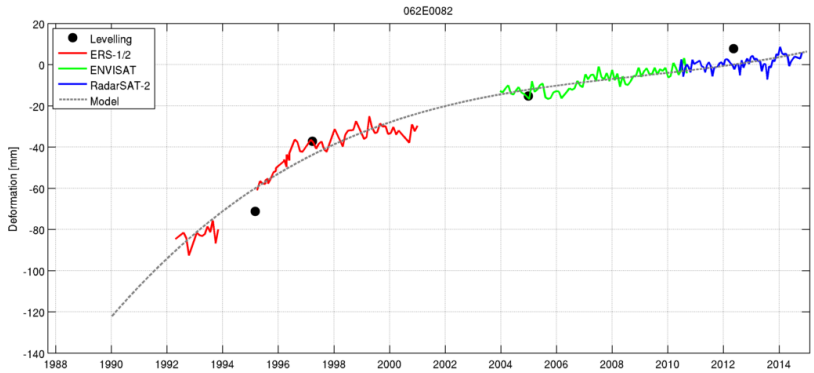
062E0082
Levelling
ERS-1/2
ENVISAT
RadarSAT-2
Model
Deformation [mm]

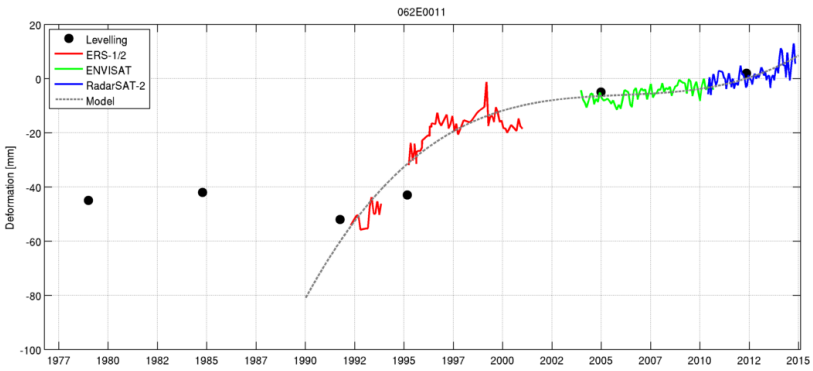
062E0011
Levelling
ERS-1/2
ENVISAT
RadarSAT-2
Model
Deformation [mm]

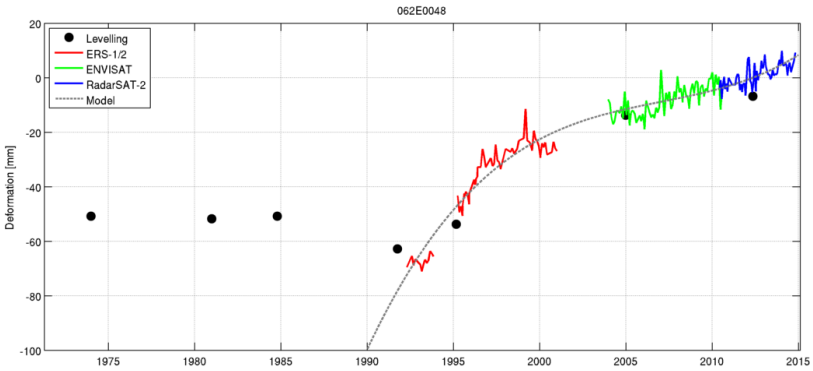
062E0048
Levelling
ERS-1/2
ENVISAT
RadarSAT-2
Model
Deformation [mm]

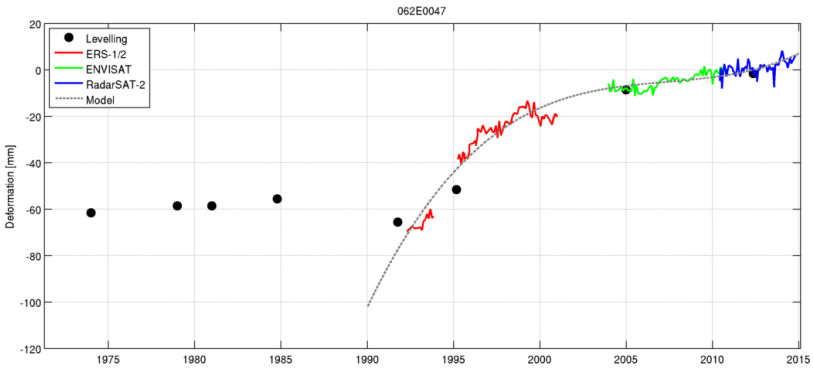
062E0047
Levelling
ERS-1/2
ENVISAT
RadarSAT-2
Model
Deformation [mm]

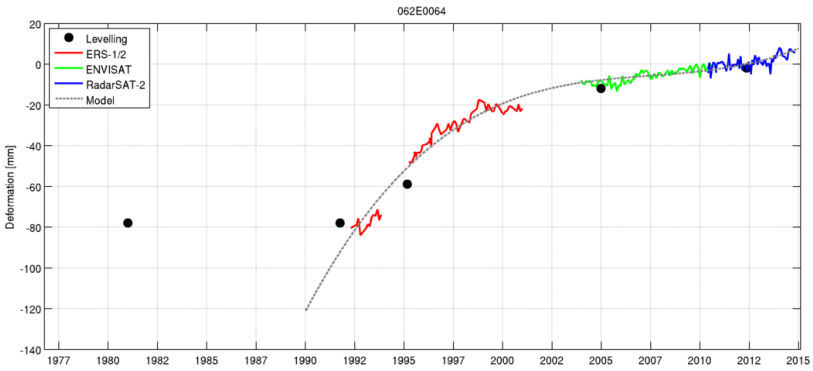
062E0064
Levelling
ERS-1/2
ENVISAT
RadarSAT-2
Model
Deformation [mm]

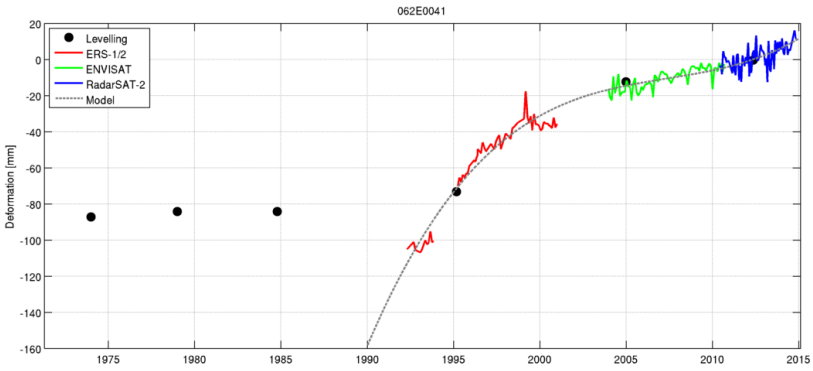
062E0041
Levelling
ERS-1/2
ENVISAT
RadarSAT-2
Model
Deformation [mm]

Appendix 3

Na-ijlende gevolgen steenkolenwinning Zuid-Limburg

Final report
on the results of the working group
5.2.1 - ground movements

Cross-profiles

by

Projectgroup
"Na-ijlende gevolgen van de steenkolenwinning in Zuid-Limburg"
(projectgroup GS-ZL)

on behalf of
Ministerie van Economische Zaken - The Netherlands

Delft, Maastricht and Aachen (D), 31. August 2016

Appendix 3 - Cross-profiles

Fig. 1: Location of PSI-based cross-profiles

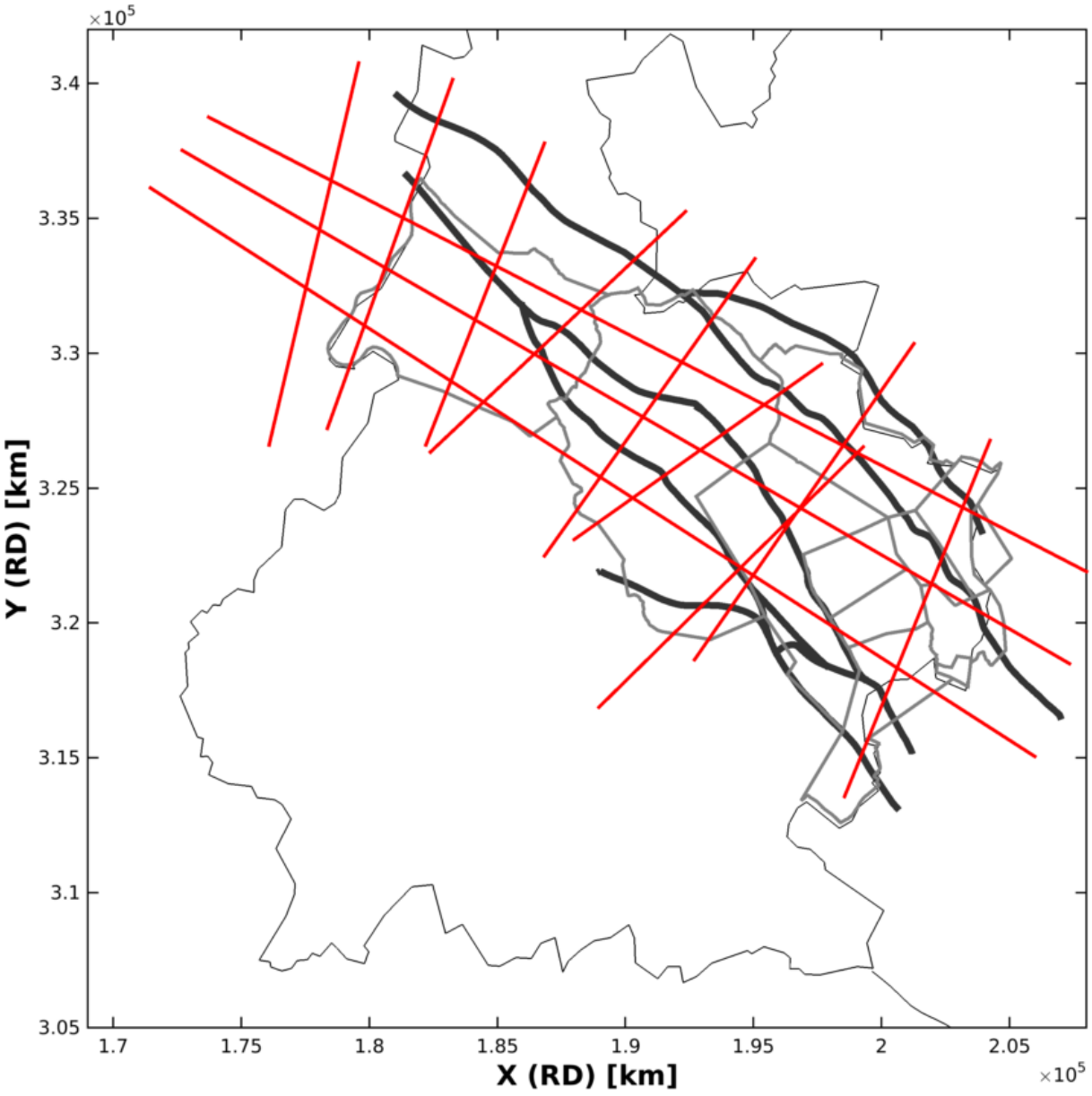

Fig. 2: PSI-based cross-profiles over the period 1 July 1992 and 1 July 2014

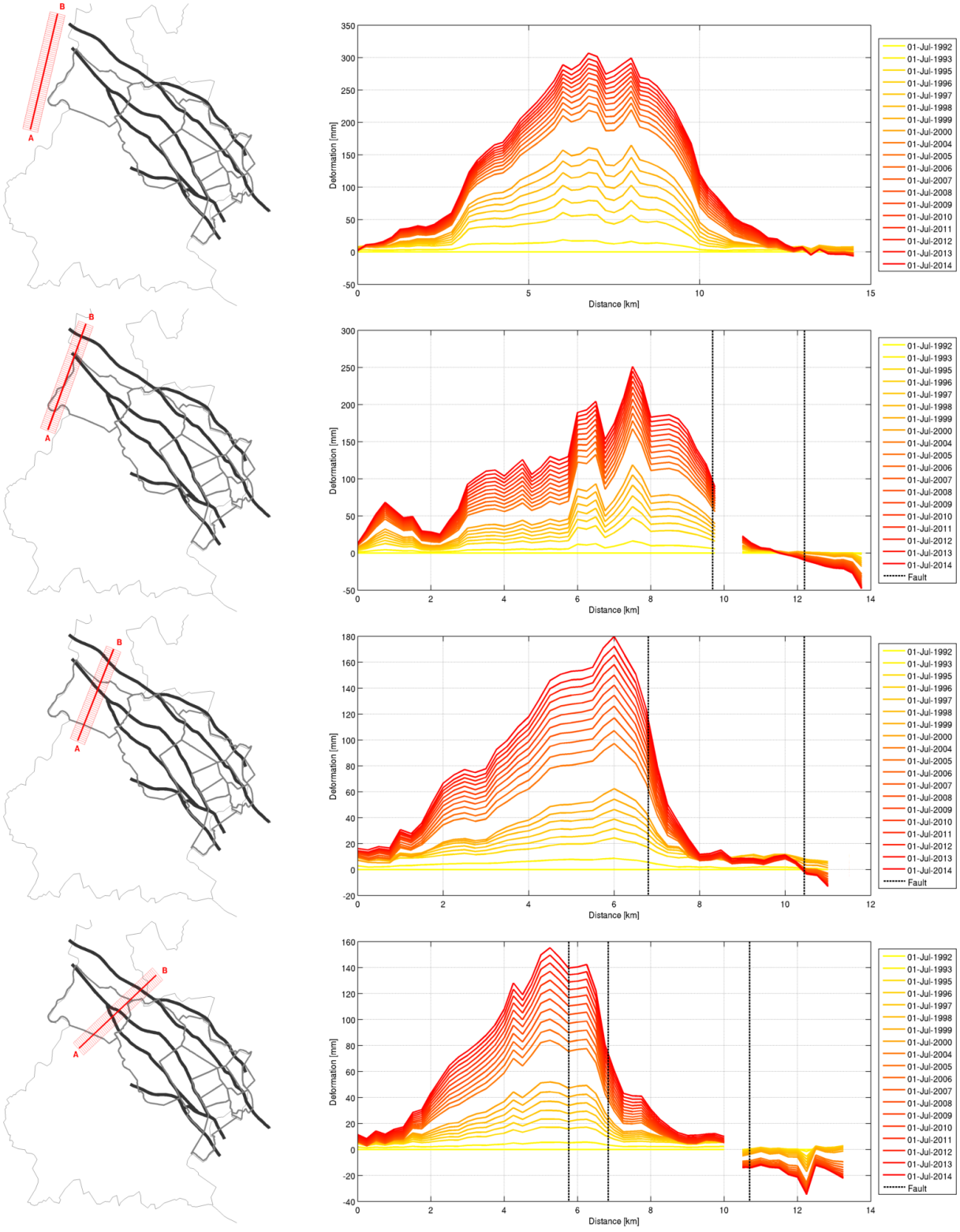

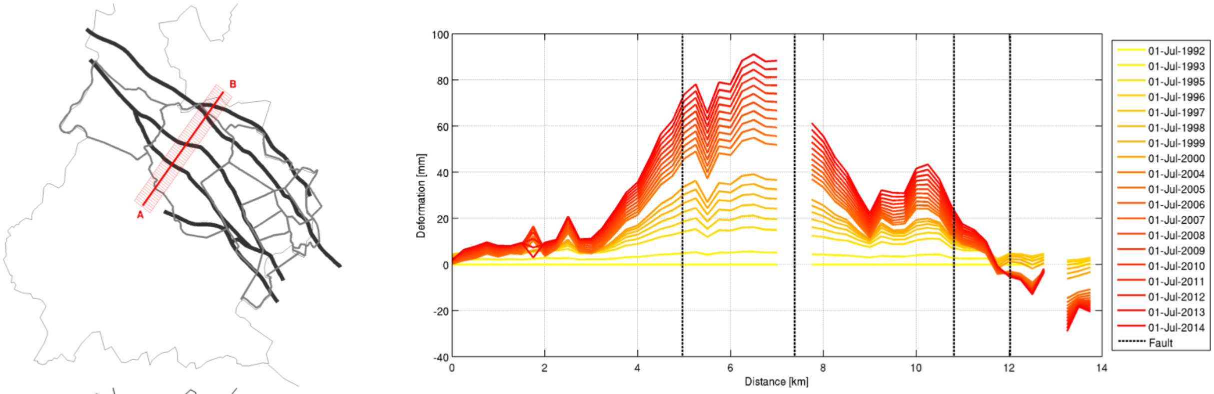

A
B
Deformation [mm]
Distance [km]
01-Jul-1992
01-Jul-1993
01-Jul-1995
01-Jul-1996
01-Jul-1997
01-Jul-1998
01-Jul-1999
01-Jul-2000
01-Jul-2004
01-Jul-2005
01-Jul-2006
01-Jul-2007
01-Jul-2008
01-Jul-2009
01-Jul-2010
01-Jul-2011
01-Jul-2012
01-Jul-2013
01-Jul-2014
Fault

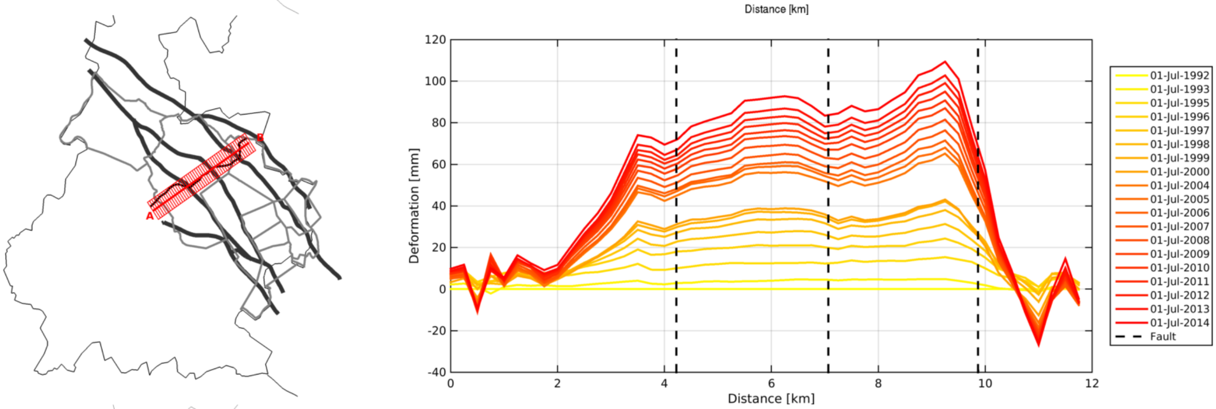

A
B
Deformation [mm]
Distance [km]
01-Jul-1992
01-Jul-1993
01-Jul-1995
01-Jul-1996
01-Jul-1997
01-Jul-1998
01-Jul-1999
01-Jul-2000
01-Jul-2004
01-Jul-2005
01-Jul-2006
01-Jul-2007
01-Jul-2008
01-Jul-2009
01-Jul-2010
01-Jul-2011
01-Jul-2012
01-Jul-2013
01-Jul-2014
Fault

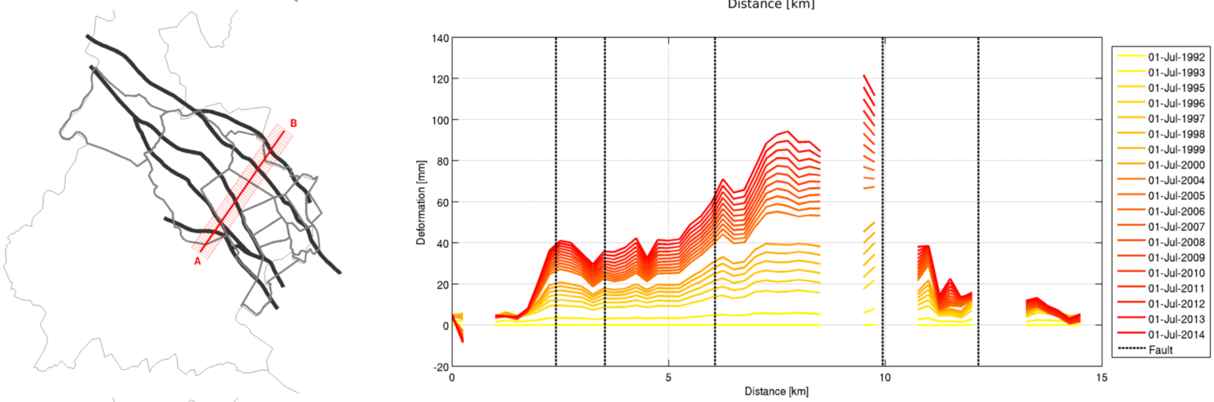

A
B
Deformation [mm]
Distance [km]
01-Jul-1992
01-Jul-1993
01-Jul-1995
01-Jul-1996
01-Jul-1997
01-Jul-1998
01-Jul-1999
01-Jul-2000
01-Jul-2004
01-Jul-2005
01-Jul-2006
01-Jul-2007
01-Jul-2008
01-Jul-2009
01-Jul-2010
01-Jul-2011
01-Jul-2012
01-Jul-2013
01-Jul-2014
Fault

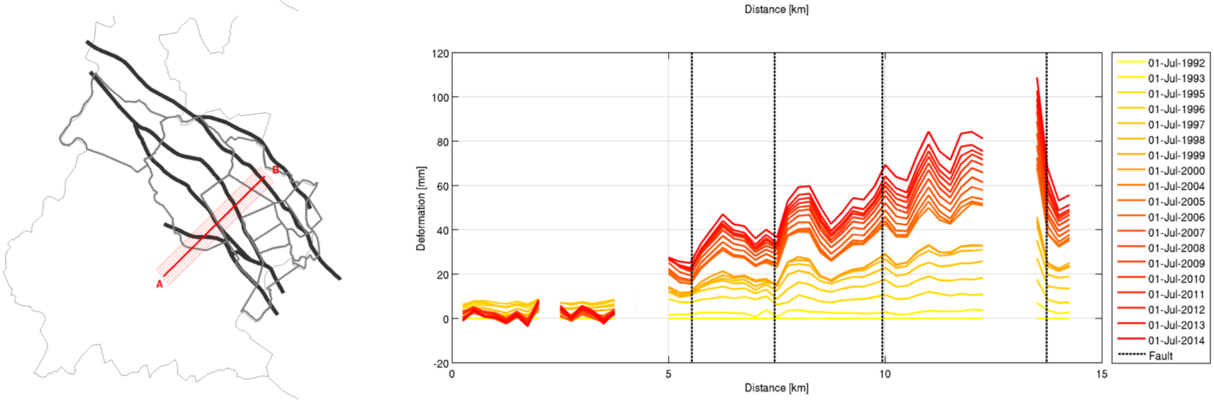

A
B
Deformation [mm]
Distance [km]
01-Jul-1992
01-Jul-1993
01-Jul-1995
01-Jul-1996
01-Jul-1997
01-Jul-1998
01-Jul-1999
01-Jul-2000
01-Jul-2004
01-Jul-2005
01-Jul-2006
01-Jul-2007
01-Jul-2008
01-Jul-2009
01-Jul-2010
01-Jul-2011
01-Jul-2012
01-Jul-2013
01-Jul-2014
Fault

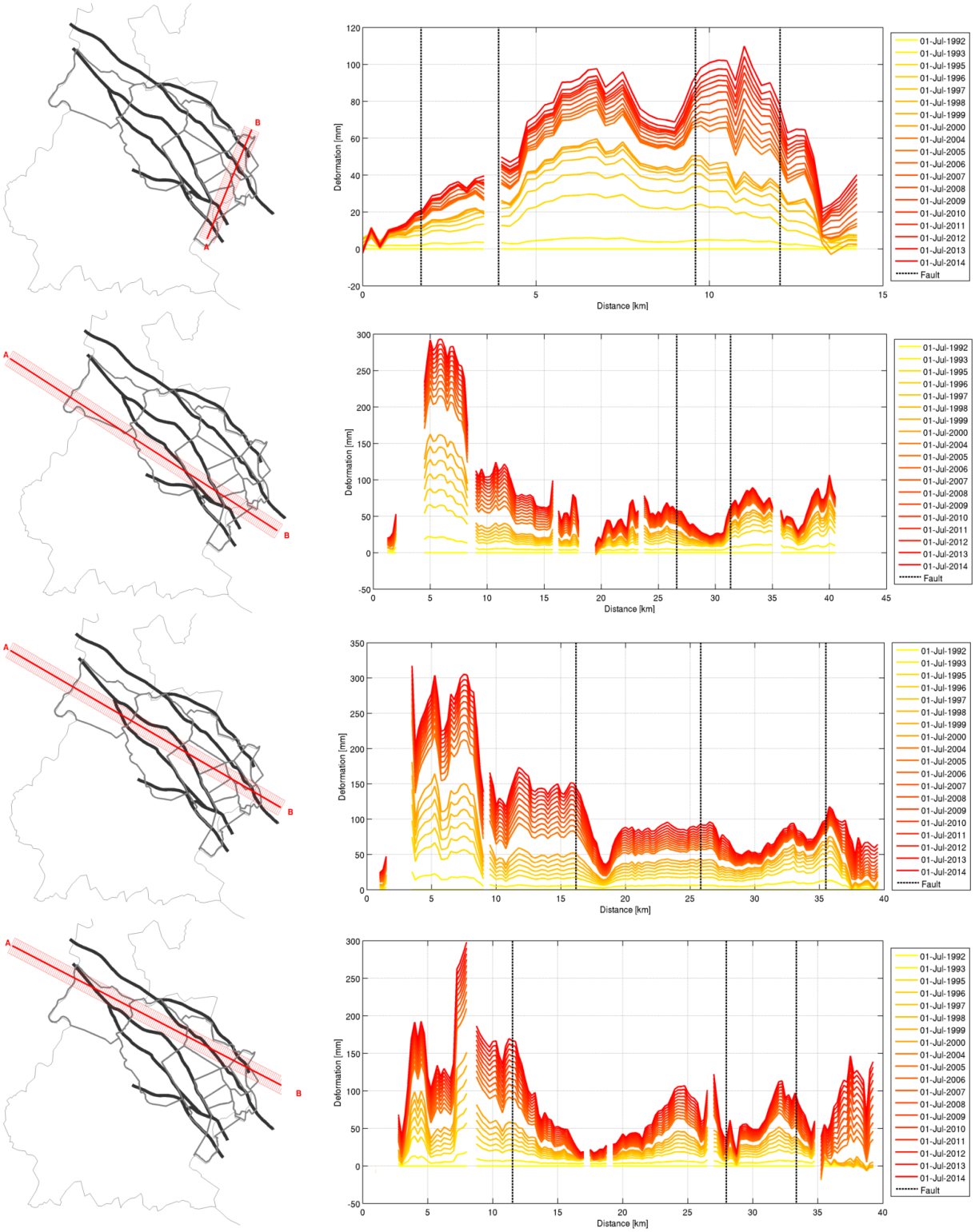
A
B
Deformation [mm]
Distance [km]
01-Jul-1992
01-Jul-1993
01-Jul-1995
01-Jul-1996
01-Jul-1997
01-Jul-1998
01-Jul-1999
01-Jul-2000
01-Jul-2004
01-Jul-2005
01-Jul-2006
01-Jul-2007
01-Jul-2008
01-Jul-2009
01-Jul-2010
01-Jul-2011
01-Jul-2012
01-Jul-2013
01-Jul-2014
Fault

Appendix 4

Na-ijlende gevolgen steenkolenwinning Zuid-Limburg

Final report
on the results of the working group
5.2.1 - ground movements

InSAR deformation maps

by

Projectgroup
"Na-ijlende gevolgen van de steenkolenwinning in Zuid-Limburg"
(projectgroup GS-ZL)

on behalf of
Ministerie van Economische Zaken - The Netherlands

Delft, Maastricht and Aachen (D), 31. August 2016

Appendix 4 - InSAR deformation maps

Fig. 1: Total vertical ground movement in the 23.04.1992 to 28.10.2014 period based on InSAR measurements

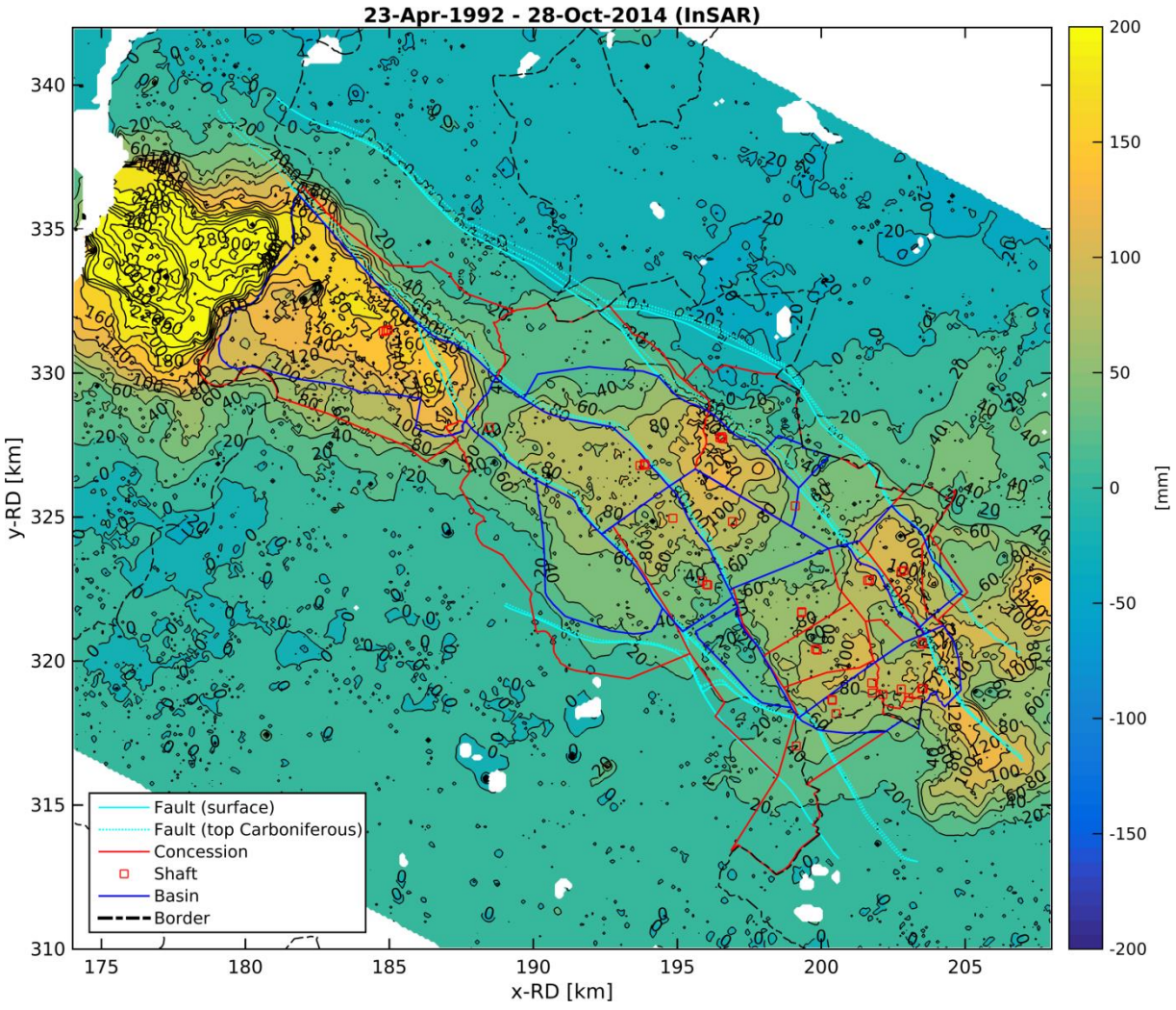

Fig. 2: InSAR-based vertical ground movement estimates for periods of five years

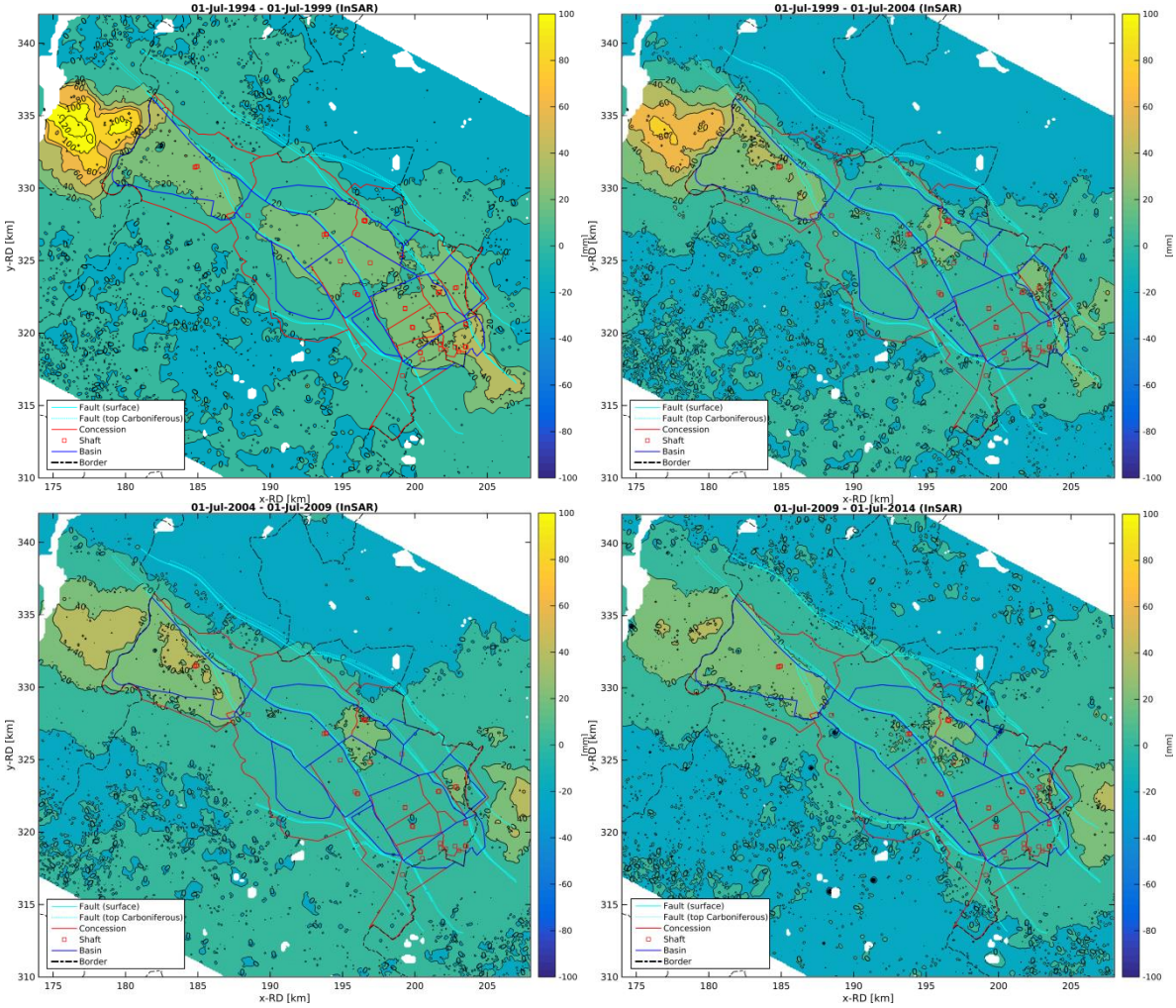

Appendix 5

Na-ijlende gevolgen steenkolenwinning Zuid-Limburg

Final report
on the results of the working group
5.2.1 - ground movements

Bow-Tie-Analysis

by

Projectgroup
"Na-ijlende gevolgen van de steenkolenwinning in Zuid-Limburg"
(projectgroup GS-ZL)

on behalf of
Ministerie van Economische Zaken - The Netherlands

Delft, Maastricht and Aachen (D), 31. August 2016
(Rev. a: 02. December 2016)

5.2.1 Ground movements

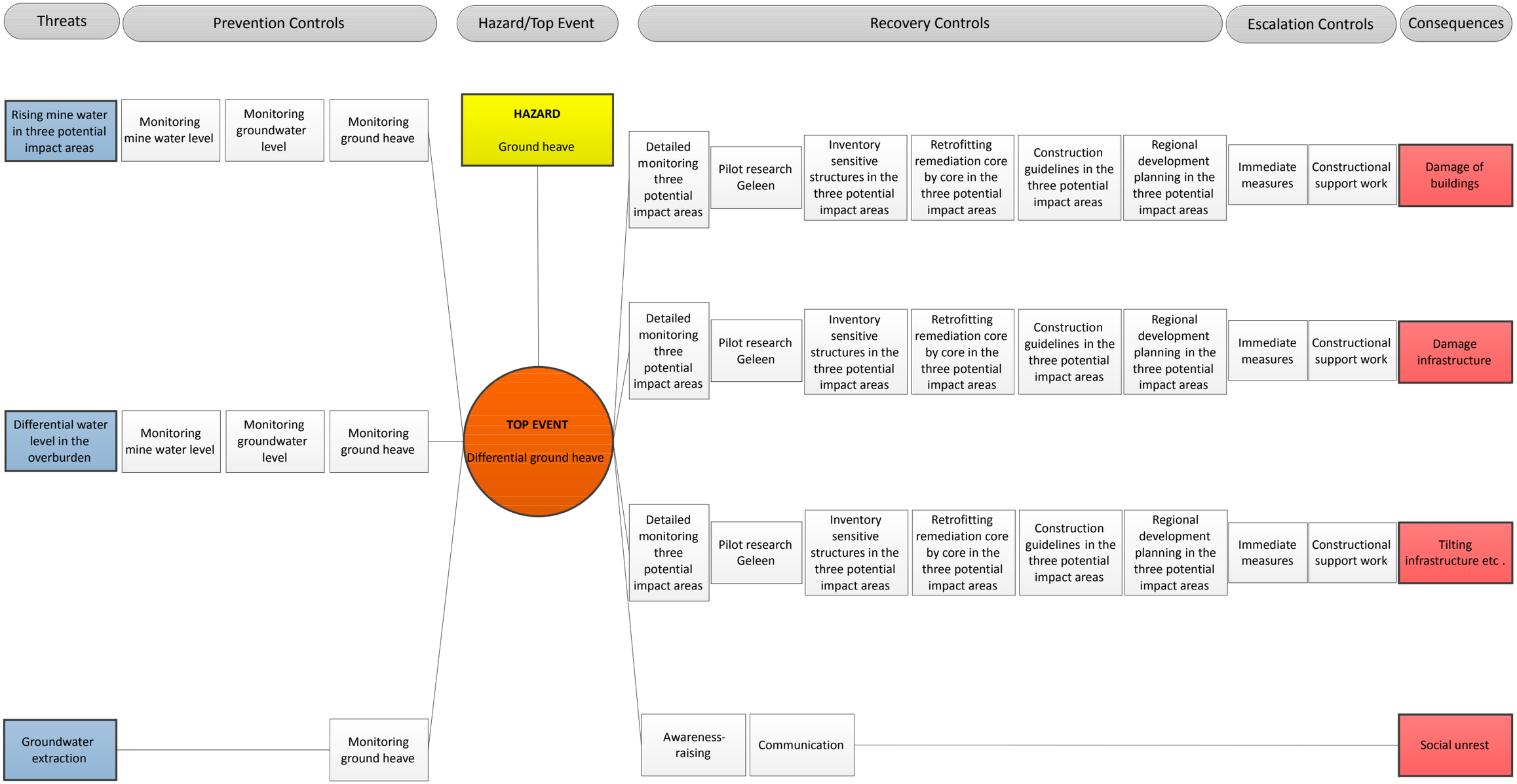

App. 5

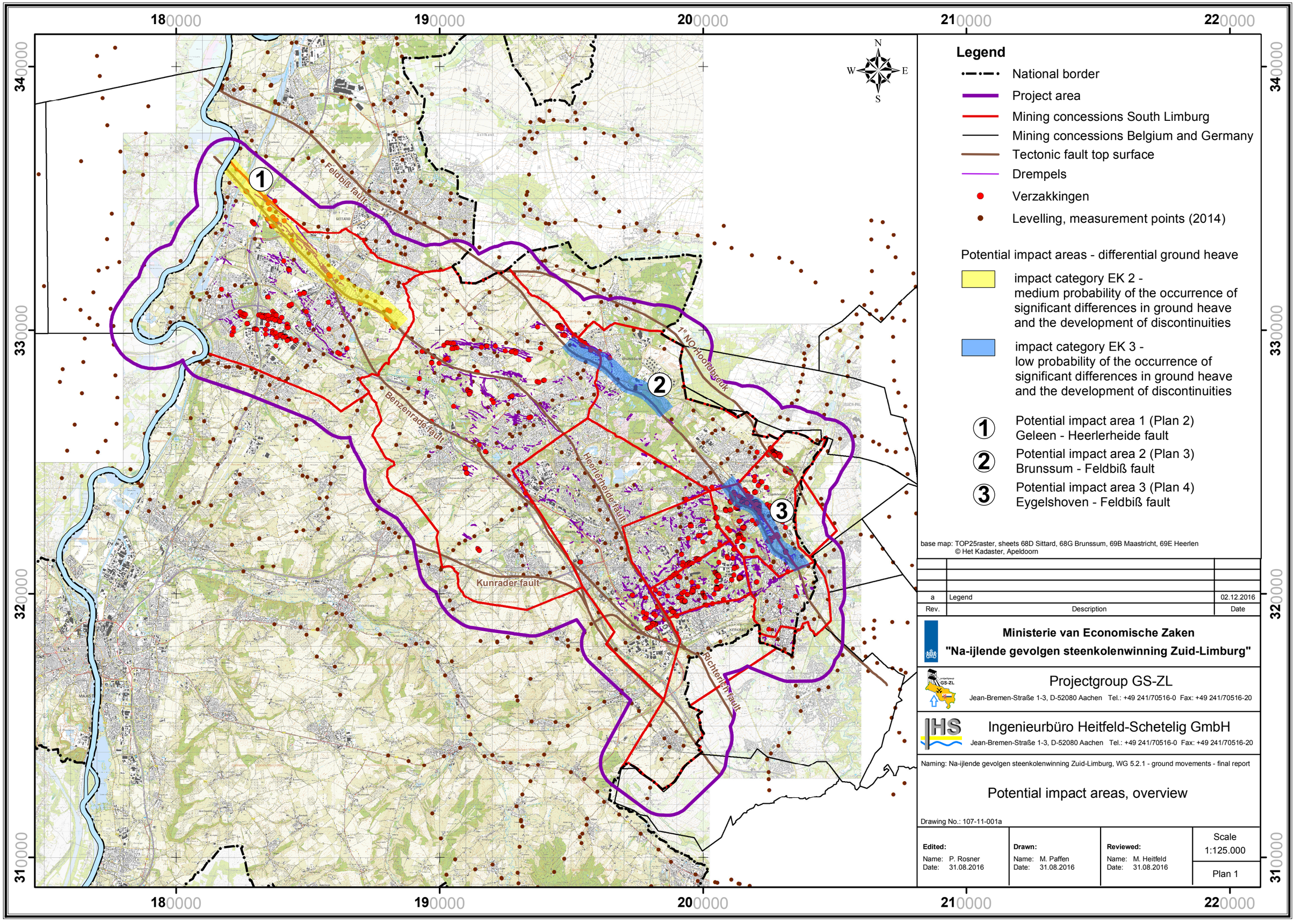

Legend

- National border
- Project area
- Mining concessions South Limburg
- Mining concessions Belgium and Germany
- Tectonic fault top surface
- Drempels
- Verzakkingen
- Levelling, measurement points (2014)

Potential impact areas - differential ground heave

- impact category EK 2 - medium probability of the occurrence of significant differences in ground heave and the development of discontinuities
- impact category EK 3 - low probability of the occurrence of significant differences in ground heave and the development of discontinuities

1. Potential impact area 1 (Plan 2) Geleen - Heerlerheide fault
2. Potential impact area 2 (Plan 3) Brunssum - Feldbiß fault
3. Potential impact area 3 (Plan 4) Eygelshoven - Feldbiß fault

base map: TOP25raster, sheets 68D Sittard, 68G Brunssum, 69B Maastricht, 69E Heerlen
© Het Kadaster, Apeldoorn

Rev.	Description	Date
a	Legend	02.12.2016

Ministerie van Economische Zaken
"Na-ijlende gevolgen steenkolenwinning Zuid-Limburg"

Projectgroup GS-ZL
Jean-Bremen-Straße 1-3, D-52080 Aachen Tel.: +49 241/70516-0 Fax: +49 241/70516-20

Ingenieurbüro Heitfeld-Schetelig GmbH
Jean-Bremen-Straße 1-3, D-52080 Aachen Tel.: +49 241/70516-0 Fax: +49 241/70516-20

Naming: Na-ijlende gevolgen steenkolenwinning Zuid-Limburg, WG 5.2.1 - ground movements - final report

Potential impact areas, overview

Drawing No.: 107-11-001a

Edited:	Drawn:	Reviewed:	Scale
Name: P. Rosner Date: 31.08.2016	Name: M. Paffen Date: 31.08.2016	Name: M. Heitfeld Date: 31.08.2016	1:125.000 Plan 1

Y:\GIS\1_Uebersichtsprojekte\Niederlande_Anlagen\Report_WG_521_part3\107_11_001_Uebersicht_v2_Rev_a.mxd

18 2000 | 18 4000 | 18 6000 | 18 8000 | 19 0000

33 6000 | 33 4000 | 33 2000

Legend

- National border
- Project area
- Mining concessions South Limburg
- Tectonic fault top surface
- Drempels
- Verzakkingen

Potential impact area
- impact category EK 2

Ground movements - InSAR data
Period 2010 - 2014
deformation rate [mm/a]

ground heave	subsidence
13 to 14	-1 to 1
12 to 13	< -1
11 to 12	
10 to 11	
9 to 10	
8 to 9	
7 to 8	
6 to 7	
5 to 6	
4 to 5	
3 to 4	
2 to 3	
1 to 2	

- Monitoring profile for detailed levelling

Rev.	Description	Date
a	Legend	02.12.2016

Ministerie van Economische Zaken
"Na-ijlende gevolgen steenkolenwinning Zuid-Limburg"

Projectgroup GS-ZL
Jean-Bremen-Straße 1-3, D-52080 Aachen Tel.: +49 241/70516-0 Fax: +49 241/70516-20

Ingenieurbüro Heitfeld-Schetelig GmbH
Jean-Bremen-Straße 1-3, D-52080 Aachen Tel.: +49 241/70516-0 Fax: +49 241/70516-20

Naming: Na-ijlende gevolgen steenkolenwinning Zuid-Limburg, WG 5.2.1 - ground movements - final report

Potential impact area 1 - Heerlerheide fault, Geleen, with monitoring measures

Drawing No.: 107-11-002a

Edited:	Drawn:	Reviewed:	Scale
Name: P. Rosner Date: 31.08.2016	Name: M. Paffen Date: 31.08.2016	Name: M. Heitfeld Date: 31.08.2016	1:25.000
			Plan 2

Y:\GIS\1_Uebersichtsprojekte\Niederlande_Anlagen\Report_WG_521_part3\107_11_002_Geleen_v2_Rev_a.mxd

194000 196000 198000 200000 202000

330000 328000 326000

Bingelrade · Schinveld · Gemeente Onderbanken · Merkelbeek · BRUNSSUM · Brunssummerheide · Schrieversheide · Gemeente Heerlen · Christinawijk

1e NO Hoofdbreuk · Feldbiß fault · Heerlerheide fault

Legend

- National border
- Project area
- Mining concessions South Limburg
- Tectonic fault top surface
- Drempels
- Verzakkingen

Potential impact area
- impact category EK 3

Ground movements - InSAR data
Period 2010 - 2014
deformation rate [mm/a]

ground heave	subsidence
14 to 15	-1 to 1
13 to 14	< -1
12 to 13	
11 to 12	
10 to 11	
9 to 10	
8 to 9	
7 to 8	
6 to 7	
5 to 6	
4 to 5	
3 to 4	
2 to 3	
1 to 2	

- Monitoring profile for detailed levelling

Rev.	Description	Date
a	Legend	02.12.2016

Ministerie van Economische Zaken
"Na-ijlende gevolgen steenkolenwinning Zuid-Limburg"

Projectgroup GS-ZL
Jean-Bremen-Straße 1-3, D-52080 Aachen Tel.: +49 241/70516-0 Fax: +49 241/70516-20

Ingenieurbüro Heitfeld-Schetelig GmbH
Jean-Bremen-Straße 1-3, D-52080 Aachen Tel.: +49 241/70516-0 Fax: +49 241/70516-20

Naming: Na-ijlende gevolgen steenkolenwinning Zuid-Limburg, WG 5.2.1 - ground movements - final report

Potential impact area 2 - Feldbiß fault, Brunssum, with monitoring measures

Drawing No.: 107-11-003a

Edited:	Drawn:	Reviewed:	Scale
Name: P. Rosner	Name: M. Paffen	Name: M. Heitfeld	1:25.000
Date: 31.08.2016	Date: 31.08.2016	Date: 31.08.2016	Plan 3

Y:\GIS\1_Uebersichtsprojekte\Niederlande_Anlagen\Report_WG_521_part3\107_11_003_Brunssum_v2_Rev_a.mxd

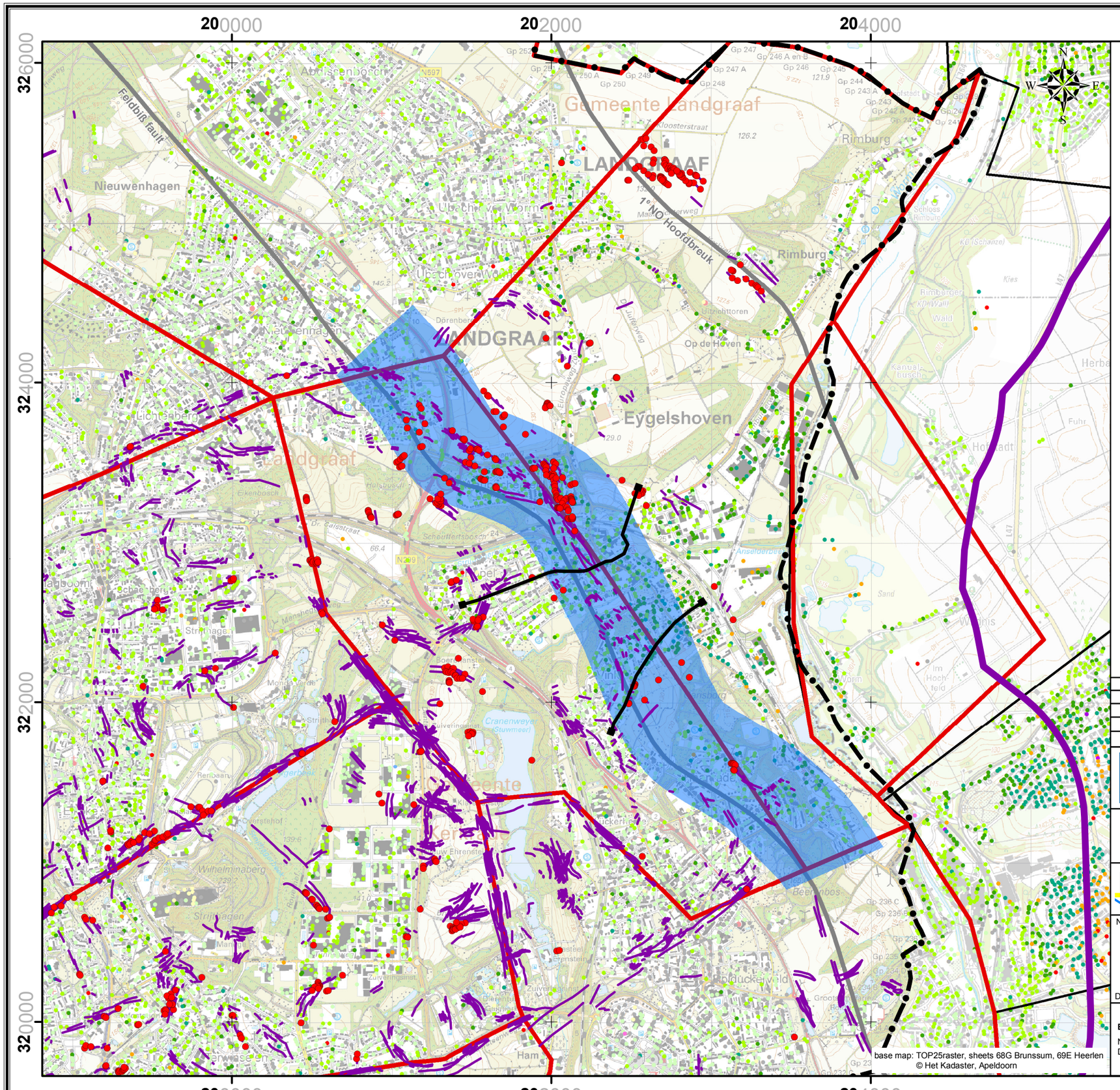

Legend

- National border
- Project area
- Mining concessions South Limburg
- Tectonic fault top surface
- Drempels
- Verzakkingen

Potential impact area

- impact category EK 3

Ground movements - InSAR data
Period 2010 - 2014
deformation rate [mm/a]

ground heave	subsidence
14 to 15	-1 to 1
13 to 14	< -1
12 to 13	
11 to 12	
10 to 11	
9 to 10	
8 to 9	
7 to 8	
6 to 7	
5 to 6	
4 to 5	
3 to 4	
2 to 3	
1 to 2	

- Monitoring profile for detailed levelling

Rev.	Description	Date
a	Legend	02.12.2016

Ministerie van Economische Zaken
"Na-ijlende gevolgen steenkolenwinning Zuid-Limburg"

Projectgroup GS-ZL
Jean-Bremen-Straße 1-3, D-52080 Aachen Tel.: +49 241/70516-0 Fax: +49 241/70516-20

Ingenieurbüro Heitfeld-Schetelig GmbH
Jean-Bremen-Straße 1-3, D-52080 Aachen Tel.: +49 241/70516-0 Fax: +49 241/70516-20

Naming: Na-ijlende gevolgen steenkolenwinning Zuid-Limburg, WG 5.2.1 - ground movements - final report

Potential impact area 3 - Feldbiß fault, Eygelshoven, with monitoring measures

Drawing No.: 107-11-004a

Edited:	Drawn:	Reviewed:	Scale
Name: P. Rosner Date: 31.08.2016	Name: M. Paffen Date: 31.08.2016	Name: M. Heitfeld Date: 31.08.2016	1:25.000 Plan 4

Y:\GIS\1_Uebersichtsprojekte\Niederlande_Anlagen\Report_WG_521_part3\107_11_004_Eygelshoven_v2_Rev_a.mxd